Forum Geografic - Studii și cercetări de geografie și protecția mediului (FG - S.C.G.P.M.)

The Journal *Forum geografic. Studii de geografie şi protecţia mediului* (Geographical Phorum – Geographical Studies and Environment Protection Research) was founded in 2002, and it seeks to publish high quality research in the domains of geography, environment protection and other related domains. It addresses a range of issues, such as geomorphology, pedology, climatology, hydrology, human geography and environment. Its content is directed to a broad audience, including both academics and policymakers. The papers selected for publication in the journal are subject to a review process using references from universities worldwide.

The journal is currently indexed by the following databases: SCOPUS, DOAJ, EBSCO, ERIH PLUS, Index Copernicus, Scipio, CrossRef, Ulrichsweb, IGU, Google Scholar, WorldCat, ProQuest, ZDB, CNCSIS, DRJI, citefactor.org journals indexing, InfoBase index, Eurasian Scientific Journal Index, ResearchBib.

Cover photo: *Metaliferi Mountains, Alba county (by Alina Vlăduț)*

For instructions for authors, subscription and all other information please visit our website
http://forumgeografic.ro
before submitting any papers please select the section *Publishing rules* from the About page and read thoroughly the submission instructions for authors

ISSN 1583-1523 (print)
ISSN 2067-4635 (online)
DOI prefix: 10.5775

Instructions for Authors

Article submission

In order to disseminate the research results in the field, researchers, scholars and professionals are welcome to submit an electronic version of the manuscript (in Microsoft Office Word format) to the editorial office (forum.geografic@gmail.com).

Submission requirements: The submission of an article for publication in our journal implies that the article has not been published before, nor it is being considered for publication in other journals. Authors are responsible for the content and the originality of their contributions. In order to be published, articles must be thoroughly researched and referenced.

IMPORTANT: All papers must be submitted in electronic format, only in English language.

Copyright statement

By submitting a scientific work to ***Forum geografic*** the submitters agree to declare the following:

- the submitted work belongs exclusively to the declared authors;
- the submitted work represents original scientific research;
- the submitted work has not been published or submitted for publishing to another journal;
- if the submitted work is published or selected for publishing in ***Forum geografic***, the authors waive any patrimonial claims derived from their authorship for the submitted work; the authors retain the moral rights for their submitted work, as granted under the Romanian applicable law; also, the authors agree to refrain from ulterior submitting of the work to other journals.

The submitters agree to be solely held accountable in case of breaching the above terms and to defend the representatives of ***Forum geografic*** in the event of a lawsuit related to the submitted work.

When submitting a paper, the authors are required to print, fill and send a scanned copy of this declaration.

Privacy statement

The submitted personal data, such as names or email addresses, are used only for the declared purpose of the ***Forum geografic*** journal (publishing original scientific research) and are not available to third parties.

Manuscripts are received at all times. However, in order to have your article published in the current year, the manuscripts must be submitted until the 15th of February for the first issue of the current year and until the 1st of September for the second issue.

Article format

All manuscripts must be edited entirely in English. Articles must include:

- Title
- Author's name(s). For each author you must mention the author's scientific title, his affiliation (institution) and e- mail address;
- Abstract (maximum 300 words);
- Keywords (not more than 5-6 words);
- Acknowledgments (if any);
- Main body of text (structured according to Introduction, Data & Methods, Results & Discussions, Conclusions);
- Illustrations (graphs, diagrams, maps, photos – should have indications of their positions in the text and title written in English) must be also submitted in electronic format, preferably in JPG, PNG or BMP format and must be referred to as Figures, which should be numbered with Arabic numbers.
- Tables must be numbered with Arabic numbers and should not repeat data available elsewhere in the text.
- References must be indicated in the text, between brackets and they must include the author's name and the date of the publication (Popescu, 2000). When three or more authors are referred, they will appear in the text as follows: (Popescu et al., 1997). References must be listed in alphabetical order at the end of the text.

The following style sheet is recommended:

- for journals:

Miletić, R., Lukić, V., & Miljanović, D. (2011). Deindustrialization and structural changes in commuting flows in Serbia. *Forum geografic*, X(2), 244-254. doi:10.5775/fg.2067-4635.2011.009.d

- for books:

Bran, F.,Marin, D., & Simion, T. (1997). Turismul rural. Modelul european, Editura Economică, București

- for papers from conference proceedings:

Deci, E. L., Ryan, R. M., (1991), A motivational approach to self: Integration in personality. In R. Dienstbier (Ed.), *Nebraska Symposium on Motivation: Vol. 38*. *Perspectives on motivations* (pp. 237-288). Lincoln: University of Nebraska Press.

Review process

All the manuscripts received by the editors undergo an anonymous peer review process, necessary for assessing the quality of scientific information, the relevance to the field, the appropriateness of scientific writing style, the compliance with the style and technical requirements of our journal, etc. The referees are selected from the national and international members of the editorial and scientific board, as well as from other scholarly or professional experts in the field. The referees assess the article drafts, commenting and making recommendations. This process leads either to acceptation, recommendation for revision, or rejection of the assessed article. Editors reserve the right to make minor editorial changes to the submitted articles, including changes to grammar, punctuation and spelling, as well as article format, but no major alterations will be carried out without the author's approval. Before being published, the author is sent the proof of the manuscript adjusted by editors. If major revisions are necessary, articles are returned to the author so that he should make the proper changes. Authors are notified by email about the status of the submitted.

Forum Geografic - Studii și cercetări de geografie și protecția mediului
www.forumgeografic.ro DOI: 10.5775/fg

CONTENTS

Volume XXII, Issue 1 / June 2023

Forum geografic. Studii și cercetări de geografie și protecția mediului
Volume **XXII**, Issue **1** (**June 2023**), pp. **5-15;** DOI: **10.5775/fg.2023.090.i**

A statistical analysis of temperature and precipitation in Belgrade, Serbia (1961-2020)

Nina ČEGAR[1,*], Uroš DURLEVIĆ[1], Milica DOBRIĆ[1], Sandra VUKAŠINOVIĆ[1]

[1] Faculty of Geography, University of Belgrade, Studentski Trg 3/III, Belgrade, Serbia
* *Corresponding author*: nina.cegar@gef.bg.ac.rs

Received on 18-10-2022, reviewed on 27-12-2022, accepted on 27-03-2023

Abstract

The most significant effects of climate change are related to temperature and precipitation. Changes in precipitation and temperature patterns affect water resource capacity, agricultural activities, global biodiversity and emergency management. In this study, using two statistical models (Mann-Kendall and Pettit's test), climate data for the territory of Belgrade in the time interval 1961-2020 were processed. Trends were analyzed: average annual temperatures, average monthly temperatures, annual and monthly precipitation amounts. The aim of the research is to determine the statistical significance of the increasing/decreasing temperature and precipitation trends on a monthly and annual basis. Based on the obtained results, it was determined that the changing point of the annual temperature is in 1997, while a statistically significant increasing trend was observed in all months except November. The increasing trend recorded by the precipitation amount is 0.345 mm/year, but without statistical significance. The most significant results corresponding to July and October.
Keywords: *Trend, Mann-Kendall test, Pettit's test, precipitation, air temperature, City of Belgrade*

Introduction

Climate change is reflected in large fluctuations in climate averages that persist for decades or even longer periods. Although climate change occurs on a global scale, impacts often vary from region to region. In the 20th century numerous climatic anomalies were observed-poor monsoon years around the turn of the century, rapid Arctic warming into the 1920s, the Dust Bowl drought and heat waves in North America in the 1930s and drought in Australia, and cold winters and hot summers in Europe in the 1940s. These anomalous events occurred during a period of strong global-scale warming, which can be attributed to a combination of external forcing (particularly, greenhouse gas increases, combined with a hiatus in volcanic events) and internal decadal variability. During the 20th century, in most European regions, a temperature increase was observed (Trajkovic & Kolakovic, 2009; Gocic & Trajkovic, 2013; Hegerl et al.,2018). Climate reconstructions show that summer air temperatures in Europe in period 1986–2015 have been the warmest for at least 2000 years, and that they lie significantly outside the range of natural variability (Luterbacher et al., 2016). Based on data from 210 weather stations on the territory of Europe, temperature increase amounts 0.051°C/year in the period 1985-2020. The highest increase was recorded in spring, the lowest in autumn (Twardosz et al., 2021). Vyshkvarkova and Sukhonos (2022) investigating the spatial distribution of temperature and precipitation extremes in Eastern Europe, conclude that there are positive and statistically significant trends for warm extremes in all seasons, with maximum values in the winter season. In contrast, negative trends were obtained for cold extremes.

Each of the last four decades has been successively warmer than any decade that preceded it since 1850. Global surface temperature in the first two decades of the 21st century (2001–2020) was 0.99 (0.84 to 1.10) °C higher than 1850–1900. Global surface temperature was 1.09 [0.95 to 1.20] °C higher in 2011–2020 than 1850–1900, with larger increases over land (1.59 [1.34 to 1.83] °C) than over the ocean (0.88 [0.68 to 1.01] °C). Hot extremes (including heatwaves) have become more frequent and more intense across most land regions since the 1950s, while cold extremes (including cold waves) have become less frequent and less severe. Globally averaged precipitation over land has likely increased since 1950, with a faster rate of increase since the 1980s. Mid-latitude storm tracks have likely shifted poleward in both hemispheres since the 1980s, with marked seasonality in trends (IPCC, 2021) According to NOAA (2022), all years in the period 2013-2021 belongs to the category of ten warmest years since measurements were made. Since 1981, the average increase in global temperature is 0.18°C per decade. In 2021 the western parts of the USA, southern South America, northern Africa and the Middle East were characterized by significantly below-average precipitation. A significant increase in annual precipitation during 2021 was observed in northern South America, eastern Europe, western and eastern parts of the Australian coast, and South Asia. Across Southern Europe, below-average rainfall was recorded in July. Dry conditions with high temperatures contributed to the spread of fires

in southern and southwestern Turkey, as well as in north-eastern Spain. In Spain, during July 2021, only 57% of the average amount of July precipitation fell. However, parts of western Europe faced torrential rainfall that caused flooding between July 13 and 15. Some locations received at least twice their normal monthly precipitation in only three days. According to preliminary reports, over 140 deaths are attributed to the floods.

Branković et al. (2013) determined for Croatia that the positive trends of the average annual temperature are caused by a statistically significant increasing trend in the summer months. The highest trend values were obtained for summer, followed by winter and spring. As the research conducted by Gocic & Trajkovic (2013) shows, there is a significant increase in temperatures in the northern, central and eastern parts of Serbia. A constant annual increase in maximum daily temperatures from 1974-2003 in Belgrade and Niš was observed by Milanovic et al. (2014). The results of the Pettit's test of average annual temperatures in the area of Sokobanja in the period 1946–2012 indicate that 1991 was a changing point in the temperature increase (Radivojević et al. 2015).

Luković et al. (2014) investigated the trend of precipitation in Serbia in the period 1961-2009. No significant trend of total annual precipitation has been detected for the whole territory of Serbia. Very slight tendencies toward drier conditions on a seasonal scale during winter and spring and wetter conditions during autumn. An increase in autumn amounts of precipitation over central parts of Serbia is a result of a significant increase in October precipitation. The results obtained by Malinovic-Milicevic et al. (2016) indicate a significant increasing trend in the amount and intensity of precipitation in Serbia during autumn. Bandyopadhyay & Perveen (2006) and Gajbhiye et al. (2015) point out that changes in the amount and frequency of precipitation, as a result of climate change, directly affect water flows, runoff, groundwater reserves and soil moisture. Determining the change in rainfall patterns is crucial for any kind of development program and planning that includes effective management of water resources, but also the food production sector.

The objectives of this study are to investigate the temperature and precipitation trends at annual and monthly level in Belgrade in the period 1961-2020 using the Mann-Kendall test. The Pettit's test was used to determine if there were changing point years of both parameters. The paper will also present a comparative analysis of the values of selected parameters in two climatological periods 1961-1990 and 1991-2020 and inter–annual variability of precipitation.

Study area

The study area is Belgrade, the capital of the Republic of Serbia (Figure 1). It covers an area of 360 km^2, while the wider city area covers 3 222 km^2. It is located in the Pannonian Plain, on the southern edge of the Pannonian Basin. It lies at the confluence of two large European rivers - the Sava and the Danube rivers, and partly belongs to the Balkan Peninsula, partly to Central Europe (Drazic et al., 2014).

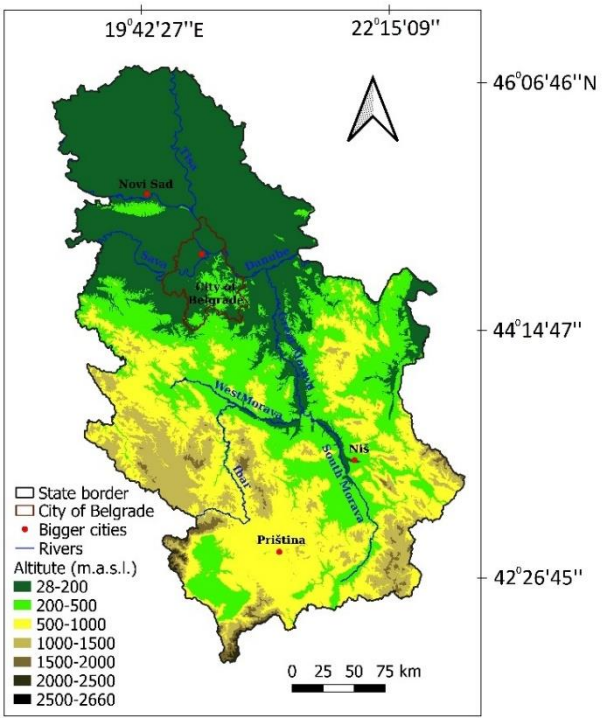

Figure 1: Geographic position of Belgrade in the Republic of Serbia

The study area map was obtained in geographic information systems, which play a major role in the analysis of phenomena and processes in the environment (Ćurić et al., 2022)

Belgrade is located in the zone of moderate continental climate (Meteologos, 2012). The climate of Belgrade is characterized by a great variability of the meteorological elements, which is caused by the circulation of air masses with different physical features. For the territory of the city, intrusions of polar and tropical air are characteristic. Relief has a significant influence on the microclimate of the capital of Serbia. It is characterized by the vast Pannonian plain in the north and the undulating surfaces of northern Šumadija and Avala Mountain (511 m) in the south. The Sava and the Danube rivers, at the confluence of which the city is located, are also significant factors.

Warm and cold periods often occur in all seasons. Cold and moist air are intruding from the northwest and west, and heavy precipitation is brought by the cyclones from the western Mediterranean Sea, which move eastward through the Sava and Danube valleys. Northern intrusions across the Pannonian plain cause a noticeable drop in temperature, while intrusions of cold air from the northeast, from the Carpathians, in winter, cause cold, windy and mostly dry weather. At the beginning of May,

the intrusions of moist and cold air appear. Local showers and thunderstorms are frequent in May and June. Shorter and longer dry periods are characteristic in summer (Unkašević, 1994). Dominant winds are košava, west and north-west winds (Meteoblue, n.d.).

Data and methods

The data come from the Republic Hydrometeological Service of Serbia (RHMSS) measured at the weather station Belgrade (Serbia). The coordinates of the meteorological station are 44°48'N and 20°28'E and it is located at an altitude of 132m (Hidmet, n.d.). The paper analyzed mean monthly and mean annual air temperatures, monthly and annual precipitation during two climatological periods - 1961-1990 and 1991-2020.

The Mann-Kendall test (Mann 1945, Kendall, 1975) was used for trend analysis. The test belongs to the group of non-parametric statistical trends that treats series that are not normally distributed, and its use is based on multi-year data series. Mann–Kendall is commonly used to detect monotonic trends in climatological and hydrological research. The Z statistic was used to test significance. A positive Z value indicates an increasing trend, while a negative Z value indicates a negative trend (Helsel & Hirsch, 2002; Westra et al., 2013; Pohlert, 2015). The null hypothesis of the Mann-Kendall test is based on the assumption that there is no monotonic trend in the time series. Control statistic is used to test the null hypothesis (Kendall, 1975).

The Mann-Kendall (S) Statistic is computed as follows (Kendall, 1962):

$$S = \sum_{i=1}^{n-1} k \sum_{j=i+1}^{n} sign(Tj - Ti),$$

where Ti and Tj are the values of sequence i, j; n is the length of the time series and:

$$Sign\ (Tj - Ti) = \begin{cases} 1\ if\ Tj - Ti > 0 \\ 0\ if\ Tj - Ti = 0 \\ -1\ if\ Tj - Ti < 0. \end{cases}$$

If the Z value (significance level) is greater than 1.96 (which corresponds to the significance threshold of 0.05), we conclude that there is a monotonic trend in the time series, and otherwise, if the value is lower, the trend does not exist (Stojković et al., 2014). Sen's estimate of the slope (Sens's estimate) shows us the estimate of the slope of the linear trend and the average value of changes in a unit of time (Salmi et. al., 2002; Ahmad et. al., 2015).

In order to detect significant changes in time series of climatological data, the Pettit's test was used. The Petit test also belongs to the group of non-parametric tests and is most often used to detect sudden changes (points of change) in climatological data. The Pettit test is a method that discover a significant change in the mean value of a time series when the exact time of the change is unknown. According to Pettitt's test, if x_1, x_2, x_3, …x_n is a series of observed data which has a change point at t in such a way that x_1, x_2 …, x_t has a distribution function F1(x) which is different from the distribution function F2(x) of the second part of the series x_{t+1}, x_{t+2}, x_{t+3} …, x_n. The non-parametric test statistics Ut for this test may be described as follows (Pettit, 1979):

$$Ut = \sum_{i=2}^{n} r \sum_{j=1}^{i-1} sign(Xi - Xj),$$

$$sign\ (Xi - Xj) = \begin{cases} 1\ if (Xi - Xj) \\ 0\ if\ (Xi - Xj) \\ -1\ if\ (Xi - Xj). \end{cases}$$

The test statistic counts the number of times that a member of the first sample exceeds a member of the second sample. The null hypothesis of Pettitt's test is the absence of a changing point. The test statistic (K) may be described as:

$$K = Max\ |Ut|$$

When the value of the test statistic is less than the chosen confidence interval, the null hypothesis is rejected and there is no distinct change point in the time series (Jaiswal et al., 2015).

The inter–annual variability of precipitation was obtained by subtracting the annual total of each year from the mean annual total over the study period and dividing the difference by the standard deviation of the series. Thus, obtaining a new series in which the mean equals to zero and the variance to 1. The obtained values enable the division of all years into three categories as follows (Kutiel et. al., 2015):

Dry (D) when $z < -0.5$
Normal (N) when $-0.5 \leq z \leq 0.5$
Wet (W) when $0.5 < z$

Results and Discussion

Temperature

The average annual air temperature in Belgrade in the period 1961–2020 is 12.5 °C. The warmest month is July with an average temperature of 22.8 °C, and the coldest is January with an average temperature of 1.1 °C (Table 1). The warmest year in the observed period was 2019 (14.8 °C), and the coldest year was 1980 (10.8 °C).

The mean annual air temperature in Belgrade shows an increasing trend of 0.042 °C/year with a significance level of 0.001. There is an increasing trend of mean monthly temperatures. Only in November the temperature increase is not statistically significant. There is a distinct trend of growth in the summer months (June, July, August) – 0.046 °C/year, 0.06 °C /year and 0.075 °C /year respectively (Table 2, Figure 2).

Table 1: Average annual and monthly temperatures in Belgrade (1961–2020)

Month	I	II	III	IV	V	VI	VII	VIII	IX	X	XI	XII	Annual
T_A (°C)	1.1	3.3	7.7	13.0	17.7	21.0	22.8	22.6	18.1	12.9	7.5	2.7	12.5

Source: Republic Hydrometeorological Service of Serbia, Climate Yearbooks 1961-2020

Table 2: Mann-Kendall test results for average annual and average monthly air temperatures in Belgrade (1961-2020)

Month	Trend (Z)	Sen's estimate (B)	Level of significance (α)
January	2.45	0.045	*
February	1.88	0.048	+
March	2.44	0.046	*
April	2.98	0.043	**
May	1.95	0.026	+
June	**3.68**	**0.046**	***
July	**5.20**	**0.060**	***
August	**4.95**	**0.075**	***
September	1.89	0.027	+
October	2.09	0.032	*
November	1.29	0.023	
December	2.67	0.041	**
Year	**6.07**	**0.042**	***

**** - significance level 0,001; **- significance level 0,01; *- significance level 0,05; +- significance level 0,1*

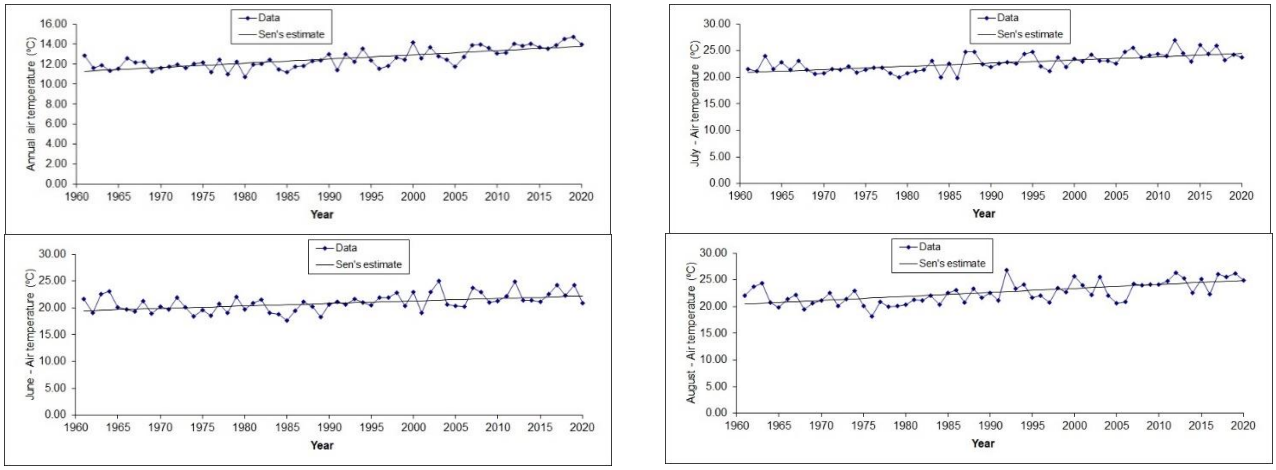

Figure 2: Trend of average annual air temperature and average temperatures of summer months in Belgrade (1961 - 2020)

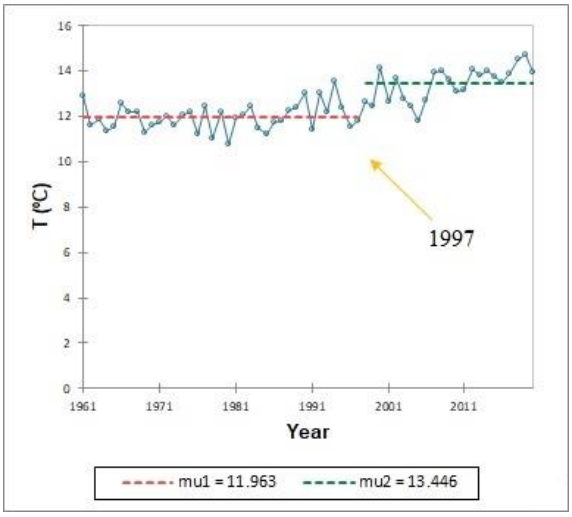

Figure 3: Pettit's test results for average annual temperatures in Belgrade (1961-2020)

The statistically significant changing point year according to the Pettit's test is 1997 (p=0.0001). The period after 1997 recorded an average annual air temperature of 13.4 °C compared to 11.9 °C in the period from 1961 to 1997 (Figure 3).

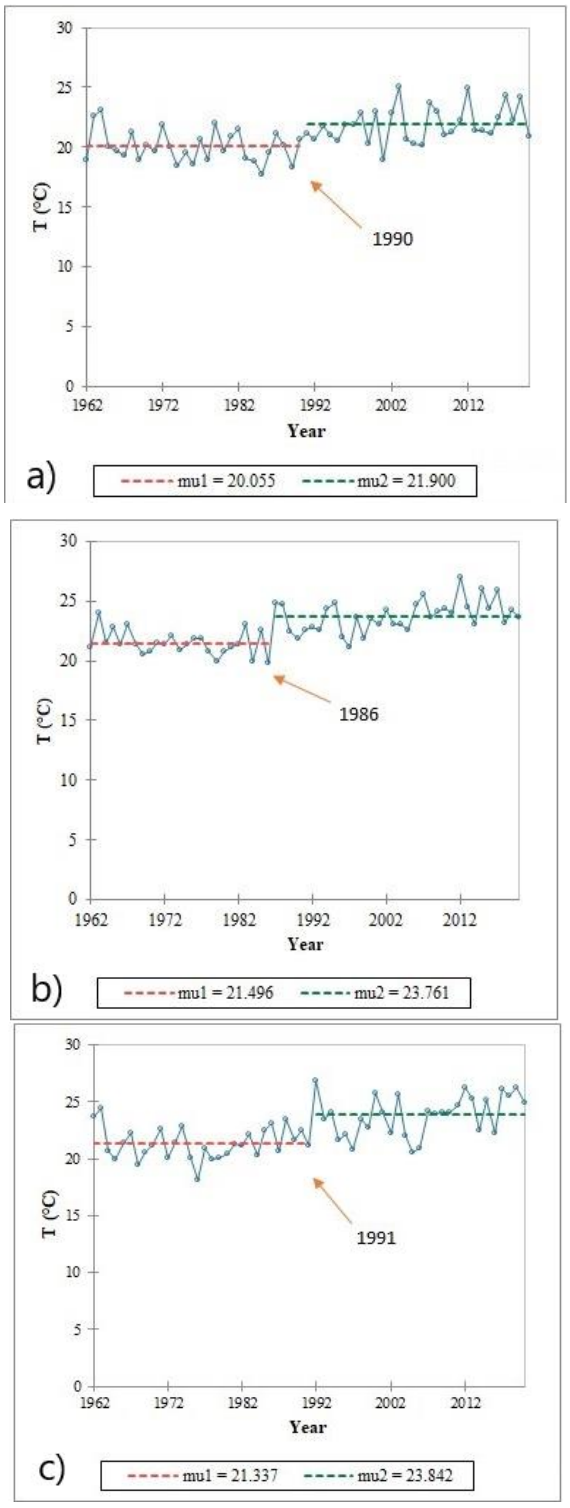

Figure 4: Pettit's test results for mean monthly air temperatures in June (a), July (b) and August (c) in Belgrade (1961-2020)

Since the statistically most significant increasing trends were recorded in the summer months, it was investigated whether there is a changing point for each of them. The average June temperature in the sixty-year period is 21.7 °C, and in 1990 there was a change (increase) in the average monthly temperature from 20.1 °C to 21.9 °C (p=0.0001). The average monthly temperature in July in Belgrade in the observed period is 21.5 °C. The statistically significant year in the average temperature change is 1986 (p p=0.0001). Until the mentioned year, the average temperature was 21.5 °C, so it corresponds to the sixty-year average. After 1986, the average July temperature in Belgrade rose to 23.8 °C. Since 1991 (p=0.0001), the average air temperature in August has increased by 2.5 °C; from 21.3 °C to 23.8 °C (Figure 4).

Table 3: Results of Pettit's test for average annual and monthly temperatures in Belgrade (1961-2020)

Parameters	Level of significance (p)	Changing point (year)	Change (°C)
Average annual temperature	0.0001	1997	+1.483
Average temperature in June	0.0001	1990	+1.845
Average temperature in July	0.0001	1986	+2.292
Average temperature in August	0.0001	1991	+2.505

The results indicate that the temperature in Belgrade is inevitably rising. An increasing trend without statistical significance was only observed in November, while in all other months the results showed a statical significant increasing trend. Pešić and Milovanović (2016) used the same methodology to determine temperature changes in the area of Šumadija (Serbia) in the period 1961-2010. They obtained a statistically significant increasing trend of annual temperature at almost all stations. The second highest mean annual temperature increase is in Belgrade (0,03°C/year), which is similar to obtained results in this paper (0,04°C/year). In Serbia, in the region of Vojvodina and Kosovo and Metohija positive air temperature trends were also obtained (Gavrilov et al., 2015; Gavrilov et al., 2016; Gavrilov et al., 2018). The average temperatures increasing trend indicates that the warming of the climate system is present in the entire territory of Bosnia and Herzegovina according to the results obtained by Trbić et al. (2017). The warming trend is more pronounced since 1990, the highest values in the period 1961–2015 were obtained in the warmest part of the year and in the area of Banja Luka and Bijeljina. In the region, temperature increase is also dominant in Montenegro (Burić et al., 2014).

Table 4: Average temperature (°C) in Belgrade during two climatic periods 1961-1990 and 1991-2020

Climatic periods	I	II	III	IV	V	VI	VII	VII	IX	X	XI	XII	Annual
1961-1990	0.4	2.8	7.2	12.4	17.2	20.1	21.8	21.4	17.7	12.5	7.0	2.3	11.9
1991-2020	1.9	3.8	8.3	13.6	18.2	21.9	23.8	23.8	18.5	13.3	8.1	3.0	13.2

Source: Republic Hydrometeorological Institute of Serbia, Meteorological yearbooks 1961–2020

Since the data of two climatological periods were used, the data on the average values of air temperature by period - from 1961 to 1990 and from 1991 to 2020 - are presented (Table 4). The average temperatures in Belgrade in the last period are higher during all months compared to the average temperatures in the period from 1961 to 1990. The biggest difference is in the summer months – August (2.4 °C), July (2 °C) and June (1.8 °C). In the same months, trend analysis showed the most significant increases in temperature. In the period from 1961-2010, according to research by Bajat et al. (2014), a significant increase in temperature in the summer period at 22 meteorological stations in Serbia was established

In July 2012, the highest average monthly temperature (27 °C) in the observed period was recorded. During 2012, which is characterized as extremely hot and dry year, temperatures in Serbia were above 35 °C for more than 50 days. Temperatures were extremely high in 2007, and precipitation were unevenly distributed (Živanović et al., 2020). The absolute maximum temperature of 43.6 °C in Belgrade was measured on July 24, 2007. On the same date, the highest temperature of 44.9 °C in the Republic of Serbia was measured in Smederevska Palanka (Anđelković, 2007). The largest number of fires (28,548) in the period from 2000 to 2010 occurred in 2007 (Živanović et al., 2020).

Precipitation

The average annual amount of precipitation in Belgrade in the period from 1961 to 2020 is 691.8 mm. On average, at monthly level, the highest amount of precipitation is in June 93 mm and May 71.5 mm, then in September 55 mm. The "driest" month is February with an average of 44 mm of precipitation (Table 5).

Table 5: Average amounts of precipitation in Belgrade (1961–2020)

Month	I	II	III	IV	V	VI	VII	VIII	IX	X	XI	XII	Annual
Average pre-cipitation (mm)	48.9	44.0	49.1	55.1	71.5	93.0	66.4	53.2	55.0	47.6	51.9	56.1	691.8

Source: Republic Hydrometeorological Service of Serbia, Meteorological yearbooks 1961–2020

Table 6. Mann-Kendall test results for annual and monthly precipitation in Belgrade (1961-2020)

Month	Trend (Z)	Sen's estimate (B)	Level of significance (α)
January	0.44	0.128	
February	0.59	0.155	
March	0.27	0.074	
April	-1.47	-0.243	
May	1.01	0.277	
June	0.85	0.386	
July	**-1.65**	**-0.416**	**+**
August	0.78	0.208	
September	-0.15	-0.026	
October	**2.67**	**0.592**	****
November	-1.39	-0.283	
December	-0.99	-0.283	
Year	0.24	0.345	

*** - level of significance 0,001; **- level of significance 0,01; *- level of significance 0,05; + - level of significance 0,1*

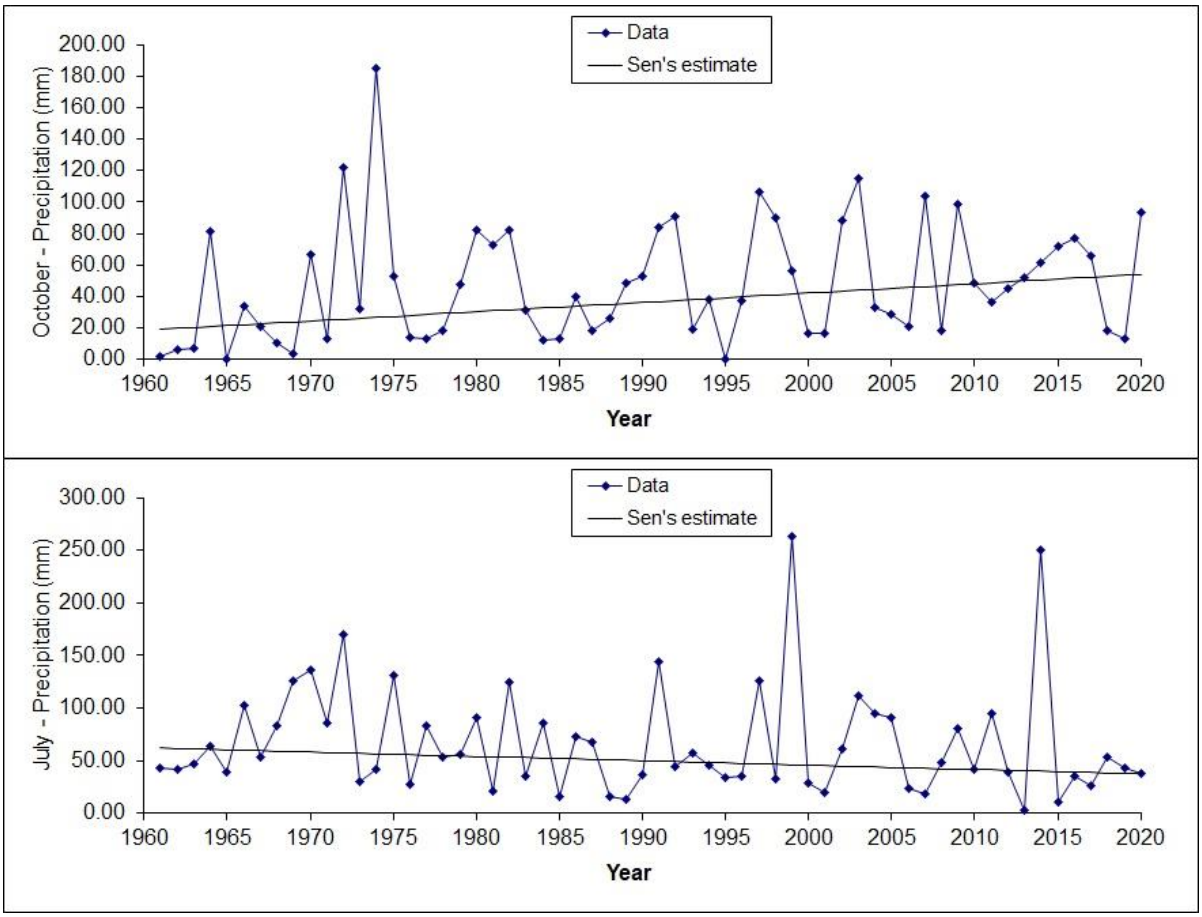

Figure 5: Precipitation trend in July and October with Sen's estimate in Belgrade 1961-2020

At the annual level, non-significant increasing trend was observed. In July, there is a decrease in the amount of precipitation (0.416 mm/year) with a significance level of 0.1. Decreasing precipitation trend is also present in April, September, November and December, but they are not statistically significant. The precipitation increase is observed in January, February, March, May, June, August but without statistically significance, while in October the increasing trend (0.592 mm/year) has a level of significance of 0.01 (Table 6, Figure 5). Changing point wasn't detected in the amount of precipitation.

No significant changes in the annual amount of precipitation were obtained in the work. Luković (2013) obtained the same results at the state level in the period 1961-2009, and Gocić and Trajković (2013) didn't found significant rainfall trend at most station in the period 1980-2010. In current paper, the most significant increasing trend was obtained in October (autumn), similar to research by and Gocić and Trajković (2013) and Tošić et. al. (2014) which obtained a significant precipitation increase during autumn and winter.

It is difficult to find similar rainfall results in the literature over a wider area. The area of south-eastern and central Europe recorded either decreases in precipitation from −20 to 0 mm/decade or an increase in precipitation from 0 to 20 mm/decade, whereby the boundary of change from the negative to the positive trend passes through Serbia to around 22° eastern longitude, but it is a generalized survey (EEA, 2017; Milentijević et al., 2020;). For most parts of Serbia, the mean annual precipitation trend for the period 1961 to 2010 falls in between −5 and +5 and +5 and +15 mm/decade (Milovanović et al., 2017). Popov and Svetozarevich (2021), analyzed annual rainfall trend on 15 weather station in Serbia The least increase in the period 1991-2019 has been observed at the stations of Belgrade, Novi Sad and Zrenjanin. The highest values are reported at Kopaonik station (84.5 mm/decade) and Crni Vrh station (70.1 mm/10 decade).

During the period 1961-2010, a slight positive trend in the annual precipitation was obtained in the eastern part of Croatia, while changes in the annual rainfall wasn't record in Hungary. (Klapwijk et al. 2013, Gajić - Čapka et al.,2015). During the period 1961-2013 some stations in western Romania recorded a statistically significant increase in the mean annual precipitation, on the other hand, the stations in the southwest of Romania recorded a statistically significant decrease in the mean annual precipitation (Croitoru et al. 2016).

The difference in monthly precipitation between the two climate periods (1961-1990 and 1991-2020) varies. A decrease in monthly precipitation is observed in the winter months (December, January and February) and in

March, April and November. The largest decrease in monthly precipitation between the two periods is in April – 7,3 mm (Table 7). The largest increase (14,5 mm) in monthly precipitation in the second thirty-year period is in October.

According to the explained methodology, in the period 1961-2020 20 dry years and 17 wet years were observed. The driest year was 2000, with z score -2.30 and total amount of precipitation of 367.7 mm. The wettest year was 2014, when 1095.1 mm of precipitation was recorded (z=2.86). Three consecutive D years are observed at the beginning of the period (1961–1963) and in the last decade of the period (2011–2013). During the entire period, no more than two consecutive W years were recorded (1969–1970, 1977–1978, 1980–1981, 2004–2005, 2009–2010). From 1964-1968 a long sequence of N years was recorded. From 1998-2020, only five N years were recorded (Figure 6).

Table 7: Average amount of precipitation (mm) in Belgrade during two climate periods 1961-1990 и 1991-2020

Climatic Periods	I	II	III	IV	V	VI	VII	VIII	IX	X	XI	XII	Annual
1961-1990	49.3	44.4	49.5	58.8	70.7	90.4	66.5	51.2	51.4	40.3	54.3	57.5	684.4
1991-2020	48.4	43.5	48.6	51.5	72.4	95.6	66.4	55.1	58.6	54.8	49.6	54.8	699.2

Source: Republic Hydrometeorogical Service f Serbia, Meteorogical yearbooks 1961–2020

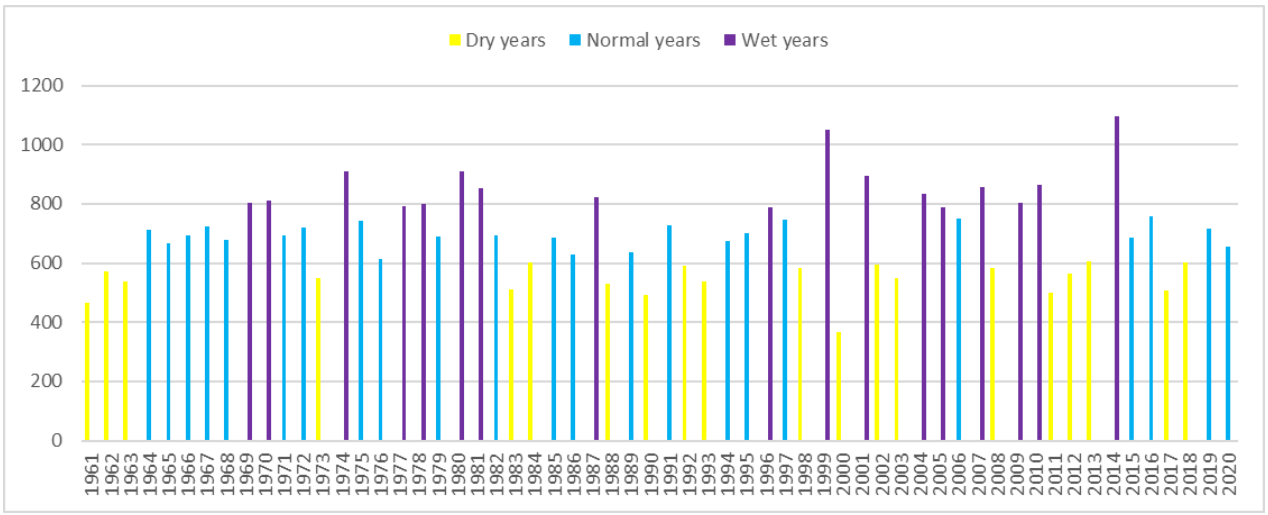

Figure 6: Annual amount of precipitation and classification of years in Belgrade 1961–2020

Conclusions

In this research, temperature and precipitation data in Belgrade in the period 1961-2020 were analyzed. Presented results were obtained using two non-parametric tests: Mann-Kendall test and Pettit's test. The Mann-Kendall test with Sen's estimate indicates the existence of statistically significant trends and shows numerical changes on an annual basis. Pettit's test was used to identify changing points in the observed time series.

The results indicate an unequivocal increase of average annual and monthly temperatures. The increasing trend is statistically significant on annual level (0.042°C/year) and during all months except November. By applying the Pettit's test, we came to the result that the changing point in the increase of the average annual temperature was 1997. The aforementioned trends can be explained by the effects of global warming, which have an impact on a regional and global scale.

The analyzed precipitation data for the same time series indicate that a trend without greater statistical significance is established. Statistically significant change at the annual level was not obtained. A statistically significant trends were detected in October (0.592 mm/year) and July (-0.416 mm/year). By monitoring the precipitation data in the research area, it was concluded that there is no significant changing point in the time series.

In order to reach a general conclusion about the change of climate elements, a comparative analysis of the data of two climate periods (1961–1990) and (1991–2020) was made. This indicates an increase in both temperature and precipitation amounts in the second thirty-year period (1991-2020). The analysis of the inter-annual precipitation variability has shown that in the last two decades the number of N years has decreased and the frequency of D and W years has increased, which points to a possible increase of extreme climate events.

This research provides an insight into the dynamics of the climate in recent decades. It can be a firm base for the

future study of climate changes in the area of Serbia, the Balkan Peninsula and Europe. Those research, firstly, must include the analysis of trends at the seasonal level, in order to accurately observe the time of year when the greatest trend decrease/increase occurs. In addition, a more complete analysis of the factors that influenced such a state of the climate should be done. Presented study should contribute a better understanding of recent climate change in Serbia. As recent studies have revealed (Tvardosz et.al., 2021), Europe continues to experience extremely cold winter months, which means that today's warming is a complex and spatially variable process (Hegerl et al., 2018; Krauskopf & Huth, 2020) that must be monitored on a continuous basis to assess its economic and social potential.

Funding

The study was supported by the Ministry of Education, Science and Technological Development of the Republic of Serbia (Contract number 451-03-68/2022-14/200091).

Conflicts of interest

The authors declare no conflict of interest.

Author contribution

Conceptualization, S.V. and M.D; methodology, U.D.; formal analysis, investigation and writing—original draft preparation, N.C; writing—review and editing, U.D., M.D, S.V. All authors have read and agreed to the published version of the manuscript.

References

Ahmad I., Tang Deshan F., Wang T., Wang M. & Wagan, B. (2015) Precipitation trends over time using Mann-Kendall and Spearman's rho tests in Swat River basin, Pakistan. *Advances in Meteorology*. doi:10.1155/2015/43186

Anđelković, G. (2007). Temperature conditions on July 2007 as extreme climatic phenomenon in Serbia.*Bulletin of the Serbian Geographical Society* 87 (2): 51-62. https://doi.org/10.2298/GSGD0702051A [In Serbian: Анђелковић, Г. (2007). Температурне прилике у јулу 2007. године као екстремна климатска појава у Србији. Гласник Српског географског друштва 87 (2): 51-62. https://doi.org/10.2298/GSGD0702051A]

Bajat, B., Blagojević, D., Kilibarda, M., Luković, J. & Tošić, I. (2014). Spatial analysis of the temperature trends in Serbia during the period 1961–2010. *Theor Appl Climatol* 121:289–301. DOI 10.1007/s00704-014-1243-7

Bandyopadhyay, J., & Perveen, S. (2006). A scrutiny of the justifications for the proposed interlinking of rivers in India. *Interlinking of rivers in India: Overview and Ken-Betwa link*, 23.

Branković, Č., Cindrić, K., Gajić-Čapka, M., Güttler, I., Pandžić, K., Patarčić, M., Srnec, L., Tomašević, I., Vučetić, V., & Zaninović, K. (2013). Sixth National Communication of the Republic of Croatia under the United Nation Framework Convention on the Climate Change (UNFCCC), Collection of papers,

Burić, D., Luković, J., Ducić, V., Dragojlović, J., & Doderović, M. (2014a). Recent trends in daily temperature extremes over southern Montenegro (1951-2010), *Natural Hazards Earth Systems. Sci.*, 14, pp. 67-72.

Croitoru A-E., Piticar A., & Burada, D-C. (2016) Changes in precipitation extremes in Romania. *Quaternary International* 415:325–335.doi.org/10.1016/j.quaint.2015.07.028 1040-61

Ćurić, V., Durlević, U., Ristić, N., Novković, I. & Čegar, N. (2022). GIS application in analisys of threat of forest fires and landslides in the Svrljiški Timok basin (Serbia). *Bulletin of the Serbian Geographical Society*, 102 (1), 107-130. https://doi.org/10.2298/GSGD2201107C

Drazic, M. D., Veselinovic, M. M., Rakonjac, B. Lj., Bojovic, R. S., Brasanac-Bosanac, B. Lj., Cule, M. N. & Mitrovic, Z. S. (2014). Geographic, landscape and the other natural characteristics of tourism. *European Journal of Geography Volume* 5 (3): 96 -122. ISSN 1792-1341

EEA report No 1 (2017) Climate change, impacts and vulnerability in Europe 2016. An indicator-based report. European Environmental Agency http://www.eea.europa.eu/publications/climate-changeimpacts-and-vulnerability-2016

Gajbhiye, S., Meshram, C., Singh, S. K., Srivastava, P. K. & Islam, T. (2015). Precipitation trend analysis of Sindh River basin, India, from 102-year record (1901–2002). *Atmospheric Science Letters* 17(1): 71–77. https://doi.org/10.1002/asl.602

Gajić-Čapka, M., Cindrić, K., &Pasarić, Z. (2014). Trends in precipitation indices in Croatia, 1961–2010. *Theoretical and Applied Climatology*, 117, 3-4, DOI 10.1007/s00704-014-1217-9

Gavrilov, M. B., Marković, S. B., Janc, N., Nikolić, M., Valjarević, A., Komac, B., Zorn, M., Punišić, M., & Bačević, N. (2018). Assessing average annual air temperature trends using the Mann-Kendall test in Kosovo. *Acta geographica Slovenica.* 58(1),pp. 8-25.

Gavrilov, M. B., Marković, S. B., Jarad, A., & Korać, V. M. (2015). The analysis of temperature trends in Vojvodina (Serbia) from 1949 to 2006. *Thermal Science* 19(2), pp. 339- 350.

Gavrilov, M. B., Tošić, I., Marković, S. B., Unkašević, M., & Petrović, P. (2016). The analysis of annual and seasonal temperature trends using the Mann-Kendall test in Vojvodina, Serbia. *Időjárás* 122(2), pp. 203-216.

Gocic, M., & Trajkovic, S. (2013). Analysis of changes in meteorological variables using Mann-Kendall and Sen's slope estimator statistical tests in Serbia. *Global and Planetary Change* 100: 172-182. https://doi.org/10.1016/j.gloplacha.2012.10.014

Hegerl G-C., Brönnimann S., Schurer A., & Cowan T. (2018). The early 20th century warming: Anomalies, causes, and consequences. *WIREs Clim Change* 9. https://doi.org/10.1002/wcc.522

Helsel, D. R., & Hirsch, R. M. (2002). Statistical methods in water resources. In *Book 4, Hydrologic analysis and interpretation, Chapter A3* (Techniques of water-resources investigations of the United States Geological Survey). https://doi.org/10.3133/tm4A3

Hidmed (n.d.). Retrived from https://www.hidmet.gov.rs/latin/meteorologija/stanica_moss1.php?moss_id=13274

IPCC, 2021: Summary for Policymakers. In: Climate Change 2021: The Physical Science Basis. Contribution of Working Group I to the Sixth Assessment Report of the Intergovernmental Panel on Climate Change [Masson-Delmotte, V., P. Zhai, A. Pirani, S.L. Connors, C. Péan, S. Berger, N. Caud, Y. Chen, L. Goldfarb, M.I. Gomis, M. Huang, K. Leitzell, E. Lonnoy, J.B.R. Matthews, T.K. Maycock, T. Waterfield, O. Yelekçi, R. Yu, and B. Zhou (eds.)]. Cambridge University Press, Cambridge, United Kingdom and New York, NY, USA, pp. 3−32, doi:10.1017/9781009157896.001.

Jaiswal, R.K., Lohani, A.K. & Tiwari, H.L. (2015). Statistical Analysis for Change Detection and Trend Assessment in Climatological Parameters. *Environ. Process*. 2, 729–749. https://doi.org/10.1007/s40710-015-0105-3

Kendall, M.G. (1962). *Rank Correlation Methods*. Hafner Publishing Company, New York.

Kendall, M.G. (1975). *Kendall Rank Correlation Methods*. Griffin: London, UK, 1-202.

Klapwijk, M., Csóka, G., Hirka, A., & Björkman, C. (2013). Forest insects and climate change: long-term trends in herbivore damage. *Ecol Evol* 3 (12):4183–4196. doi:10.1002/ece3.717

Krauskopf, T., & Huth, R. (2020). Temperature trends in Europe: Comparison of different data sources. *Theoretical and Applied Climatology*, 139, 1305–1316. https://doi.org/10.1007/s00704-019-03038-w

Kutiel, H., Luković, J. & Burić, D. (2015), Spatial and temporal variability of rain-spells characteristics in Serbia and Montenegro. *Int. J. Climatol*., 35: 1611-1624. https://doi.org/10.1002/joc.4080

Luković, B. J. (2013). Spatial pattern of climate change in Serbia in the instrumental period. Doctoral Dissertation. Belgrade: University of Belgrade, Faculty of Geography. [In Serbian: Луковић, Б. Ј. (2013). Увођење просторне димензије у проучавању колебања климе у Србији у инструменталном периоду. Докторска дисертација. Београд: Универзитет у Београду, Географски факултет, 1-204.]

Luković, J., Bajat, B., Blagojević, D. & Kilibarda, M. (2014) Spatial pattern of recent rainfall trends in Serbia (1961–2009). *Reg Environ Change* 14, 1789–1799. https://doi.org/10.1007/s10113-013-0459-x

Luterbacher, J., Werner, J.P., Smerdon, J.E., Fernandez-Donado, L., Gonzalez-Rouco, F.J., Barriopedro, D., Ljungqvist, F.C., Büntgen, U., Zorita, E. & Wagner, S. (2016) European summer temperatures since Roman times. *Environmental Research Letters*, 11, 1–12. DOI 10.1088/1748-9326/11/2/024001

Malinovic-Milicevic, S., Radovanovic, M. M., Stanojevic, G. & Milovanovic, B. (2016). Recent changes in Serbian climate extreme indices from 1961 to 2010. *Theoretical and Applied Climatology* 124: 1089-1098. https://doi.org/10.1007/s00704-015-1491-1

Mann, H. B. (1945). Nonparametric tests against trend. *Econometrica*, 13, 245-259.

Meteologos, (2012). Retrived from http://www.meteologos.rs/karakteristike-gradske-klime-beograda/

Meteoblue (n.d.) Simulirani istorijski podaci o klimi i vremenu za Beograd. Retrived from). https://www.meteoblue.com/sr/vreme/historyclimate/climatemodelled/beograd_%D0%A1%D1%80%D0%B1%D0%B8%D1%98%D0%B0_792680

Milanovic, M., Gocic, M. & Trajkovic, S. (2014). Analysis of Extreme Climatic Indices in the Area of Nis and Belgrade for the Period between 1974 and 2003. *Agriculture and Agricultural Science Procedia* 4: 408-415. https://doi.org/10.1016/j.aaspro.2015.03.046

Milentijevic, N., Bacevic, N., Ristic, D., Valjarevic, A., Pantelic, M. & Kicovic, D. (2020). Application of Mann-Kendal (MK) test in trend analysis of air temperature and precipitation: Case of Macva district (Serbia). *Publication in Natural Sciences* 10 (1): 37-43. https://doi.org/10.5937/univtho10-24774

NOAA National Centers for Environmental Information (2022), State of the Climate: Monthly Global Climate Report for Annual 2021. https://www.ncei.noaa.gov/access/monitoring/monthly-report/global/202113.

Pešič, A. M., & Milovanović, B. (2016). Thermic regime and air temperature trends in Sumadija region (Serbia). *Journal of the Geographical Institute Jovan Cvijic SASA* 66(1):19-34. DOI: 10.2298/IJGI1601019M

Pettitt, A.N. (1979). A Non-Parametric Approach to the Change-Point Problem. *Journal of the Royal Society: Series* C (Applied Statistics), 28, 126-135.

Pohlert, T. (2015). Trend: Non-Parametric Trend Tests and Change-Point Detection, R package version 0.0.1. DOI: 10.13140/RG.2.1.2633.4243

Popov, H., & Svetozarevich, J. (2021). Changes and contemporary trends in the annual amounts of precipitation in Serbia. *Journal of the Bulgarian*

Geographical Society, Volume 44 (2021) 73–79. DOI 10.3897/j77102

Radivojević, R. A., Martić Bursać, M. N., Gocić, J. M., Filipović, M. I., Pavlović, A. M., Radovanović, M. M., Stričević, S. Lj. & Punišić, R. M. (2015). Statistical analysis of temperature regime change on the example of Sokobanja basin in eastern Serbia. *Thermal science* 19 (2): 323-S330 https://doi.org/10.2298/TSCI150119019R

Republic Hydrometeorological Service of Serbia – RHMZ (2022). Meteorological yearbook - climatological data 1961-2020.

Salmi, T., Määttä, A., Anttila, P., Airola, T. & Amnell, T. (2002). Detecting trends of annual values of atmospheric pollutants by the Mann-Kendall test and Sen's slope estimates—the Excel template application MAKESENSE. *Helsinki: Finish Meteorological Institute*.

Stojković, M., Plavšić, J. & Proharska, S. (2014). Long-term changes of annual and seasonal flows: A case of the Sava River. *Vodoprivreda*, 46, 39-48. [In Serbian: Stojković, M., Plavšić, J. & Proharska, S. (2014). Dugoročne promene godišnjih i sezonskih proticaja: primer reke Save. *Vodoprivreda*, 46, 39-48.]

Tošić, I., Hrnjak, I., Gavrilov, M. B., Unkašević, M., Marković, S. B., & Lukić, T. (2014a). Annual and seasonal variability of precipitation in Vojvodina. *Theoretical and Applied Climatology*, 117,pp. 331-341. doi:10.1007/s00704-013- 1007-9

Trajkovic, S. & Kolakovic, S. (2009). Wind-adjusted Turc equation for estimating reference evapotranspiration at humid European locations. *Hydrology Research* 40 (1): 45–52. https://doi.org/10.2166/nh.2009.002b

Trbić, G., Popov, T. & Gnjato, S. (2017). Analysis of air temperature trends in Bosnia and Herzegovina. *Geographica Pannonica*. 21 (2): 68-84 DOI: 10.18421/GP21.02-01

Twardosz, R., Walanus, A. & Guzik, I. (2021). Warming in Europe: Recent Trends in Annual and Seasonal temperatures. *Pure Appl. Geophys*. 178, 4021–4032. https://doi.org/10.1007/s00024-021-02860-6

Unkašević, M. (1994). The climate of Belgrade. Belgrade: Naučna knjiga. [In Serbian: Unkašević, M. (1994). Klima Beograda. Beograd: Naučna knjiga.]

Vyshkvarkova, E., & Sukhonos, O. (2022). Compound Extremes of Air Temperature and Precipitation in Eastern Europe. *Climate*, 10, 133. https://doi.org/10.3390/cli10090133

Westra, S., Alexander, L.V., & Zwiers, F.W. (2013). Global increasing trends in annual maximum daily precipitation. *J. Clim.*, 26 (11), 3904–3918. DOI: https://doi.org/10.1175/JCLI-D-12-00502.1

Živanović, S., Ivanović, R., Nikolić, M., Đokić, M. & Tošić, I. (2020). Influence of air temperature and precipitation on the risk of forest fires in Serbia. *Meteorology and Atmospheric Physics* 132:869–883. https://doi.org/10.1007/s00703-020-00725-6

http://www.meteologos.rs

https://climateknowledgeportal.worldbank.org

https://www.meteoblue.com

Forum geografic. Studii și cercetări de geografie și protecția mediului
Volume **XXII**, Issue **1** (**June 2023**), pp. **16-27;** DOI: **10.5775/fg.2023.066.i**

The changing river course and its impact on riverine society: A case study on the Padma River, Murshidabad District, West Bengal (India)

Dr. Sanatan GHOSH[1*]

[1] Associate Professor, Department of Geography, Krishnath College & Coordinator (Ad hoc) Department of Geography, Murshidabad University, Berhampore, Murshidabad, West Bengal, India.
* *Corresponding author*: sghosh2871972@gmail.com

Received on 20-01-2023, reviewed on 22-02-2023, accepted on 20-03-2023

Abstract

River bank erosion within Murshidabad district is a tragedy, which happens haphazardly along the bank of the Padma River system. The main objective of the study is to analyze the changing river course and its impact on society. By comparing the toposheet and Landsat (5 and 8) images of the Padma River of the Murshidabad district from the years 1924, 1990, and 2020, it is clearly observed that there have been significant changes on the southern portion of the river since 1924 (Bhagawangola II, Raninagar II, and Jalangi Block), while less changes occur on the central part of the river, which is near the Lalgola block. But in the year 2020 significant changes have been found in the northern and middle portion of the district near Samserganj and Lalgola block. Those parts belong to a highly vulnerable zone of bank erosion. This study analyzed some factors, such as soil stratification of the river bank and human encroachment as an obstruction to the natural river flow, also responsible for bank failure. The river has been consuming the vast portions of the right bank every year due to its increasing sinuosity. The victims are mostly in the Samserganj, Lalgola, Bhagawangola II, Raninagar II and Jalangi blocks, who suffered greatly from 1924 to 2020 due to moving of river course by 27% on the right side, which is notified from cross sectional analysis. Additionally, the predicted erosional impact of the region highlights the socio-economic perspective of the research area.
Keywords: *dynamic river course, cross section, lateral erosion, Landsat, Padma River, socio-economic perspective*

Introduction

Murshidabad district is situated in the moribund deltaic region of the lower Ganga plain in India. The deltaic rivers have the tendency to oscillate within a wide limit. The alteration of river channels is almost a universal occurrence. Murshidabad district's people have probably been affected by the river for a long time. Murshidabad was the capital and important Business centre of Bengal, Bihar and Orissa in the British period. Murshidabad has lost its earlier glory due to historical and geographical reasons. Another historic town that perished naturally was Karnasubarna. The probable cause may be the severe erosion of the Bhagirathi River or the lack of a sufficient water supply when the main flow of the Ganga was diverted through Padma. Researchers have been studying the geomorphological phenomenon of river bank erosion and channel shifting for the past few years (Mukhopadhyay & Das Gupta 2010; Parua, 2006, 2009, 2010; Rudra, 2005, 2010; Ghosh 2015; Islam et al., 2019; Rahman, 2010; Raman et al., 1986). The changing river courses also led to river bank erosion, devastating floods, extensive silt deposition along river beds, meandering cut-off which are the serious threat to human habitation as well as environment. The river system is made up of mainly the Ganges, the Padma, the Bhagirathi, Jalangi, and Bhairab. These river systems are constantly altering their paths, and deltaic rivers do so in a wide range. The river systems of the district are generally meandering and braided in nature. Rivers help the systems in dynamic equilibrium. When river channels are altered due to naturally dynamic hydrologic conditions, the river readjusts itself in terms of size, profile, and pattern to re-establish its previous balance or equilibrium (Couture, 2008). The free-flowing river is always adjusting the equilibrium condition through erosion, transportation, and deposition processes. When the deposition process is underway on one side, the erosion process is underway on the other bank side. Mid channel bar or char formation is restricted to mid channel flow pattern and flow concentrated to bank side, as result of severe bank erosion. The erosion and deposition of a meandering river are continuously characterized by the processes of emergence, submergence, and re-emergence. This phenomenon has been explained as follows: "accumulated silt leads to the rise of a sand-bed in the interfluves (the region of higher land between channels); being obstructed by this bed of the river then divides into two channels with the sand-bed in between. This makes the flow oblique. The flow gets obstructed with the river-bank eventually causing river bank erosion. The eroded silt and sediment are carried by the river which again

accumulates to form a new sand-bed and cycle continues" (Mukherjee, 2011).

One of the few morphological systems, meandering streams, provide a rich historical record of changes in channel design and related erosion and deposition of flood plains (Panda & Bandyopadhyay, 2010). The changes of river courses have been contributing to many international problems such as boundary dispute, land reallocation problems, identity problems for the people of charland etc. in the border areas between Bangladesh and Murshidabad (India). Smuggling is also another social problem in the border area. Many people are displaced from their homeland, lost their agricultural land and property etc. A description of the uses of space-based remote sensing data for river research was presented by various researchers. This study has emphasized the most recent applications of satellite remote sensing data to studies of river systems. All sorts of these data are presently available. Malda and Murshidabad, two districts in West Bengal, are the worst affected and experiencing a long-term natural disaster as a result of the Padma river's altered route and ensuing river bank failure. The present study is significant in the context of an alarming situation in the district due to changing of river courses which is aggravated due to human interferences. Many people lost their homeland, agricultural land, domestic animals and even their lives. In such alarming situations people are shifted to other places as environmental neo-refugees without permanent houses and proper sanitation and drinking water. People are forced to migrate to other states for work or are engaged in illegal activities. Both Central and State Governments spend huge amounts of money to tackle these problems. So, this study is significant both internationally and nationally.

Objectives

The main objectives of this study are:

i. To analyze the changes of river course from early 1920 to present time.

ii. To identify and analyze the impact of changing river courses on socio-economic and environmental conditions on the riverine people.

iii. To identify the predicted erosion impact areas.

iv. Planning and mapping to give suggestions and remedy measures to tackle these problems.

Data and Methodology

Data and information are collected from primary and secondary sources. The major sources of primary data include observation, questionnaire survey and interviews of the selected displaced households settled in new areas. The secondary sources of information are satellite images, old records, published reports and articles (Table1).

The following methodology is taken for study work:

• Changes of river channels in early times have been documented from reports, documents when map is not available.

• Extensive field investigation was undertaken to places of river bank erosion areas with the help of Garmin GPS survey.

• Lateral dynamics of the river channel was established and mapped from earlier maps which are available such as SOI Topographical Map (1924), other thematic maps and LANDSAT Satellite Imagery1990 and 2020, with help of ArcGIS software.

• The questionnaire survey and interview method has been done in the displaced household settled in new areas in the district such as – Muradpur (Jalangi), Hasanpur, Mithipur (Raghunathganj -II), Hasanpur and Nirmalchar (Bhagawangola II), Maya and Khandua (Lalgola), Bamnabad (Raninagar II) and Dhusaripara and Dhuliyan (Samerganj). 600 household samples were collected using the stratified random sampling approach. Basically, they belong to a low economic group and a minority (Muslim) community.

Table1: Data source of this Study

DATA TYPE		SOURCE	SCALE
SPATIAL DATA	GEOMORPHOLOGY	National Remote Sensing Centre, Hyderabad	1:50,000
	SOIL	FAO & UNESCO 1972	1:5000
	RAINFALL	Center for Hydrometeorology and Remote Sensing	4km x 4km
	SLOPE	CARTO DEM	PAN(2.5m) Stereo Data
	TOPOSHEET	US ARMY TOPOSHEET NG 45 -15 & NG 45 -16	1:250000
	LANDSAT 5	PATH 138 ROW 43 & DATE 05.06.1990	30m
		PATH 139 ROW 43 & DATE 01.06.1990	30m
	LANDSAT 8	PATH 138 ROW 43 & DATE 04.06.2020	30m
		PATH 139 ROW 43 & DATE 28.05.2020	30m
NON SPATIAL DATA		Primary field survey data	

Study area

The research samples were drawn from the affected villages in the Jangipur, Lalbagh, and Domkal sub-divisions of the Murshidabad district of West Bengal (Figure 1). The Padma and its tributaries are the primary rivers of the research area. The research area is located quite near the Bangladesh-India border region. Nine cadastral units along with the banks of the Padma River which are prone to erosion were chosen as study units to satisfy the needs of the study.

Figure 1: Location of the study area

The study units are – Dhulian, Dhusaripara, Bamnabad, Nirmal char, Khandua, Maya, Mithipur, Hasanpur and Muradpur. According to the district statistics handbook for Murshidabad published in 2011, the district was split into two essentially equal-sized geographic sections by the river Bhagirathi. But there is a geological distinction between them. The Western part of the Bhagirathi River is known as the Rarh region. It is a sequence of lateritic clay from the Sub-Vindhyan period characterized by nodular ghuting. Bagri area is located along the eastern portion of the Bhagirathi River and it is made of Gangetic alluvial sediments of the Quaternary period. The slope of the entire research area ranges from 0 to 15 degrees. Monsoonal climates have been found in the area and a huge amount of rainfall (approx. 1500 mm) occurs due to the south west monsoon. The bulk of the population is employed in agricultural sectors, while just a tiny fraction is involved in industrial activities, according to the district statistics handbook, Murshidabad (2011).

Results and discussion

Lateral dynamics of Padma River course

Most of the dams in India are constructed due to irrigation and generation of hydroelectric power, but the construction of Farakka Barrage served different purposes. The Farakka Barrage (2.64 km long) was designed to divert 40,000 cubic feet per second (1133 cubic metre per second) of the Ganga water towards the Bhagirathi river through a feeder canal (38 km long) to save the Kolkata port. The interface of the Ganga regime by construction of Farakka Barrage gives many hydrological and morphological changes of water level, discharge, sediment movement, bed slope characteristics etc. (Ghosh, 2015). Such changes of river course have been analyzed within two temporal windows from 1924 to 1990 and 1990 to 2020 (Figure 2).

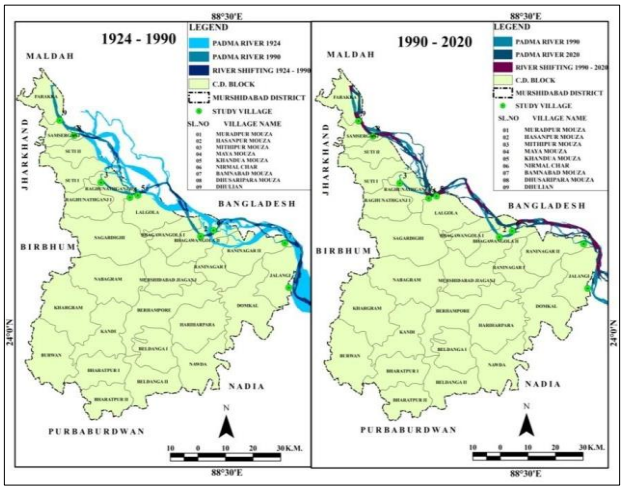

Figure 2: Lateral dynamics of the Padma River (1924 to 2020)

Table 2: Changing point of Padma River

SL.	LATITUDINAL &	VILLAGE	COMMUNITY	SHIFTING OF RIVER WITHIN STUDY PERIOD

NO.	LONGITUDINAL VALUE	NAME	DEVELOPMENT BLOCK (C.D. BLOCK)	1924 - 1990 (k.m.)	REAMRKS	1990 - 2020 (k.m.)	REMARKS
1	88°42′00′′ E, 24°08′24′′ N	MURADPUR	JALANGI	3.41	**Right side**	6.31	**Left side**
2	88°24′36′′ E, 24°18′36′′ N	HASANPUR	BHAGAWANGOLA II	5.11	**Right side**	3.87	**Left side**
3	88°04′48′′ E, 24°28′48′′ N	MITHIPUR	RAGHUNATHGANJ II	3.67	**Right side**	5.21	**Leftside**
4	88°10′48′′ E, 24°25′48′′ N	MAYA	LALGOLA	2.3	**Right side**	1.5	**Right side**
5	88°12′00′′ E, 24°26′24′′ N	KHANDUA	LALGOLA	1.8	**Right side**	1.05	**Right side**
6	88°27′18′′ E, 24°19′48′′ N	NIRMALCHAR	BHAGAWANGOLA II	1.3	**Left side**	1.41	**Left side**
7	88°41′06′′ E, 24°17′06′′ N	BAMNABAD	RANINAGAR II	1.85	**Right side**	2.11	**Left side**
8	88°00′00′′ E, 24°37′48′′ N	DHUSARIPARA	SAMSERGANJ	1.6	**Right side**	1.71	**Rightside**
9	88°57′00′′ E, 24°40′48′′ N	DHULIAN	SAMSERGANJ	2.24	**Right side**	1.46	**Right side**

The Ganges River split into two major streams once it reached the northern part of Murshidabad district near Dhulian before the construction of Farakka Barrage. Following the construction of Farakka Barrage and feeder canal (dedicated to Nation 1975), only a small amount of water flows from the Bhagirathi River through a very small channel and reaches the Padma River at Mithipur, although natural flow of the Bhagirathi was started after crossing the Jangipur Barrage. The northern and eastern boundaries of the Murshidabad district are defined by the Padma branch of the river Ganga, which flows towards the south-east. On the other hand, the Bhagirathi River branch flows southwards. This section of the Padma River discharges a large amount of water. The main channel is constantly shifting except the high bank. As a result, shoal or island or charland is continually rising in the channel. The people of the islands such as Nirmalchar of Bhagawangola -II block and Bamnabad char of Raninagar –II block live in temporary huts due to the annual bank flooding. Within this study area, nine different locations have been identified where the Padma River has shifted its course in different directions, on a distance exceeding one kilometer (Table 2 and Fig. 3).

Lateral dynamics of the Padma River from 1924 to 1990

From Table 2, Figure 2 and Figure 3 it is observed that the Padma River has been shifted on a maximum distance of 3 to 5.11 km towards the right side, near Bhagawangola-II, Raghunathganj-II and Jalangi block, while the minimum distance can be found near Lalgola, Raninagar, and Samserganj block, while the river shifted towards east direction or left-hand direction about 1.3 km near Nirmal char of Bhagawangola II block. During this time period, significant river bank erosion has been registered in Bhagawangola II and Jalangi blocks.

Lateral dynamics of Padma River from 1990 to 2020

The Padma has been shifted on a maximum distance from 3 to 7 km towards its left side near Bhagwangola-II, Raghunathganj-II and Jalangi block; the minimum distance where it shifted was registered near Raninagar II block, while the river shifted towards west direction or right hand about 2 km near Samserganj (Dhulian & Dhusaripara) and Lalgola (Maya & Khandua) block. During this time period, Samserganj and Lalgola blocks have seen significant river bank erosion due to right side sifting of river courses. Figure 4 basically shows the vulnerable river bank erosion zone after the average weight analysis of data. The vulnerable river bank erosion zone along the Padma River bank are Zone I, which consists of Farakka, Samserganj and Suti-II block, Zone-II consists of border area of Raghunathganj and Lalgola block, Zone-III consists of Bhagawangola –I and Bhagawangola-II block, Zone-IV consists of small area of Raninagar-II and Jalangi block. Currently, Samserganj and Lalgola blocks are the most vulnerable river bank erosion zone.

It has been observed that average changes of the Padma River course from 1924 to 1990 is 76.580 metre/year and after the construction of Farakka Barrage, the river bank erosion is 79.2187 metre/year from 1990 to 2020. River bank erosion has increased since the Farakka barrage was constructed. Figure 5 & 6 basically show cross-sections of the minor bed-major bed along the Padma in 1990 and 2020 which identified the thalweg shifting of the river. At the block level, the average changes in river course are greatest (98.75 metre/year) in the Jalangi block following the construction of the barrage, while river bank erosion is 57.24 metre/year, which is less than the previous phase. Overall, the highest river course change after the completion of the dam took place at Suti II block, 67.5 metre/year (1990 to current years), although river course

change before dam construction was 38.44 metre/year. Besides, it is also observed that river course changes have gradually decreased after the construction of dam at Bhagawangola II, Bhagawangola I and Raninagar I block.

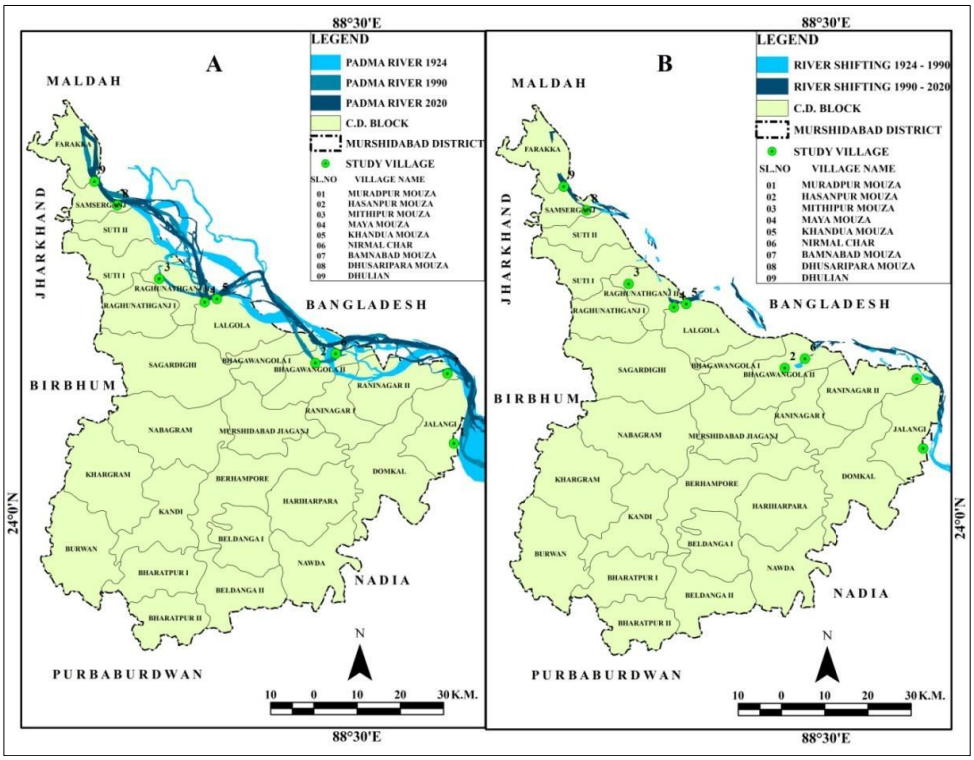

Figure 3: Major shifting points of the Padma River (1924 to 2020)

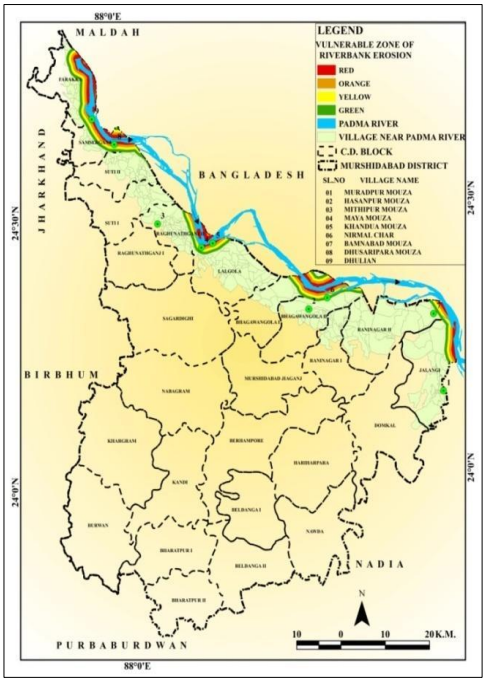

Figure 4: Vulnerable zone to erosion along the Padma River, 2020

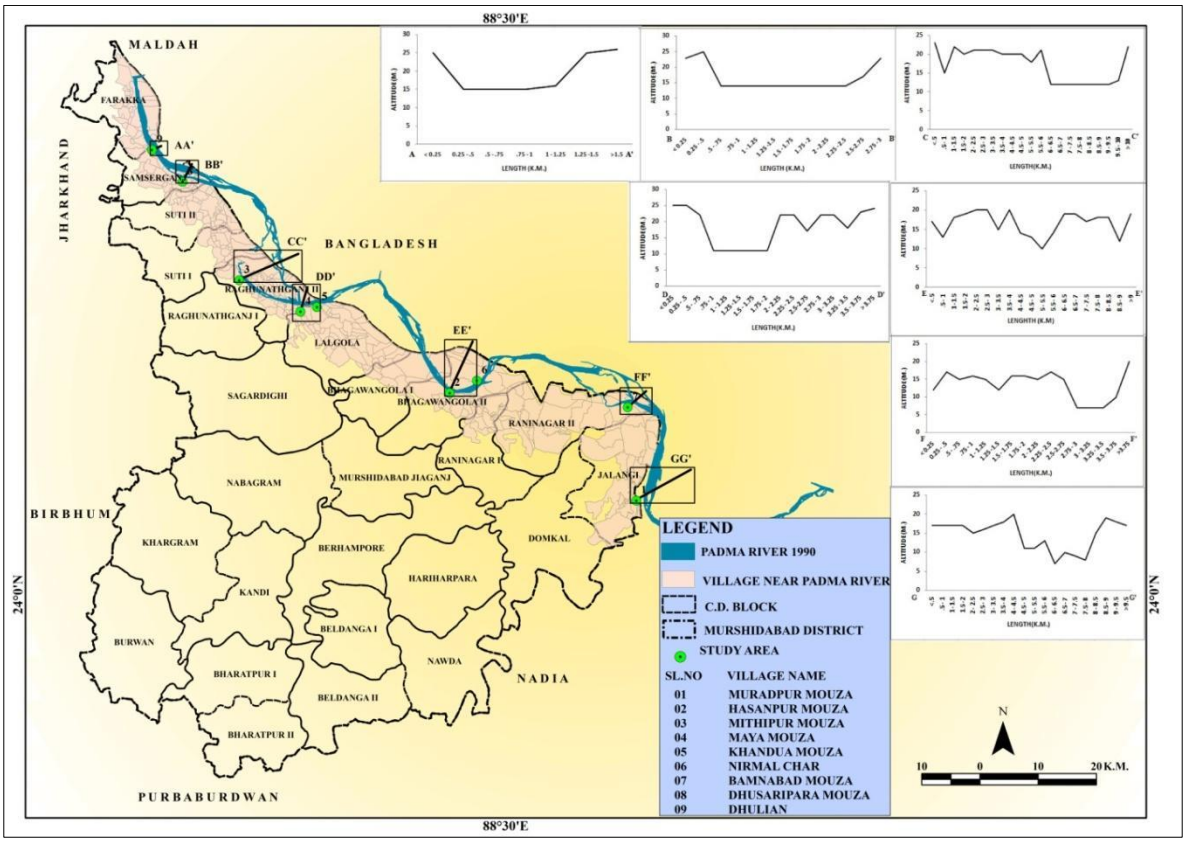

Figure 5: Analysis of cross-sections of the minor bed-major bed along the Padma River, 1990

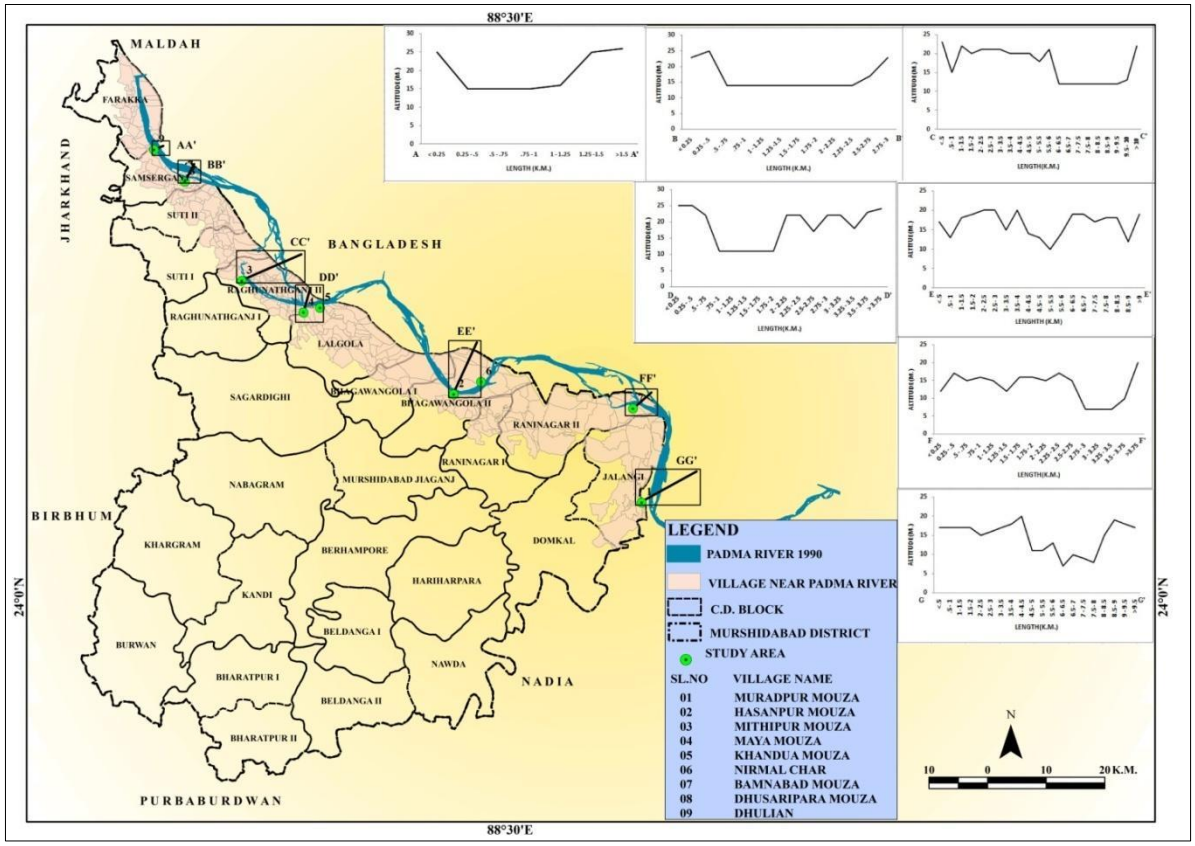

Figure 6: Analysis of cross-sections of the minor bed-major bed along the Padma River, 2020

Trigger factors of lateral erosion

i. The river channel in moribund deltaic region varies from braided to meander with limited straight channel. Within the meandering reach, the river course is sinuous and deep banks.

ii. Stratigraphy of a bank composed of micaceous unconsolidated sand at bottom and thin silt clay at top causes severe bank erosion (Figure 7).

iii. Fluctuation of river water discharge of the Ganga (from 1,100 a cubic metre per second to 76,000 a cubic metre per second) as well as fluctuation of water level (10 to 12 metres) causes alternately drying and wetting of the river bed. As a result, bank materials are dislodged and bank erosion accelerated.

iv. Seepage of groundwater towards the river leads to liquefaction and flowage of basal development of cracks ultimately accelerated bank erosion in early post monsoon period.

v. Sediment load of the river water also plays an important role in bank erosion. Fine sediment in river water will increase the viscosity of flow, increase the force, decrease the bed irregularities and bed form roughness and thus enhance the instability of river bank resulting in bank erosion.

vi. Current and wave action are also important factors in bank erosion. River current is turbulent in nature and acts along the bank obliquely and undercut the lower portion of the river bank. As a result, unconsolidated bank materials of the upper part have collapsed. If the velocity, discharge and depth of river water will increase, the current and wave action are more concentrated along the river bank. That is why river bank erosion is more in the rainy season.

vii. Anthropogenic activities along the bank side such as digging of the land for preparation of brick, furrowing of land for cultivation, construction for habitation etc. also accelerate the process of river bank erosion. Brick fields are concentrated in different parts of Murshidabad district along the bank side of the Padma and Bhagirathi River. Digging of land on the river bank also causes bank erosion at Dhulian and Maya and other places by land mafia. Apart from the 2.64 km. the long Farakka Dam which was built across the river during 1962-1971, bank revetment with boulders, construction of the spurs to deflect the impinging current, the flood control embankment, excessive withdrawal of groundwater are all combined causes for river bank failure.

Figure 7: Trigger factors of lateral erosion - ***A. Unconsolidated Sand at bottom and thin silt clay soil at top at Maya, Lalgola; B. Human interference (Brick field) along the river bank at Maya; C. River bank characteristics near Dhulian; D. Construction of Bank Protection Wall at Dhulian; E. Illegal digging along the river bank at Maya***

Socio-economic impact of the river bank erosion

A serious environmental risk caused by river bank erosion also contributes to social and economic inequality. Loss of nutrients of soil required for plant development, harm to downstream ecosystems by erosion-generated sediments, and reduction of water storage capacity are the three main impacts of erosion. Flood plains are heavily populated since they are fertile and easily accessible and riverine locations have always attracted human settlements. Each and every year the

Padma riverine societies are highly affected by river bank erosion during the post monsoonal phase. In the eastern portion of the Murshidabad district, nine severely affected human settlement areas have been chosen in order to better understand the extent and degree of river bank erosion as well as the nature of people's adjustment with the erosion. Out of these selected areas, two blocks, namely Samserganj block (Dhusaripara and Dhulian) and Lalgola block (Khandua and Maya) were severely affected from 1990 to present and rest of the villages (Muradpur, Hasanpur, Mithipur, Nirmal char and Bamnabad) were affected from 1924 to 1990.

Occupational structure

The physical environment provides natural resources, while human activities create the economic environment. The occupational structure of inhabitants is greatly affected by riverbank erosion. The main or marginal farmers work as day labourers but now their lifestyle and social status have been changed.

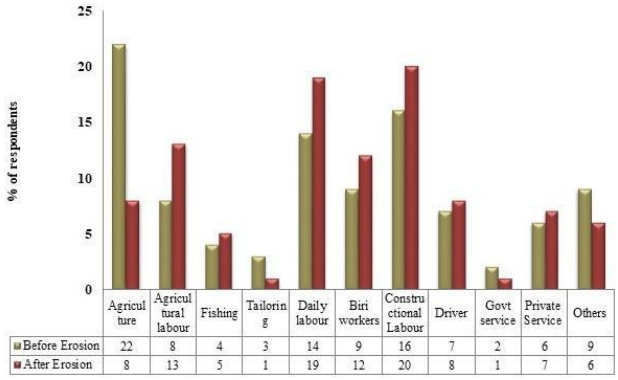

	Agriculture	Agricultural labour	Fishing	Tailoring	Daily labour	Biri workers	Constructional Labour	Driver	Govt service	Private Service	Others
Before Erosion	22	8	4	3	14	9	16	7	2	6	9
After Erosion	8	13	5	1	19	12	20	8	1	7	6

Figure 8: Occupational status of population, before and after bank erosion

From Figure 8, it is clear that 22% of respondents are engaged in agricultural activities and 14% -16% of respondents are working as daily labourers and constructional laborers. But after the river bank erosion this occupational scenario has dramatically changed. Within a very short time due to the loss of 48% of the agricultural land, people shifted their jobs from agriculture to daily labourers, construction labourers or e - rickshaw drivers. They are also forced to migrate to other states as construction labourers and other countries, mainly Saudi Arabia and Dubai as workers.

Educational status

A man can become qualified to serve his country and live a happy life by getting education. Most often, an illiterate guy is engaged in basic economic pursuits with no understanding of how to enhance or change such pursuits. The majority of them do not know what to do or how to deal with loss when a tragedy occurs. It is clear from the data that about 49% of the respondents spend Rs. 600 on schooling. Among the respondents, just 21% spend more than Rs.1000 for education. After river bank erosion there is a significant change in literacy rate. As a result, many students are not attending school. Children and young people must find employment in order to survive. It is observed from primary data, that the percentage of illiteracy has climbed from 30% to 43% and other educational levels (primary, upper primary, secondary, higher secondary and so on) show a very badly affected educational system within the study area. Education is the best option for raising income levels and improving living conditions, thus individuals should focus more on this area. Figure 9 clearly shows that 36% of family members of respondents have only primary education, 27% secondary education and the rest of 19%, 11% and 7% family members of respondents are engaged in higher education. But after river bank erosion this educational scenario has been changed due to loss of their land, destruction of school buildings and occupational changes. Currently, 90% of total members of respondents are engaged in primary education with the help of ICDS and NGOs, but there is no one with higher education.

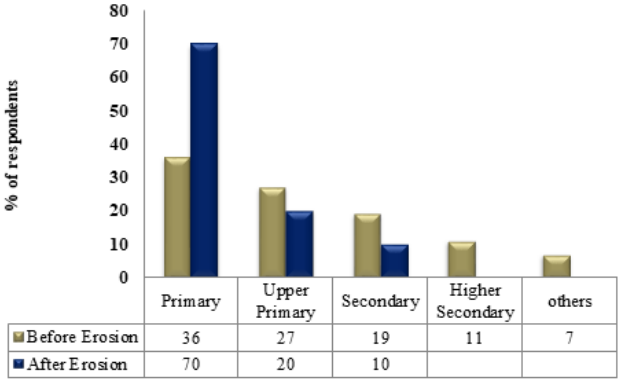

	Primary	Upper Primary	Secondary	Higher Secondary	others
Before Erosion	36	27	19	11	7
After Erosion	70	20	10		

Figure 9: Educational status of before and after bank erosion

Housing conditions

Housing conditions are another indicator of social status. The vulnerability to river bank erosion affects the strength of the house structure. Residents in the study region are aware that they may have to leave their home at any time. Therefore, they build their houses by using materials which can quickly be moved during calamities. According to our study, 82% of the homes are *kacha houses* (a type of houses which is made of bamboo, mud, grass, leaves etc.), while 16% houses are *semi- pucca* (a house that has fixed walls but roofs are generally made of hay) and the rest 2% are pucca (a pucca house is one which has walls and roofs are made of burnt brick and stones. Losing homesteads makes the population more vulnerable to leading a good life, which is the serious consequence of bank erosion. People have little choice but to stay behind when erosion occurs and deal with the consequences. Prior to the onset of erosion, they never

moved their homestead. The primary cause of this behavior is because their meager income prevents them from replacing their dwellings before they completely collapse.

Neo refuges

Many people have been displaced from their household due to river bank erosion and make them environmental neo-refugees. River bank erosion causes continuous forced migration in the following manner (Figure 10):

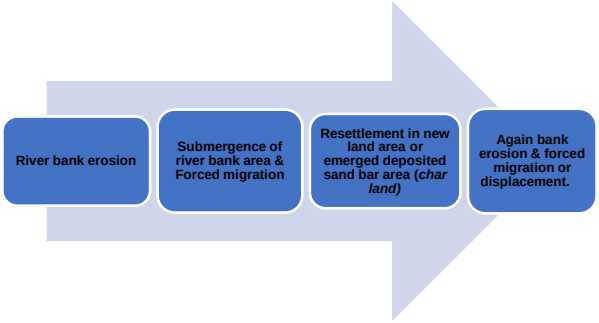

Figure 10: Migration Process due to river bank erosion

Data of socio-economic conditions of the displaced people are collected through household surveys. The results are explained below: about 40 to 50% of the displaced people are illiterate. The illiteracy rate also increases to *charland*. About 60% people are illiterate at Mahishmara Char (Nirmal char). The literate people are mostly below Madhyamik pass such as Tekpara village (Hasanpur Mouza) about 46%, Muradpur mouza (Totally) about 33%. Due to lack of educational institutions and economic distress, education is the least priority among these displaced people. It has been observed in these areas that many children and even teenagers have never been to school and are illiterate. Medical facilities in the neo-refugees' areas are very poor. Most of the areas even have no primary health centre. Most of the children suffer from malnutrition, and there are several reports of children dying due to malnutrition. Immunizations programmed for children are not properly done in many resettled areas. Sometimes deaths of pregnant women were reported because of their delayed arrival at hospitals. Socio-economic study of erosion affected displaced people has been done in the different places in Murshidabad district. Those that are displaced typically relocate locally, but there are some who migrate to far-off places. The maximum number of displacements was four times among the sample respondents. More than a third (37%) of the population within the study area has relocated at least once. Approximately 12% of respondents said they had been affected five to six times. Due to the erosion, it is utterly difficult for them to support themselves. According to the field survey, more than 15% of displaced construction workers are thought to have relocated to Kochi, Chennai, and Mumbai. Figure 11 shows migration of labourers from the affected river bank erosional zone to other parts of India and abroad.

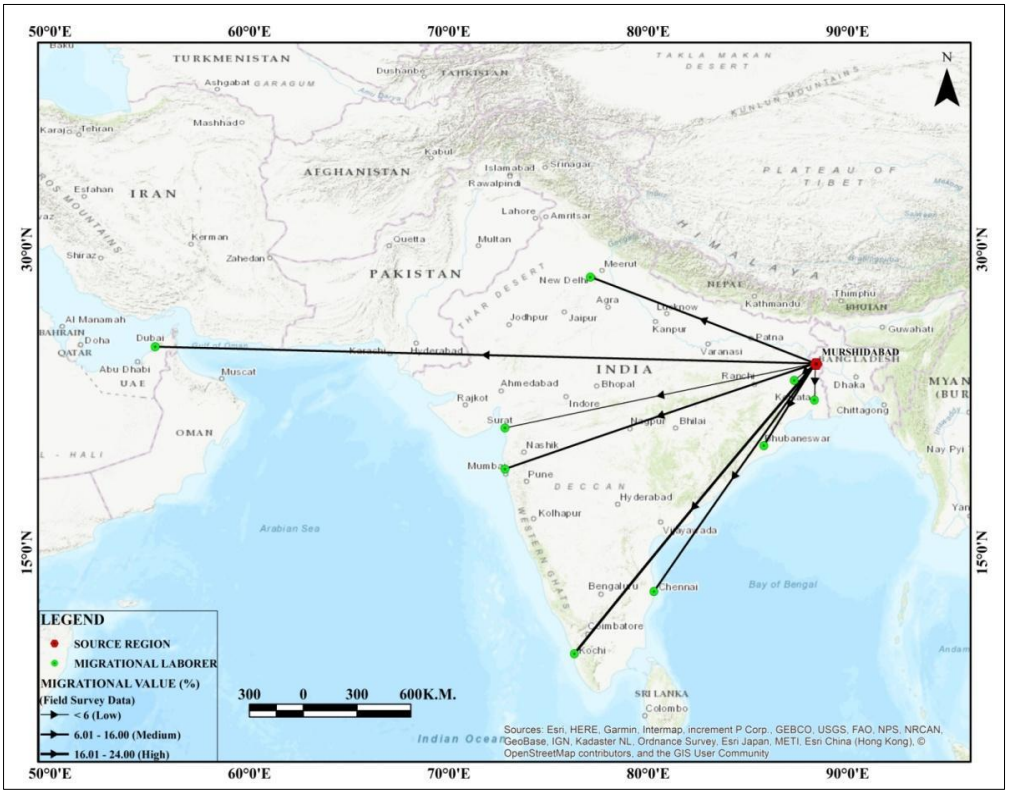

Figure 11: Flow path of emigrational labourers from riverine society

Major Findings

i. The majority of displaced individuals suffer greatly from poverty, with monthly incomes ranging from Rs 2000 to Rs 5000.

ii. 72% of the homes in the region are kacha.

iii. Previously, agriculture served as the majority of people's source of income, but due to the loss of all agricultural land, the situation has changed completely. The majority of individuals now work as construction labourers to support their families.

iv. According to the study, 22% of the study area's residents are at risk for river bank erosion since they reside close to the bank line (Figure 12).

v. In the research region, 65% of the population has lost their homes costing at least Rs1.5 lakh rupees.

vi. 13% of people have lost 2.5 acres of agricultural land, and 25% have suffered from financial losses up to Rs5 lakh.

vii. The monthly expenditure of about 81% people is less than Rs 5000.

viii. 49% of people spend just Rs 600 per month on education.

ix. 37% of the population in the study region has relocated once or more.

x. The study has found that most of the construction labourers have migrated to Kerala, Chennai, Mumbai and Delhi.

Figure 12: Present status of the Padma River bank erosion – ***A. Recent River Bank Erosion Ground truth evidence at Farakka; B, D & E. Recent River Bank Erosion Ground truth evidence at Dhulian (During Bank Erosion); C. Recent River Bank Erosion Ground truth evidence at Maya (Lalgola); F.Recent River Bank Erosion Ground truth evidence at Dhulian Municipality ward no 17***

Conclusions

The river bank erosion takes place at an alarming rate due to low level technological adjustment and ill directed planning. As the district is situated near the border area, since the independence of India (1947) a large number of people have emigrated from East Pakistan (Bangladesh), changing the socio-economic and demographic scenario in the district, people becoming marginalized. The environmental neo-refugees of Murshidabad district have faced multi-dimensional problems and have lacked basic amenities for survival. In these circumstances, the preventive measures and human preparedness must be undertaken to control the river bank erosion. Simultaneously basic amenities have to be provided to environmental neo-refugees for uplifting the socio-economic condition of these people. The changing river courses have both positive and negative impacts on human life. Many landscapes are developed due to changing river courses in the district such as river cut-off, *charland* and alluvial deposition etc. Later river cut-off is transformed into *bills* or swampy lands. These *bills* act as wetlands. Excessive flood water holds these wetlands and reduces the flood. These wetlands also produce

fishes and other aquatic animals and plants and also recharge the groundwater and use recreation purposes such as Mothijil. *Charlands* emerged on the river bank due to changing river courses. Victims affected by erosion take shelter at these *charlands* such as Nirmal*char*, Bamnabadchar etc. *Charlands* are also used for agricultural purposes such as vegetables, Pulses, Turmeric etc. But changing river courses have many folds negative effect than positive effect. Changing river courses have badly affected human society. River bank erosion due to changing river course causes the displacement of thousands of people in the district every year, turning them into environmental refugees.

While the total taming of the tremendous eroding force of the Padma River is impossible, local people have to learn to live upon continuous adjustment to erosion. The low-cost house building with easily detachable and movable materials like corrugated sheets, bamboo, wood etc. may be provided on *chars* and vulnerable areas. The Government should pay more attention to protect non-displaced people and relief generally provided for displaced people rather than spending huge amounts of money for engineering works. Construction of special type schools in suitable areas which plays a dual role such as education as well as shelter.

Hectares of agricultural land are also lost due to river bank erosion and flood. Displaced people live without proper shelter, sanitation, drinking water, even electricity such as Nirmal*char*, Bamnabad*char* etc. They are forced to migrate to other states and countries to get jobs. Huge amounts of money every year are used for bank protection but in many cases bank protection with boulders is futile. In these circumstances, a holistic approach with human preparedness will be undertaken to save the displaced people. Basic needs of the displaced people are to be ensured with providing facilities such as housing, food, drinking water, education, medical, proper sanitation, jobs etc. Establishment of police outposts or BSF camps may also develop a sense of security in *charland*. An arrangement of elevated flood shelter is absolutely necessary as chars are submerged during the rainy season. They also granted pattas or right to the *charland* for peaceful life of the *charland*.

Bank protection in this sector is mostly dependent on engineering work such as concrete spur, net wire fill boulders, and so on, but never takes into account the societal aspect. Therefore, better preparedness and scientific resettlement strategies as well as holistic planning may improve the socio-economic status of the thousands of erosion and flood victims lastly, displaced people are considered as Indian citizens; otherwise, they are helpless and hopeless.

Funding

This research received no external funding.

Author contribution

Conceptualization, methodology, writing – original draft, MM, GB. The author has read and agreed to the publication.

Conflicts of interest

The author declares no conflict of interest.

Acknowledgement

I am grateful to the thousands of erosion victims who shared their stories with me throughout the questionnaire survey and interviews. I'd also like to thank my student, Mr. Subham Kumar Roy, for preparing the text. Thank you to my students who assisted me during the questionnaire survey and interview processes.

References

Couture, S. (2008): River Dynamics and Erosion, Presented to Great Bay Siltation Commission, December1, 2008

Ghosh, S. (2015). River bank erosion and environmental neo-refugees: A case study of Murshidabad District,West Bengal, India. *International Journal of Current Research*, 7 (5), 16582-16589

Islam, T., Azman, A., Singh, P., Ali, I., Akhtar, T., Rafatullah, M., ...&Hossain, K. (2019). Socio-economic vulnerability of riverbank erosion of displacees: Case study of coastal villages in Bangladesh. *Indian Journal of Ecology*, 46(1), 34-38. https://www.sciencedirect.com/science/article/abs/pii/S1470160X16303703

Mukherjee, J. (2011). NO VOICE, NO CHOICE: RIVERINE CHANGES AND HUMAN VULNERABILITY IN THE 'CHARS' OF MALDA AND MURSHIDABAD. *INSTITUTE OF DEVELOPMENT STUDIES KOLKATA*, 28, 1- 30

Mukhopadhyay, S. C., & Das Gupta, A. (2010). River Dynamics of West Bengal: Physical Aspects (Vol. 1). *Kolkata: Prayas Publishers and Book Shellers*

Panda, S., & Bandyopadhyay, J. (2011). Morphometric Changes of Bhagirathi River at Murshidabad District Using Geoinformatics. *Journal of Geographic Information System*, 3 (01), 85 - 97. DOI:10.4236/jgis.2011.31006

Parua, P. K. (2006). Some Facts About Farakka Barrage Project (Vol. 1). *Berhampore: Silpanagari Prakasani*

Parua, P. K. (2009). Some Facts About Farakka Barrage Project (Vol. II). *Berhampore: Silpanagari Prakasani*

Parua, P. K. (2010). The Ganga: Water Use in the Indian Subcontinent (Vol. 64). *Springer, Water Science and Technology*

Rahman, M. R. (2010). Impact of riverbank erosion hazard in the Jamuna floodplain areas in Bangladesh. *Journal of Science Foundation*, 8(1-2), 55-65

https://www.banglajol.info/index.php/JSF/article/view/14627

Raman, K. S., Kumar, S., & Neogi, B. B. (1986). Exploration in Bengal Basin India - An Overview. *Singapore: Offshore South East Asia Show*

Rudra, K. (2010). Dynamics of the Ganga in West Bengal, India (1764–2007): Implications for science–policy interaction. *Quaternary International*, 227 (2), 161-169.https://doi.org/10.1016/j.quaint.2009.10.043

Rudra, K. (2005). The Encroaching Ganga and Social Conflicts: The Case of West Bengal, India.

Census of India, (2011): Population Census of Murshidabad district, West Bengal

Govt. of West Bengal (Office of the District Magistrate, Murshidabad) (2014). Flood Preparedness & Management Plan (Murshidabad District)

Murshidabad District Gazetteers (1997): West Bengal District Gazetteers, Government of West Bengal,Calcutta, pp 1-22

Murshidabad District Gazetteers (2003): West Bengal District Gazetteers, Government of West Bengal,Calcutta, pp: 14-45

Forum geografic. Studii și cercetări de geografie și protecția mediului
Volume **XXII**, Issue **1** (**June 2023**), pp. **28-43;** DOI: **10.5775/fg.2023.094.i**

Flood risk modelling using HEC-RAS and GIS in the semi-urban watershed of Oued Ziad (Constantine, North-Eastern Algeria)

Manel YAKHLEFOUNE[1*], Chaouki BENABBAS[2], Florina GRECU[3], Abdeldjalil BELKENDIL[4], Takki-Eddine KHARCHI[1]

[1] Department of Urban Techniques and Environment, Institute of Urban Techniques Management, University of Constantine3, Constantine, Algeria. Geo-prospective, Environment, and Development Laboratory
[2] Territory Planning Research Center, Constantine, Algeria
[3] Department of Geomorphology, Pedology, Geomatics, Faculty of Geography, University of Bucharest, Bucharest, Romania
[4] Department of Hydraulic Engineering, Faculty of Science and Technology, University of Tlemcen, Tlemcen, Algeria. Laboratory 60: Water Resources Valorization
* *Corresponding author*: manel.yakhlefoune@univ-constantine3.dz

Received on 03-05-2023, reviewed on 05-06-2023, accepted on 12-06-2023

Abstract

The study of flood risk in Algerian cities has become essential given the multiple issues at stake (urbanization, urban sprawl, easements, infrastructure, soil structure, etc.), which constitute vulnerable elements, as well as their frequency and repetition in time and space. This has become a problem for the city and the urban environment, particularly in large metropolises such as Constantine. The watershed of Oued Ziad located in the northwestern part of the city of Constantine has experienced exceptional flooding, causing loss of life and property in the Jebli Ahmed agglomeration in the Hamma Bouziane township. The main objective of this research is to identify the factors aggravating the risk of flooding in the Oued Ziad watershed, to analyze the frequency of maximum daily rainfall to determine peak flows for different return periods of 10, 20, 50, 100 and 1000 years, and to map the extent of the flood hazard in the Oued Ziad watershed for a centennial flow, using geographic information systems and HecRas software. The simulation results show the overflow of Oued Ziad on national road N°27, affecting a part of the agglomeration located downstream by a centennial peak flow equal to 50. 98 m3/s and a water height exceeding 3 m, which confirms the extent of the area exposed to risk during the flood that occurred on 19/9/2018. The field survey shows that several anthropic factors increase the risk of flooding while the capacity of the existing hydraulic structures is insufficient to evacuate water during floods, which requires the development of this watercourse and its banks to protect the population and its property from the risk of flooding and to reduce the impact on the city's environment and socio-economic activities.
Keywords: *Constantine, Flood risk, hydrological modelling, geographic information system, Hec-Ras, Oued Ziad watershed*

Introduction

Natural hazards constitute a real environmental problem, threatening people and their property, the environment, and infrastructure. Among natural hazards, floods constitute one of the world's worst natural disasters causing significant human, material, and economic losses. Over the last decade, there have been multiple investigations carried out utilizing spatial analysis to evaluate flood and sedimentation management in large geographical areas. (Rai and Mohan, 2014; Mătreaţă et al., 2016; Grecu, 2016; Grecu et al., 2017; Costache et al., 2020; Jalilzadeh and Behzadi, 2020; Nkwunonwo et al., 2020; Ongdas et al., 2020; Tegenie and Berhe, 2021; Abdelshafy and Mostafa, 2021; Xafoulis et al, 2022), these extreme hydro-climatic events due essentially to the complex interaction and concomitance of several topographical, geological, hydrological and meteorological factors, are often intensified by climate change which increases their frequency and repetition in time and space (Lasri 2019; Prăvălie and Costache, 2014). The risk of flooding is not a characteristic of the urban environment. High population density and soil impermeabilization increase the probability of flooding due to urban runoff, especially in areas with steep slopes (Nkwunonwo et al., 2020). In general, flooding is limited to the overflow of water from river beds. In the case of cities, flooding includes the amount of water that appears in public spaces, including water resulting from non-functioning sewage systems.

Flooding has become one of the most frequent and devastating natural disasters in Algeria (Derdour et al., 2017), the country's northern territories being highly threatened by this phenomenon. Indeed, the main physical features as well as the natural characteristics of these territories (aggressive climate, type of fragile plant cover, soil sealing, nature of the hydrographic network (shape, density), tend to favour torrential flows (Grecu, 2018a), which induces the overflowing of wadi beds, thus consti-

tuting a major constraint for economic and social development, by consequence: loss of human life, destruction of infrastructures (bridges, roads), destruction of housing and agricultural areas.

The study of flood risk in North-Eastern Algeria has become a priority in the context of climate change and the recurrence (frequency and repetition) of extreme events. The high concentration of the population in northern Algeria, which is experiencing accelerated and often poorly controlled urbanization, has led to the establishment of activities in flood-prone areas, reducing the permeability of the soil surface to infiltration, and consequently the formation of flash floods (Gao et al., 2021). This problem has become a serious concern for decision-makers and city managers. Intense rainfall is the main factor in the formation of flash floods, occurring within a short period (Buta et al., 2017). Several regions of the country are regularly threatened by these floods, whose effects are often intensified by anarchic urbanization involving the occupation of flooded land and even wadi banks.

The city of Constantine was severely affected by flooding, including the historic flooding of the Djebli Ahmed agglomeration on 19/09/2018, mainly due to the overflowing of the Oued Ziad watercourse following intense rainfall, causing severe damage to the population (the death of two people, and 11 others injured), and to material assets (many cars were swept away by the flooding of the wadi), as well as to infrastructures (blocked roads, disruption of economic activity) (Fig.1) (Bekhira et al., 2019). During this exceptional downpour, the rain gauge at the Hamma Bouziane station, which is the closest to Oued Ziad, recorded 33.5 mm in just 40 min, resulting in a very high flow rate of 60 m3/s and an intensity equal to 139. 6 l/s/h according to the National Agency for Hydraulic Resources (ANRH), this strong flow collected several tree trunks and blocks and deposited them in the downstream section, where they blocked the culvert and the water overflowed on the national road 27 (Fig.1). This event underlines the importance of studying flood risk in small torrential urban catchments.

The present work aims to highlight the role of torrential precipitation in the flooding of an area subject to slope runoff, by i) Identifying the factors triggering the risk of flooding in the Oued Ziad watershed, which has already been affected by a historical flood of the unknown return period. ii) Hydrological modelling of flood risk to determine the extent of the hazard and the height of water (Uca et al., 2022), also to protect people, their property, and infrastructure from the risk, and for better management and prevention of flood risk in the city by:

- The analysis of the hydro-morphometric characteristics of the watershed using geographic information systems.
- Statistical analysis of maximum daily rainfall using Hyfran plus software to determine peak flows for different return periods (10, 20, 50, 100, and 1000 years), and analysis of short-duration rainfall to determine the return period of the historic flood that has already occurred in the agglomeration located downstream of the watershed.
- Hydrological modelling of the flood hazard using Hec-Ras software, to determine water levels during floods.
- The autumn flood on 19/09/2018 is used to validate the simulation results, which serve as a decision-support document for city managers and local authorities, to protect this watercourse from flooding and Presenting a methodology for the strategic management of floods to mitigate their damage in areas invaded by human activity by calibrating it and stabilizing its banks (Bilașco et al., 2022).

Study area

Geographically, the Oued Ziad watershed is part of the Kebir Rhumel watershed (Benabbas,2006), a tributary of Oued Rhumel with a surface area of 12.02 km^2 and a perimeter of 19.47 km, drained mainly by Oued Ziad with a length of 7.11 km, it is a mountainous watershed, originating from the Djebel El Wahch mountains, a mountainous area marked by a rugged relief varying between 350 and 980 meters characterized by steep to medium slopes. Oued Ziad crosses National Road N° 27, national road N° 03, and the urban limits of the Bekira agglomeration and the Constantine-Skikda railroad, it flows into Oued Rhumel downstream, characterized by a semi-arid Mediterranean climate (cold winters and hot, dry summers).

Figure 1. The exceptional flooding of the township Djebli Ahmed caused by the overflow of Oued Ziad, photos taken by the civil protection of Constantine on 19/09/2018

Oued Ziad is administratively located in the north-western part of the city of Constantine, in the Djebli-Ahmed agglomeration, commonly known as "El-Cantoli", which lies between the administrative boundaries of the Hamma-Bouziane municipality and the municipality of Constantine. Over half of the catchment area is built-up (Fig.2).

Methodology

The hydraulic efficiency of different adaptation strategies was evaluated by utilizing a simplified two-dimensional flow model. This model was developed in HEC RAS Hydrologic Engineering Center River Analysis System version 6 0 by the US Army Corps of Engineers (Kashfy et al., 2021). The fundamental concept underlying the utilized modelling approach is that rainwater quantities usually gather over the urban landscape and eventually flow into the nearby canal system; a physically based model for rainfall runoff HEC RAS made its debut in 1995 and since then it has undergone validation through numerous case studies in similar settings (Yalcin, 2020). Due to the presence of local data, the entire configuration of the employed model relies on open access input data which includes freely available topographical and hydro meteorological information. The research methodology is based on 3 stages:

The first step is to study the physical and hydro-morphometric characteristics of the watershed. Indeed, knowledge of the physical characteristics of the watershed enables the determination of its morphometric parameters, which form the basic foundation for all hydrological studies (Grecu, 2018b). To process this part of the study, we used a 10 m resolution digital elevation model obtained by digitizing the contour lines of the 1:25,000 scale topographic map produced by the National Institute of Cartography and Remote Sensing (INCT) in 2006 and processed using ArcMap 10.8 software to extract the various slope, hypsometric and hydrographic network maps to calculate the morphometric parameters of the watershed. The second step is to carry out a statistical analysis of flooding. For this, we used observation data from the National Hydraulic Resources Agency (ANRH) at the station closest to our watershed, Hamma Bouziane (Table. 1), and maximum daily rainfall data over 51 years (1968-2021).

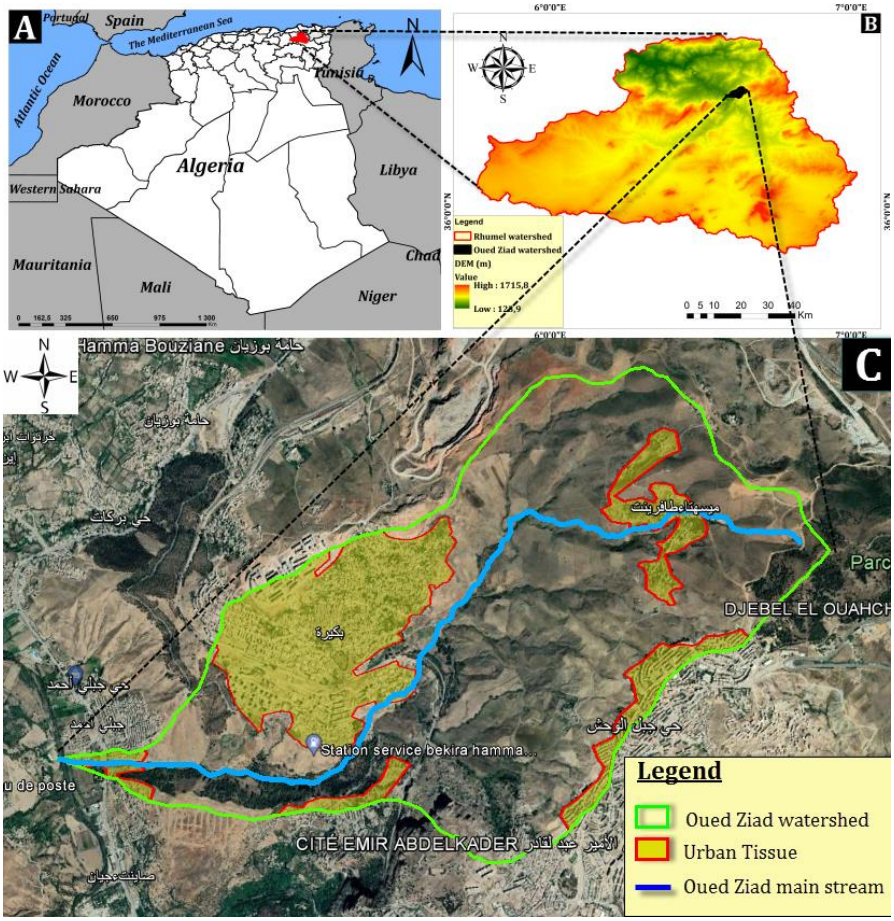

Figure 2. Geographical location of the study area: A) Location in Algeria, B) Location in Oued Rhumel Watershed, C) Google-Earth location of the Oued Ziad watershed

Table 1. Characteristics of the Hamma Bouziane rainfall station

Station	Code	Longitude (X)	Latitude (Y)	Altitude (Z)	Years of observation	Average annual rainfall (mm)
Hamma Bouziane	10-06-03	848.5	352.8	460	51 years	528

Source: national water resources agency

For rainfall adjustment, we used HYFRAN Plus software. HYFRAN Plus is a statistical data analysis program that can be used to fit a large number of statistical distributions to a series of data observations and to check hypotheses of independence, homogeneity, and stationarity. It has been designed for frequency analysis in hydrology, especially for extreme events, or for flows for each return period recorded.

We used the Normal, Log-Normal, and Gumbel laws to analyze flood frequency. Then, we calculated the Intensity, Duration, and Frequency (IDF) curve.

IDF curves represent the evolution of rainfall intensity as a function of duration and frequency, expressed in return periods. The development of IDF curves is an extremely important tool in flood risk management and prevention. They help us to design hydraulic protection structures.

The intensity duration frequency relationship is given by the formula:$I(t,T) = a(T)/t\hat{}b$

I: intensity mm / h

a (T): maximum intensity in mm/h for a rainfall return period T

b: Montana coefficient

According to the National Hydraulic Resources Agency (ANRH), the Montana coefficient for El Hamma station is equal to 0.63. We then proceed to determine short-duration rainfall, time of concentration and peak flows for the various return periods using empirical formulas.

The third stage is devoted to the hydrological modelling of peak flows using HEC RAS (Hydrological Engineering Centers - River Analysis System) software, designed by the US Corporation Engineers Hydraulic Engineering Centre to model river flow (Brunner, 2016). This program calculates water level and velocity in rivers and builds one- or two-dimensional models to simulate water movement, whether in a stable or unstable state, including sediment transport modelling (Zellou and Rahali, 2016; AL-Hussein et al., 2022).

To generate the flood hazard map, we used the topographic survey (Sunilkumar and Vargheese, 2017; Thapa et al., 2020) of Oued Ziad, obtained from the hydro project East engineering company of Constantine. The data required for this hydraulic modelling are the flows resulting from the hydrological study and the geometry of the watercourse. Wadi modelling is based on cross-sections, as well as longitudinal slope and bed and bank roughness at the various calculation points.

The integration of HEC-RAS (Hydrologic Engineering Centers River Analysis System) and GIS (Geographic Information System) technologies to obtain scientifically derived information has been effective in the simulation, identification, and analysis of flood events in a geospatial environment (Yerramilli, 2012; Lasri, 2019; Tegenie and Berhe, 2021; Awad et al., 2022).

Results

Determination of watershed physical characteristics and morphometric parameters

The study of the physical characteristics (slope, hypsometry, hydrographic network) of the Oued Ziad watershed is essential for the calculation of the morphometric parameters required for our hydrological study, as well as for the study of river dynamics (Benabbas et al., 2011; Grecu et al., 2021).

The study of the slope is fundamental to any hydrological study, it enables us to determine the type and characteristics of runoff, the type of surface runoff, and the areas affected by flood risk.

According to the slope map (Figure. 3), our terrain is dominated by steep slopes ranging from 12% to 25%, the steep slope that dominates the watershed accelerates flow velocity, reducing the time of concentration (table. 2).

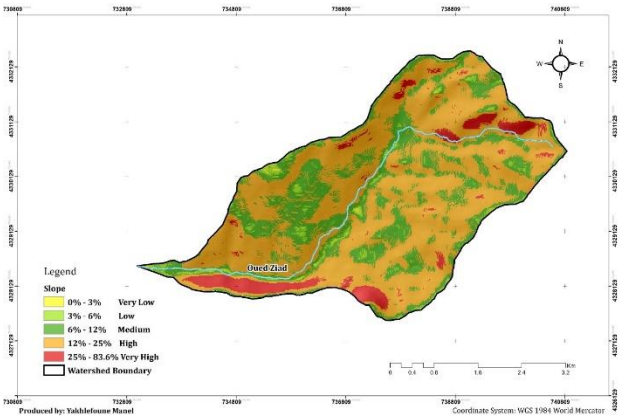

Figure 3. Slope map

Basin morphology is an essential element. It enables us to determine the areas likely to be affected by flooding and therefore to combat this risk. The longitudinal profile is traced using the Oued Ziad topographic survey and is presented by the altitude and length of the watercourse.

Table 2: Slope Classes and area percentage

Slope classes	Area (Km^2)	Area (%)
0% - 3%	0.59	0.07
3% - 6%	2.02	0.24
6% - 12%	17.97	2.16
12% - 25%	68.97	8.29
25% - 83.6%	10.44	1.25
Total	12.02	100

It can include major infrastructures (railroads, dams) and various tributaries. From the longitudinal profile below (Figure. 4), we can see that there is a variation in slopes; the further north-east we go, the steeper the slopes (corresponding to areas of high relief). The further south we go, the steeper the slopes (corresponding to the watercourse).

Relief is one of the physical characteristics of the watershed, defined as the variation in altitude; these variations influence runoff, precipitation, vegetation, etc. To characterize the relief of the study area, we produced a hypsometric map (Figure. 5), then we calculated the distribution of the watershed surface according to the altitude, using Arcmap 10.8 to produce the hypsometric curve.

The relief of the Oued Ziad watershed is too rugged (Benabbas, 2006), with altitudes ranging from 350 m to 980 m and a relatively steep slope.

The hypsometric curve in (Figure. 6) provides a synthetic view of the slope of the watershed, hence its relief. This curve represents the distribution of the watershed's surface area as a function of its altitude. The results are detailed in (table 3).

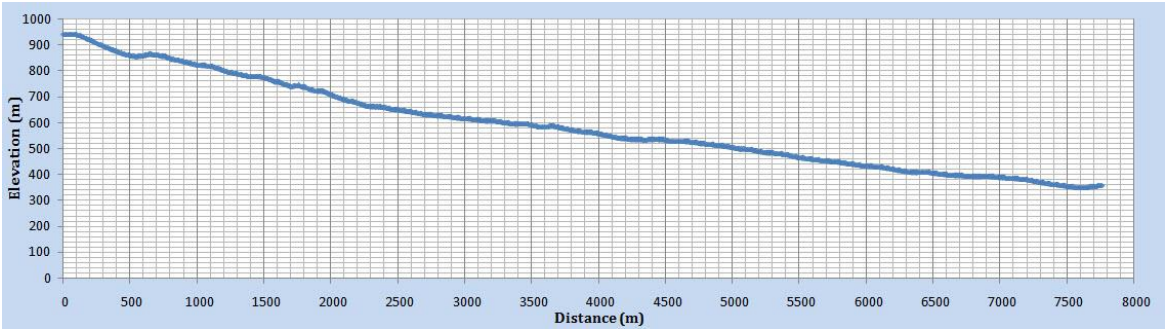

Figure 4. Longitudinal profile of Oued Ziad

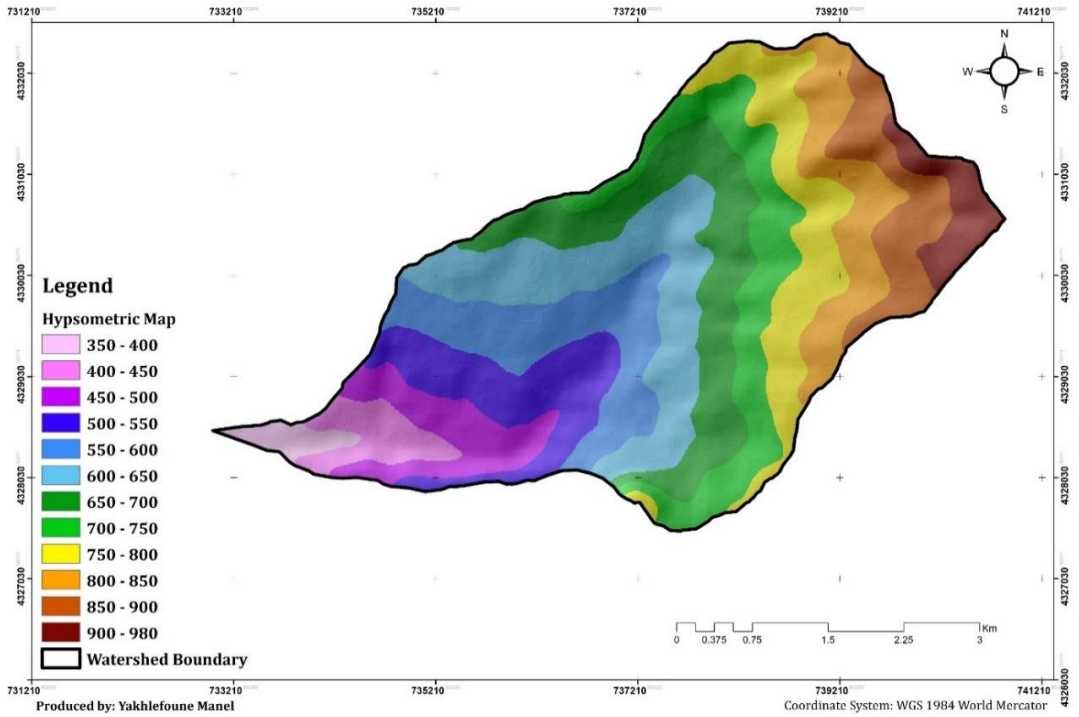

Figure 5. The hypsometric map of the Oued Ziad watershed

Table 3: Hypsometric characteristics of the Oued Ziad watershed

Elevation (m)	Area between curves		Cumulative areas	
	Km²	%	Km²	%
350 – 450	0,58	4,83	0,580	4,83
450 – 550	1,87	15,58	2,450	20,41
550 – 650	3,1117	25,93	5,562	46,34
650 – 750	3,0153	25,12	8,577	71,46
750 – 850	2,26	18,83	10,837	90,29
850 – 950	1,113	9,27	11,950	99,57
950 - 980	0,052	0,43	12,002	100,00
	12.02	100		

This table shows the percentage of accumulated surface area above a certain altitude.

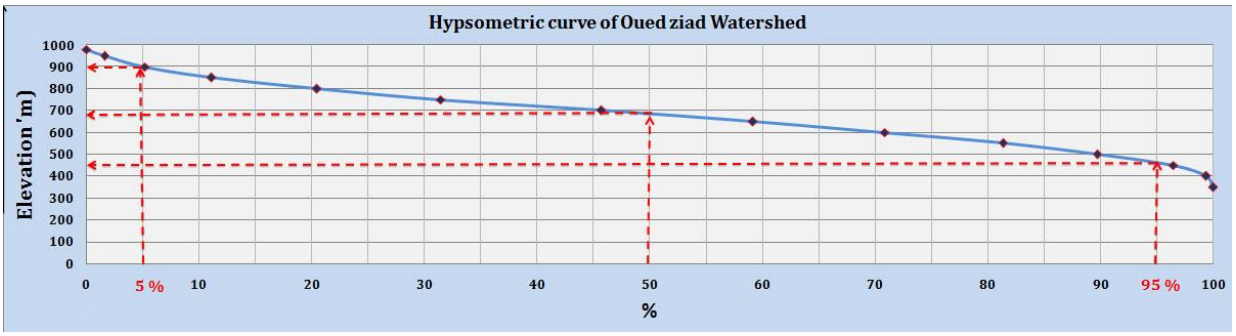

Figure 6. The hypsometric curve of the Oued Ziad watershed

The Oued Ziad watershed is characterized by a well-developed hydrographic network (Figure. 7), with an average drainage density of 2.43 km/km^2. Its main watercourse (Oued Ziad) is torrential, with an estimated length of 7.11 km, and starts flowing at an altitude of 980 m, reaching its outlet at an altitude of 350 m. The main direction of the watercourse is North-East to South-West upstream and becomes East-West downstream, the watercourse is not very sinuous and seems to follow segments of linear accidents.

The physical characteristics of the Oued Ziad watershed have enabled us to calculate its morphometric parameters (Table. 4), which help us to understand its behaviour and hydrological response, as well as the factors that aggravate hydrological risks.

Concentration-time calculation

The time of concentration (Tc) is defined as the time required for the raindrop falling at the furthest point in the watershed to reach the stream outlet; based on the physical characteristics of the watershed, we calculated the time of concentration using various empirical formulas that are adapted to the characteristics of our watershed (Ventura's formula, Turraza's formula, Passini's formula and Giandotti's formula), then calculated the average of the values obtained (Table. 5).

Statistical analysis of rainfall data

Statistical analysis of hydrological data aims to determine the extent of extreme events in terms of their frequency of occurrence, using probability laws (Zegait et al., 2022). The analysis of maximum daily rainfall is necessary for estimating peak flood discharges, and we used the most recent maximum daily rainfall ANRH data from the Hamma Bouziane station for the entire observation period (1968-2021), which is long enough to carry out our study.

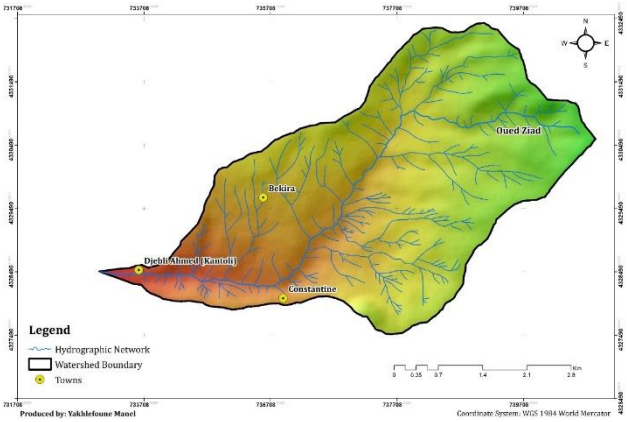

Figure 7. Hydrographic network of the Oued Ziad watershed

Table 4: Morphometric characteristics of the Oued Ziad watershed

Morphometric parameters		Units	Oued Ziad watershed
Area (A)		Km^2	12.02
Perimeter (P)		Km	19.46
Main Talweg Length (L)		Km	7.11
Compactness index (the GRAVILIUS capacity coefficient)		/	1.58
Equivalent Rectangle	Length (L)	Km	8.37
	Width (W)	Km	1.43
Elevation Characteristics	elevation at 5%	m	900
	elevationat 95%	m	455
	Maximum elevation (H_{max})	m	980
	Minimum elevation (H_{min})	m	350
	Average elevation	m	667
Overall slope index (Ig)		m/Km	53.76
Useful height difference (Du)		m	450
Specific height difference (Ds)		m	186.4
Watershed relief (R)		/	Relief Fort
Drainage density (Dd)		Km/Km^2	2.43

Table 5: Result of concentration time calculation

Empirical formulas	Giandotti	Turazza	Passini	Ventura	Mean
Equations	$Tc = \frac{4\sqrt{A+1.5L}}{0.8\sqrt{Hmedian - Hmin}}$ Where A: Area (km^2) L: length of the equivalent Rectangle (m)	$Tc = 0.108\frac{\sqrt[3]{A \times L}}{\sqrt{P}}$ Where A: Area (Ha) L: Main Talweg Length (m) S: Slope (m/m)	$Tc = 0.108 \times \left(\frac{(A \times L)^{1/3}}{S^{0.5}}\right)$ Where A: Area (km^2) L: Main Talweg Length (km) S: Slope (m/m)	$Tc = 0.13\sqrt{\frac{A}{S}}$ Where A: Area (km^2) S: Slope (m/m)	/
Tc(hour)	1.44	1.5	1.94	1.59	1.62

The value adopted is the result closest to the averages of the results of the four formulas used. The concentration time is 1.59 h.

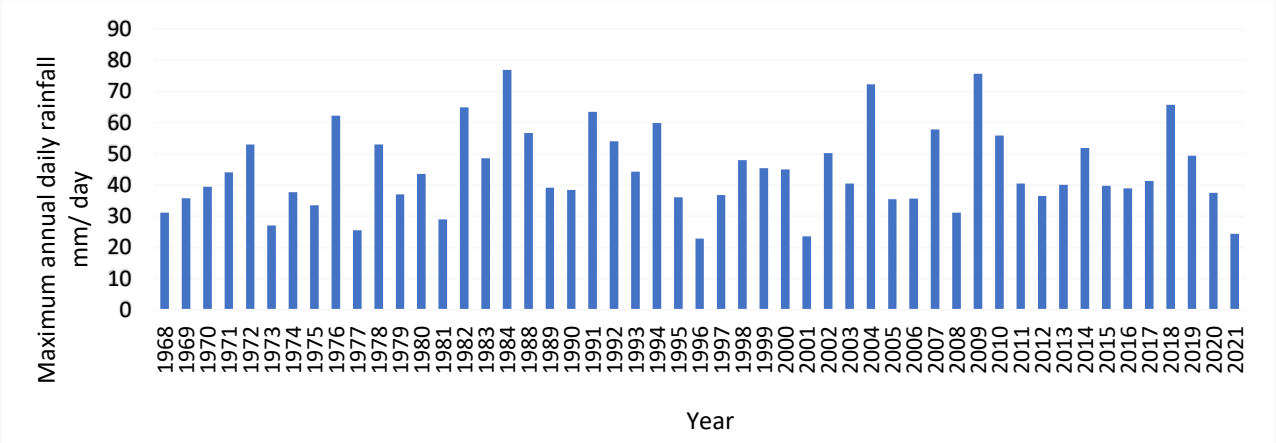

Figure 8. Maximum annual daily rainfall of Hamma Bouaziane station from 1968 to 2021

The highest value recorded of the maximum daily rainfall is equal to 76.9 mm/day, for the hydrological year 1984, and the lowest value recorded of the maximum daily rainfall is equal to 22.8 mm/day, for the hydrological year 1996 (Figure. 8).

Statistical adjustment to the Gumbel probability law

Algeria is subject to a highly unpredictable and irregular climate; however, the choice of an asymmetrical statistical law is essential for the statistical analysis of maximum daily rainfall. To obtain more accurate results, we adjusted the series of observations of maximum daily rainfall at the rainfall station in our study to the Gumbel, Normal and Log-Normal laws (Kim et al., 2020), which are well adapted to the Mediterranean hydrological climate. The maximum daily rainfall series is adjusted by Hyfran plus software, using the (maximum likelihood) method**.**

The results obtained show that the best-fitting law is Gumbel's law, which gives good frequency values (Figure. 9). This result has been validated by the National Hydraulic Resources Agency (ANRH) of Constantine for the selected Hamma Bouziane station, then we obtained the peak flows by Gumbel adjustment using the maximum likelihood method (table 6).

Calculation of Intensity - duration - frequency curve

The IDF curve is a relationship between rainfall, return period, and duration: for each selected return period, rainfall is plotted against duration. It has the practical advantage of lending itself well to interpolation for different durations. To produce IDF curves, we transform maximum daily rainfall into short-duration rainfall expressed in (mm), using K. Body's formula (ANRH, 1984). The figure 10 gives us the different intensity values for different return periods.

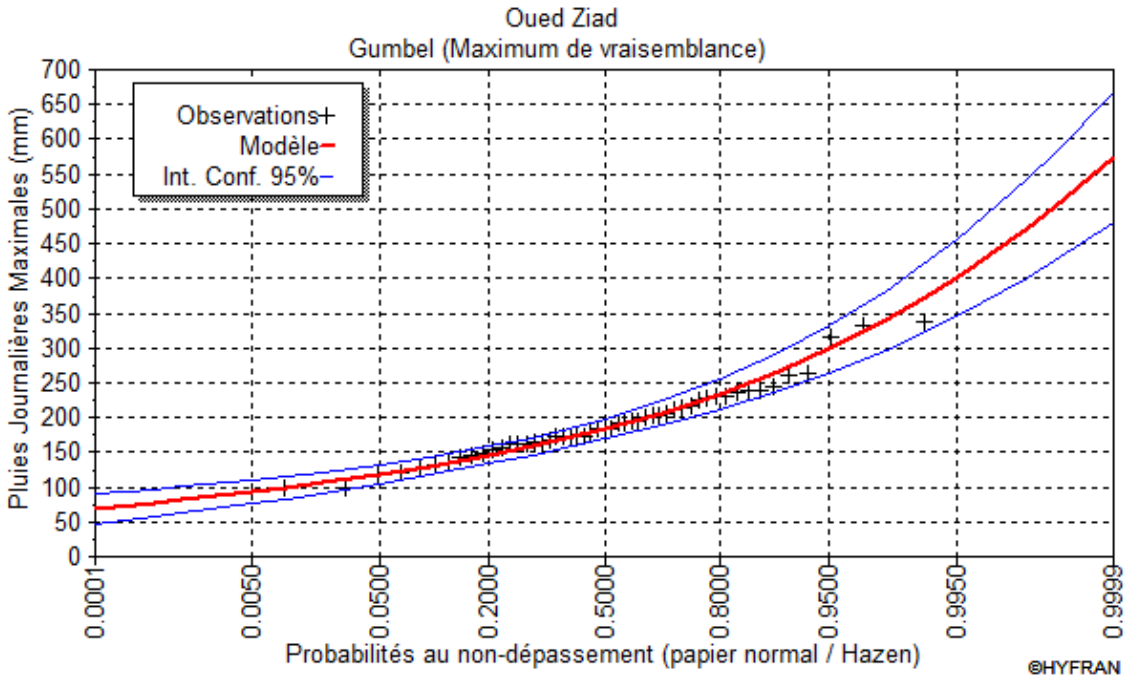

Figure 9. Adjustment to the Gumbel low (Source; HYFRAN software, june 2023)

Table 6: Statistical results of peak flows by Gumbel adjustment using the maximum likelihood method, between (1968 and 2021)

Return Period (T)	Probability of not being exceeded	flow for different return periods	Standard deviation	Confidence interval (95%)
1000	0.999	472	36.3	401- 543
100	0.99	370	25.3	320-419
50	0.98	339	22.0	296-382
20	0.95	298	17.6	263-333
10	0.9	266	14.4	238-294
5	0.8	233	11.2	211-255
2	0.5	183	7.24	169-197

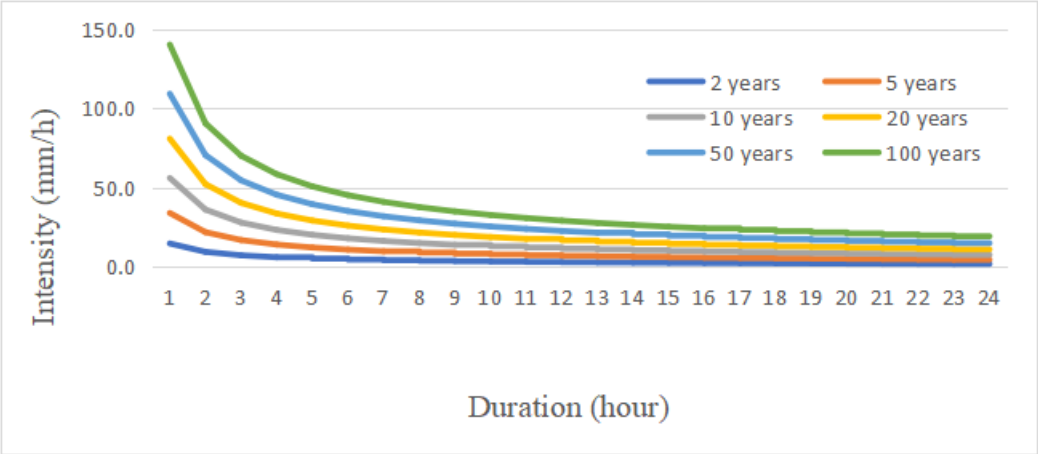

Figure 10. Intensity-Duration-Frequency (IDF) curve for Hamma Bouziane station

Determination of short-duration rainfall

The event of 19-09-2018 was recorded at the Hamma station, according to ANRH sources. An important value of 33.5 mm during 40 minutes, that is to say, an intensity of 139.6 l/s/h, made an exceptional flood, which caused important human and material damages. Using the following relationship, we transform maximum daily rainfall into short-duration rainfall of the same frequency: $Ptc = DR \max(tc / 24)^b$

Where:

Ptc: short-term rainfall of given frequency, (mm).

DR max: maximum daily rainfall of the same frequency, (mm).

Tc: time of concentration, (hours).

b: climatic exponent = 0.34.

Short-term rainfall values are shown in the following table: 07 The results obtained in the table above show that the flooding event that occurred on September 19, 2018, has a return period of 100 years.

Determining maximum point flows

Flow rates can be calculated using several empirical formulas. The empirical formulas used for this study are often applied to basins in northern Algeria (Zegait et al., 2022), and these formulas are also well adapted to the conditions of our watershed: (the Turraza formula, the Rational formula, the Giandotti formula, and the Mallet Gautier formula) (Table. 8).

Flood hydrograph

Flood hydrographs are determined using the SOKOLOVSKY method. From the graph, we can determine the three times: time of flood rise, time of flood fall, and the base time as well as the peak flow for each return period. The rising flow reaches an estimated value of 50.98 (m^3/s) for a return period of 100 years, this rise has a time of 1.59 h.

Hydraulic modeling of Hec Ras flooding hazard

To achieve the objectives of the study, we first built an HEC-RAS model of the entire Oued Ziad, made up of 39 cross-sections distributed over the entire length of the main watercourse (7 kilometers) (Figure 11). The profiles chosen are perpendicular to the direction of water flow, do not cross each other, cross the entire alluvial plain and take account of geomorphological changes in the major bed. Manning's coefficient or bed roughness coefficient provides the closest possible model to reality, taking into account water velocity on the Wadi bed and banks. On each cross-sectional profile, Manning's coefficient is set at 0.028 for the Oued Ziad banks and 0.035 for the main watercourse.

The cross-sections (in figure 12) shows the water level reached as a function of distance, and the flow velocity varies with the slope of the wadi, the values of these velocities show that the flow has a torrential regime,

The different cross-sections tell us about a series of elements:

1/ The asymmetry of the banks

2/ The narrowing and deepening of the bed of the Oued in certain sectors.

These particularities would be intimately linked to the active geological context of this region.

The elevation of the water line exceeds the minimum elevation of the Wadi Canal. Consequently, the wadi overflows on both banks.

Table 7: Short-duration rainfall of different frequencies

Frequency	0.999	0.99	0.98	0.95	0.90
Return period (years)	1000	100	50	20	10
Ptc (mm)	44.44	34.73	31.84	27.97	24.99

Table 8: Peak flow in m3/s for different return periods

Frequency	0.90	0.95	0.98	0.99	0.999	Equations
Return period (year)	10 years	20 years	50 years	100 years	1000 years	
Turraza	28.82	35.19	43.39	50.98	74.55	$Qmax = \frac{Rc \times Ptc \times A}{Tc \times 3.6}$ Rc: Runoff Coefficient Pct.s hort-term rainfall for t=Tc, (mm) A: Area in (Km²) Tc: Time of concentration (H)
Rational Formula	23.77	31.04	40.37	49.55	70.45	$Qmax = C \times i \times A$ C: runoff coefficient. i: rain intensity in (mm/h) of a given frequency. A: area of the watershed in (Km²).
Giandotti	34.51	38.63	43.97	47.96	61.37	$Qmax = \lambda \times A \times Ptc \times \sqrt{\frac{(Hmedium - Hmin)}{4\sqrt{A}}} + 1.5 \times L$ A: area of the watershed in (Km²). L: length of the main thalweg in (m). Ptc: short duration rainfall for a given frequency (m) H_{medium}: mean elevation of the watershed. H_{min}: minimum elevation of the watershed. λ: coefficient depending on the climatic and physical parameters of the watershed (λ= 0.16)
Mallet-Gautier	37.76	43.17	49.42	53.67	65.84	$Qmax = 2K \times Log(1 + 20H)\frac{A}{\sqrt{L}}\sqrt{1 + 4LogT - LogA}$ K: constant depends on the characteristics of the basin between 1 and 3. H: average interannual precipitation in (m). A: area of the watershed in (Km²). L: length of the main thalweg in (Km). T: return period (years)
Average formulas	31.21	37.01	44.29	50.54	68.05	/
Maximum flow (Qmax)	28.82	35.19	43.39	50.98	74.55	/

The results that are closest to the average of the calculated methods will be used as frequency flood flows in our study: Q1000yr = 74.55 m3/s; Q100yr = 50.98 m3/s; Q50yr = 43.39 m3/s; Q20yr = 35.19 m3/s; Q10yr = 28.82 m3/s

The results of the hydrological modelling of Oued Ziad during the centennial flood show the overflow of the Oued Ziad on the national road N ° 27, affecting part of the agglomeration located downstream (Fig. 13 B). These overflows, combined with high velocities ranging from 0.03 m/s to 3.76 m/s, threatened homes, and flooded areas, particularly downstream, are significant (Fig. 13 A); hence, the hydraulic section is insufficient to evacuate these flows during flood periods. The height of water varies between 0 and 15m.

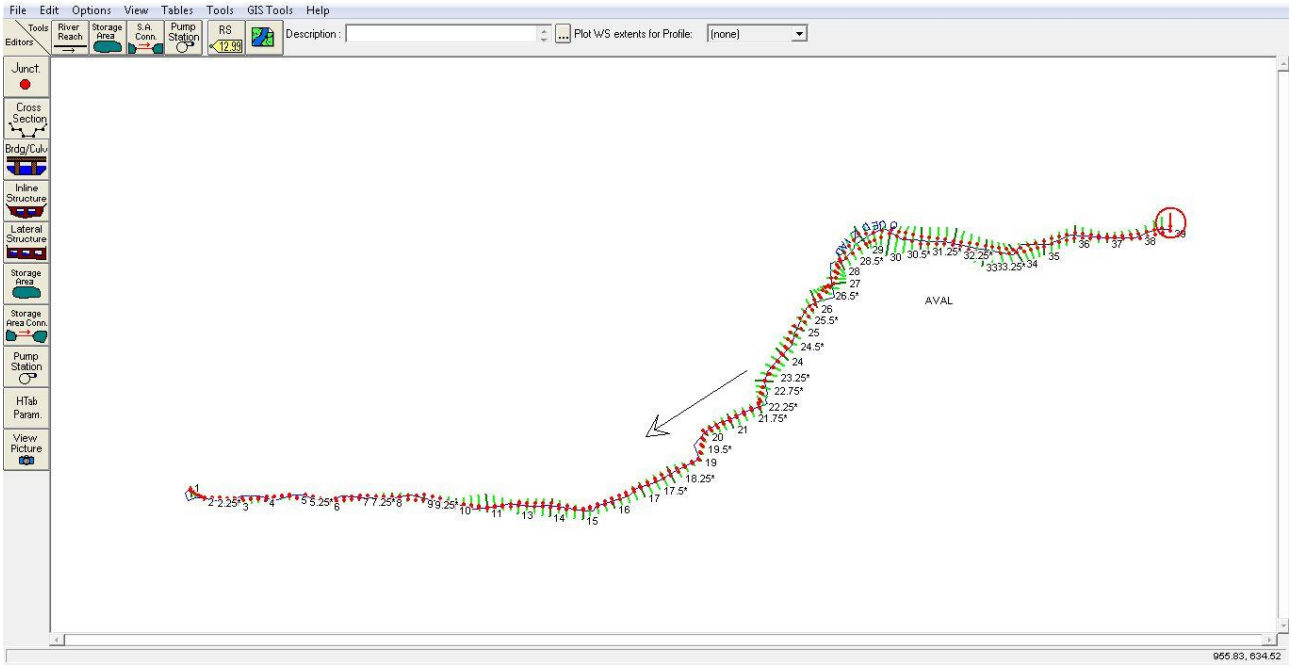

Figure 11. Cross-sections on the Oued Ziad Watercourse

Source; Hec-Ras software, june 2023

Discussion

Morphometric analysis is used to characterize the hydrological behaviour of the watershed. The surface area of the watershed is the most important parameter because it controls the intensity of several hydrological phenomena such as flow, precipitation volume, and infiltration. For this watershed, the surface area is equal to 12.02 km2, and the perimeter is equal to 19.46 km.

The compactness index and the equivalent rectangle show that the Oued Ziad watershed has an elongated shape (Kc = 1.53, L = 7.64 km, l = 2.53 km), which means that it is more drained. The overall slope index is 53.76 m /km and the drainage density is equal to 2.43 Km / Km2, reflecting the dynamics of the watershed, the stability of the hydrographic network, and the type of surface runoff (Table.4).

The time of concentration determines the speed at which the water reaches the watershed outlet, so this variable influences the maximum flow. The result shows that the time of concentration in this catchment is very short (Tc = 1.59 h) (Table 5).

The HEC-RAS simulation is used to calculate the water level based on a specified flow rate (simulation of the 100-year flow rate). For a flow rate of 50.98 m³/s, we can observe (Table 9):

- A rise in water level to an altitude exceeding that of the sills, and consequent overflow along the channel.

- Flow velocity values vary from upstream to downstream, until cross-section number 28, where they increase to reach a maximum value of 3.76 m/s. (Table 9)

The results obtained from this simulation are close to the extent of the surface overflowed by water during the flood that occurred in September 2018 in the same study area, which confirms that this extreme hydroclimatic event has a return period of 100 years. This simulation shows that the capacity of the existing hydraulic structures is insufficient to handle the 100-year flood.

Assessment of factors aggravating the risk of flooding from the Oued Ziad overflow channel

Based on field investigations, we have observed that several factors are responsible for triggering the risk of flooding in the downstream part of the watershed, thus affecting the Djebli Ahmed agglomeration even during low rainfall, thus causing low peak flows. Based on this field investigation, we have identified the following conclusions:

- Anarchic urbanization and the positioning of buildings and commercial activities close to the minor bed of Oued Ziad in its downstream part of Djebli Ahmed agglomeration without taking into consideration the distance necessary for the easement (Oued), make the soil impermeable and cause an increase in the volumes of water runoff, consequently increasing the vulnerability of people and their property to the risk of flooding, which even risks collapsing their very vulnerable dwellings (Fig. 14. A).

- Lack of flood protection facilities (undeveloped/uncalibrated wadis).

-the steepness of the watershed accelerates runoff and water concentration, which can exacerbate flooding.

- Lack of cleaning, maintenance, and effective management of the problem of waste deposited in the minor bed, due to ignorance and lack of awareness on the part of the population (Fig. 14 B).
- The high flow rate and velocity of the water transport the waste and soil particles removed by the erosion process, depositing them downstream and clogging the wadi's drainage channels. The lack of maintenance of the wadi is worsening the situation, and the size of the culvert of the Wadi is insufficient to transport these dumps.

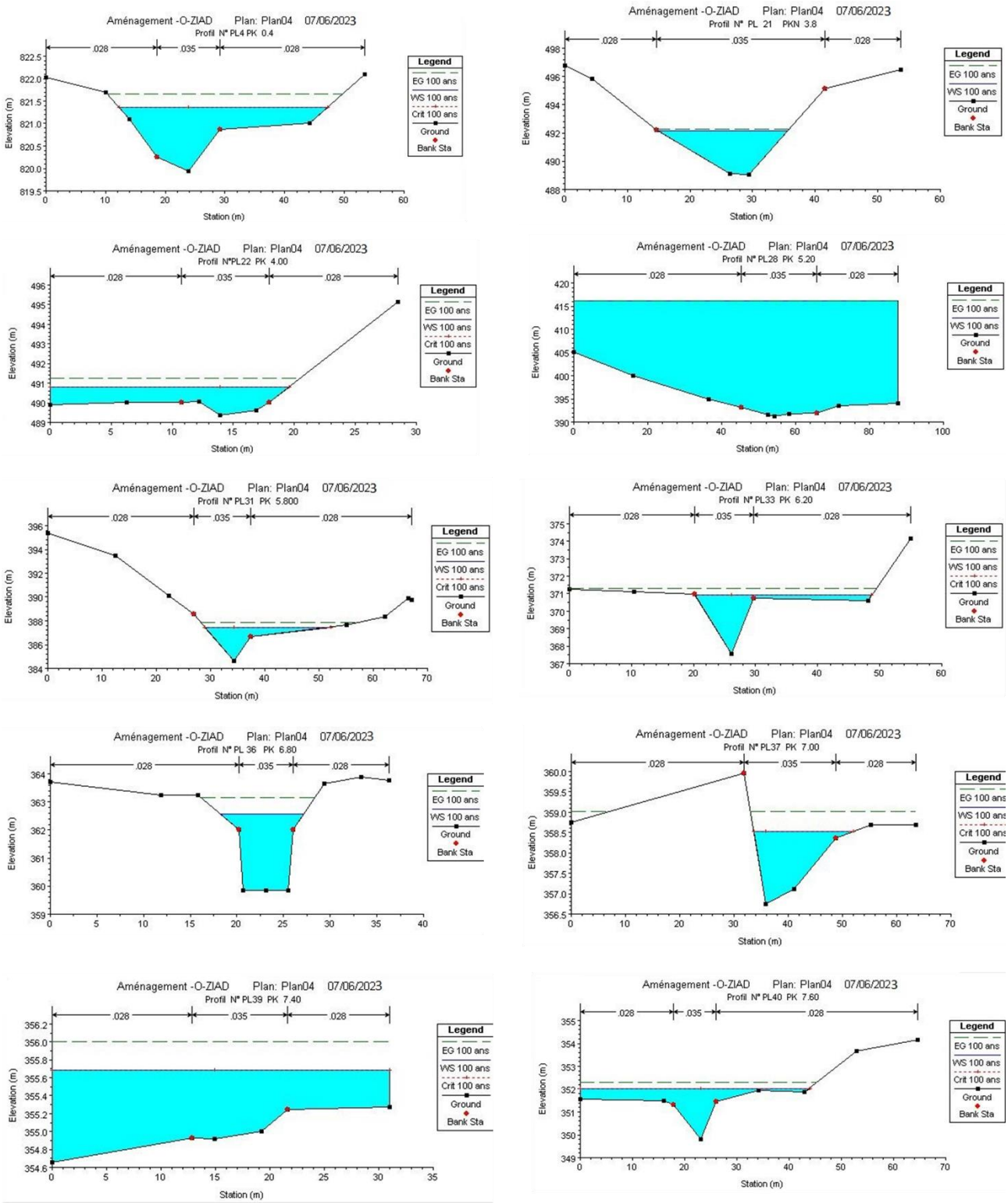

Figure 12. Cross-sections and water levels during the 100-year flood.

Source: Hec-Ras software, June 2023

Table 9: Simulation results on Hec Ras

Reach	River Station	Q Total (m^3/s)	Min Ch El (m)	W.S. Elev (m)	Crit W.S. (m)	E.G. Elev (m)	E.G. Slope (m/m)	Velocity Chnl (m/s)	Flow Area (m^2)	Top Width (m)	Water level (m)
AVAL	39	50.98	886.92	888.14	888.14	888.65	0.011952	3.2	16.18	16	1.22
AVAL	38	50.98	832.24	834.53	834.53	835.11	0.012476	3.36	15.18	13.26	2.29
AVAL	37	50.98	819.93	821.36	821.36	821.66	0.008033	2.74	22.09	34.99	1.43
AVAL	36	50.98	775.23	777.63	777.63	778.24	0.012609	3.46	14.75	12.28	2.4
AVAL	35	50.98	762.55	765.08	765.08	765.72	0.012809	3.55	14.38	11.38	2.53
AVAL	34	50.98	711.71	712.76	712.76	713.17	0.013238	2.84	17.95	22.07	1.05
AVAL	33	50.98	675.95	676.71	676.71	677.02	0.014647	2.45	20.83	34.84	0.76
AVAL	32	50.98	652.75	654.07	654.07	654.53	0.012896	3	16.99	18.78	1.32
AVAL	31	50.98	610.38	612.22	612.22	612.68	0.012719	3	16.97	18.48	1.84
AVAL	30	50.98	606.23	607.43	607.43	607.88	0.012902	2.97	17.15	19.07	1.2
AVAL	29	50.98	593.62	594.3	594.3	594.55	0.015579	2.2	23.19	47.87	0.68
AVAL	28	50.98	576.78	579.64	579.64	580.36	0.013474	3.76	13.55	9.49	2.86
AVAL	27	50.98	561.25	562.75	562.75	563.29	0.012478	3.26	15.64	14.47	1.5
AVAL	26	50.98	555.02	557.13	557.13	557.68	0.012576	3.26	15.62	14.56	2.11
AVAL	25	50.98	548.29	550.03	550.03	550.4	0.013854	2.7	18.9	25.44	1.74
AVAL	24	50.98	541.81	543.97	543.97	544.65	0.012505	3.68	14.11	10.68	2.16
AVAL	23	50.98	537.38	538.88	538.88	539.22	0.009446	1.61	20.02	29.8	1.5
AVAL	22	50.98	516.97	519.1	519.1	519.64	0.012405	3.23	15.77	14.78	2.13
AVAL	21	50.98	507.21	509.52	509.52	510.17	0.012444	3.6	14.18	10.79	2.31
AVAL	20	50.98	489.03	492.16		492.26	0.00122	1.4	36.4	20.76	3.13
AVAL	19	50.98	489.38	490.8	490.8	491.25	0.010267	3.01	17.24	19.55	1.42
AVAL	18	50.98	474.88	476.93	476.93	477.53	0.012236	3.41	14.93	12.53	2.05
AVAL	17	50.98	463.84	465.87	465.87	466.5	0.012535	3.52	14.49	11.67	2.03
AVAL	16	50.98	447.09	449.35	449.35	449.82	0.01352	3.03	16.83	18.41	2.26
AVAL	15	50.98	441.73	444.11	444.11	444.84	0.012474	3.8	13.46	9.39	2.38
AVAL	14	50.98	425.34	427.3	427.3	427.89	0.012518	3.4	15	12.97	1.96
AVAL	13	50.98	401	416.06		416.06	0	0.03	1781.57	87.79	15
AVAL	12	50.98	413.66	415.45	415.45	416	0.01284	3.29	15.51	14.39	1.79
AVAL	11	50.98	407.77	409.67	409.67	410.23	0.009389	3.39	15.9	14.75	1.9
AVAL	10	50.98	384.65	387.46	387.46	387.88	0.007782	3.08	19.17	23.17	2.81
AVAL	9	50.98	374.75	376.31	376.31	376.77	0.0129	2.99	17.05	18.75	1.56
AVAL	8	50.98	367.55	370.93	370.93	371.3	0.006173	2.82	20.98	28.46	3.38
AVAL	7	50.98	363.92	365.97	365.97	366.56	0.011085	3.44	15.11	12.84	2.05
AVAL	6	50.98	360.89	363.75		363.99	0.003029	2.2	23.18	12.15	2.86
AVAL	5	50.98	359.85	362.57		363.14	0.00761	3.4	15.56	8.93	2.72
AVAL	4	50.98	359.28	361.2	361.2	361.9	0.012728	3.68	13.84	10.05	1.92
AVAL	3	50.98	356.75	358.53	358.53	359.02	0.011309	3.11	16.62	18.38	1.78
AVAL	2	50.98	354.92	355.68	355.68	356.01	0.008066	1.99	21.36	30.97	0.76
AVAL	1	50.98	349.79	352.03	352.03	352.3	0.005691	2.62	25.09	43.94	2.24

These results confirm the need for additional preventive measures to protect people and property from the risk of flooding. Hence the need to install additional gutters to allow water to flow away during extreme floods, to raise public awareness of the risk of flooding, and to clean and maintain the Oued and its banks on an ongoing basis.

Figure 13. A/Flood hazard modelling map during the centennial return period of Oued Ziad; B/ the overflow of Oued Ziad on national road 27

Figure 14. Status of Oued Ziad and causal factors; A) Anarchic urbanization occupying the right bank of the Wadi; B) waste deposited in the minor bed of the Wadi

Conclusions

This study enables us to determine the overflow areas in the Oued Ziad watershed. Hydraulic modelling using HEC-RAS software allows us to simulate the 100-year flood and determine that protection against floods requires forecasting and prevention measures, which integrate the various factors likely to influence the risk of flooding. It is not only a question of mapping flood-prone areas, but also regulating land use, maintaining waterways and minimizing anthropogenic factors, and managing watersheds (Lahsaini & Tabyaoui, 2018).

This work has shown that flooding has also become a critical risk in Constantine. They must be taken seriously into account in development programs.

The use of geographic information systems (Arcmap) in conjunction with Hec Ras hydrological modelling software provides a powerful spatial decision support system that enables flood risk to be mapped effectively, providing a clear understanding of the extent and height of the water, as well as identifying the factors aggravating its dynamics for better management and maintenance of water resources, which are a non-renewable natural resource.

Funding

This research received no external funding.

Author contribution

Conceptualization, M.Y, and A.B; T.E. K, methodology, M.Y, A. B; formal analysis, M.Y; investigation, C.B, M.Y, F, G; writing – original draft preparation, M. Y, writing – review and editing, F. G, C. B, and M. Y.

All authors have read and agreed to the published version of the manuscript.

Conflicts of interest

The authors declare no conflict of interest.

References

Abdelshafy, M., & Mostafa, A. (2021). Flash Flood Modeling Using HEC-RAS (2D) model on Wadi Reem in the western region, Kingdom of Saudi Arabia. J. Egypt. Acad. Soc. Environ. Develop, 22(1), 17–32. www.jades.journals.ekb.eg

AL-Hussein, A. A. M., Khan, S., Ncibi, K., Hamdi, N., & Hamed, Y. (2022). Flood Analysis Using HEC-RAS and HEC-HMS: A Case Study of Khazir River (Middle East—Northern Iraq). Water (Switzerland), 14(22). https://doi.org/10.3390/w14223779

Awad, T., Bansode, M., Chavan, R., & Bhise, R. (2022). FLOOD MANAGEMENT BY USING HEC-RAS SOFTWARE. In International Research Journal of Modernization in Engineering Technology and Science. Vol 04, Issue 06. www.irjmets.com.

Bekhira, A., Habi, M., & Morsli, B. (2019). Management of hazard of flooding in arid region urban agglomeration using HEC-RAS and GIS software: The case of the Bechar's city. Journal of Water and Land Development, 42(1), 21–32. https://doi.org/10.2478/jwld-2019-0041

Benabbas, C. (2006). Mio-Plio-Quaternary evolution of the continental basins of north-eastern Algeria: contribution of photogeology and morpho-structural analysis). Ph.D thesis. University of Mentouri, Constantine, Algeria. 256 p. (in French)

Benabbas. C., Bouedja, F., & Benzid, Y. (2011). Néotectonique, déformation du relief et risque sismique dans la région de Constantine. IV éme Colloque International « directions contemporaines dans l'étude du territoire-Gestions du territoire, des aléas et de la ville » ; Bucarest, 22-27 Juin.

Bilașco, Ș., Hognogi, G. G., Roșca, S., Pop, A. M., Iuliu, V., Fodorean, I., ... & Sestras, P. (2022). Flash flood risk assessment and mitigation in digital-era governance using unmanned aerial vehicle and GIS spatial analyses case study: small river basins. Remote Sensing, 14(10), 2481

Brunner, G. W. (2016). HEC-RAS river analysis system user's manual version 5.0. US Army Corps of Engineers, 962. http://www. hec.usace.army.mil/software/hec-ras/downloads.aspx

Buta, C., Mihai, G., & Stănescu, M. (2017). Flash floods simulation in a small drainage basin using HEC-RAS hydraulic model. Ovidius University Annals of Constanta - Series Civil Engineering, 19(1), 101–118. https://doi.org/10.1515/ouacsce-2017-0009.

Costache, R., Popa, M. C., Bui, D. T., Diaconu, D. C., Ciubotaru, N., Minea, G., & Pham, Q. B. (2020). Spatial predicting of flood potential areas using novel hybridizations of fuzzy decisionmaking, bivariate statistics, and machine learning. Journal of Hydrology, 585, 124808.

Derdour, A., Bouanani, A., & Babahamed, K. (2017). Hydrological modeling in semi-arid region using HEC-HMS model. case study in Ain Sefra watershed, Ksour Mountains (SW-Algeria). Journal of Fundamental and Applied Sciences, 9(2), 1027. https://doi.org/10.4314/jfas.v9i2.27

Gao, P., Gao, W., & Ke, N. (2021). Assessing the impact of flood inundation dynamics on an urban environment. Natural Hazards, 109(1), 1047–1072. https://doi.org/10.1007/s11069-021-04868-6

Grecu, F. (2016). Hazarde si riscuri naturale, Editura Universitara, Bucuresti, ISBN 978-606-28-0392-6, https://doi 10.5682/9786062803926, 354 p

Grecu, F., Zaharia, L., Ioana-Toroimac, G., Armas, I. (2017), Floods and flash-floods related to river channel dynamics in vol. Radoane M., Vespremeanu Stroe F. eds, Landform dynamics and evolution in Romania, Springer Verlag, p. 821 – 844, ISBN 978-3-319-32589-7 DOI 10.1007/978-3-319-32589-7_33

Grecu, F. (2018 a). Geomorphologic Hazard in Romania.Typology and Areal distribution In Water Management and the Environnment. Case Studies ed. Martina Zelenakova, Springer International Publ, https://doi.org 10.1007/978-3-319-79014 -5_5, p.85 - 99.

Grecu, F. (2018 b). Geomorfologie dinamică pluviofluvială. Teorie şi aplicaţii, Editura Universitară, 480 p., 264 figuri, 70 tabele, 503 titluri bibliografice, index de termini, simboluri

Grecu, F., Benabbas, C., Teodor, M., Yakhlefoune, M., Săndulache, I., Manchar, N., Vișan, G. (2021). Risk of Dynamics of the River Stream in Tectonic Areas. Case studies: Curvature Carpathian - Romania and Maghrebian Chain - Algeria. Forum geographic. XX(1), 5-22. doi:10.5775/fg.2021.021.i

Jalilzadeh, A., & Behzadi, S. (2020). Flood Mapping and Estimation of Flood Water-Level Using Fuzzy Method and Remote Sensing Imagery (Case Study: Golestan Province, Iran). Vol XIX, Issue 2, pp. 165-174 http://dx.doi.org/10.5775/fg.2020.062.d

Kashfy, M., Aminuddin, A., Nor, Z., Ngai, CW. (2020). HEC-RAS One-Dimensional Hydrodynamic Modelling for Recent Major Flood Events in Pahang River. In: Mohamed Nazri, F. (eds) Proceedings of AICCE'19. AICCE 2019. Lecture Notes in Civil Engineering, vol 53. Springer, Cham. https://doi.org/10.1007/978-3-030-32816-0_83

Kim, V., Tantanee, S., & Suparta, W. (2020). Gis-based flood hazard mapping using hec-ras model: A case study of lower mekong river, cambodia. Geographia Technica, 15(1), 16–26. https://doi.org/10.21163/GT_2020.151.02

Lahsaini, M., & Tabyaoui, H. (2018). Modelisation Hydraulique Mono Dimensionnel Par HEC RAS, Application Sur L'oued Aggay (Ville De Sefrou). European Scientific Journal, ESJ, 14(18), 110. https://doi.org/10.19044/esj.2018.v14n18p110

LASRI, M. (2019). Flood hazard mapping in the town of Fez: From hydrological modeling to hydraulic simulation. Environmental and Water Sciences, public Health and Territorial Intelligence Journal, 3(2), 113-123. https://doi.org/10.48421/IMIST.PRSM/ewash-ti-v3i2.16083

Mătreaţă, M., Mătreaţă, S., Costache, R.-D., Mihalcea, A., & Manolache, A. V. (2016). Assessment of Flash Flood Hazard Maps Using Different Threshold Values and Indices Methods. Forum Geografic, XV(Suppl. 2), 49–54. https://doi.org/10.5775/fg.2016.059.s.

Nkwunonwo, U. C., Whitworth, M., & Baily, B. (2020). A review of the current status of flood modelling for urban flood risk management in the developing countries. Scientific African, 7, e00269.

Sunilkumar, P., & Vargheese, K. O. (2017). Flood modelling of mangalam river using GIS and HEC-RAS. Department of Civil Engineering, Government Engineering College, Thrissur, India.

Ongdas, N., Akiyanova, F., Karakulov, Y., Muratbayeva, A., & Zinabdin, N. (2020). Application of hec-ras (2d) for flood hazard maps generation for yesil (ishim) river in kazakhstan. Water (Switzerland), 12(10), 1–20. https://doi.org/10.3390/w12102672

Prăvălie, R., & Costache1, R. (2014). The analysis of the susceptibility of the flash-floods' genesis in the area of the hydrographical basin of Bâsca Chiojdului river. Forum geografic. Studii și cercetări de geografie și protecția mediului XIII(1), 39–49. https://doi.org/10.5775/fg.2067-4635.2014.089.i

Rai, P. K., & Mohan, K. (2014). Remote Sensing data & GIS for flood risk zonation mapping in Varanasi District, India. Forum Geografic, XIII(1), 25–33. https://doi.org/10.5775/fg.2067-4635.2014.041.i

Tegenie, E. B., & Berhe, F. T. (2021). Floodplain Inundation Modeling and Mapping for Geray River: Nile Basin, Ethiopia. Vol (3). Issue (6). https://doi.org/10.3759/jowrem.v6i3.3057

Thapa, S., Shrestha, A., Lamichhane, S., Adhikari, R., & Gautam, D. (2020). Catchment-scale flood hazard mapping and flood vulnerability analysis of residential buildings: The case of Khando River in eastern Nepal. Journal of Hydrology: Regional Studies, 30. https://doi.org/10.1016/j.ejrh.2020.100704

Uca, Lamada, M., Nyompa, S., & Haris, N. A. (2022). Morphometry and Topographic Wetness Index Analysis for flood inundation mapping in Mata Allo watershed (South Sulawesi, Indonesia). Forum Geografic, 21(2), 133–145. https://doi.org/10.5775/fg.2022.105.d

Xafoulis, N., Farsirotou, E., Kotsopoulos, S., & Alamanis, N. (2022). Flood hazard assessment in a mountainous river basin in Thessaly, Greece, based on 1D/2D numerical simulation. Energy Nexus, 8, 100142. https://doi.org/10.1016/j.nexus.2022.100142

Yalcin, E. (2020). Assessing the impact of topography and land cover data resolutions on twodimensional HEC-RAS hydrodynamic model simulations for urban flood hazard analysis. Natural Hazards, 101(3), 995-1017.

Yerramilli, S. (2012). A Hybrid Approach of Integrating HEC-RAS and GIS Towards the Identification and Assessment of Flood Risk Vulnerability in the City of Jackson, MS. American Journal of Geographic Information System, 1(1), 7–16. https://doi.org/10.5923/j.ajgis.20120101.02

Zegait, R., Şen, Z., Pulido-Bosch, A., Madi, H., & Hamadeha, B. (2022). Flash Flood Risk and Climate Analysis in the Extreme South of Algeria (the Case of In-Guezzam City). Geomatics and Environmental Engineering, 16(4), 157–185. https://doi.org/10.7494/geom.2022.16.4.157

Zellou B, Rahali H (2016) Assessment of reduced-complexity landscape evolution model suitability to adequately simulate flood events in complex flow conditions. Nat Hazards 86 (1):1–29

Forum geografic. Studii și cercetări de geografie și protecția mediului
Volume **XXII**, Issue **1** (**June 2023**), pp. **44-53;** DOI: **10.5775/fg.2023.073.i**

Determination for automated land-use / land cover change detection of Keti Bunder, Indus Delta, Pakistan, by using satellite remote sensing techniques

Zia ur REHMAN[1,*], Asif GUL[1], Jamil Hasan KAZMI[1]

[1] Department of Geography, University of Karachi, 75270, Pakistan
* *Corresponding author*: ziarockies86@gmail.com

Received on 03-01-2023, reviewed on 14-03-2023, accepted on 03-04-2023

Abstract

The Land use/Land cover (LULC) has a substantial role in planning and monitoring natural resource utilization, in the framework of the ongoing surge in human demands in the current ecosystem. Satellite remote sensing provides modern methods for locating and mapping Land use/Land cover patterns and their spatial changes. This paper discusses the evaluation of the LULC classes characteristic of Keti Bunder during the years 2015 and 2020, by using satellite remote sensing; the paper also uses Geo-informatics to study and investigate the temporal LULC variations that occurred over time. According to the empirical findings, there have been significant spatial changes, with less dry mudflats and unoccupied land overall. In comparison, the findings of the research point to inter-conversion of the area between LULC classes, i.e. mangrove areas, turbid water, wet mudflat, dry mudflat and barren land/vacant land. Overall, these geographical alterations show that the environment has been significantly impacted due to recent extreme weather events in the region.
Keywords: *GIS, satellite remote sensing, environment, mangrove, ecology*

Introduction

Studies on the patterns of land use and land cover have made extensive use of Satellite Remote Sensing technology. It is essential for locating and measuring various physical characteristics on the planet's surface. Digital mapping with Geomatics enables the collection of recurring data over a predetermined period, has a digital format that can be processed by computers, and has locational precision (Jensen, 1996; Rehman et al., 2016). Satellite Remote Sensing (SRS) offers several spectral and synoptic evaluations. It is also useful for observing coastal changes and land degradation, as well as sea tides, wave currents, shallow water, suspended materials, mudflats, wetlands, mangroves, vegetation, and land degradation (SCCDP, 2013; Rehman & Kazmi, 2018).

To observe environmental changes, Satellite Remote Sensing (SRS) and Geographic Information System (GIS) technology offer a set of potent tools that allow us to perform spatial analysis using both spatial and non-spatial information (Osei et al., 2006; Ibrahim, 2008; Tariq et al., 2020). These tools are used in environmental monitoring studies, notably for mapping the spatial distribution of biophysical restrictions on the surfaces that significantly affect climate (Henderson, 1999). SRS and GIS technologies are now widely used. Comprehensive monitoring of LULC changes is provided by SRS in conjunction with GIS and GPS. In Satellite Remote Sensing, comparing two or more satellite pictures is a typical practice to find LULC changes.

Change detection commonly uses pixel-to-pixel comparison and post-classification comparison (Nelson et al., 1983; Martin, 1989; Green et al., 1994; Raza et al., 2020). The first method (pixel-by-pixel) combines satellite images taken at various times and dates. Image classification is not involved. In these studies, the pixel-to-pixel comparison is typically used. In the post-classification detection technique, two or more classed satellite images from various times and dates are examined (Pylon, 1988; Fung & Zhang, 1989; Johnson & Howarth, 1989; Frihy et al., 1998).

This approach is the most widely used and it is regarded as one of the most effective approaches to identify LULC alterations (Jensen et al., 1993; Dewidar K. M., 2004). Human activities that have an impact on a specific area of land can be linked to changes in land cover, whereas changes in land usage are directly impacted by changes in land cover (Jensen, 2007; Abbas, 2012; Jackson & Attia, 2013). The changes in LULC are related to various environmental and landscape characteristics of the land surface, such as the land, water quality, and air resources, as well as the living conditions, method, practices, and functions (Jackson & Attia, 2013).

Keti Bunder is situated in the deltaic zone of the Indus River, at about 200 km southeast of the port city of Karachi, Sindh. Administratively, Keti Bunder is a taluka (tehsil) of the Thatta district, it is spread over 60,969 hectares and consists of 42 *dehs* (clusters of villages). Historically, Keti Bunder was the main port city of this

part of the world, connecting the Indus Valley with international sea trade routes before the dams and barrages were constructed over the Indus River, which caused the insufficient discharge of the Indus waters into the sea (delta zone).

This area has four major creeks, i.e. the Chann, the Hajamro, the Khobar, and the Kangri, as well as numerous small creeks. This area has been exposed to sea intrusion, which has caused severe environmental degradation and loss of livelihood opportunities for the locals. WWF mentioned that the sea has engulfed around 46,137 hectares in 28 *dehs* of Keti Bunder (WWF Pakistan, 2004). The progressive seawater intrusion and freshwater scarcity in the rivers of these lands have caused resettlements and migration flows in the study area, where the smaller villages had to shift their location more than once in the last 70 years because of the increased salinity in their agricultural land. The study region for this research is Keti Bunder, Sindh (Figure 1).

For many decades, in the Indus Delta region, the mangrove ecosystem has been adversely affected by the acute freshwater scarcity downstream of the last barrage on the Indus River and by water diversion for inland agriculture in upstream areas, as well as by coastal urbanization, population increase and industrialization and pollution. Overall, out of eight mangrove species previously found in the Indus Delta, four have been completely depleted; currently, three of the remaining four are on the verge of extinction (*Rhizophora mucronata* 8%, *Aegiceras corniculatum* 1.5% and *Ceriops tagal* 0.5%), whereas *Avicennia* covers 90% of mangroves in this region (Figure 1).

The main objectives of the paper are the following:

1. to extract the Keti Bunder land use/land cover classification for the years 2015 and 2020, by using Satellite Remote Sensing;

2. to explore temporal land-use / land cover (LULC) changes of Keti Bunder between 2015 and 2020, by using Geo-informatics;

3. to investigate the LULC classes in relation to ground realities.

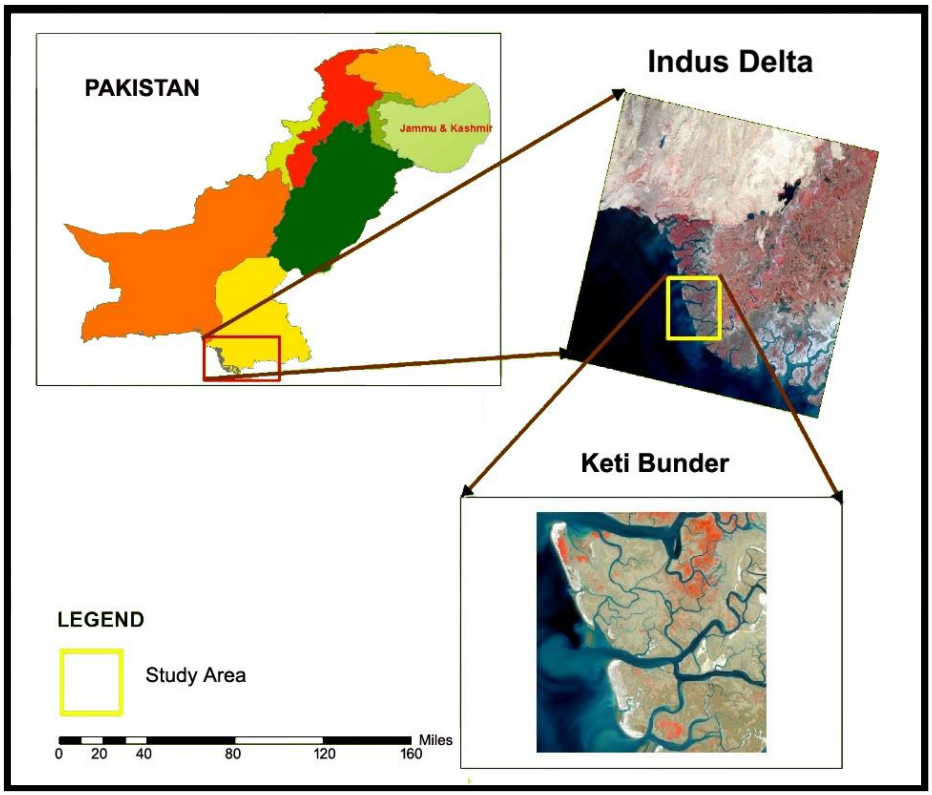

Figure 1: Location of the study area

Data and methods

Data

This study particularly attempts to identify and interpret the land use/land cover changes over five years (2015 - 2020 period) through satellite remote sensing and ground-truthing. The methodological framework is shown in Figure 2. For this, Landsat-8 OLI/TIRS datasets of 21-11-2015 and 18-11-2020 were extracted from the online archives of USGS Earth Explorer, which covers the study area (path 152 and row 043). There are nine (1-9) spectral bands with 30 m spatial resolution in the Landsat-8 OLI dataset, while Landsat-8 TIRS dataset has two spectral bands (10 and 11), with 100 m spatial resolution.

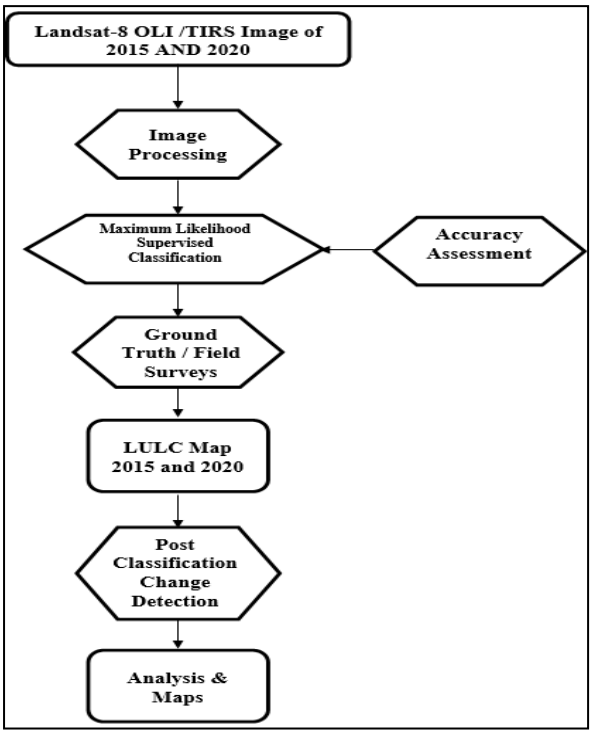

Figure 2: Methodological framework

Techniques and analysis

Maximum likelihood classification

In satellite image classification, there are three main classification techniques: supervised classification, unsupervised classification, and object-based image classification. The supervised classification was chosen for this study, where particularly the Maximum Likelihood Classifier (MLC) algorithm was used. This approach has been widely applied by many scholars for the classification of medium-resolution satellite datasets (Ratnaparkhi et al., 2016; Zaidi et al., 2017; Zubair & Javed, 2018).

Based on the visual interpretation of land use features on the satellite image and Google Earth, the sample polygons were marked as training areas. Based on their spectral signature, seven major LULC classes were delineated, namely dense mangrove, sparse mangrove, barren/vacant land, wet and dry mudflat, deep water and turbid water. The maximum likelihood of unknown pixels in each class would be computed and assigned to these seven main land use classes.

Accuracy assessment

The satellite image classification process is followed by accuracy assessment, which evaluates to what degree the ground features are truly classified to the corresponding LULC class (Foody, 2002). The ERDAS imagine software and its toolset, i.e. the accuracy assessment tool of the supervised classifier, have been used to perform this procedure. Using stratified random sampling approach, random reference points were generated (i.e. 187 in 2015 and 294 in 2020). The associated class of the point on the classified image was matched with the visually interpreted point on Google Earth. The kappa statistics and error matrix for both 2015 and 2020 classified images were generated from ERDAS Imagine. In the error matrix, the rows denote the points where the pixels are classified to certain LULC classes and the columns show the LULC classes recognized by the user from the referenced data.

The diagonal cells show the correctly recognized pixels for each land use class of classified and reference data. The pixels incorrectly designated to the right LULC class do not occur in diagonal and indicate inaccuracy between reference and classified data.

Ground survey

Field surveys were conducted to assess the socio-economic conditions of the selected area through interviews; this went along with the GPS survey of ground features for image classification.

Change detection

Because of its cost-effectiveness and accessibility of high temporal resolution, RS and GIS-based change detection methods are widely used across the Globe.

Some researchers have used the post-classification comparison technique, employing maximum likelihood supervised classification, with overall greater classification accuracy (Torahi & Rai, 2011; Muttitanon & Tripathi, 2005).

The classification of satellite images and the comparison of the related individual classes allow for the spatial identification of the locations where the change occurred.

Results and discussion

Kappa coefficient and overall accuracy for the 2015 and 2020 images

The accuracy assessment was performed for the LULC classification maps of 2015 and 2020. In the case of the 2015 LULC map, 187 points were randomly selected. The overall kappa statistics value for the 2015 LULC map was found at 0.9280, whereas the overall accuracy was computed at 90.67% (Table 1). The producer's accuracy for each LULC class was found to be equal to or higher than 85.75% and the user's accuracy for each LULC class was observed to be equal to or higher than 76.42%.

In the case of the 2020 LULC classification, there were selected 294 random points. The overall kappa statistics and LULC classification accuracy were found to be 0.9670 and 96.82%, respectively (Table 2). The producer's accuracy of all individual LULC classes was higher than 92%. The user's accuracy of all LULC classes was more than 90%, except for the dense mangrove (87.50%).

Overall, in both LULC classification maps, the accuracy of each LULC class was found to be satisfactory. The general accuracy results and kappa coefficient for the LULC classification maps of 2015 and 2020 are presented in Tables 1 and 2, respectively.

Table 1. The accuracy assessment of classified image 21-11-2015

S. no.	LULC Class Name	Producers Accuracy (%)	Users Accuracy (%)	Kappa Atatistics
1	Dense mangrove	99.20	99.54	0.9017
2	Sparse mangrove	93.71	88.00	0.7378
3	Wet mudflat	87.50	100.00	1
4	Dry mudflat	100.00	82.61	0.8009
5	Barren/Vacant Land	85.75	76.42	0.8504
6	Turbid water	100.00	100.00	1
7	Deepwater	94.00	98.15	0.8352
Overall Classification Accuracy = 90.67%. Overall Kappa Statistics = 0.9280				

Table 2. The accuracy assessment of classified image 18-11-2020

S. no.	LULC Class Name	Producers Accuracy (%)	Users Accuracy (%)	Kappa Statistics
1	Dense mangrove	100.00	87.50	0.8689
2	Sparse mangrove	100.00	100.00	1
3	Wet mudflat	92.31	92.31	0.9069
4	Dry mudflat	96.43	90.00	0.877
5	Barren/Vacant Land	100.00	100.00	1
6	Turbid water	100.00	100.00	1
7	Deepwater	100.00	94.74	0.9402
Overall Classification Accuracy = 96.82%. Overall Kappa Statistics = 0.9670				

Land use/land cover classification

Land use/land cover pattern of Keti Bunder in 2015

The LULC classification map of 2015 generated from the Landsat-8 data set is depicted in Figure 3. The largest category was found to be the turbid water, which covered 14,265.7 ha (as shown in Figure 4) (31.19% of the total area), whereas the deep water accounted for 2,417.31 ha (5.28%), and the wet mudflat for 12,631.2 ha (27.61%). The sparse mangrove accounted for 5,324.76 ha (11.64%) and the area under dense mangroves covered 197.55 ha (0.43%).

On the other hand, the barren land/vacant land covered 6,508.8 ha (14.23%) and the dry mudflats, including Goths and villages, accounted for 4,398.84 ha (9.62%).

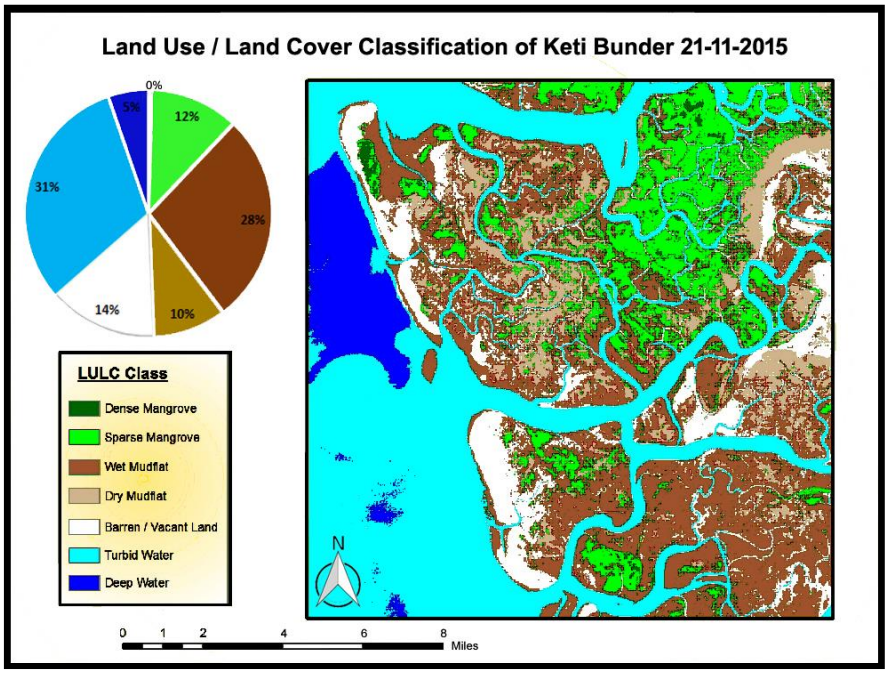

Figure 3: LULC map of the study area in 2015

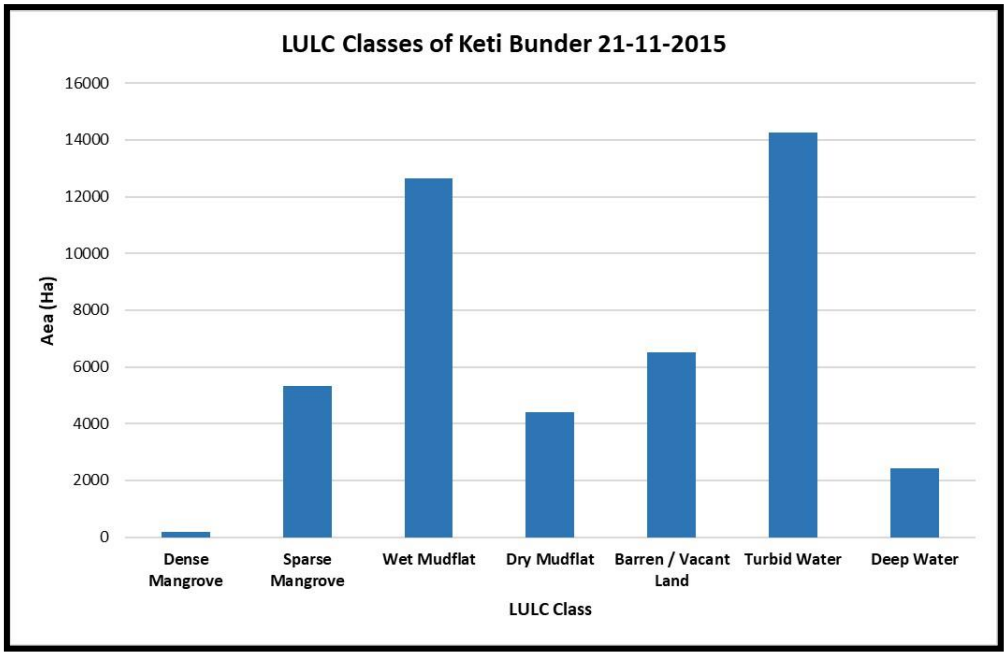

Figure 4: LULC characteristics of Keti Bunder in 2015

Land use/land cover pattern of Keti Bunder in 2020

According to the 2020 LULC classification dataset (Figure 5), the turbid water accounted for 21,044.20 ha (as shown in Figure 6), i.e. 46% of the study area, the deep water covered over 3,860.01 ha (8.44%), while the area under wet mudflat accounted for 487.80 ha (1.07%).

The sparse mangroves covered 12,113.10 ha (26.48%), while the dense mangroves covered 335.61 ha (0.73%). In the same year, the dry mudflat covered 7,210.80 ha (15.76%) and the barren/vacant land accounted for 692.73 ha (1.51%).

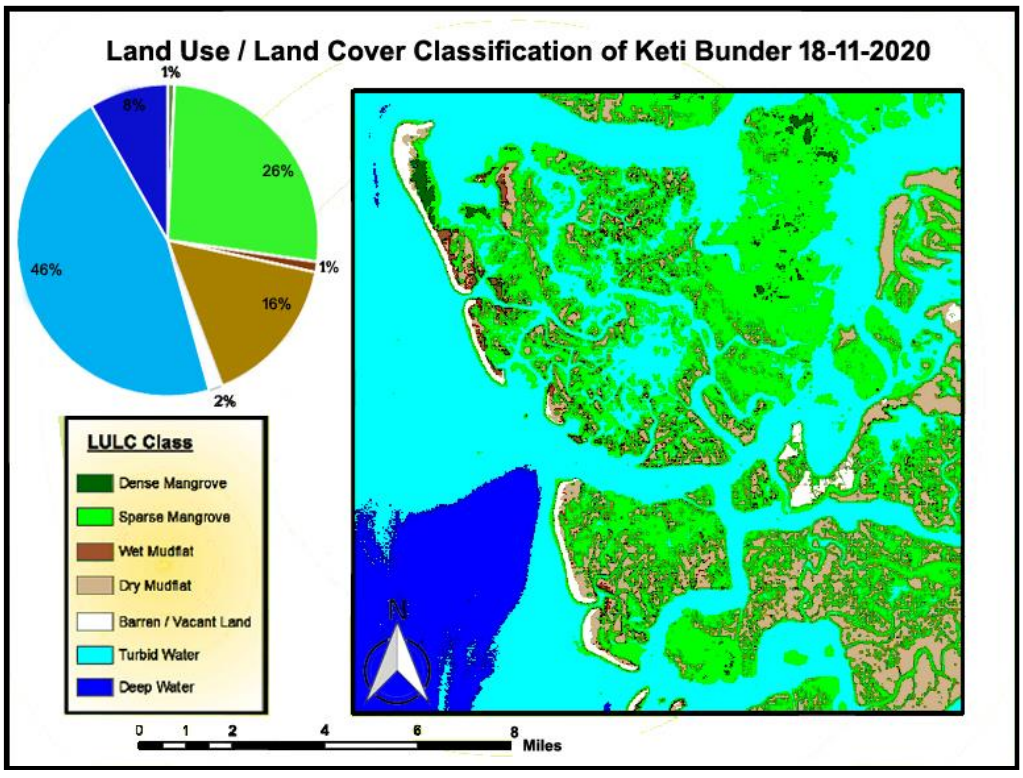

Figure 5: LULC map of the study area in 2020

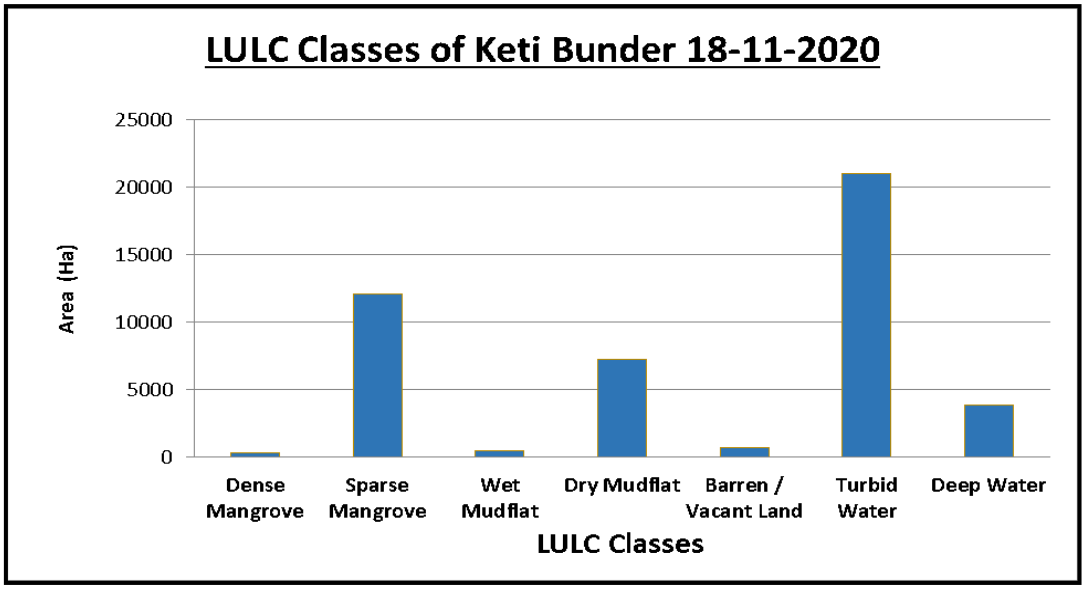

Figure 6: LULC characteristics of Keti Bunder in 2020

LULC classification comparative analysis and change detection between 2015 and 2020

The area under the LULC classes and its changes between 2015 and 2020 are presented in Table 3, Figure 7, and Figure 8. During these five years, significant changes were observed among the LULC classes within the area under study. The wet mudflat and the barren/vacant land use categories revealed a considerable decrease in their covered area, while the mangroves (dense and sparse) and the water bodies, particularly the turbid water category, exhibited an increase.

Dense mangrove

The area under dense mangroves increased from 197.55 ha in 2015 to 335.61 ha in 2020, representing a net increase of 138.06 ha (shown in Table 3, Figure 7, and Figure 8). Figure 8 shows that the dense mangrove converted to sparse mangrove represents about 61 ha (0.13%). At the same time, the dense mangrove area that shifted to barren/vacant land represented about one ha (0.01%). Some dense mangrove was converted to dry mudflat.

Sparse mangrove

The area under sparse mangroves increased from 5,324.76 ha in 2015 to 12,113.1 ha in 2020, which represents a net increase of 6,788.34 ha (shown in Table 3, Figure 6, and Figure 7). Figure 8 and Figure 9 show the sparse mangrove area conversion to other LULC classes. About 72 ha (0.16%) were converted to dense mangroves, 23 ha (0.05%) to wet mudflat, 778 ha (1.70%) to turbid water, 107 ha (0.23%) to dry mudflat, while about 5 ha (0.01%) shifted to barren/vacant land.

Wet mudflat

The area under the wet mudflat decreased significantly about 12,143.40 ha, from 12,631.20 ha (in 2015) to 487.8 ha (in 2020) (Table 3, Figure 8, and Figure 9). It is important to mention the conversion of wet mudflats to certain other LULC categories, i.e. about 7,392 ha (16.16%) to turbid water, 4,408 ha (9.64%) to sparse mangroves, 599 ha (1.31%) to dry mudflat, while some 5 ha (0.01%) of wet mudflats shifted to barren/vacant land.

Dry mudflat

The area under dry mudflat increased significantly, namely with circa 2,811.96 ha, from 4,398.84 ha (in 2015) to 7,210.80 ha (in 2020). Figure 9 shows the conversion of dry mudflat into other LULC classes. About 2,686 ha (5.87%) of dry mudflat were converted to wet mudflat, 1411 ha (3.08%) to sparse mangroves, and 58 ha (0.13%) to wet mudflat.

Barren/Vacant land

The area under barren/vacant land decreased from 6,508.80 ha in 2015 to 692.73 ha in 2020, which represents a net decrease of 5,816.07 ha. This decrease is due to the rise in the plantation of mangroves.

Figure 9 shows the area under barren/vacant land that was converted to other LULC classes. About 2,257 ha (4.93%) were converted to dry mudflat, 1,671 ha (3.65%) to sparse mangrove cover, 1,591 ha (3.48%) to turbid water, 212 ha (0.46%) to wet mudflat, and 128 ha (0.28%) to dense mangrove.

Turbid water

The area under turbid water increased around 6,778.50 ha, from 14,265.70 ha (in 2015) to 21,044.20 ha (in 2020). Figure 9 shows the area under turbid water that was converted to other LULC classes. About 3,738 ha (8.17%) were converted to deep water, while 223 ha (0.49%) shifted to sparse mangrove cover.

Table 3: The area under each LULC class in the 2015 and 2020 data sets, along with changes in the area of each LULC class over the five years

S. no.	LULC classes	2015 Area (hectares)	2020 Area (hectares)	Change (2015-2020) Area (hectares)
1	Dense mangrove	197.55	335.52	138.15
2	Sparse mangrove	5324.76	12113.1	6788.34
3	Wet mudflat	12631.2	487.8	-12143.4
4	Dry mudflat	4398.84	7210.8	2811.96
5	Barren/vacant Land	6508.8	692.73	-5816.07
6	Turbid water	14265.7	21044.2	6778.5
7	Deep water	2417.31	3860.01	1442.7
TOTAL		45744.16	45744.16	

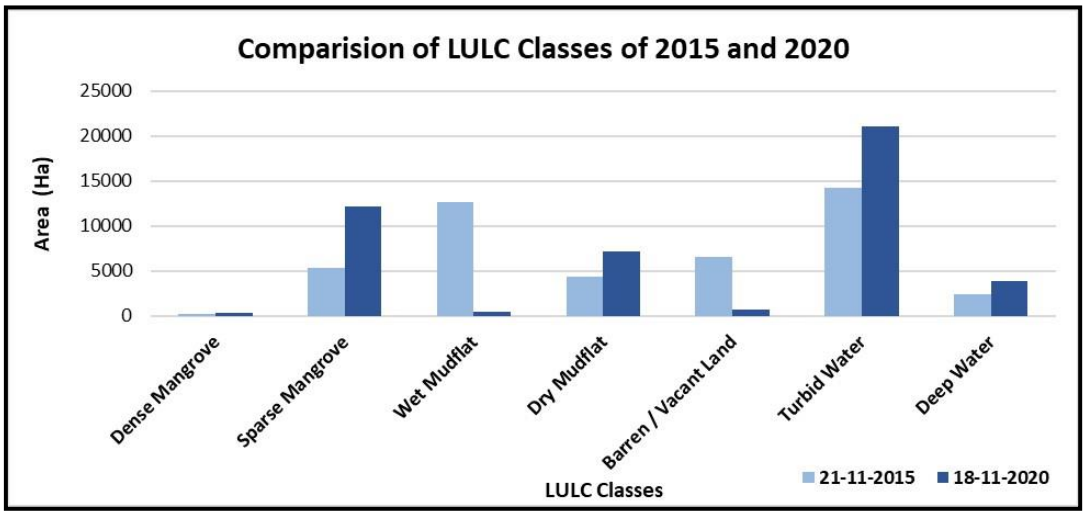

Figure 7: Comparison of LULC classes specific to different years

Deepwater

As shown in Figure 8, the area under deep water increased 1,442.70 ha (from 2,417.31 ha in 2015 to 3,860.01 ha in 2020). Around 2,298 ha (5.02%) of the area underwater shifted to the turbid water class.

The field surveys revealed that certain drastic changes in the socio-economic conditions have been triggered by climate change impacts associated with the LULC transformations in the Indus Delta regions. The agricultural land, mangroves and biodiversity of this region face severe conditions. During the survey, the responses regarding the last few decades revealed that red rice used to be grown in the area, but it has almost become non-existent at present. Apart from rice, this area was also suitable for producing different types of fruits, i.e. bananas, coconuts, and melons. Over the years, because of a number of factors, among which the reduced water flows of rivers and the sea intrusion, which caused water logging and salinity, it was estimated that more than 117,823 acres of agricultural land have been affected.

Because of climate changes, the Indus Delta region is more prone to floods, droughts, and cyclones. Keti Bunder is also vulnerable to cyclones and tsunamis. In the last 30 years, because of global warming, the intensity and frequency of cyclones have particularly increased. The migration within local communities is obvious over time, this also being an effect of extreme weather incidents, which may increase in the coming few years because of the impacts of storms, rising sea levels, and other expected effects of climate change (Gowdy & Salman, 2010). The climate projection indicates that at least a 5°C rise will occur in the Indus Delta by the end of the 21st century (Rehman et al., 2015).

In the year 2020, the rainfall was 38% above the average precipitation specific to Pakistan (the 4th wettest year since 1961), while Sindh received 105.5% additional annual rain as compared to its average rainfall.

Particularly in August, the monsoon rains were the highest ever recorded, as 363% of the average rain fell during this month. The seasonal rain from July to September accounted for 332 mm, which was 148% more than the seasonal average of 133 mm. This led to floods along the Indus River in August and September. The same has been reflected in the inter-conversion of land cover classes, where a significant area under wet mudflats was converted into turbid water, while a substantial proportion of barren/vacant land has been transformed into sparse mangroves, turbid water, and dry mudflats. In the case of mangroves, a significant proportion of dry and wet mudflats contributed 3% and 9.6% of their respective area in 2015 to the sparse mangroves.

For the last decade, on administrative grounds, the Provincial Forest Department and nongovernmental organizations have been aggressively working for the plantation and conservation of mangroves in the Indus Delta region (IUCN, 2018; WWF Pakistan, 2021).

Generally, these geographical alterations in the Indus Delta area show that the environment has been significantly impacted because of recent extreme weather events in the region.

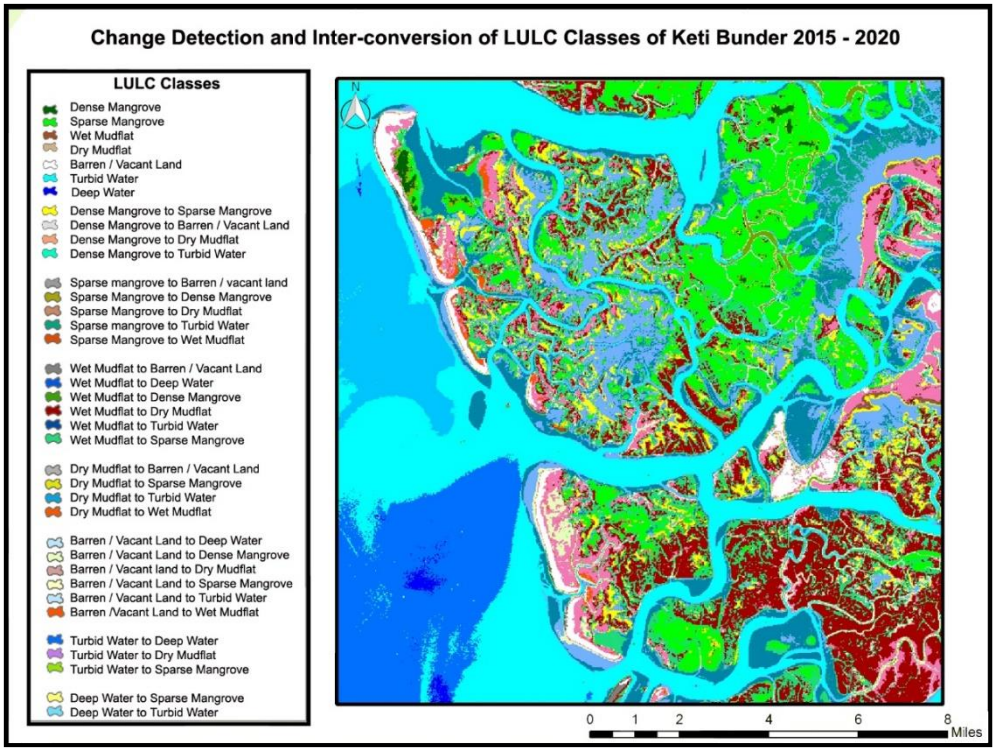

Figure 8: Change detection and Inter-conversion of LULC Classes in Keti Bunder between 2015 and 2020

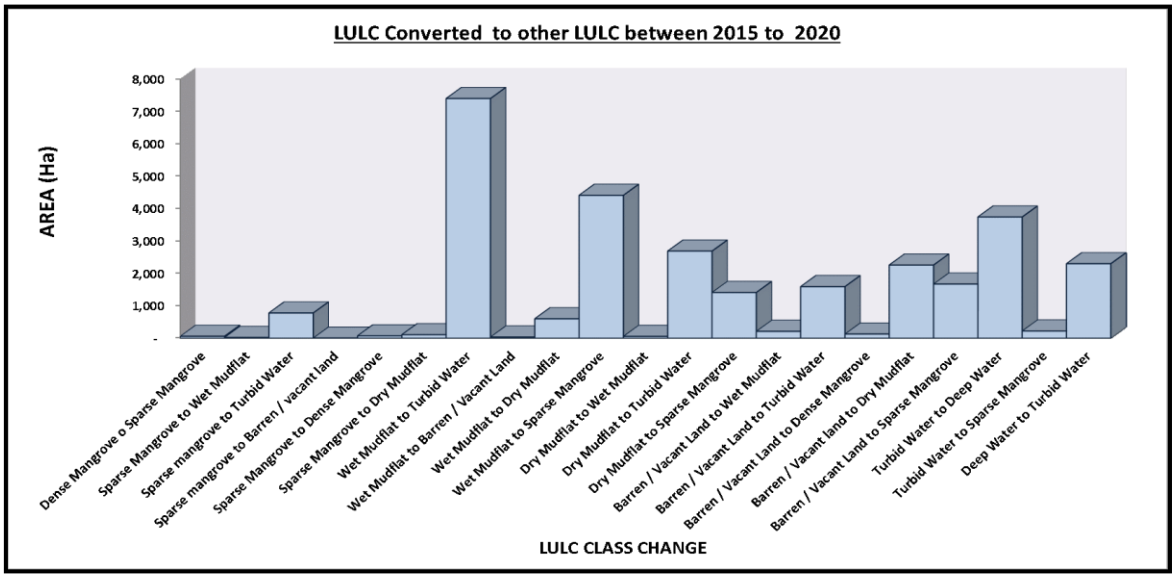

Figure 9: Post-classification changes of LULC classes between 2015 and 2020

Conclusions

This work has quantified the spatial variations in LULC between 2015 and 2020, based on GIS and remote sensing methods. The methods used in this investigation are reasonably straightforward and inexpensive.

The multi-temporal satellite imagery has been used in order to determine the extent of land use changes in Keti Bunder. The overall classification accuracy for the present analysis was determined to be within acceptable limits. In the post-classification comparison, significant changes were seen in the LULC of the region under study, during the research period.

Over the course of these five years, an increase in the area under thick mangroves, sparse mangroves, murky water, and deep water was observed, while the effects of extreme weather events in recent months have also been noticed. Mangrove species were abundant, but now only four species survived because of the lack of fresh water, along with the sea water intrusion. The findings could be used in the ecological management and planning.

Acknowledgments

We would like to express our sincere gratitude to Dr. Imran Ahmed Khan (Assistant Professor Department of Geography, University of Karachi) for his valuable feedback and support throughout the research process.

Authors contributions

Dr. Zia ur Rehman conceived the original idea. While Dr. Zia ur Rehman, Dr. Asif Gul and Prof. Dr. Jamil Hasan Kazmi contributed to the design and implementation of the research, to the analysis of the results and the writing of the manuscript. Prof. Dr. Jamil Hasan Kazmi supervised the project.

Funding

This research received no external funding.

Declaration of interests

We declare that this submission has not been published elsewhere, nor is under consideration for publication and there is no conflict of interest among the authors before submitting it in this reputed journal.

References

Abbas, I. I. (2012). An assessment of land use/land cover changes in a section of Niger Delta, Nigeria. *Frontiers in Scienc*e, 2(6), 137-143. DOI:10.5923/j.fs.20120206.02

Dewidar, K. M. (2004). Detection of land use/land cover changes for the northern part of the Nile Delta (Burullus region), Egypt. *International Journal of Remote Sensing*, 25(20), 4079-4089. DOI:10.1080/01431160410001688312

Foody, G. M. (2002). Status of land cover classification accuracy assessment. *Remote Sensing of Environment*, 80(1), 185–201. https://doi.org/10.1016/S0034-4257(01)00295-4

Frihy, O. E., Dewidar, K. M., Nasr, S. M., & El Raey, M. M. (1998). Change detection of the northeastern Nile Delta of Egypt: shoreline changes, Spit evolution, margin changes of Manzala lagoon and its islands. *International Journal of Remote Sensing*, 19(10), 1901-1912. https://doi.org/10.1080/014311698215054

Fung, T., & Zhang, Q. (1989). Land use change detection and identification with Landsat digital data in the Kitchener–Waterloo area. *Remote Sensing and Methodologies of Land Use Change Analysis*, 135-153

Gowdy, J. M., & Salman, A. (2010). Institutions and ecosystem functions: the case of Keti Bunder, Pakistan. In *Valuation of Regulating Services of Ecosystems* (pp. 213-233). Routledge

Green, K., Kempka, D., & Lackey, L. (1994). Using remote sensing to detect and monitor land-cover and land-use change. *Photogrammetric Engineering and Remote Sensing*, 60(3), 331-337

Henderson, F. M. (1999). Mapping coastal ecosystems over a steep development gradient using C-CAP protocols. *International Journal of Remote Sensing*, 20(4), 727-744. https://doi.org/10.1080/014311699213163

Ibrahim, A. A. (2008, November). Using remote sensing technique (NDVI) for monitoring vegetation degradation in semi-arid lands and its relationship to precipitation: Case study from Libya. In *The 3rd International Conference on Water Resources and Arid Environments* (pp. 16-19)

Jackson, M. & Attia, F. (2013). Land use and Land cover Change Analysis Using Satellite Remote Sensing: A case Study of the Upper Niger Delta Region of Rivers. *European Journal of Geoengineering*, Voll.11 2013, ISSN (paper) 2668-3296 ISSN (online) 2668-3598. www.BellPress.org

IUCN. (2018, April). Sindh Forest Department brings pride to nation by planting Maximum Number of Mangroves for 3rd Guinness World Record. Retrieved from The International Union for Conservation of Nature (IUCN): https://www.iucn.org/news/pakistan/201804/sindh-forest-department-brings-pride-nation-planting-maximum-number-mangroves-3rd-guinness-world-record

Jensen, J. (2007). Remote sensing of the Environment. An Earth Resources Perspective (2nd Edition), 450 p., Pearson Education, Inc.

Jensen, J. R. (1996). Introductory digital image processing (3rd ed.) Upper Saddle River, NJ: Prentice Hall.

Jensen, J. R., Cowen, D. J., Althausen, J. D., Narumalani, S. & Weatherbee, O. (1993). An evaluation of the CoastWatch change detection protocol in South Carolina. *Photogrammetric Engineering and Remote Sensing*, 59(6), 1039-1044. https://www.asprs.org/wp-content/uploads/pers/1993journal/jun/1993_jun_1039-1046.pdf

Johnson, D. D., & Howarth, P. J. (1989). The effects of spatial resolution on land cover/land use theme extraction from airborne digital data. *Remote Sensing and Methodologies of Land Use Change Analysis*, 117-134

Martin, L. R. (1989). An evaluation of Landsat-based change detection methods applied to the rural–urban fringe. Remote Sensing and Methodologies of Land Use Change Analysis, 101-116

Muttitanon, W., & Tripathi, N. (2005). Land use/land cover changes in the coastal zone of Ban Don Bay, Thailand using Landsat 5TM data. *International Journal of Remote Sensing*, 26(11), 2311–2323. https://doi.org/10.1080/01431160512331326666.

Nelson, R. F. (1983). Detecting forest canopy change due to insect activity using Landsat MSS. *Photogrammetric Engineering and Remote Sensing*, 49(9), 1303-1314

Osei, A. J., Merem, C. E. & Twumasi Y. A. (2006). Use of GIS and Remote Sensing Technology as a Decision Support Tool in Land Administration the Case of Lagos, Nigeria. *Regional Conference for Africa Promoting Land Administration Good Governance*. Accra, Ghana, https://www.oicrf.org/-/use-of-gis-and-remote-sensing-technology-as-a-decision-support-tool-in-land-administration-the-case-of-lagos-nigeria

Pakistan Meteorological Department. (2021). The State of Pakistan's Climate in 2020. Pakistan Meteorological Department. Karachi: Pakistan Meteorological Department. Retrieved from http://www.pmd.gov.pk/cdpc/Pakistan_Climate_2020.pdf

Pylon, P. (1988). An enhanced classification approach to change detection in semiarid environments. *Photogrammetric Engineering and Remote Sensing*, 54(12), 1709-1716

Ratnaparkhi, N. S., Ajay, D. N. & Bharti, G. (2016). Analysis of land use/land cover changes using remote sensing and GIS techniques in Parbhani City, Maharasthra, India. *International Journal of Advanced Remote Sensing and GIS*, 5(1), 17021708. https://doi.org/10.23953/cloud.ijarsg.54

Raza, D., Shu, H., Khan, S. U., Ehsan, M., Saeed, U., Aslam, H., ...& Arshad, M. (2022). Comparative geospatial approach for agricultural crops identification in interfluvial plain - A case study of Sahiwal district, Pakistan. *Pak. J. Agri. Sci*., Vol. 59(4), 567-578. DOI:10.21162/PAKJAS/22.127

Rehman, Z., & Kazmi, S. J. H. (2018). Land Use/Land Cover Changes Through Satellite Remote Sensing Approach: A Case Study of Indus Delta, Pakistan. *Pakistan Journal of Scientific & Industrial Research*. Series A: Physical Sciences, 61(3), 156-162. DOI:10.52763/PJSIR.PHYS.SCI.61.3.2018.156.162

Rehman, Z., Farheen, K., & Kazmi, S. J. H. (2016). Evaluation of land cover changes at the coast of Sindh through successive Landsat imageries. *Journal of Earth Science & Climatic Change*, 7(1)

Rehman, Z., Kazmi, S. J. H., Khanum, F. & Samoon, Z. A. (2015). Analysis of land surface temperature and NDVI using geo-spatial technique: A case study of Keti Bunder, Sindh, Pakistan. *Journal of Basic & Applied Sciences*, 11, 514-527. DOI:10.6000/1927-5129.2015.11.69

Sindh Forest Department. (2023, March). Mangroves. Retrieved from Sindh Forests: https://sindhforests.gov.pk/page-mangroves

Tariq, A., Riaz, I., Ahmad, Z., Yang, B., Amin, M., Kausar, R., & Rafiq, M. (2020). Land surface temperature relation with normalized satellite indices for the estimation of spatio-temporal trends in temperature among various land use land cover classes of an arid Potohar region using Landsat data. *Environmental Earth Science*s, 79(1), 1-15. https://doi.org/10.1007/s12665-019-8766-2

Torahi, A. A., & Rai, S. C. (2011). Land cover classification and forest change analysis, using satellite imagery-A case study in Dehdez area of Zagros Mountain in Iran. *Journal of Geographic Information System*, 3(1), 1–11. https://doi.org/10.4236/jgis.2011.31001

WWF Pakistan (2004). GIS Remote Sensing Based Assessment of Mangrove Resources of Selected Project Sites of Indus Delta and Makran Coast. *World Wildlife Fund for Nature and Natural Resources*, Pakistan, Lahore, 55 pp

WWF Pakistan (2021, July). Despite challenges, mangrove cover is increasing in the Indus Delta. Retrieved from www.wwfpak.org: https://www.wwfpak.org/?369559/Despite-challenges-mangrove-cover-is-increasing-in-the-Indus-Delta

Zaidi, S. M., Akbari, A., Abu Samah, A., Kong, N. S. & Gisen, J. I. A. (2017). Landsat-5 Time Series Analysis for Land Use/Land Cover Change Detection Using NDVI and Semi-Supervised Classification Techniques. *Polish Journal of Environmental Studies*, 26(6), 2833-2840. https://doi.org/10.15244/pjoes/68878

Zubair Iqbal, M. & Javed Iqbal, M. (2018). Land use detection using remote sensing and GIS (A case study of Rawalpindi Division). *American Journal of Remote Sensing*, 6(1), 39–51. https://doi.org/10.11648/j.ajrs.20180601.17

Forum geografic. Studii și cercetări de geografie și protecția mediului
Volume **XXII**, Issue **1** (**June 2023**), pp. **54-66;** DOI: **10.5775/fg.2023.030.i**

A multi-temporal Landsat data analysis for land-use/land-cover change in the Northwest mountains region of Vietnam using remote sensing techniques

Vu Thi PHUONG[1,2], Bui Bao THIEN[3,4*]

[1] Faculty of Social Sciences, Hong Duc University, Thanh Hoa, Vietnam
[2] Innovation Startup Support Center, Hong Duc University, Thanh Hoa, Vietnam
[3] Southern Federal University, Rostov-on-Don, 344006, Russia
[4] Faculty of Social Sciences, National University of Laos, Vientiane, Laos
* *Corresponding author*: buibaothienha@gmail.com

Received on 20-01-2023, reviewed on 07-04-2023, accepted on 26-04-2023

Abstract

Land-use change is one of the challenges that exacerbate environmental problems. Understanding the scope of land-use and land-cover change, past and present drivers and consequences is crucial for properly managing land resources. This study applies the supervised classification maximum likelihood algorithm in ArcGIS 10.8 software to detect changes in land use and cover in Hoa Binh city, Hoa Binh province, Vietnam using multimedia satellite data obtained from Landsat 7-ETM+, Landsat 5-TM and Landsat 8-OLI for the years 2000, 2010 and 2020 respectively. In addition, for each satellite scene we also applied spectral indices (NDVI-Normalized Differential Vegetation Index and NDWI-Normalized Differential Water Index) to classify and evaluate the change of LULC. The study area, located in the Northwest mountainous region of Vietnam, is classified into five land-use/cover classes: Agriculture, Forest, Water, Urban or built-up land and Bare soil or rock. The results reveal significant changes in the study area between 2000 and 2020. Accounting for the largest proportion of total area, the forest area has decreased from 243.20 km^2 in 2000 to 217.40 km^2 in 2020. Conversely, the urban/built-up land area has increased continuously for the last 20 years, from 9.31 km^2 in 2000 to 13.27 km^2 in 2010 and 51.80 km^2 in 2020. Changes in land use and cover have severe environmental impacts, such as climate change, loss of biodiversity, deterioration of water availability and quality, and reduced crop yields. Therefore, appropriate measures must be taken to limit drastic land-use changes and harmonize environmental conservation and human livelihoods.
Keywords: *Land use/cover change, Remote Sensing, GIS, Northwest Vietnam, Hoa Binh city*

Introduction

Land is an essential natural resource with numerous economic, social and ecological uses. A change in land use denotes the conversion of an area of land for a specified purpose and is caused by anthropogenic activities, while a change in land cover describes alterations in the characteristics of the land surface (Patel et al., 2019). Changes in land use/land cover (LULC) on the earth's surface are significant drivers of biodiversity loss and environmental problems worldwide (Homer et al., 2020; Field & Barros, 2014). LULC also impacts climate variability (Pielke Sr, 2005; Deng et al., 2013), land degradation (Meaza et al., 2016) and hydrology (Garg et al., 2019), affecting the capacity of ecosystem services (Arowolo et al., 2018; Rimal et al., 2019). Driven by changes in LULC, continuous environmental changes and their associated adverse impacts are becoming central issues globally (Li et al., 2020). Consequently, studying LULC dynamics is fundamental for the proper planning and use of natural resources as well as their management (Ahmad, 2012; Kotoky et al., 2012; Fonji & Taff, 2014; Rawat & Kumar, 2015; Belete et al., 2021; Thien et al., 2022a).

Remote Sensing (RS) and Geographic Information Systems (GIS) are effective tools to promote transboundary studies and explore transboundary data opportunities. Using overlays, they permit the detection and analysis of LULC variations over a given period to improve the selection of sites for agricultural, urban or industrial development (Selçuk et al., 2003; Dewan & Corner, 2013; Thien et al., 2022b). Remote sensor data allows for studying land cover changes in less time, with lower costs and higher accuracy (Kachhwala, 1985). Combined with GIS, RS provides a suitable platform for data analysis, updating and retrieval (Cihlar, 2000). Consequently, RS and GIS help stakeholders map where changes are occurring and gain insight into how development patterns are affected by human actions and climate change. Natural climates and seasonal landscapes can vary over time; hence, evaluating current actions and policies while anticipating and planning for appropriate changes in the future is critical (Mubako et al., 2018).

The study area is located in the Northwest mountainous region of North Vietnam, sharing the border with Laos and China. The terrain in this area is rugged, with numerous block-fault mountains and high mountain

ranges running in the northwest-southeast direction. The highest peaks range from 2,800 to 3,000 m in altitude. The Northwest has a total area of 50,728 km^2, accounting for 15% of Vietnam's land area. However, the land area used for agricultural production is limited to around 7,000 km^2, about 13% of the region's total land area. The unused flat and forest production land area is approximately 6,000 km^2 or 12% of the total land area. Hence, there remains a significant potential for expansion of agricultural production in this region. However, agricultural production faces numerous challenges in the region. The productive land is scattered due to the strongly fragmented terrain, the rate of erosion in the area is increased, and the weather and climate are challenging, with prolonged droughts and unpredictable salt fog. While the irrigation system has been developed, the amount of water available for irrigation remains low. In the Northwest, the land, forest and water resources have a significant influence on land cover changes (Trincsi & Turner, 2014; Ngo et al., 2015; Phuong & Son, 2017; Son & Binh, 2020).

Therefore, our goal is to integrate open access RS data and GIS to examine the spatial trends of LULC change in the Northwest mountainous region (Hoa Binh city, Hoa Binh province, Vietnam) over a 20-year period (2000-2020). This study aims to provide basic information to support informed land use planning in the mountainous region of northwest Vietnam. Our specific objectives are as follows: (1) identify and delineate different types of LULC and patterns of land use change in the area of Hoa Binh city between 2000 and 2020, (2) determine the potential of integrating RS and GIS to study the spatial distribution of different LULC changes, and (3) identify shifts in LULC classes through the spatial comparison of maps.

Materials and methods

Study Area

The study was carried out in Hoa Binh city, Hoa Binh province, in the Northwest mountainous region of Vietnam. The geographical position of the study area lies in the coordinates of latitude 20°44'34.88"N–21°1'16.53"N and longitude 105°15'47.42"E–105°27'48.50"E (Fig. 1). Hoa Binh city has an average mountain topography with elevations ranging from 200 to 700 m, craggy, fragmented terrain, and steep slopes.

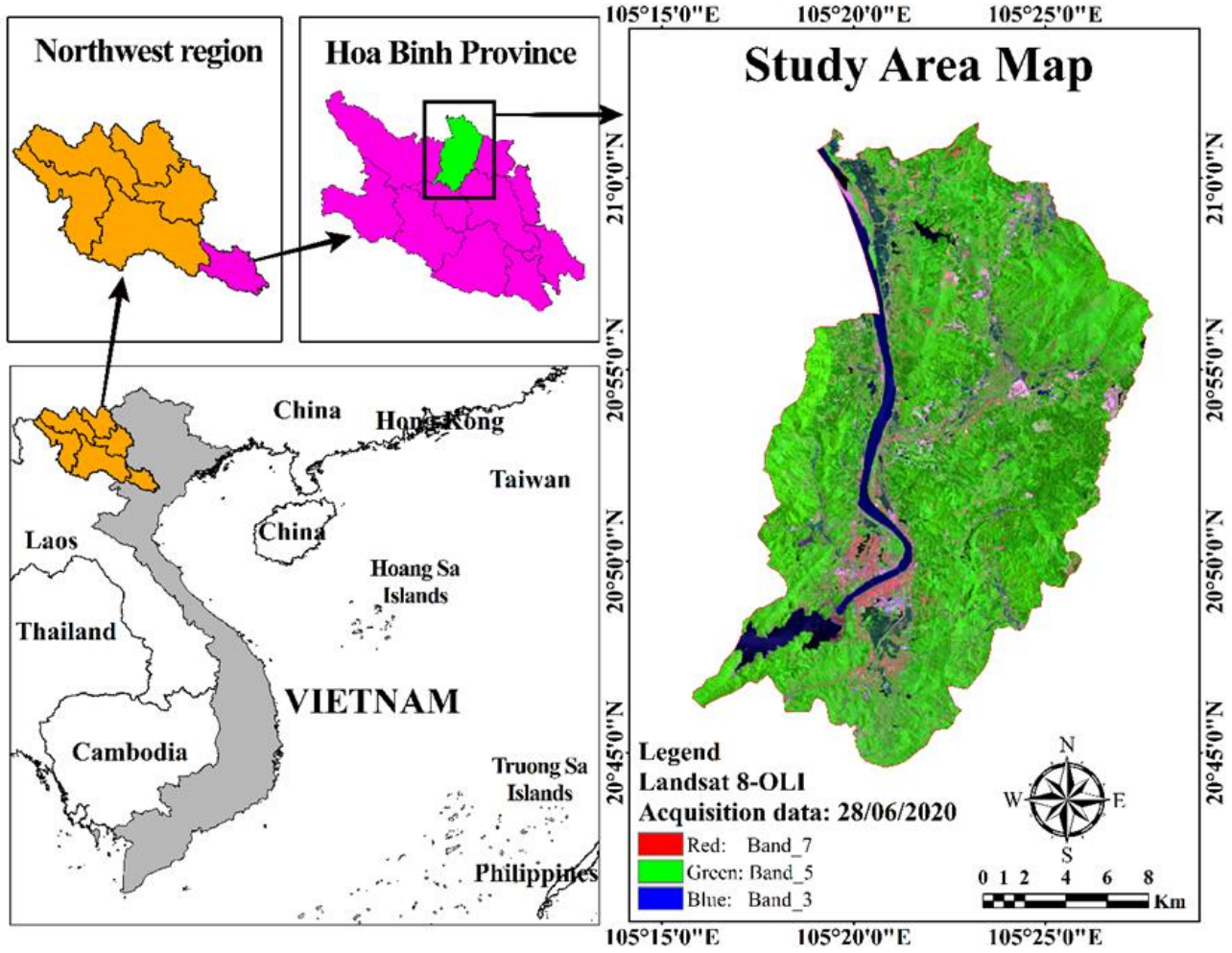

Figure 1. Map of the study site in Hoa Binh city, Hoa Binh province, Viet Nam

The study area has a humid subtropical climate: cold, dry, non-tropical winters with little rain and hot, rainy summers, with average rainfall from 1,400 mm to 2,800 mm per year. The average annual temperature is above 24 °C. June has the highest temperature of the year, averaging 30–32 °C, whereas January has the lowest temperature, averaging 17.4–19.5 °C (HoaBinh Statistics Office, 2021) (Fig. 2).

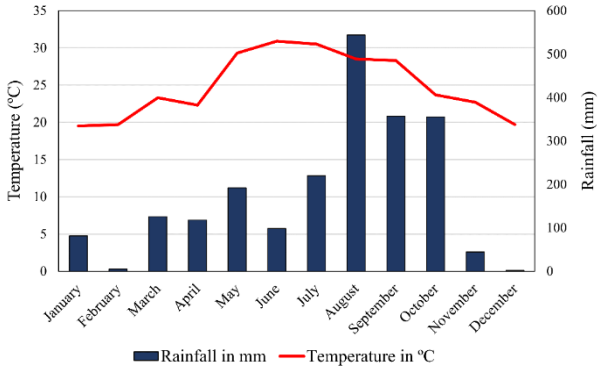

Figure 2. Mean monthly rainfall and temperature values of the study area

The Da River is the largest confluence of the Red River flowing through the study area. The river has a large volume of water and is considered a critical resource for the Vietnamese electricity industry. The Hoa Binh Dam, constructed between November 6, 1979 and December 20, 1994, was the largest hydroelectric plant in Vietnam and Southeast Asia from 1994 to 2012. The Hoa Binh hydroelectric plant is the main power supply for the entire Vietnamese electricity system. It is also the primary flood protection facility of the northern delta, facilitating transport in the downstream river and providing irrigation water.

Data Collection

The data used in this study were divided into satellite data and ancillary data. Ancillary data include accurate ground-truth data, aerial images of the study area and its vicinity, and topographic maps. The ground-truth data were collected using a Global Positioning System (GPS) from May to December 2020. An image from 2020 was used for image classification and assessment of the overall accuracy of the classification results. Landsat satellite data for three years, including multispectral data, were obtained free of charge from USGS EarthExplorer (http://earthexplorer.usgs.gov/) and USGS GloVis (http://glovis.usgs.gov/). The ArcGIS 10.8 software was used for image classification and zoning of the study area. The acquisition dates, sensors, path/row resolutions and image sources used in this study have been summarized in Table 1.

Table 1: Satellite data specifications of the study area

Satellite image	Sensor	Path/row	Resolution (m)	Acquisition data	Source
Landsat 7	ETM+	127/46	30*30	17/09/2000	USGS GloVis
Landsat 5	TM	127/46	30*30	17/06/2010	USGS GloVis
Landsat 8	OLI	127/46	30*30	28/06/2020	USGS EarthExplorer

Image pre-processing and classification

Image pre-processing was performed to extract meaningful information from satellite data so that they may become easier to interpret (Thien & Phuong, 2023). This process is used for the initial processing of the raw data and typically involves procedures like geometric corrections, image enhancement, noise removal, and topographic corrections (Jianya et al., 2008). All satellite images were geometrically corrected to the Universal Transfer Mercator (UTM) coordinate system and georeferenced to the data for the study area selected by the World Geodetic System (WGS) zone 48N. Data were processed in ArcGIS 10.8 to stitch and crop images based on existing study area boundaries. Satellite data were processed by assigning signatures per pixel and categorizing watersheds into five classes depending on the specific numerical values of various landscape elements: Agriculture, Forest, Water, Urban or built-up land and Bare soil or rock (Table 2).

Table 2: Classes delineated on the basis of supervised classification

No.	Class name	Description
1	Agriculture	Cultivated outfields, homestead garden fields and small scattered plots of grazing lands
2	Forest	Land covered with natural and plantation forests
3	Water	River, open water, lakes, ponds and reservoirs
4	Urban/built-up land	Residential, commercial, industrial, transportation, roads, mixed urban
5	Bare soil/rock	Land areas of exposed soil and barren area influenced by human influence

For each predefined LULC class, training samples were selected by delineating polygons around representative locations. Spectral signatures for the respective types of land cover obtained from satellite images were recorded using the pixels within these polygons. A satisfactory spectral signature ensures "minimum confusion" among the land cover types (Gao & Liu, 2010).

The study has used the rule-based supervised classification - maximum likelihood classifier (MLC) algorithm for LULC classification for acquired images of 1992, 2010, and 2022 (Rawat & Kumar, 2015; Thien et al., 2022b). The analyst controls this picture classification method by choosing the appropriate classes of pixels. Therefore, due to its simplicity and efficacy, post-classification refinement was employed to enhance classification accuracy and decrease misclassifications (Harris & Ventura, 1995). The approved LULC categorization characteristics defined class boundaries and consistent category definitions based on anthropogenic and natural factors changes within the study area. Additionally, as a size-independent, this categorization strategy can be successfully used at any spatial scale or level of detail. The LULC differences between the categorized photos were found utilizing a post-classification comparison method that used change detection comparison (pixel by pixel) to measure the change in LULC (Thien et al., 2022b). The methodology for classification is shown in Fig. 3.

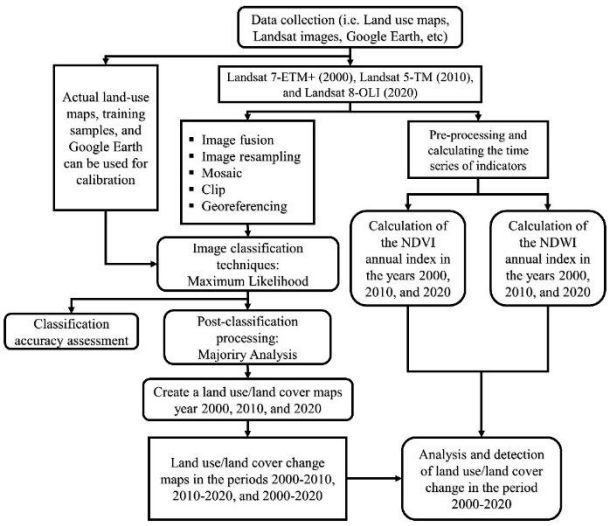

Figure 3. Overall process of land use/land cover change technique

Accuracy Assessment

The classification accuracy of 2000, 2010 and 2020 images were evaluated to determine the quality of the information obtained from the data. We sampled the reference points using a stratified random sampling approach, a probabilistic sampling method applied to assess the precision of each class (Olofsson et al., 2014; Thien & Phuong, 2023) that allows the selection of a relative number of points proportional to the size of each type of land cover. This ensures that each land cover is accurately represented by reference points to reduce bias in accuracy estimates. The accuracy assessment was conducted using 700 validation points on Google Earth Pro satellite images for the years 2000, 2010 and 2020. A comparison of reference data and classification results was performed to generate an error matrix. In addition, the accuracy of the classifier was measured using a nonparametric kappa test that considers not only the diagonal elements but also all elements in the error matrix (Rosenfield & Fitzpatrick-Lin, 1986; Ariti et al., 2015). The kappa coefficient is a measure of agreement between a predefined manufacturer rating and a user specified rating (Viera & Garrett, 2005). According to (Cohen, 1960), the kappa coefficient is calculated using the formula (Equation (1)):

$$Kappa\ coefficient\ (K) = \frac{Po-Pe}{1-Pe} \quad (1)$$

where *Po* is the number of times the k raters agree, and *Pe* is the number of times the k raters are expected to agree only by chance.

NDVI and NDWI analysis

The Normalized Difference Vegetation Index (NDVI) is suitable to detect vegetation cover of the study area (Gao, 1996; Cao et al., 2014). NDVI is a satellite-based index to quantify vegetation greenness and to understand plant density and health. The NDVI of an area can be obtained from a range of numerical values from -1 to 1, depending on the response of photosynthetic activity carried out by green vegetation. High values of NDVI represent high vegetation density, and negative values indicate water. The more active the NDVI, the greener the vegetation within a pixel and the NDVI index calculated using equation (2) given below:

$$NDVI = \frac{\mathrm{NIR-RED}}{\mathrm{NIR+RED}} \quad (2)$$

where NIR is the reflectance radiated in the near-infrared wave band, and RED is the reflectance radiated in the visible red wave band of the satellite radiometer.

Similarly, the Normalized Disparity Water Index (NDWI) is an index developed to analyze the features of open water and the water content of vegetation (Huete, 2012). The NDWI is a valuable indicator for monitoring drought, water stress and land degradation. NDWI has no dimensions and its value ranges from -1 to +1. High values of NDWI represent water content in vegetation and high open water features, and low values indicate lower water content, and the NDWI index is calculated using equation (3) given below:

$$NDWI = \frac{\mathrm{GREEN-NIR}}{\mathrm{GREEN+NIR}} \quad (3)$$

where NIR is the reflection in the near-infrared spectrum, GREEN is the reflection in the green range spectrum.

Land use/land cover Change Detection

The post-classification change detection technique was applied using the ArcGIS 10.8 software. Information that changes on a pixel-by-pixel basis was generated using a pixel-based comparison. Therefore, the changes were interpreted more efficiently by taking advantage of "from-to" information. Pairs of categorical images of two different data were compared using cross-tabulation to identify qualitative and quantitative aspects of changes between 2000 and 2020. This procedure generated a two-way cross-matrix that was used to characterize the main patterns of change in the study area.

Results and discussion

Results of Classification and Analysis

The classification results of the pre-processed images for the years 2000, 2010 and 2020 are presented in Fig. 4.

The three-year statistics of the land-use classes and their corresponding importance rates are shown in Table 3. The classification results shown in 2000, most of the study area was covered by forest, accounting for 69.75% (243.20 km^2), followed by agriculture area with 22.78% (79.41 km^2), water area with 4.61% (16.09 km^2), and urban/built-up land and bare soil/rock area with at least 2.67% (9.31 km^2) and 0.18% (0.64 km^2), respectively (Table 3). In 2010, the size of the forest and water class all decreased by 64.22% (223.90 km^2) and 4.12% (14.35 km^2), respectively (Table 3). On the other hand, in terms of agriculture, urban/built-up land, and bare soil/rock, the class increased by 27.29% (95.13 km^2), 3.81% (13.27 km^2), and 0.57% (2.00 km^2), respectively (Table 3). In 2020, the forest, agriculture, water and bare soil/rock classes area decreased by 62.36% (217.40 km^2), 18.34% (63.95 km^2), 4.04% (14.09 km^2) and 0.40% (1.41 km^2), respectively. Meanwhile, the area of the urban/built-up land class increased sharply by 14.86% (51.80 km^2) (Table 3).

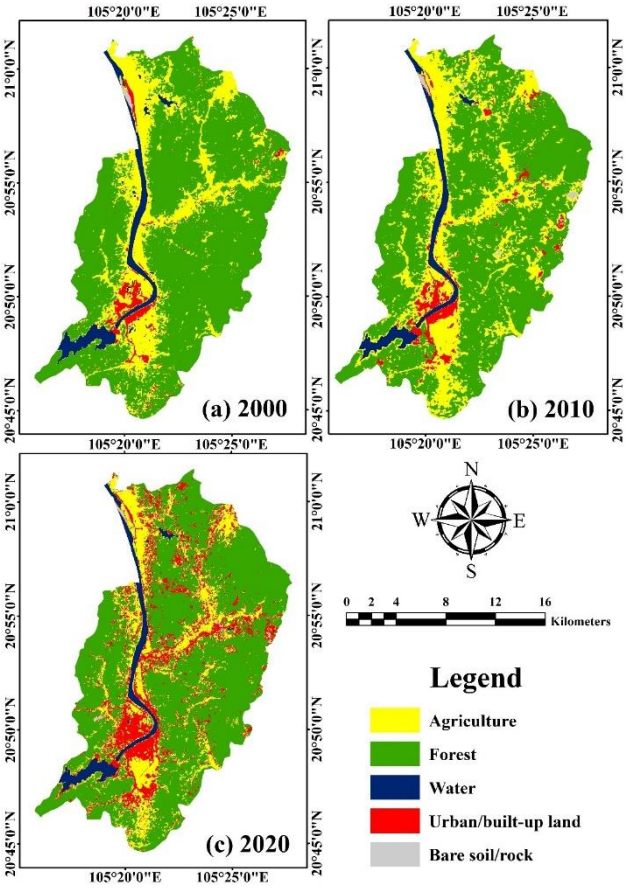

Figure 4. Maps of classified land use/land cover in Hoa Binh city (a) in 2000, (b) in 2010 and (c) in 2020

A total of 700 points were randomly selected to assess the accuracy of three land-use status maps in 2000, 2010, and 2020. The confirmation data were manually and randomly selected using Google Earth Pro. The overall classification accuracy was 95.56%, 95.09% and 94.07% and the overall kappa coefficients were 0.944, 0.938 and 0.926 for 2000, 2010 and 2020, respectively. The study requirements were met, as evidenced by the overall classification accuracy of more than 90% and kappa coefficients over 0.9 (Lea & Curtis, 2010).

Table 3: Area statistics land use/land cover in Hoa Binh city for 2000, 2010 and 2020

LULC classes	2000		2010		2020	
	Area (km^2)	Area (%)	Area (km^2)	Area (%)	Area (km^2)	Area (%)
Agriculture	79.41	22.78	95.13	27.29	63.95	18.34
Forest	243.20	69.75	223.90	64.22	217.40	62.36
Water	16.09	4.61	14.35	4.12	14.09	4.04
Urban/built-up land	9.31	2.67	13.27	3.81	51.80	14.86
Bare soil/rock	0.64	0.18	2.00	0.57	1.41	0.40
Total	**348.65**	**100.00**	**348.65**	**100.00**	**348.65**	**100.00**

Analysis of land-use/land cover changes

Table 4 presents statistics on LULC in Hoa Binh city in the periods 2000-2010, 2010-2020, and 2000-2020. The results in Table 4 and Fig. 5a show that between 2000 and 2010, the forest area exhibited the most significant change, losing 19.30 km^2 or 5.54% of its area. During this period, the agricultural land area increased the most, with

the total area of 15.72 km^2, showing an increase of 4.51% increase in 2000 as compared to 2010. The water area decreased by 1.74 km^2 or 0.50%. In addition, urban/built-up land and bare soil/rock areas showed a slight increase of 3.96 km^2 and 1.36 km^2, respectively, equivalent to 1.14% and 0.39%.

The results presented in Table 4 and Fig. 5b give an overview of the change in land cover from 2010 to 2020. During this period, the urban/built-up land area displayed the largest increase, with its total area increasing by 11.05% or 38.53 km^2. Agricultural land decreased the most, with a loss of 31.18 km^2 or 8.94% as compared to the previous period. Land areas covered by forest, water and bare soil/rock were reduced by 6.50 km^2 (1.86%), 0.26 km^2 (0.07%) and 0.59 km^2 (0.17%), respectively in the period 2010-2020 mentioned above (Table 4).

Table 4: Table of area land use/land cover changes in Hoa Binh city from 2000 to 2010, 2010 to 2020, 2000 to 2020

LULC classes	2000-2010		2010-2020		2000-2020	
	Area (km^2)	Area (%)	Area (km^2)	Area (%)	Area (km^2)	Area (%)
Agriculture	15.72	4.51	-31.18	-8.94	-15.46	-4.43
Forest	-19.30	-5.54	-6.50	-1.86	-25.80	-7.40
Water	-1.74	-0.50	-0.26	-0.07	-2.00	-0.57
Urban/built-up land	3.96	1.14	38.53	11.05	42.49	12.19
Bare soil/rock	1.36	0.39	-0.59	-0.17	0.77	0.22

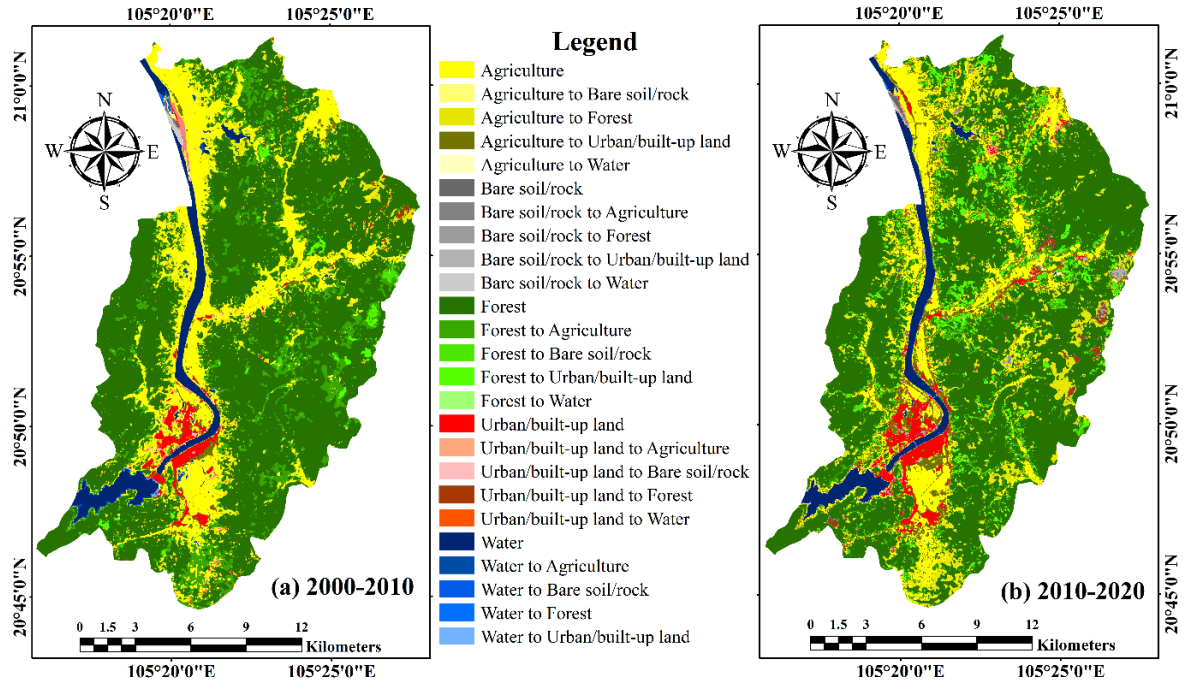

Figure 5. Land use/land cover changes maps in Hoa Binh city from (a) 2000 to 2010, (b) 2010 to 2020

Based on Table 3 and Table 4, the results for the period 2000-2020 show a considerable decline in the land cover area for the Forest, Agriculture and Water classes while the area of the Urban/built-up and Bare soil/rock classes increased. Forest land decreased from 69.75% to 62.36% of the total area and agricultural land decreased from 22.78% to 18.34%. Although the water surface area was relatively small in 2000, it was further reduced from 4.61% to 4.04%. The proportion of urban/built-up land was 2.67% of the total area in 2000, substantially increasing to 14.86% in 2020. The bare soil/rock area has also increased from 0.18% to 0.40% (Table 3).

The comparison of each class showed a marked change in LULC over the 20-year study period (Fig. 6). Between 2000 and 2020, the percentage of the area belonging to the Urban/built-up class in the study area increased by 12.19% (Table 4), an increase attributable to residential, farm and recreational projects that have been flourishing in the city center and surrounding areas. In addition, the dynamism of residential areas is closely related to urban population growth, specifically an increase in population size due to natural increase and higher fertility as well as migration from rural areas out into the city. According to the Department of Statistics of Hoa Binh province, the study area reached 92,754 people in 2014, and by 2020

the population has increased to 137,091, with an increase of nearly 7,400 people/year. Hoa Binh city is the political, administrative, economic, cultural and social center of Hoa Binh province, so the city attracts the most investment in the province with 203 projects, mainly in the public sector industry, infrastructure and cities. Along with these developments, infrastructure to access the area, such as new sidewalks, highways and roads, has been constructed (Zhang et al., 2018). The Bare soil/rock class exhibited a total increase of 0.22% during the study period (Table 4). This increase in the Bare soil area is associated with the loss of agricultural land, with previously cultivated land becoming barren open space, as farmers abandoned unproductive land due to economic inefficiencies. In addition, several construction site planning projects, where the land has been cleared but is left unconstructed, contribute to this increase in vacant land. The area covered by the Forest class decreased by 7.40% from 2000 to 2020 (Table 4). The main drivers of forest depletion in this typical study area are human activities such as illegal logging of high-value forest wood (Malhi et al., 2008). In addition, the lack of effective and strict forest fire management played an important role in forest decline. The area of Agricultural land decreased by 4.43% from 2000 to 2020 (Table 4), primarily due to challenges in land cultivation. In addition, rapid urbanization caused a large area of Agricultural land to be converted to Urban/built-up land, further contributing to the decline in the agricultural land area (Peerzado et al., 2019; Youssef et al., 2020). Therefore, the increase in the settlement land can be termed a positive increase, whereas the decrease in the agricultural land can be called a negative change. In addition, plowing, improper farming practices, and overgrazing are the leading causes of anthropogenic soil erosion, which drives decreases in agricultural land area. The area covered by water has decreased by 0.57% between 2000 and 2020 (Table 4). Water depletion, drought or little precipitation and intense evaporation in downstream river basins were factors in this decrease, as were the impacts of global climate change, the El Niño phenomenon and human activities (Haddeland et al., 2014; Gosling & Arnell, 2016). Moreover, the Hoa Binh hydroelectric power plant and irrigation efforts caused a considerable change in the water regime, water quality and aquatic systems in both upstream and downstream rivers (Young et al., 2011).

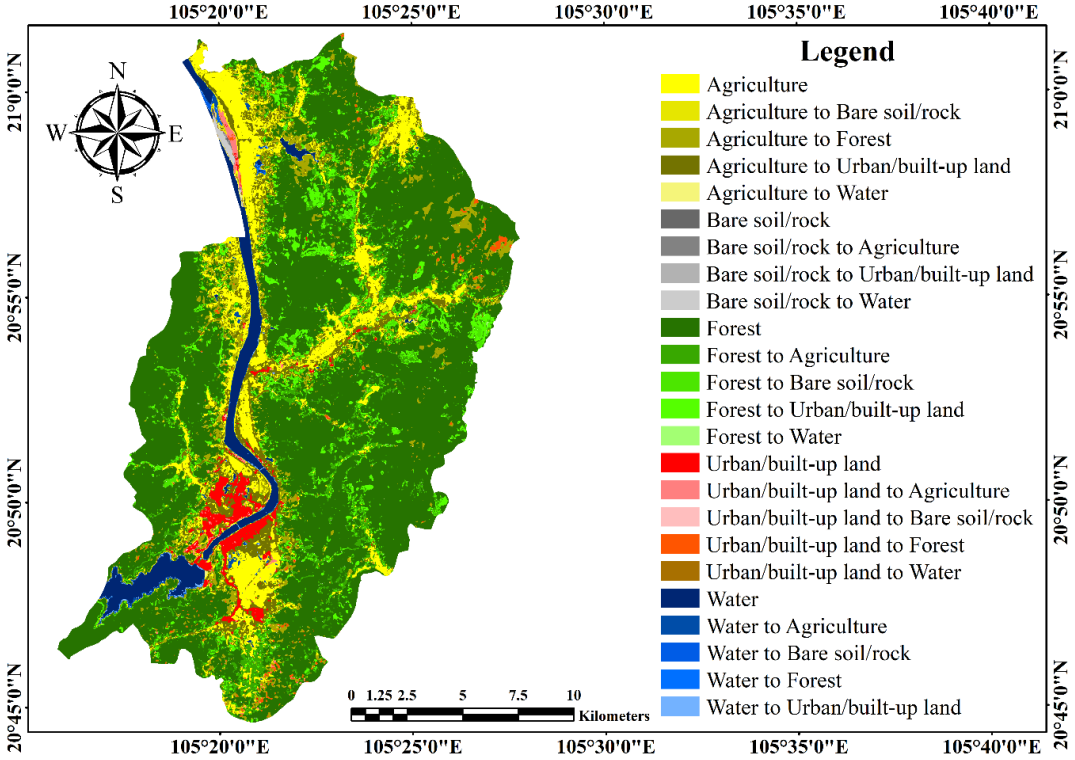

Figure 6. Land use/land cover changes map in Hoa Binh city from 2000 to 2020

Post-classification comparison of the detected change was conducted using GIS by mapping change to understand its spatial pattern (Fig. 5, Fig. 6). The 2000, 2010 and 2020 classified maps were overlaid in stages to create a map of LULC changes. The cross-tabulation matrix was also generated to assess the "from-to" transition between land covers.

The cross-tabulation matrices (Table 5) show the shift in the land cover classes. Out of the 243.79 km^2 that was Forest area in 2000, 199.38 km^2 was still Forest area in 2020 but 43.58 km^2 was converted to Agriculture and Urban/built-up, and rest to Water and Bare soil/rock. At the same time the increase of Forest, from 2000 to 2020, was mainly from Agriculture (16.53 km^2). Agriculture out of 78.81 km^2 in 2000 lost area mainly to Forest as

mentioned before, Bare soil/rocks, a small part to Urban/built-up and Water, and retained 38.56 km^2 of total in 2020. Urban/built-up increased from 9.32 km^2 in 2000 to 51.80 km^2 in 2020. It retained 6.46 km^2 of it and was mainly replaced by Agriculture and Forest. The class which Urban/built-up mainly replaced in 2020 was Agriculture (23.09 km^2) (Table 5). Water class retained 13.18 km^2 of the total 16.09 km^2 in 2000. It was reduced to 14.09 km^2 and mainly replaced by Agriculture and Urban/built-up. The area of other land cover classes replaced by Water was small. Bare soil/rock area increased from 0.64 km^2 in 2000 to 1.41 km^2 in 2020. Bare land/rock only retained 0.05 km^2 of the total area in 2000 and was mainly replaced by Water (Table 5).

Table 5: Crosstabulation of the change in land cover between 2000 and 2020 (area in km^2)

2020 \ 2000	Agriculture	Forest	Water	Urban/built-up land	Bare soil/rock	**Total**
Agriculture	**38.56**	22.14	1.86	1.33	0.06	63.95
Forest	16.53	**199.38**	0.09	1.40	0.00	217.40
Water	0.31	0.04	**13.18**	0.06	0.50	14.09
Urban/built-up land	23.09	21.44	0.78	**6.46**	0.03	51.80
Bare soil/rock	0.32	0.79	0.18	0.07	**0.05**	1.41
Total	78.81	243.79	16.09	9.32	0.64	

This study emphasizes the importance of incorporating RS and GIS for LULC change detection. This method offers crucial information about the spatial distribution as well as the nature of changes in land cover. The 90% overall accuracy of LULC maps indicates that integrating supervised classification of satellite imagery with visual interpretation is an effective method for characterizing and analyzing LULC change in an area such as the Northwest mountainous region of Vietnam.

Spatial distribution of NDVI and NDWI over 2000 to 2020

The study area was also analyzed with two widely used NDVI and NDWI indices. Both indices produce similar types of results. The selected five land cover features are distinguishable by both indices. The values of NDVI show the amount of chlorophyll content present in vegetation, where the greater NDVI value shows healthy and dense vegetation, but a lower NDVI value shows sparse vegetation. Fig. 7 represents the spatial distribution of NDVI values for three specified years (2000, 2010 and 2020) and values range between −0.53 to 0.66. The NDVI values in 2000 ranged from −0.53 to 0.45; in 2010, the NDVI value indicated the minimum value that is −0.20 and maximum 0.62; while in 2020, the NDVI value indicated the minimum value that is −0.19 and maximum 0.66. The highest values of NDVI were found in 2020, while the lowest were in 2000. Higher values showed the most productive areas like forest and crops. Similarly, lower values showed fewer and least productive areas like built-up area, water and bare soil. The NDVI analysis also revealed that urban/built-up land areas have risen dramatically while forest areas have significantly been reduced over time period.

The study area was also investigated with the NDWI, and the results are quite similar to the NDVI results. Fig. 8 represents the spatial distribution of NDWI values of three specified years. The NDWI values range between −0.58 and 0.56 in the specified period. The NDWI values in 2000 ranged from −0.33 to 0.56. In 2010, the NDWI value indicated a minimum of −0.58 and a maximum of 0.18. In 2020, it slightly increased from −0.58 to 0.29. The spatial variation of the NDWI values is evident across different years. The NDWI analysis also shows that the forest area shown in red has shrunk significantly between 2000 and 2020, and the urban/built-up land area shown in green has expanded centrally and along the length of the foot of the mountain over time, as can be seen in Figure 8. From these results, we can conclude that both NDVI and NDWI are good indicators that can effectively support the classification and spatial mapping of LULC layers in Hoa Binh city, especially to quickly assess the fluctuation of LULC layers.

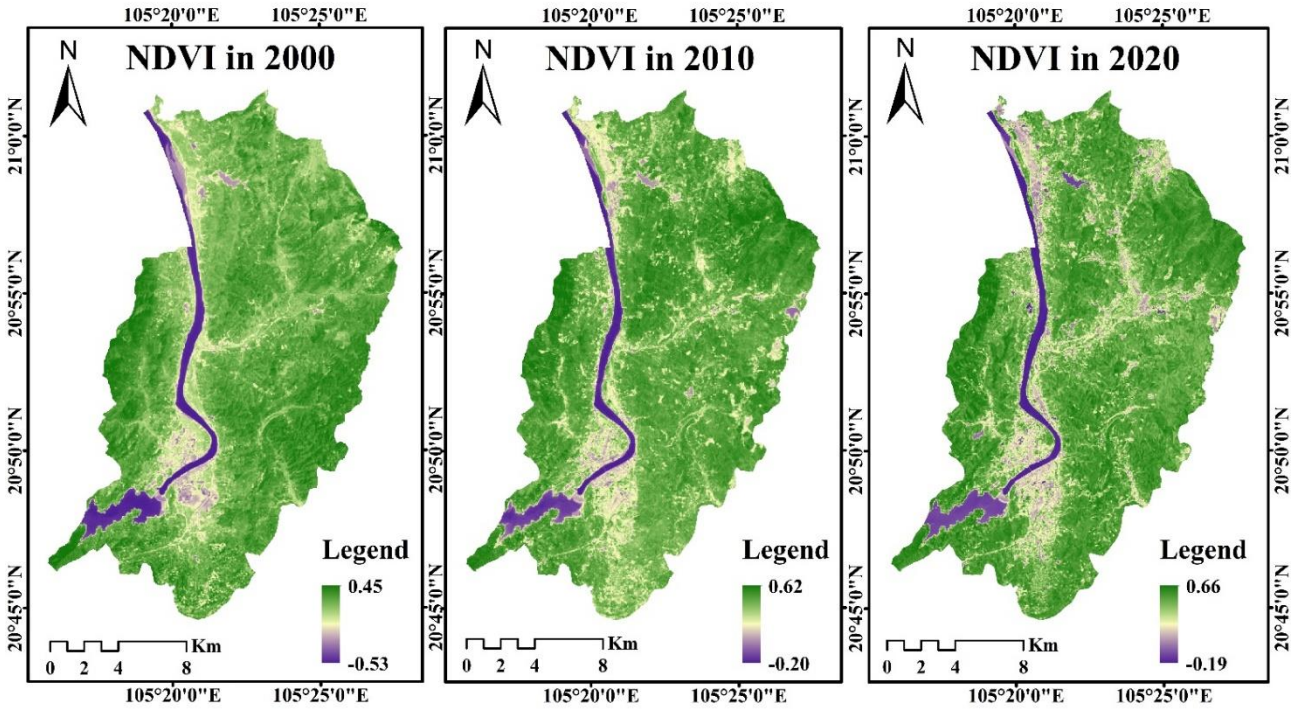

Figure 7. Spatial distribution of NDVI for 2000, 2010 and 2020

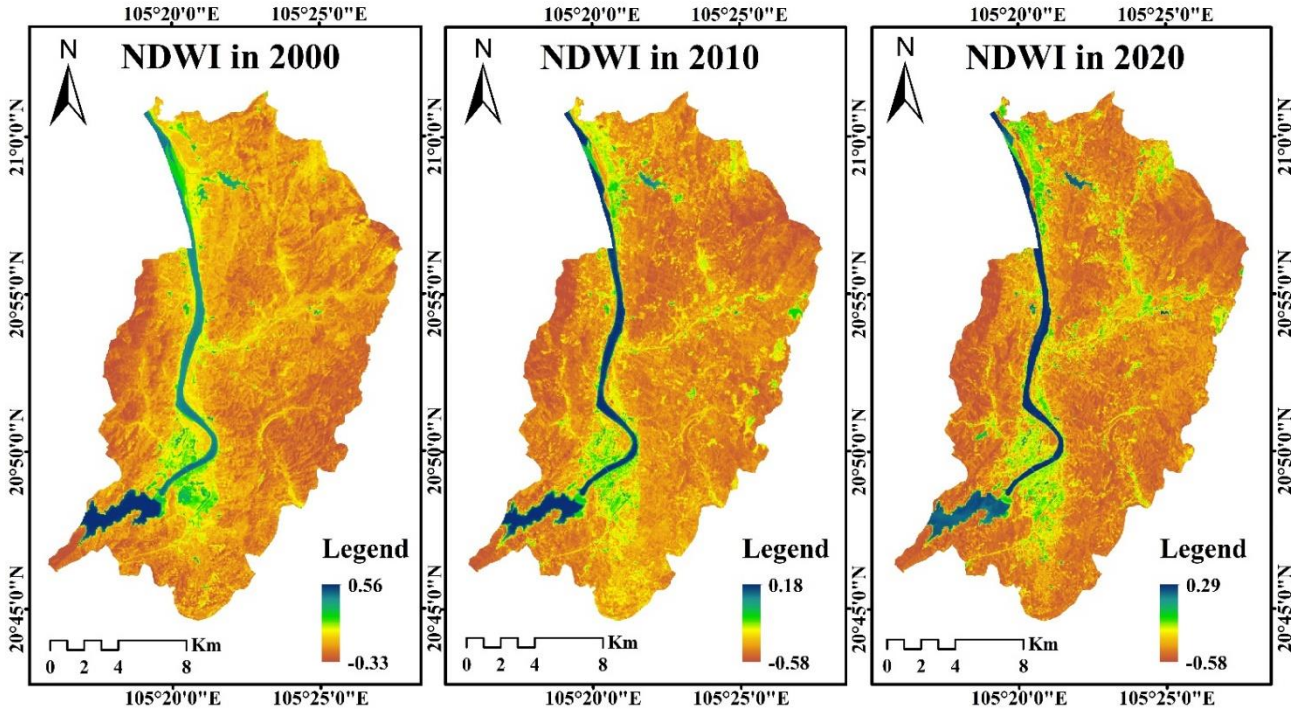

Figure 8: Spatial distribution of NDWI for 2000, 2010 and 2020

Relationships between NDVI and NDWI were created using linear regression analysis. In Hoa Binh city, the consequences of urban expansion were visible in both the calculated NDVI and NDWI. To determine how variations in LU intensity inside LULC units vary across space and lead to intra-LU fluctuation of NDWI, regression analysis (R^2) is conducted. However, NDVI and NDWI had a negative connection, as shown in Fig. 9, between the vegetation index (NDVI) and NDWI-derived built-up fractions, with correlation coefficients of R^2 = 0.9737 for 2000, 0.9656 for 2010, and 0.9639 for 2020 displayed in all images. Regression analysis reveals that NDWI values were lowest in the area with the highest NDVI values.

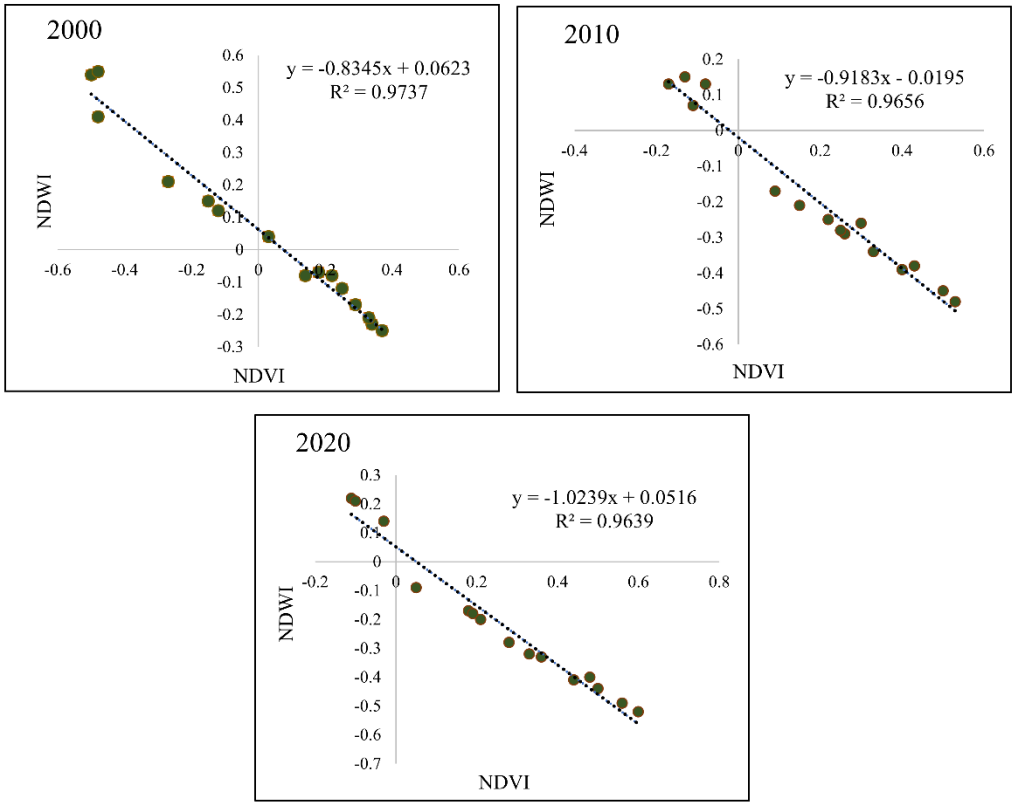

Figure 9: Regression analyses between NDVI and NDWI in the study area

Limitation of the study

This study faced some limiting factors that need to be highlighted. Firstly, the satellite data used in this investigation has a resolution of 30 m. Although it might work for small-scale studies, it isn't the best option for in-depth research. The investigation had to be done with free, average-quality Landsat pictures because the current study couldn't access high-resolution images. Since small-scale green spaces cannot be seen due to the 30 m pixel size, many rooftop gardens or plants growing along roadways may have gone unnoticed throughout the investigation, leading to errors. Second, the land cover map was produced using maximum likelihood classification algorithms, but due to Vietnam's diverse and complex land use pattern, the Landsat pictures may have been misclassified or significantly incorrectly classified. We used the post-classification feature in the ArcGIS 10.8 program to get the most out of this restriction. To address the aforementioned issues and employ a different and multi-model approach for further elucidation, more study is required.

Conclusion

Since the 2000s, the land use of Hoa Binh city, located in the Northwest mountainous region of Vietnam, has substantially changed due to economic development and the impact of human activities. In this study, Landsat 7-ETM+, Landsat 5-TM and Landsat 8-OLI image data were used to obtain LULC maps for 2000, 2010 and 2020. The results obtained by integrating RS and GIS analysis demonstrate that LULC has changed significantly in Hoa Binh city between 2000 and 2020. According to the classification results, the land cover class with the largest area was forest, with 234.20 km^2 in 2000, 223.90 km^2 in 2010 and 217.40 km^2 in 2020. The area of urban/built-up land increased steadily from 2000 to 2020, while changes in the Water, Agriculture, and Bare soil/rock classes were closely related to human activities. The NDVI and NDWI indices have also contributed to clarifying notable changes in land cover characteristics between 2000 and 2020.

Persistence of this trend of LULC change will result in severe environmental and economic consequences, impacting the livelihood of the local people. The outcome of the study shows that the policy maker and stakeholder of this region need to be conscious about the rapid development and changes in the land use pattern in Hoa Binh city. Implementing appropriate measures to ensure the sustainable use of natural resources and the efficient use of land is, therefore, critical. Moreover, this study offers evidence that integrating open-access RS and GIS constitutes a valuable approach for providing baseline spatial information. Therefore, it is suggested that RS and GIS techniques be used to detect the change in LULC in other parts of Vietnam as well as the world. Such spatial information is vital to informed land use and sustainable regional development worldwide. In addition, the complementary future studies may integrate quantitative

and qualitative methods to understand and discuss the reasons for these quantitative descriptive results.

Acknowledgments

The authors are grateful to the Ministry of Science and Higher Education of the Russian Federation for a scholarship to Bui Bao Thien.

Authors contributions

Conceptualization, B.B.T. and V.T.P.; methodology, B.B.T. and V.T.P.; software, B.B.T.; validation, V.T.P.; formal analysis, B.B.T.; writing—original draft preparation, B.B.T. and V.T.P.; writing—review and editing, B.B.T. All authors have read and agreed to the published version of the manuscript.

Funding

This research received no external funding.

Declaration of interests

The authors declare no conflict of interest.

References

Ahmad, F. (2012). Detection of change in vegetation cover using multi-spectral and multi-temporal information for District Sargodha, Pakistan. *Sociedade & Natureza*, 24, 557-571. doi:10.1590/S1982-45132012000300014

Ariti, A. T., van Vliet, J., & Verburg, P. H. (2015). Land-use and land-cover changes in the Central Rift Valley of Ethiopia: Assessment of perception and adaptation of stakeholders. *Applied Geography*, 65, 28-37. doi: 10.1016/j.apgeog.2015.10.002

Arowolo, A. O., Deng, X., Olatunji, O. A., & Obayelu, A. E. (2018). Assessing changes in the value of ecosystem services in response to land-use/land-cover dynamics in Nigeria. *Science of the Total Environment*, 636, 597-609. doi: 10.1016/j.scitotenv.2018.04.277

Belete, F., Maryo, M., & Teka, A. (2021). Land use/land cover dynamics and perception of the local communities in Bita district, south western Ethiopia. *International Journal of River Basin Management*, 1-12. doi:10.1080/15715124.2021.1938092

Cao, L., Liu, T., & Wei, L. (2014). A comparison of multi-resource remote sensing data for vegetation indices. *IOP Conference Series: Earth and Environmental Science*, 17(1), 012067. doi:10.1088/1755-1315/17/1/012067

Cihlar, J. (2000). Land cover mapping of large areas from satellites: status and research priorities. *International Journal of Remote Sensing*, 21(6-7), 1093-1114. doi:10.1080/014311600210092

Cohen, J. (1960). A coefficient of agreement for nominal scales. *Educational and Psychological Measurement*, 20(1), 37-46. doi:10.1177/001316446002000104

Deng, X., Zhao, C., & Yan, H. (2013). Systematic modeling of impacts of land use and land cover changes on regional climate: a review. *Advances in Meteorology*, 2013. doi:10.1155/2013/317678

Dewan, A., & Corner, R. (2013). Dhaka megacity: Geospatial perspectives on urbanisation, environment and health. *Springer Science & Business Media*, 1-22.

Field, C. B., & Barros, V. R. (2014). Climate change 2014–Impacts, adaptation and vulnerability: Regional aspects. *Cambridge University Press*, 1820 p.

Fonji, S. F., & Taff, G. N. (2014). Using satellite data to monitor land-use land-cover change in North-eastern Latvia. *SpringerPlus*, 3(1), 1-15. doi:10.1186/2193-1801-3-61

Gao, B.C. (1996). NDWI—A normalized difference water index for remote sensing of vegetation liquid water from space. *Remote Sensing of Environment*, 58(3), 257-266. doi:10.1016/S0034-4257(96)00067-3

Gao, J., & Liu, Y. (2010). Determination of land degradation causes in Tongyu County, Northeast China via land cover change detection. *International Journal of Applied Earth Observation and Geoinformation*, 12(1), 9-16. doi: 10.1016/j.jag.2009.08.003

Garg, V., Nikam, B. R., Thakur, P. K., Aggarwal, S. P., Gupta, P. K., & Srivastav, S. K. (2019). Human-induced land use land cover change and its impact on hydrology. *Hydro Research*, 1, 48-56. doi: 10.1016/j.hydres.2019.06.001

Gosling, S. N., & Arnell, N. W. (2016). A global assessment of the impact of climate change on water scarcity. *Climatic Change*, 134(3), 371-385. doi:10.1007/s10584-013-0853-x

Haddeland, I., Heinke, J., Biemans, H., Eisner, S., Flörke, M., Hanasaki, N., Konzmann, M., Ludwig, F., Masaki, Y., Schewe, J., Stacke, T., Tessler, Z. D., Wada, Y., & Wisser, D. (2014). Global water resources affected by human interventions and climate change. *Proceedings of the National Academy of Sciences*, 111(9), 3251-3256. doi:10.1073/pnas.1222475110

Harris, P. M., & Ventura, S. J. (1995). The integration of geographic data with remotely sensed imagery to improve classification in an urban area. *Photogrammetric Engineering and Remote Sensing*, 61(8), 993-998.

HoaBinh Statistics office. (2021). HoaBinh Statistical Yearbook 2020. *Statistical Publishing House – 2021*, 682 p.

Homer, C., Dewitz, J., Jin, S., Xian, G., Costello, C., Danielson, P., Gass, L., Funk, M., Wickham, J., Stehman, S., Auch, R., & Riitters, K. (2020). Conterminous United States land cover change patterns 2001–2016 from the 2016 national land cover database. *ISPRS Journal of Photogrammetry*

and Remote Sensing, 162, 184-199. doi: 10.1016/j.isprsjprs.2020.02.019

Huete, A.R. (2012). Vegetation indices, remote sensing and forest monitoring. *Geography Compass*, 6(9), 513-532. doi:10.1111/j.1749-8198.2012.00507.x

Jianya, G., Haigang, S., Guorui, M., & Qiming, Z. (2008). A review of multi-temporal remote sensing data change detection algorithms. *The International Archives of the Photogrammetry, Remote Sensing and Spatial Information Sciences*, 37(B7), 757-762.

Kachhwala, T. S. (1985). Temporal monitoring of forest land for change detection and forest cover mapping through satellite remote sensing. In *Proceedings of the 6th Asian Conf. on Remote Sensing*. *Hyderabad*, 77-83.

Kotoky, P., Dutta, M. K., & Borah, G. C. (2012). Changes in landuse and landcover along the Dhansiri River channel, Assam—A remote sensing and GIS approach. *Journal of the Geological Society of India*, 79(1), 61-68. doi:10.1007/s12594-012-0002-6

Lea, C., & Curtis, A. C. (2010). Thematic accuracy assessment procedures: National Park Service Vegetation Inventory. *US Department of the Interior, National Park Service, Natural Resource Program Center*.

Li, K., Feng, M., Biswas, A., Su, H., Niu, Y., & Cao, J. (2020). Driving factors and future prediction of land use and cover change based on satellite remote sensing data by the LCM model: a case study from Gansu province, China. *Sensors*, 20(10), 2757. doi:10.3390/S20102757

Malhi, Y., Roberts, J. T., Betts, R. A., Killeen, T. J., Li, W., & Nobre, C. A. (2008). Climate change, deforestation, and the fate of the Amazon. *Science*, 319(5860), 169-172. doi:10.1126/science.1146961

Meaza, H., Tsegaye, D., & Nyssen, J. (2016). Allocation of degraded hillsides to landless farmers and improved livelihoods in Tigray, Ethiopia. *Norsk Geografisk Tidsskrift-Norwegian Journal of Geography*, 70(1), 1-12. doi:10.1080/00291951.2015.1091033

Mubako, S., Belhaj, O., Heyman, J., Hargrove, W., & Reyes, C. (2018). Monitoring of land use/land-cover changes in the arid transboundary middle Rio grande basin using remote sensing. *Remote Sensing*, 10(12), 2005. doi:10.3390/rs10122005

Ngo, T. S., Nguyen, D. B., & Rajendra, P. S. (2015). Effect of land use change on runoff and sediment yield in Da River Basin of Hoa Binh province, Northwest Vietnam. *Journal of Mountain Science*, 12(4), 1051-1064. doi:10.1007/s11629-013-2925-9

Olofsson, P., Foody, G. M., Herold, M., Stehman, S. V., Woodcock, C. E., & Wulder, M. A. (2014). Good practices for estimating area and assessing accuracy of land change. *Remote Sensing of Environment*, 148, 42-57. doi: 10.1016/j.rse.2014.02.015

Patel, S. K., Verma, P., & Shankar Singh, G. (2019). Agricultural growth and land use land cover change in peri-urban India. *Environmental Monitoring and Assessment*, 191(9), 1-17. doi:10.1007/s10661-019-7736-1

Peerzado, M. B., Magsi, H., & Sheikh, M. J. (2019). Land use conflicts and urban sprawl: Conversion of agriculture lands into urbanization in Hyderabad, Pakistan. *Journal of the Saudi Society of Agricultural Sciences*, 18(4), 423-428. doi: 10.1016/j.jssas.2018.02.002

Phuong, T. T., & Son, N. T. (2017). Land use change and its interactions with soil, water resources, and rural livelihoods in Hoa Binh province. *Vietnam Journal of Agricultural Sciences*, 15(3), 249-262.

Pielke Sr, R. A. (2005). Land use and climate change. *Science*, 310(5754), 1625-1626. doi:10.1126/science.1120529

Rawat, J. S., & Kumar, M. (2015). Monitoring land use/cover change using remote sensing and GIS techniques: A case study of Hawalbagh block, district Almora, Uttarakhand, India. *The Egyptian Journal of Remote Sensing and Space Science*, 18(1), 77-84. doi: 10.1016/j.ejrs.2015.02.002

Rimal, B., Sharma, R., Kunwar, R., Keshtkar, H., Stork, N. E., Rijal, S., Radman, S. A., & Baral, H. (2019). Effects of land use and land cover change on ecosystem services in the Koshi River Basin, Eastern Nepal. *Ecosystem Services*, 38, 100963. doi: 10.1016/j.ecoser.2019.100963

Rosenfield, G. H., & Fitzpatrick-Lins, K. (1986). A coefficient of agreement as a measure of thematic classification accuracy. *Photogrammetric Engineering and Remote Sensing*, 52(2), 223-227.

Selçuk, R. E. I. S., Nisanci, R., Uzun, B., Yalcin, A., Inan, H., & Yomralioglu, T. (2003). Monitoring land-use changes by GIS and remote sensing techniques: case study of Trabzon. In *Proceedings of 2nd FIG Regional Conference*, *Morocco*, 1-11.

Son, N. T., & Binh, N. D. (2020). Predicting Land Use and Climate Changes Scenarios Impacts on Runoff and Soil Erosion: A Case Study in Hoa Binh Province, Lower Da River Basin, Northwest Vietnam. *Environment Asia*, 12(2), 67-77. doi:10.14456/ea.2020.30

Thien, B. B., & Phuong, V. T. (2023). Using Landsat satellite imagery for assessment and monitoring of long-term forest cover changes in Dak Nong province, Vietnam. *Geographica Pannonica*, 27(1), 69-82. doi:10.5937/gp27-41813

Thien, B. B., Phuong, V. T., & Huong, D. T. V. (2022b). Detection and assessment of the spatio-temporal land use/cover change in the Thai Binh province of Vietnam's Red River Delta using remote sensing and GIS. *Modeling Earth Systems and Environment*, 1-12. doi:10.1007/s40808-022-01636-8

Thien, B. B., Sosamphanh, B., Yachongtou, B., & Phuong, V. T. (2022a). Land use/land cover changes in the period of 2015–2020 in AngYai Village, Sikhottabong District, Vientiane Capital, Lao PDR. *Geology,*

Geophysics and Environment, 48(3), 279-286. doi:10.7494/geol.2022.48.3.279

Trincsi, K., & Turner, S. (2014). Mapping mountain diversity: Ethnic minorities and land use land cover change in Vietnam's borderlands. *Land Use Policy*, 41, 484-497. doi: 10.1016/j.landusepol.2014.06.022

Viera, A. J., & Garrett, J. M. (2005). Understanding interobserver agreement: the kappa statistic. *Fam Med*, 37(5), 360-363.

Young, P. S., Cech, J. J., & Thompson, L. C. (2011). Hydropower-related pulsed-flow impacts on stream fishes: a brief review, conceptual model, knowledge gaps, and research needs. *Reviews in Fish Biology and Fisheries*, 21(4), 713-731. doi:10.1007/s11160-011-9211-0

Youssef, A., Sewilam, H., & Khadr, Z. (2020). Impact of urban sprawl on agriculture lands in greater Cairo. *Journal of Urban Planning and Development*, 146(4), 05020027. doi:10.1061/(ASCE)UP.1943-5444.0000623

Zhang, Y., Su, Z., Li, G., Zhuo, Y., & Xu, Z. (2018). Spatial-temporal evolution of sustainable urbanization development: A perspective of the coupling coordination development based on population, industry, and built-up land spatial agglomeration. *Sustainability*, 10(6), 1766. doi:10.3390/su10061766

Forum geografic. Studii și cercetări de geografie și protecția mediului
Volume **XXII**, Issue **1** (**June 2023**), pp.**67-77;**DOI:**10.5775/fg.2023.022.i**

Change detection analysis using Landsat images on Balurghat Municipality, West Bengal, India

Manash LAHA[1*]

[1] Faculty, Department of Geography, Islampur College,Islampur, North Dinajpur,West Bengal, India
* *Corresponding author*: manashlaha1986@gmail.com
Received on 23-03-2023, reviewed on 23-05-2023, accepted on 30-05-2023

Abstract

The major focus of the current study is a spatio-temporal analysis of land use and land cover changes in Balurghat Municipality, West Bengal, using remote sensing and geographic information systems (G.I.S.) from 1990 to 2020. The primary goals are to identify changes in land use and land cover and to look at the key influences and how they affect the dynamics of the landscape. The Landsat images of the study area are classified into five categories with the help of GIS software and Google verified and validated by the process of accuracy assessment. An image has been classified digitally with the help of the Supervised Image Classification method under Maximum Likelihood Classification techniques which also helps to identify the transformation of land from vegetation cover to built up area.
Keywords: *Change detection, Transformation of land, Supervised Image Classification, Maximum likelihood classification, Land use and Land cover.*

Introduction

The land is a product of nature and it is an example of three-dimensional dynamic complex bodies. A part of land developed through the interaction of lithology, structure, drainage, climate, vegetation, and the geomorphological processes operating through time. As a result, different types of landforms have evolved in different parts of the earth (Roy& Shaikh, 2021). Top most solid layer of earth surface which is known as land and Land cover is the biophysical state of the earth's surface particularly immediate surface (Turner et al., 1995). Land cover refers to the natural vegetative cover types that characterize a particular area. These are generally a reflection of the local climate and landforms, though they too can be altered by human actions. Therefore, land use change may involve either Conversion from one type of use to another, or, Modification of a certain type of land use. We have already noted that Land Use describes human uses of the land, or immediate actions modifying or converting land cover and includes such broad categories as human settlements, protected areas and agriculture. The land use change may involve either (a) conversion from one type of use to another or (b) modification of a certain type of land use (Briassoulis, 2002, Roy& Shaikh, 2021). Changes in Land Use and Land Cover have significant impacts on local physical environmental conditions and economic and social welfare. A landscape is a natural arrangement on interrelated tracts of land which is very complicated in nature, the study of landscape dynamics it is very much relevant for land use land cover planning management (De & Jana, 1997). Recent research on land use and land cover change detection has drawn attention of many researchers (Liang et al. 2002; Ayele et al. 2016).Change detection has a significant process for managing and monitoring natural resources and urban development mainly due to the provision of quantitative analysis of the spatial distribution based on a temporal scale. There are a lot of available techniques that serve the purpose of detecting and recording differences and might also be attributable to change (Singh, 1989). Remote Sensing (RS) and Geographic Information System (GIS) are now providing new tools for advanced ecosystem management. The collection of remotely sensed data facilitates the synoptic analyses of Earth – system function, patterning, and change at local, regional and global scales over time; such data also provide an important link between intensive, localized ecological research and regional, national and international conservation and management of biological diversity (Wilkie & Finn 1996, Patra &Gavsker,2021). Balurghat is the headquarter of the Dakshin Dinajpur district but in 60 years ago it had been a mere village, in the historical context of the partition of India and East Pakistan(1971), overnight made its appearance as a town and today it has been turned into a Class-I urban centre of district. Due rapid urbanization, still different problems such as population growth, dramatically changed land cover and land use pattern, urban environmental degradation and gaps are related to the development, don't use any kind statistical based and satellite image based study on urban growth and landscape dynamics of this town are (Kundu,2018).

Objectives:

The present study focused on the following major objectives-

a) To examine the pattern of population growth.
b) To identify the land use and land cover change detection.
c) To identify major land use and land cover problems and provide some probable solutions.

Study area

The name of the town Balurghat has been probably derived from 'BALUKAKIRNAGHAT' meaning a 'ghatfull of sand' (Roy, 2000). The study area is Balurghat municipality under Balurghat community development block of South Dinajpur district. Balurghat, Khadimpur, Bongi, Narayanpur, Barargunathpur, part of Hosseinpur, and Dakra are all included in the Balurghat municipal area. It is lies between 25°12’29’’ N to 25°16’17’’ N and 88°44’48E to 88°47’27’’ E (Figure1). The study area had 151,299 people living there as of the 2011 Census, covering an area of just under 10.74 sq. km. 23wards are available in this municipality and river Atreyee runs across the city, dividing it into disproportionate halves. On the eastern bank of the river is where the city's vital administrative, cultural, and entertainment units are located. The border between India and Bangladesh is 3 km away from the township (Kundu,2018).

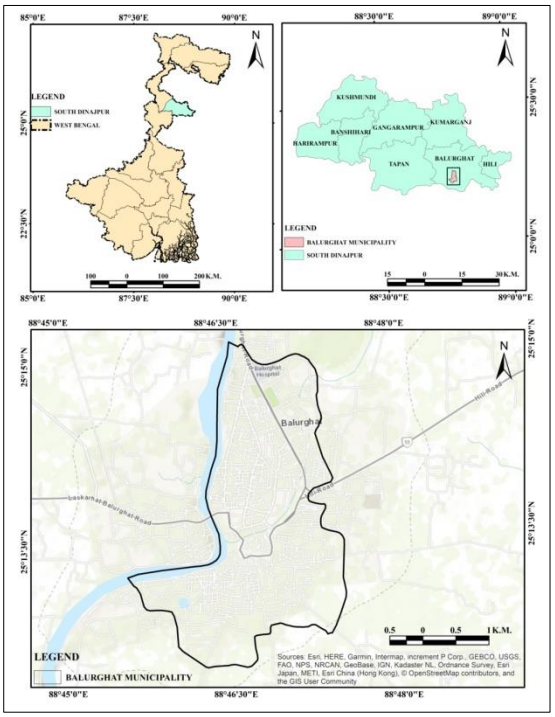

Figure1.Map of study area

Materials and methods

This research is based on cloud free, error free satellite images from USGS data archive on various dates (Table1). For the improving the image accuracy, satellite images should be preprocessed before using. GIS mapping techniques, cartographic techniques and various statistical analyses have been done to fulfill our research objectives. Arc GIS 10.2 and QGIS 2.18 have been used for location map, supervised image classification with maximum likelihood algorithm and transformation of land characteristics. MS-Excel (07) and Power Bi software have been used for statistical calculation and cartographic techniques. Figure 2's flow chart illustrates the approach used in the current study.

Supervised Image Classification

The goal of image classification is to classify all of the pixels in digital image into various landuse and landcover classes. There are two forms of classification, depending on how the computer and interpreter interact during the process. When an analyst has extensive expertise of the field, supervised classification—one of the two main approaches of picture classification—is typically selected. The analyst performs these classifications using a three-stage method that includes training, classification, and output. The analyst chooses training sites to reflect regions with well-known cover kinds throughout the training phase. In this process, the analyst selects training pixels that are representative of the desired land use classes. In the present study, for each class around 25 training samples are taken into account. The sample selection sites from various landuse and land cover categories are shown in Table 1.The classification stage is the second step in supervised classification; it involves categorizing a variety of spectral bands into precise categories of land use and land cover. The output stage is the final outcomes of the image which are presented, visualized, and interpreted using output products. In this research supervised image classification method has been adopted to demonstrate the change detection over a 30-year period. In this classification five different landuse and landcover features have been identify to validate our research goal. Each and every image is independently classified in a supervised classification method with the help of a maximum likelihood algorithm using Arc GIS (10.2) software.

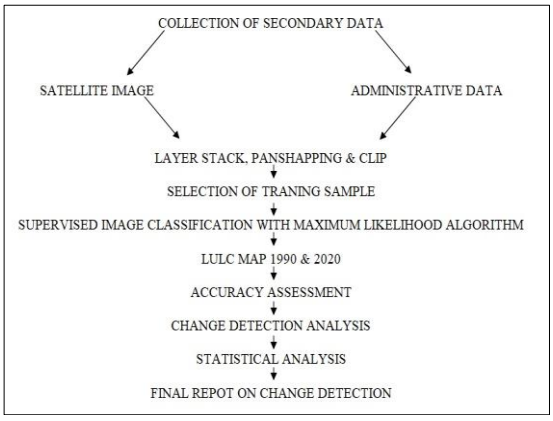

Figure 2.Flowchart of methodology

Table 1: Secondary Data source of this research

SPATIAL DATA	DATA	DATA SOURCE	DATE OF ACQUISITION
SATELLITE IMAGE	Landsat 5 TM	USGS Earth Explorer	30.01.1990
	Landsat 8 OLI/TIRS	PATH : 138/ ROW:48	20.02.2020
ADMINISTATIVE AREA	Village Shape file	https://sedac.ciesin.columbia.edu	01.07.2022
NON SPATIAL DATA	South Dinajpur District Census Hand Book,2001 & 2011		
	District Statistical Hand Book South Dinajpur 2014		

Source: *Prepared by author, 2022.*

Table 2: Land use and land cover classes of the study area

LANDUSE AND LAND COVER CLASS	DESCRIPTION
Waterbody	Rivers, Canals, Ponds.
Sand	Riverian Sands.
Vegetation area	Deciduous Forest Lands,Gardens, Mixed ForestLands, Roadside or Riverside vegetation areas etc.
Open space	Stadium, Play Ground, Park, Recreational spot and Project area under construction, permanent or current fallow.
Builtup area	Residential,Commercial and Services lands.

Source: *Prepared by author, 2022.*

Accuracy Assessment

The term 'accuracy' is often used to indicate the measure of correctness of a derive map which can be tested by using an error-matrix. Remote sensing studies have been focused on accuracy assessment as a key component. It is necessary to gather some in-situ data or a priori knowledge about specific features before comparing them to the classification map produced by remote sensing in order to quantitatively evaluate classification accuracy. Consequently, comparing two classification maps is required to evaluate classification accuracy. 1) The map obtained from remote sensing, and 2) real map. The presumed genuine map may be from on-the-ground research or, more frequently, from the interpretation of remotely sensed data collected at a greater scale or resolution. The most popular method for determining accuracy is error matrix analysis (Khorram et al. 2013). The change detection process relies heavily on individual classifications.

Table 3: Status of Kappa (Rwanga, 2017)

VALUE OF KAPPA	STATUS OF KAPPA
< 0	Poor
0 – 0.2	Slight
0.21 – 0.4	Fair
0.41 – 0.6	Moderate
0.61 – 0.8	Good
> 0.81	Very good

Source: *Prepared by author, 2022 & Das &Sahu, 2020*

As a result, a thorough examination of accuracy must include a report on overall accuracy, user accuracy, and producer accuracy, all of which were examined using the Kappa coefficient (Table3).

Statistical Calculation

Correlation analysis is a statistical analysis which allows researchers to explore the degree of association within independent and dependent variables (Schober&Schwarte, 2018; Senthilnathan, 2019).

$$\mathbf{r} = \frac{\sum(X\mathrm{i}-\bar{\mathrm{x}})(\mathrm{Yi}-\bar{\mathrm{y}})}{\sqrt{(X\mathrm{i}-\bar{\mathrm{x}})^2\sum(\mathrm{Yi}-\bar{\mathrm{y}})^2}}$$

Where, 'r' is the Pearson's product moment correlation coefficient, 'x_i' is values of x variable in a sample,'$\bar{x}_i$' is mean values of x variable, y_i is the value of y variable in a sample and '$\bar{y}_i$'is mean values of y variable.

Scatter plots were created by using regression analysis to demonstrate the pattern of transformation of land from the year 1990 to 2020. Pearson's product-moment correlation coefficient (PPMCC) has been used to measure the direction and strength of the relationship between two variables and regression analysis established the functional relationship between independent (x) and dependent (y) variables (Zhao, 2013). Linear regression is used to ascertain the impact of several numbers of independent variables like X1, X2,X3…Xi on a single dependent variable y Symbolically.

$$y = \beta_0 + x_1 \beta_{1+\ldots} x_p \beta_p + \varepsilon$$

Where, 'β' reflects how much x effects on yand 'Ɛ' is the error term.

Results and discussion

Population Growth

The political reasons for the country's split in 1947 and in 1971 as a result of the Bangladesh war are the key factors that led to the formation of Balurghat Town. This area was first incorporated in East Pakistan by British attorney Sir Radcliff. Later, Radcliff was forced to reverse his choice as a result of the persistent efforts of Mr. Satindranath Basu and Dr. Sushil Ranjan Chatterjee. So, three days later, on August 18, 1947, Balurghat experienced the taste of independence and it was designated as the administrative centre of the West Dinajpur District. Previously a little settlement patches were converted into Balurghat municipality status in 1951 at a small room of the "1928 Club" by Notification No. M1M-40/50 (1) dt. 24th May, 1951 with a population of 18,121 and an area of 6.37 sq. km. The Municipality began operations formally on June 18, 1951, with five wards operating under a nominated authority (Kundu,2018). The population data are collected from census handbook of South dinajpur district showing the continuous population growth in Balurghat municipality from 1951 to 2011 and r2 value showing the population growth over time.

According to Census (2011), present Municipality has 23 wards with 10.74 sq.km total area and total population is 1, 53279. The town is primarily an administrative town having overall population density 6213 persons per sq km. According to census highest decadal growth rate had been recorded in the year 1971, which was 148.48% due to independence war of Bangladesh. **Figure 3** line graph illustrates the continuous flow of population growth.

Infrastructural development is the major threshold area on which developments depends upon in an area (Arif, 2018). It is one of the most significant pull factor for the migrate people. The phenomenon of urbanization therefore occurs on an area and involves links and nodes to create a total system (Sharma, 2012). We are classified urban service basic on their functionality in to six categories such as administrative sector, educational sector, health sector, transport sector, market and recreational sector. The degree of urbanization generally refers to the relative or absolute number of people who live in places defined as urban (Kundu, 2013).

$$\text{Degree of urbanization} = \frac{Urban\ Population}{Total\ Population)} * 100$$

$$= (153279/248907)*100 = 61\%$$

The rate of urbanization is 61 percent, which is significantly greater than India's rate of urbanization. Due to a lack of adequate urban infrastructure, Balurghat is getting increasingly crowded and congested.

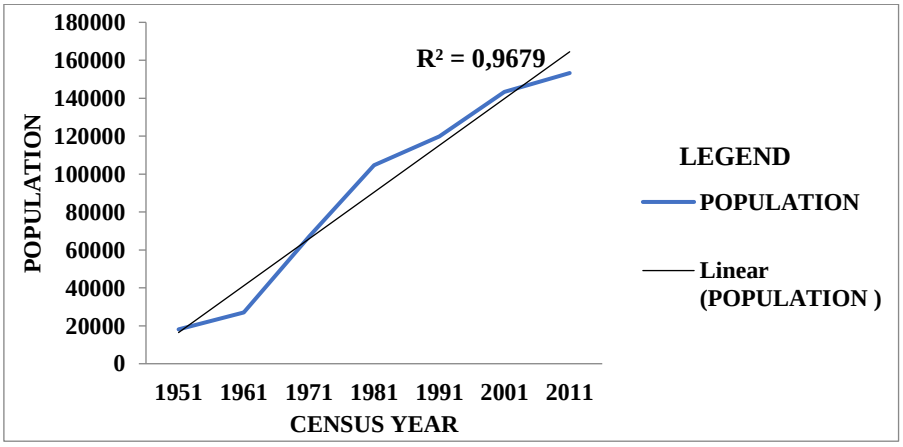

Figure 3: Population Growth of Study Area from 1951 to 2011

Land use and Land cover Change

Detection of changes in the land use / land cover involves use of at least two period data sets (Jenson, 1996). Therefore, spatial changes including surface organization of the land use and land cover and their inter-relationship with a focus on direction and spread are well explained (Patra and Gavsker, 2021). A substantial portion of the research region is revealed to be urban in nature, with little in the way of greenery or open space (Figure4)

Land use and Land Cover Classification 1990

Land use land cover classification was done in the study area under the supervised classification method using maximum likelihood algorithm. On the basis of the number of pixels, the area of each class was calculated

(Das & Sahu, 2020). Based on the land use land cover map of 1990 the area and percentage of areas as classified are water bodies 2.88 % (0.31 Sq.Km.), sand 0.93%(0.1Sq.Km.), vegetation area 33.79 % (3.63Sq.Km.), open space 16.79 % (1.8Sq.km.) and built up area 45.62% (4.9 Sq.Km.). The dominated land use class was built up area and main land cover type was vegetation cover.

Land use and Land Cover Classification 2020

In other hand based on the land use land cover map of 2020 the area and percentage of areas as classified are water bodies 4.18 % (0.45Sq.Km.), sand 1.86 %(0.2 Sq.Km.), vegetation area 14.05 % (1.51 Sq.Km.), open space 18.43 % (1.98 Sq.Km.), and built up area 61.45% (6.6 Sq.Km.). The dominated land use class was built up area and main land cover type was vegetation cover. In case of spatio temporal change it is very indicated that most part of the vegetation cover and open space are transform into or built up area.

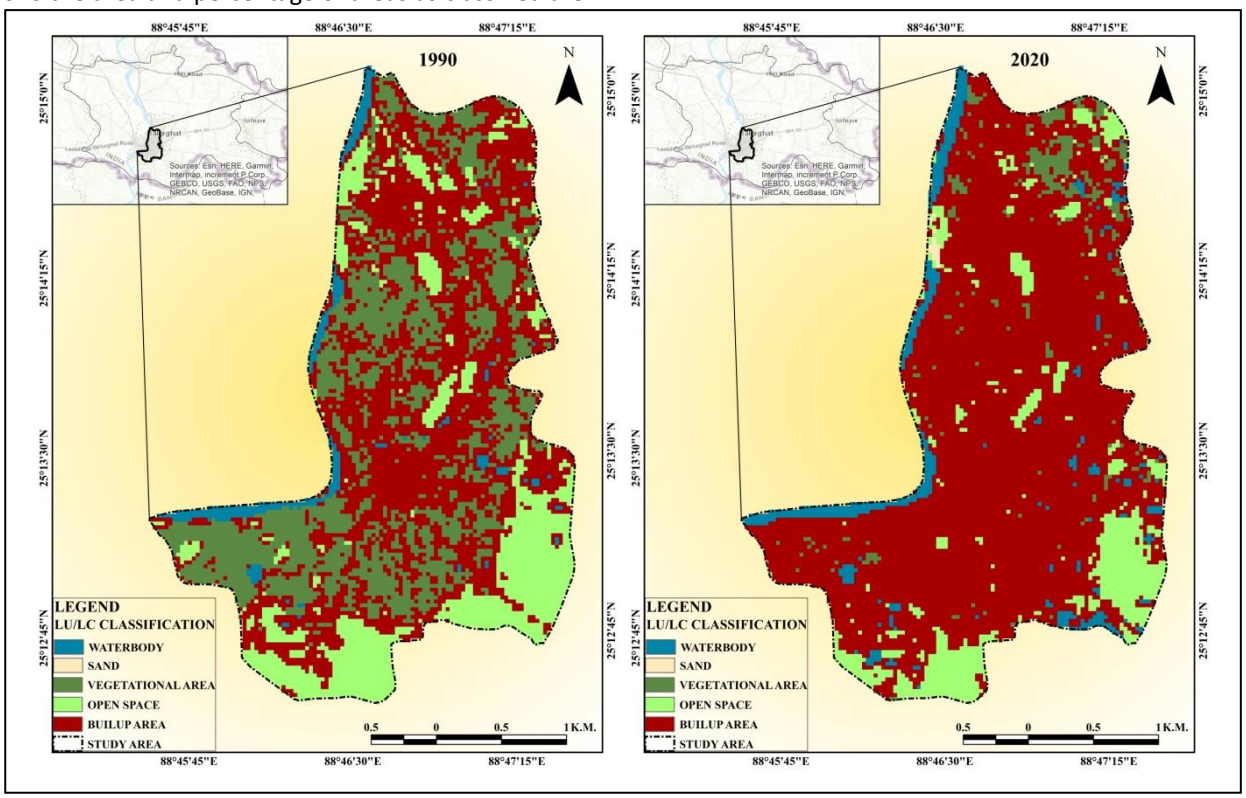

Figure 4: Land use and Land cover map of the study area from 1990 to 2020

Accuracy Assessment:

Accuracy assessment is one of the most crucial stages of the research to confirm our work with genuine earth. Kappa coefficient analysis is one of the most helpful approaches to determine the accuracy evaluation of a study. For the accuracy assessment random sampling method has been used over 100 samples, collected samples are compared between Google Earth image and Landsat images and Table 4 are represent the kappa value which was express the level of accuracy of our research (Kaimais& Patidar,2016). According to Rwanga's (2017) classification (Table 3) the values of kappa are under good to very good scale.

Table4:Summary of Accuracy Assessment from 1990 to 2020

LU/LC CLASSIFICATON TYPE	1990		2020	
	USER'S ACCURACY	PRODUCER'S ACCURACY	USER'S ACCURACY	PRODUCER'S ACCURACY
WATERBODY	0.78	0.88	0.8	0.94
SAND	0.8	0.75	0.82	0.87
VEGETATION	0.76	0.76	0.8	0.92
OPEN	0.8	0.85	0.85	0.85
BUILUP	0.92	0.81	0.92	0.81
OVERALL ACCURACY	**0.815**		**0.881**	
KAPPA	**0.769**		**0.834**	

Source: Prepared by author, 2022

Change detection

Boriah et al., (2008) have performed a new change detection technique for the landcover change detection, especially for remote sensing data. An important aspect of change detection is to determine, which is actually changing to what extent, in other words to check, which landuse class is changing. The outcome results will reveal both the desirable and undesirable changes along with relatively stable categories overtime. This information works as a vital tool in management decisions (Opeyemi, 2006). In this section the attempt is made to check the trend, rate and magnitude of changes in land use / land cover of study area. Table 5 and Figure 5 are representing the spatial change over study area.

Table 5: Summary of Accuracy Assessment from 1990 to 2020

LU/LC CATEGORIES	1990		2020		Area Change		VALUE OF R SQUARE
	Area	%	Area	%	Area	%	
WATERBODY	0.31	2.88	0.45	4.18	0.14	1.3	**0.826**
SAND	0.1	0.93	0.2	1.86	0.1	0.93	**0.89**
VEGETATION COVER	3.63	33.79	1.51	14.05	-2.12	-19.74	**0.858**
OPEN SPACE	1.8	16.79	1.98	18.43	0.18	1.64	**0.79**
BUILTUP AREA	4.9	45.62	6.6	61.45	1.7	15.83	**0.811**

Source: Prepared by author, 2022

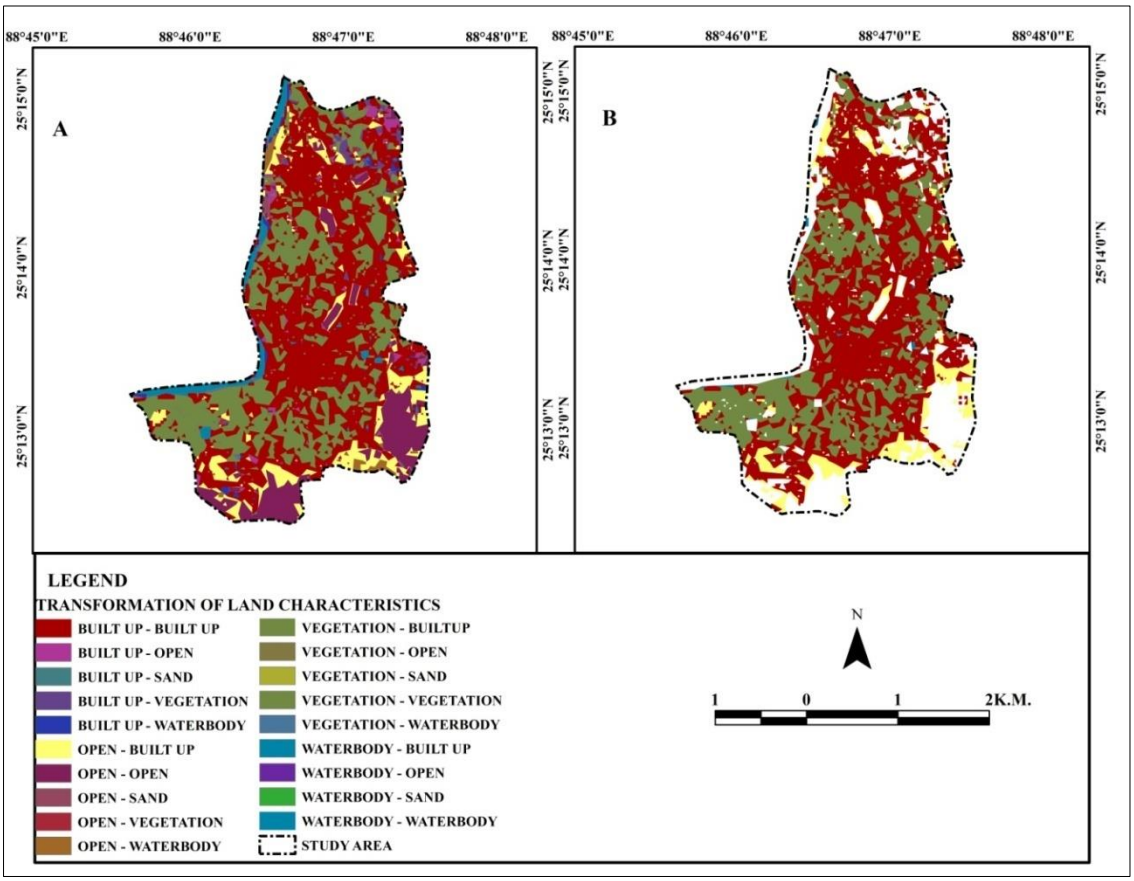

Figure 5: A. Change Detection of land characteristics of the study area from 1990 to 2020 and B. Expansion Built up area

- **Water body**

A river called River Atreyee flows from north to south direction in this region and there are many lakes, ponds and tanks etc have been found. In 1990 the water bodies hold 0.31 sq.km areas which were almost 2.88 % of the total area. But in 2020 the water bodies hold 0.45 sq.km areas which were almost 4.18 % of the total area. So it's clear that from 1990 to 2020 total areas of water bodies continuously increasing nearly 1.3% and the r2 value of water body is 0.826 which indicates the rate growth of water body within this time (Table 5 and Figure 6).

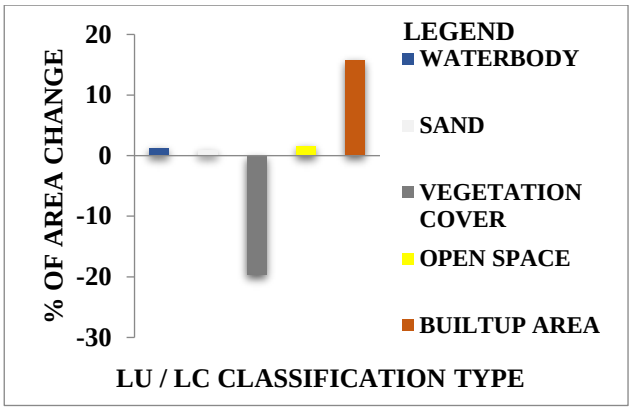

Figure6: Change detection of the study area from 1990 to 2020

- **Sand**

Sand area mainly found in the river floodplain. Sand covered 0.1 sq. km in 1990, or roughly 0.93 percent of the total area but in the 2020 sand holds 0.2 sq.km areas which were almost 1.86 % of the total area. Therefore, it is evident that total sand areas was increased by roughly 0.93 percent between 1990 and 2020, and the r2 value 0.89, so it is shows the pace at which sand will expand during this period (Table 5 and Figure 6).

- **Vegetation cover**

North Eastern, South and South Western parts of the region are covered by dense forest (Figure4). In 1991the vegetation cover was 3.63 km2 areas, about 33.79 % of the total area. But the area decreased to 1.51 km2 (14.05%) in 2020. Hence it's clearly analyzed that from 1990 to 2020 the amount of vegetation cover continuously decreased nearly 19.74 percentage of area. Also the r2 value of vegetation cover is 0.858 which indicates the rate of extensive declining of vegetation cover within this time (Table 5 and Figure 6).

- **Open space**

Stadium, Play Ground, Park, Recreational spot, Project area and under construction area etc are categorized as open area in LULC map. Generally this natural open area has been converted into urban sector and few of them remain static. This area experience a little change with an aerial extent of 1.8 km2 in 1990 which was 16.79% of the total area and 1.98 km2 (18.43%) in 2020. Value of r2 open area is 0.79 indicating the low positive value and showing its significant level of complexness according to time (Table 5 and Figure 6).

- **Builtup area**

An urban sector's area are includes residential, commercial, and other administrative buildings. Accordingly the area included under built up area was 4.9 km2 in 1991 which was 45.62 % of the total area and in the year 2020 the area is 6.6 km2 (61.45%) of the total area respectively. The transformation and growth of built up areas mainly from eastern to south eastern part of the municipality area (Figure 4). Value of r2 built up area is 0.811 is the indication of highly positive development of built up area within time and roughly 15.83 percentage area had been take a positive change(Table 5 and Figure6).

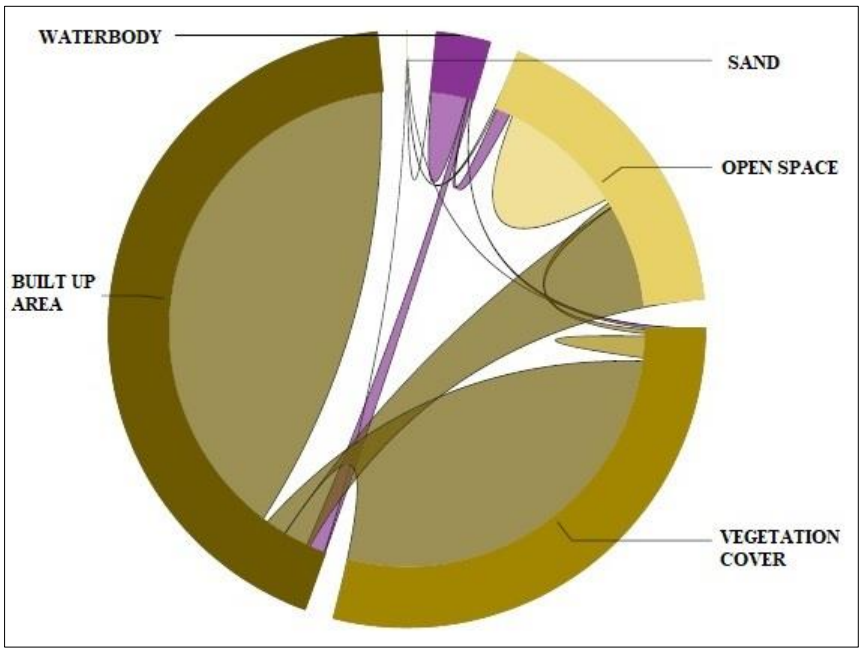

Figure 7: Transformation of land characteristics of the study area from 1990 to 2020

Figure 7 is useful for determining the rate of change, whereas Table 5 and Figure 6 primarily aid in identifying the region of change during the course of the research. The primary land characteristics have shifted from vegetation cover (2.44%) and open space (0.63%) to built-up area.

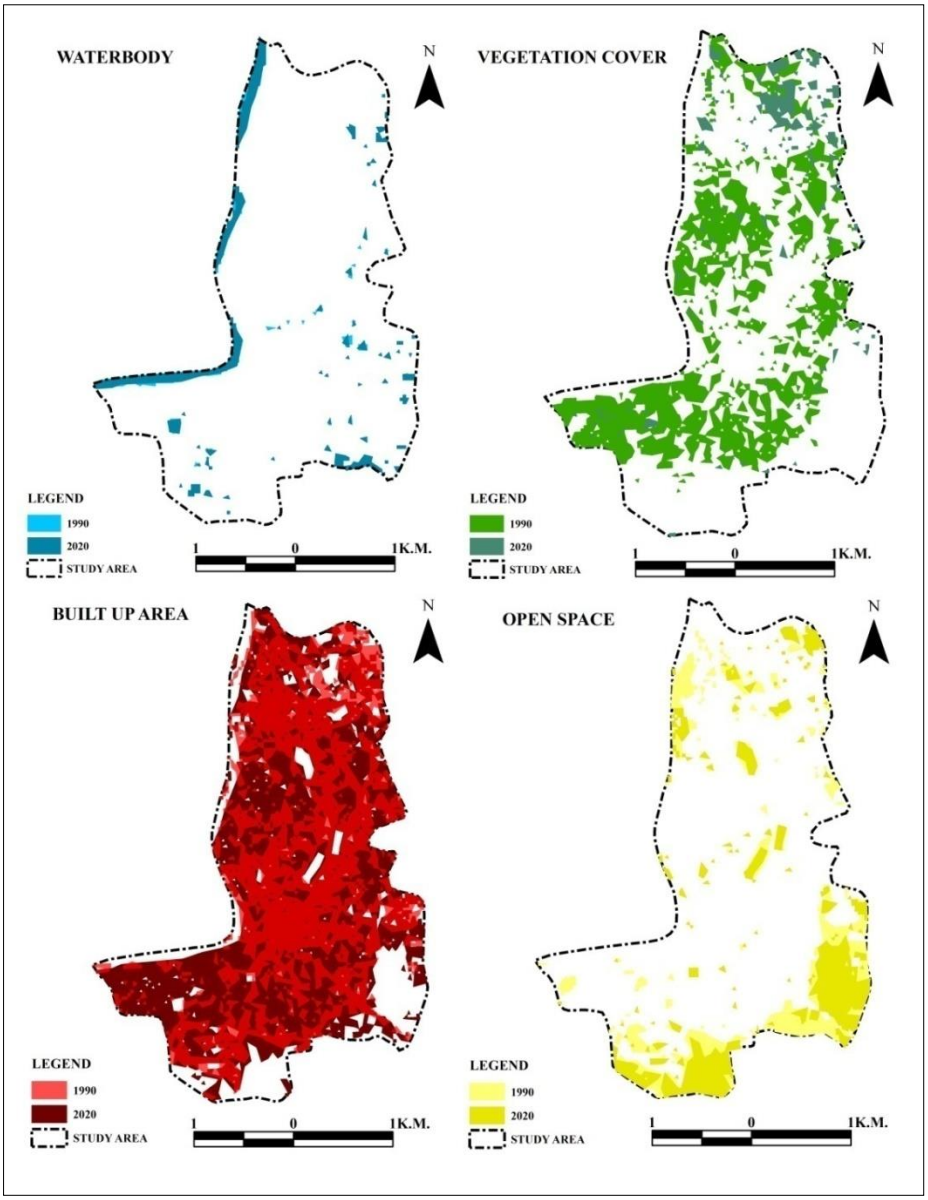

Figure 8: Spatial distribution of land characteristics of the study area from 1990 to 2020

The spatial transformation of each significant land use and land cover characteristic over the study area is plotted in Figure 8. Positive changes have been discovered in land use and land cover elements such water body (1.3%), open space (1.64%), and built-up areas (15.83), while negative changes have been recorded in vegetation cover (almost 19.74%).

Major problem associated with land use and land cover changes

•Clearing of forest areas in some parts of Balurghat city has increased the level of carbon-di-oxide is what is called greenhouse gas. It causes a general rise in temperature. It is also observed that due to concretization of the open land the area is now becoming heat islands.

•Water logging in the rainy season is one of the most important problems in the town as a result of unplanned rapid urbanization.

•Construct residential apartment is major crime to encroaching of water bodies in my study area.

•Land is one of the most precious natural resources on the planet. Due to the sprawling and unplanned growth the fetching of ground water increased and it affects the soil character of the land. Due to the improper management system the soil gets polluted and it affects the soil health and microbial statues of the soil, and the quality of soil is degraded over time.

•Overcrowding refers to the situation in which more people are living within a single dwelling. It is observed from the current study that, the central portions (Ward No.4, 6, 9, 11, 12, 14 &17) have over crowded rather than others.

•Transport plays an important role in economic growth and globalization, but has a deteriorating impact on the congestion, particularly in portions where there are encroachments. Most of the traffic in Balurghat is made up with slow moving vehicles.
•Solid waste is the waste matter which is generated by domestic, commercial, industrial healthcare, agricultural activities etc and accumulates in study area. It is another burning issue in study area.

Probable solution

•The new underground drainage system should be made to control the hygienic condition of the environment

environment. Many areas of the study area have traffic

•The system of collection and management of solid wastes should be improved.
•Urban sprawl and expansion of the city should be controlled.
•Large scale afforestation programmes should be undertaken by the Balurghat municipality.
•Proper manage the urban wetland to check the water scarcity in summer and urban flood.
•New automatic traffic system should be made to control the traffic system.
•One way transportation system should be made to control the overcrowding.

Picture Plate1: Major problem associated with land use and land cover changes

A. Soil pollution &degradation; B. Slum &overcrowding; C. Water logging; D. Traffic congestion; E. Urban waste and F. Drainage problem

Conclusions

This study pinpoints the fundamental issue and suggests some potential solutions. It mostly focuses on change detection from 1990 to 2020. With the use of satellite images and statistical measurements, supervised image classification, accuracy assessment and Pearson's Product Moment Correlation coefficient(r) are used to detect the current situation. It is vital to note that changes in land use and land cover, as well as prompt corrective actions, are crucial for the best and most sustainable use of land resources and the prevention of additional unfavorable degradation. According to the research, Balurghat municipal policy makers should be concerned about future urban growth and create a detailed strategy for environmentally friendly constriction. The study also projected that Land use and land cover change detection can improve the overall urban health and environment and there is further scope for research in this arena to look into population growth, correlation among NDVI, NDWI and NDBI, Land surface temperature and solid waste management program etc. This may be further studied in relation to overall

biophysical and human-induced changes in the region

Funding

This research received no external funding.

Author contribution

Conceptualization, methodology, writing – original draft, ML. The author has read and agreed to the published.

Conflicts of interest

The author declare no conflict of interest.

References

Arif, M., & Gupta, K. (2018). Mapping peri-urbanization in a non-primate city:A case study of Burdwan, India. European Academic Research , V (11), 6065 - 6081.

Ayele, G. T., Demessie, S. S., Mengistu, K. T., Tilahun, S. A., Melesse, A. M. (2016): Multitemporal Land Use/Land Cover Change Detection for the Batena Watershed, Rift Valley Lakes Basin, Ethiopia. In: Melesse, A.,Abtew, W. (eds.) Landscape Dynamics, Soils and Hydrological Processes in Varied Climates. Springer Geography. Springer, https://doi.org/10.1007 /978-3-319-18787-7_4

Boriah, Shyam., Kumar, Vipin., Steinbach, Michael., Potter, Christopher.s and Klooster Steven (2008): Land Cover Change Detectin: A Case Study. http://cucis.ece.northwestern.edu/projects/DMS/publications/BoriahBKSPK2008.pdf

Briassoulis, H. (2000). Analysis of Land Use Change: Theoretical and Modeling Approaches. The Web Book of Regional Science, West Virginia University. http://www.rri.wvu.edu/WebBook/Briassoulis/contents.html

Census of India, 2001 & 2011: District Census Handbook, Dakshin Dinajpur District.

Das, S., & Sahu, A. S. (2020). Monitoring Landuse/ Landcover Changes Using Remote Sensing and GIS: A Casestudy on Kanchrapara Municipality and Its Adjoining area, WestBengal,India. Regional Science Inquiry , XII (2), 43 - 54.

District Statistical Hand Book South Dinajpur 2014.

De, N. K., & Jana, N. C. (1997). The Land Multifaced Appraisal and Management. Calcutta: Sribhumi Publication Company.

Jensen, J. R. (1996). Introductory digital image processing: A remote sensing perspective. Prentice-Hall Inc.

Kaimaris, D., & Patias, P. (2016). Identification and Area Measurement of the Built-up Area with the Built-up Index. International Journal of Advanced Remote Sensing and GIS , 5 (6), 1844-1858

Khorram, S., Nelson, S., Cakir, H., & Wiele, C. V. (2013). Digital Image Processing: Post-processing and Data (Patra & Gavsker, 2021).

Integration. (J. N. Pelton, S. Madry, & S. C. Lara, Eds.) Handbook of Satellite Applications, Springer , 839 - 862. DOI 10.1007/ 978-1-4419-7671-0.

Kundu, T. (2013). Urbanization in the South - East Resource Region of India - A Case Study of Jharkhand , Orissa and Chattisgarh : 1901 - 2001. (N. C. Jana, & L. Sivaramakrishnan, Eds.) Reources and Development Issues and Concerns , 280 – 298

Kundu, P. K. (2018). Emergence of Balurghat as a Class-i City: Demographic Impact of Partition and Bangladesh Liberation War. International Journal of Research and Analytical Reviews , 5 (3), 955Z-964Z.

Liang, S., Fang, H., Morisette, J. T., Chen, M., Shuey, C. J.,Walthall, C. L., Daughtry, C. S. (2002): Atmospheric correction of landsat ETM+ land surface imagery. II.Validation and applications. IEEE Transactions on Geoscience and Remote Sensing 40(12), 2736–2746, https://doi.org/10.1109/TGRS.2002.807579.

Opeyemi, Z. A. (2006): Change Detection in Land Use and Land Cover Using Remote Sensing Data andGIS. http://www.gisdevelopment.net/thesis/OpeyemiZubair_ThesisPDF.pdf

Patra, S., Gavsker, K. K. (2021): Land use and land cover change-induced landscape dynamics: a geospatial study of Durgapur Sub-Division, West Bengal (India). AUC Geographica 56(1), 79–94 https://doi.org/10.14712/23361980.2021.3

Roy, D., (2000). River is the another name of Creation: The Atreyee River (in Bengali) in Dadhichi Uttaradhikar Balurghat, eds. by M. Chakraborty, Banerjee Press, Balurghat, pp. 4-17.

Roy, S. K., & Shaikh, A. S. (Dec.2021). Spatio - temporal change - An analytical Geospatial study using satellite data - Farakka block,Murshidabad district,West Bengal(India). Territorio Della Ricercasu Insediamenti e Ambiente International Journal of Urban Planning. 27 (2/2021) 111-126.

Rwanga, S. S. & Ndambuki, J. M. (2017). Assessment of Land Use/Land Cover Classification Using Remote Sensing and GIS. International Journal of Geosciences. Accuracy. (8): 611-622. https://doi.org/10.4236/ijg.2017.84033

Schober, P., & Schwarte, L. A. (2018). Correlation coefficients: Appropriate use and interpretation. Anesthesia and Analgesia, 126(5), 1763–1768. https://doi.org/10.1213/ANE.0000000000002864

Senthilnathan, S. (2019). Usefulness of Correlation Analysis. SSRN Electronic Journal, 2009(July). https://doi.org/10.2139/ssrn.3416918

Singh, A. (1989). Digital change detection techniques usingremotely sensed data. International Journal of Remote Sensing 10(6), 989–1003, https://doi.org/10.1080 /01431168908903939.

Sharma (Sarkar), S. (2012). Trend of Urbanisation in Berhampore Municipality: A Geographical Analysis. Geo-Analyst , 2 (2), 49 – 56.

Turner, B.L. II and Meyer, W.B., Skole, D., Sanderson, S., Fischer, G., Fresco, L., and Leemans, R. (1995): Global Land Use and Land Cover Change: An Overview, In Changes in Land Use and Land Cover: A Global Perspective, eds. W.B. Meyer and B.L. Turner II, Cambridge: Cambridge University Press, pp.3-10.

Wilkie, D. S., Finn, J. T. (1996). Remote Sensing Imagery for Natural Resources Monitoring: A Guide for First-Time Users. Columbia University Press.

Zhao, J. (2013). The impact on Personality knowledge sharing of personality traits: organizational trust as intermediary variable. Information Studies:Theory & Application, 36(5), 34–38. http://search.ebscohost.com/login

Forum geografic. Studii și cercetări de geografie și protecția mediului
Volume **XXII**, Issue **1** (**June 2023**), pp. **78-91;** DOI: **10.5775/fg.2023.086.i**

Fire signal in lakes and peatlands in Romania during the Holocene: A review of methods, groundwork and achievements

Anca PETRAȘ[1], Anișoara FILIP[1], Diana ISTRATE[1], Marcel MÎNDRESCU[1,2,*]

[1] Department of Geography, Ștefan cel Mare University, 720229 Suceava, Romania
[2] Geoconcept Association of Applied Geography, 727110 Cârlibaba, Romania
* *Corresponding author*: mindrescu@atlas.usv.ro

Received on 12-01-2023, reviewed on 24-05-2023, accepted on 20-06-2023

Abstract

In this article, we provide a review of research that explores the extensive history of wildfires across Europe, focusing specifically on Romania's territory. Lakes and peatlands serve as ideal sources for reconstructing charcoal fluxes resulting from vegetation burning. These natural resources are extremely sensitive to local environmental changes, and the deposition of allochthonous material is exclusively atmospheric. The analysis of macro-charcoal is the primary method for reconstructing local and regional wildfires. This article aims to emphasize the significant studies on paleofires, and the processing and identification methods of macroscopic charcoal particles, which include charcoal number, morphology, and CharAnalysis. The review of scientific achievements in Europe and Romania provides valuable insights into these methods. We aim to investigate the potential of modern international paleofire databases, such as the Global Charcoal Database and Reading Palaeofire Database, which provide updated information on local and regional paleofire occurrences during the Holocene period. We will also make use of software tools that generate maps based on network data, such as VOSviewer Bibliometric Analysis, to visualize and study the wildfire in Romania. Furthermore, we will analyze the publications related to this topic that are available in the Web of Science database. We analyzed the results of paleofire studies in Europe and Romania to determine the primary research directions linked to fire reconstruction. Our review revealed that most of the study sites in Romania are in the Carpathians, particularly at higher elevations, followed by mid-elevation areas. However, lowlands have been less investigated up to this date.
Keywords: *macro-charcoal analysis, lake and peatland sediments, Holocene, paleofire*

Introduction

Charcoal is the result of incomplete combustion of organic matter by a natural or anthropogenic fire (Whitlock & Larsen, 2001). In most cases, charcoal data from lake sediments and peat cores have been used to examine the links between fire and past climate, vegetation, and sometimes anthropogenic activities (Bal et al., 2011; Blarquez et al., 2015; Leys & Carcaillet, 2016; Vanniere et al., 2016). The charcoal layers detected in the thickness of lake and peat deposits can indicate large local fires in certain areas, although they may not entirely reflect all the fires that have occurred in the region. Modern methods of investigation make it possible to reconstruct past fire activity in the local and regional landscape based on data from macro-charcoal analyses of lake and peatbog sediments (Mooney & Tinner, 2011). Moreover, approaches for researching past wildfires also rely on using dedicated software to determine local fire episodes, such as “CharAnalysis” (Higuera, 2009).

The increasing use of fire activity reconstructions based on charcoal analysis over the last millennium reflects the growing interest within the palaeoecological scientific community to consider fire as an ecosystem process operating at both long- and short-time scales, as well as the need for forest managers to understand past fire regimes to identify sustainable management strategies for current and future landscapes (Whitlock & Larsen, 2001; Whitlock et al., 2018). Numerous global studies based on fossil charcoal analysis reflect the need for an understanding of past vegetation fires, particularly during the Holocene (Whitlock et al., 2003; 2010), which represents a key interval for the reconstruction of paleofire activity due to the greater human impact on the environment and the ability to more accurately assess its influence on the fire regime. In recent years, several papers (Mooney & Tinner, 2011; Mustaphi & Pisaric, 2014) have reviewed methods for charcoal analysis in lake sediment and peat cores and their use as a tool for reconstructing fire history. The aim of our research is to review modern methods, achievements, foundations, and perspectives in the study of the long-term dynamics of past fires based on macro-charcoal analyses of various natural archives (lake and peat sediments), and to present a bibliometric analysis of Web of Science paleofire studies linked to climate change. To assess the performance of VOSviewer, paleofire simulations were performed and compared with proxy-based data. Although VOSviewer is primarily designed to analyze bibliometric networks, it can also be used to create, visualize, and explore maps based on any type of network data (Van Eck et al., 2018). Our

research on paleofires contributes to understanding the long-term variations in fire occurrence, by complementing historical records (Feurdean et al., 2015).

Long-term history determination methods for paleofires

The formation and evolution of environments are affected by any fire, natural or anthropogenic. After fires, "traces" in the form of ash and charcoal particles are dispersed by air and water currents and then deposited in peat sediments, preserving palaeoecological information for millennia. Such dispersed charcoal particles can be found and counted in fossil peat sediments using specific methods (macro-charcoal analysis) (Whitlock & Larsen, 2002; Mooney & Tinner, 2011). Peat records are considered the most suitable for reconstructing fire history because sedimentation is continuous, and these sediments preserve palaeodata for many thousands of years in their thickness (Conedera et al., 2009).

Macro-charcoal and dating analysis

In the international literature, two terms are used to designate the same method – macroscopic charcoal analysis (Whitlock & Larsen, 2002) or macro-charcoal analysis (Feurdean et al., 2020). Macroscopic charcoal particles (> 90/150 μm) are transported by the wind over short distances from the fire perimeter (up to 1-2 km), and within the local catchment area and deposited on the surface (Mîndrescu et al., 2013; 2023). Over time, they are buried under new layers of sediment in peat bogs where soil accumulates. Large macro-charcoal particles preserved in post-fire sediments indicate local wildfire activity (Whitlock & Larsen, 2002; Mooney & Tinner, 2011).

There are two main methods for quantification of macroscopic charcoal in lake and peat sediments, namely charcoal number and charcoal area. The use of the charcoal area can reduce uncertainties in the charcoal analysis due to taphonomic processes and breakage during sample preparation. However, it can also introduce measurement errors due to very large individual particles that cannot be associated with a fire event (Finsinger et al., 2014). Therefore, in environments where taphonomic processes are considered important, such as the Mediterranean (Leys et al., 2013; 2016), charcoal areas may be preferred. Conversely, taphonomic processes may be at a minimum in environments at higher latitudes or in ombrotrophic peatlands (Mustaphi & Pisaric, 2014; Florescu et al., 2018).

For reliable reconstructions of fire activity, several studies (Finsinger et al., 2014; 2018) recommend combining both methods. Despite this, there are few studies in Europe (e.g., Leys et al., 2013, 2016; Finsinger et al., 2014; Carter et al., 2018) that compare number- and area-based macroscopic charcoal methods for fire activity reconstruction. Furthermore, there are only two studies in Romania (Retezat Mts.) that reconstruct fire regimes based on both charcoal number and charcoal area (Finsinger et al., 2014; 2018). Macro-charcoal particles are therefore reliable indicators of palaeofires that are specific in systems. The statistical processing of the data obtained on the concentration of macro-charcoal preserved in sediments is carried out using the "CharAnalysis" software (Higuera, 2009), adapted for the R-space. The program uses calculations on a chronological basis to age the samples according to the depth-aged model of sediments based on available radiocarbon dates for the sediment section studied. In general, the data obtained from macro-charcoal analysis make it possible to reconstruct the local history of fire activity in each area, to identify relationships between changes in vegetation, climate, and fire, and to identify the possible causes of wildfire activity and its effects on the surrounding areas (Whitlock et al., 2010; Feurdean et al., 2020).

Current state of research on vegetation fires in Europe

Interest in studying paleofire appeared in the 1960s when the concept of fire regime was first introduced to the scientific community. The main issue on which the concept was based was the study of the ecological role of fires (Conedera et al., 2009). These first studies on the long-term history of paleofire were published in the 1970s and were based on novel methods for identifying paleofire in peatbog sediments using macro-charcoal analysis (Clark, 1983; Patterson et al., 1987). The studies focusing on the reconstruction of paleoecological and paleofire conditions (e.g., Barnosky, 1984) and the progress of charcoal analysis (Patterson et al., 1987; Whitlock & Larsen, 2002; Mooney & Tinner, 2011) describe the general features and properties of charcoals, the conditions for their deposition and accumulation, possible relationships between the components of systems, and the probable causes of fires (Whitlock & Larsen, 2002; Mooney & Tinner, 2011).

In several works (e.g., Enache & Cumming, 2006; Mustaphi & Pisaric, 2014; Feurdean et al., 2017) various morphotypes of charcoal particles are distinguished, such as wood, roots, needles, etc., revealing the type of burned vegetation. As these research methods become widespread, technologies for identifying fire episodes are being modernized through the development of software tools, such as CharAnalysis (Higuera, 2009), which allows for the calculation of the rate of accumulation of macro-charcoal particles, the background and threshold values of the concentration of charcoal in sediments and the identification of local fire episodes, and CharTool (The Charcoal Quantification Tool) dedicated to determining, identifying, and classifying the morphological type of charcoal (Snitker, 2020; Pupysheva et al., 2023).

The increasing interest in the reconstruction of wildfires in different parts of the world using macro-

charcoal analyses indicates the relevance of this field of research. In addition to general issues of reconstructing the history of vegetation, fires, and climate in certain areas, possible links between components are considered (Marlon, 2020). In these studies, fire is seen as a natural evolutionary factor contributing to the maintenance and increase of biodiversity, and as a response to changing climatic conditions. In addition, the authors question the dominant role of humans in the increase in modern fire activity, emphasizing the climatic factor. Fire control through changes in land use is considered, since it leads to the elimination of fires and the reduction of the consequences of fires for human infrastructure, while it also introduces an imbalance in the natural process of ecosystem development, sometimes creating favorable conditions for more powerful fires (Harrison et al., 2010; 2021). Another relevant area of wildfire research is to identify the mechanisms of control and variability of fires and their modelling to make probable forecasts on the dynamics of fires (Harrison et al., 2010; 2021). It is recognized that burning biomass has an impact on the climate itself and is a component of regional climate dynamics, as well as a key link in human interaction with the climate.

The purpose of the Global Paleofire Working Group (GPWG) was to collect and analyze data on the content of dispersed charcoal in sediments of different genesis around the world by creating the Global Charcoal Database (GCD) (Power et al., 2008; Harrison et al., 2022; Pupysheva et al., 2023). The main directions of paleofire studies include reconstructing local and regional paleofire events to reveal the dynamics of fires in the Holocene; accumulating a database on paleofire history to identify local and global patterns; identifying relationships between fires and other components of environments including assessing anthropogenic impacts; contributing to the improvement of research methods including software development.

A review of palaeoenvironmental reconstruction research in Romania

Many studies on paleoenvironmental and paleoclimatic reconstructions in Romania have been carried out based on the analysis of sediments from lakes and peatbogs, due to their property of integrating and preserving climatic signals (Feurdean et al., 2012; 2017; 2020; Tanțău et al., 2011; 2014; Fărcaș et al., 2013; Florescu et al., 2017; 2018; Finsinger et al., 2014; 2018; Peters et al., 2020). This research was mostly conducted to understand the evolution of climate change, including the manner in which climate variability and anthropogenic disturbances relate to past fire history. In Romania, studies have been carried out at 15 sites to reconstruct the regime and impacts of wildfires in central and northwestern Transylvania, Retezat Mts. (Tăul betwen Brazi and Galeș), Rodnei Mts., Țibles Mts., Maramureș Mts., and Apuseni Mts. (Feurdean et al., 2012, Mîndrescu et al., 2023) (Fig. 1 and Table 1).

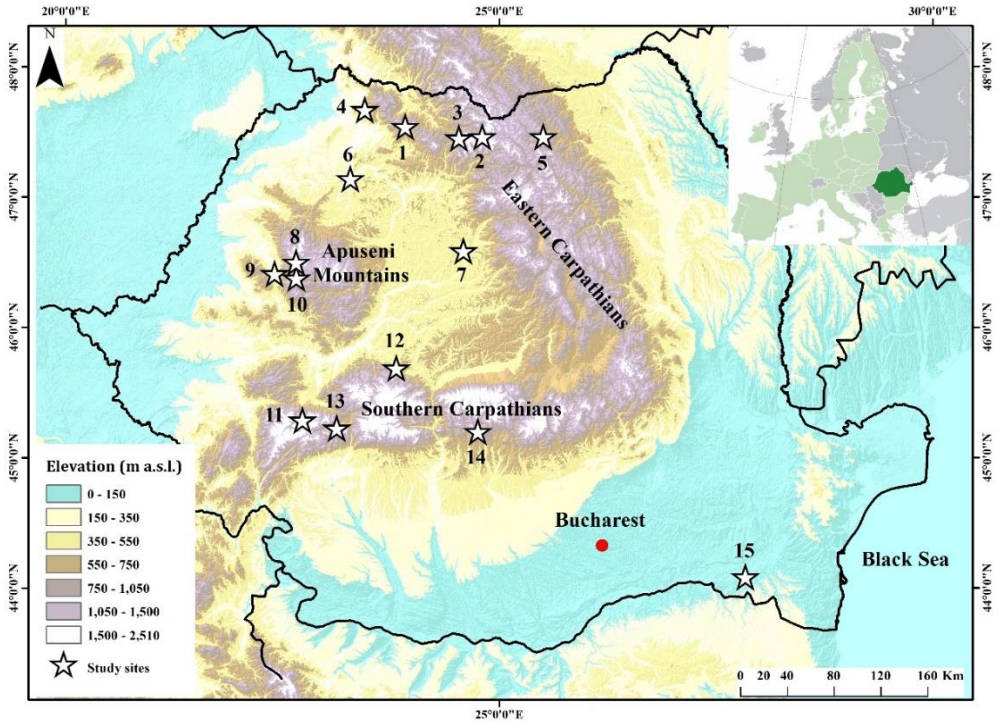

Figure 1. Map of sites where reconstructions of the paleofire regime have been carried out: 1. Tăul Negru; 2. Poiana Știol; 3. Tăul Muced; 4. Preluca Țiganului; 5. Iezerul Feredeu; 6. Turbuța; 7. Știucii; 8. Padiș Sondori; 9. Pietrele Onachii; 10. Molhașul Mare; 11. Brazi (Tăul dintre Brazi); 12. Galeș; 13. Lia; 14. Bucura; 15. Oltina

Table 1. Lacustrine sites investigated in Romania for various proxies, including charcoal

No.	Site name	Geographic location	General information (Elevation, area, maximum water depth, thickness of sediment sequence, age yrs. cal. BP)	Type of investigated site	Proxies	References
1	Tăul Negru	Eastern Carpathians-Lăpuș Mts. 47° 39' 38.39" N 23° 55' 58.43" E	Elev. = 1143 m a.s.l Site = 2 ha Age = 10500 at 5.54 m	Peat bog Late Pliocene volcanic rocks (andesites)	Micro and macro-charcoal, lithostratigraphy, pollen.	Peters *et al.* 2020
2	Poiana Știol	Eastern Carpathians-Rodna Mts., northern slope 47° 35' 14" N 24° 48' 99" E	Elev. = 1540 m a.s.l. St = 3.20 m Site = 0.6 ha CA= 10 ha Age = 10380 at 2.93 m	Peat bog Located in a cirque floor sinkhole Rock type = crystalline limestone	Charcoal, lithostratigraphy, pollen.	Tanţău *et al.* 201l a Tanţău and Fărcaș 2004 Tanţău 2006 Fărcaș *et al.* 2006 Feurdean *et al.* 2017
3	Tăul Muced	Eastern Carpathians-Rodna Mts. 47° 34′ 26″ N 24° 32′ 42″ E	Elev. = 1360 m a.s.l. St = 5.6 m Site = 2 h Age = 8850 at 5.15 m	Peat bog	Charcoal, lithostratigraphy, pollen.	Feurdean *et al.* 2015 Gałka *et al.* 2016 Diaconu *et al.* 2017
4	Prelipca	Eastern Carpathians-Gutâi Mts., western slope 47° 48' 83" N 23° 31' 91" E	Elev. = 830 m a.s.l Site = 2.374 ha CA = 29 St = 10 m (hiatus) Age = 14400 at 9.88 m	Peat bog Located in rock slope failure (sackung)	Charcoal, lithostratigraphy, pollen, plant macrofossil, mineral magnetic analyses (SIRM), organic matter content via LOI, and petrographic analyses (clay mineralogy and grain size measurement).	Feurdean and Beimike 2004 Feurdean 2005 Feurdean and Astalos 2005 Feurdean *et al.* 2007a, b, 2008
5	Iezerul Sadovei	Eastern Carpathians-Western part of the Feredeu Mts., southern Bucovina 47º 36' 13" N 25º 26' 58" E	Elev. = 930 m a.s.l. Site = 0.70 ha CA = 2 ha St = 4.4 m Age = 1300 at 0.98 m	Lake Landslide-dammed located at the bottom of the valley	Charcoal, lithostratigraphy, pollen, plant macrofossil, mineral magnetic analyses (SIRM), organic matter content via LOI, and petrographic analyses (grain size measurement).	Florescu *et al.* 2017
6	Turbuța	Transylvanian Basin, northwestern part 47° 15' 26.5" N 23° 18' 42.9" E	Elev. = 275 m a.s.l. Site = 1.5 ha St = 1.9 m (hiatus)	Paleolake landslide dammed	Micro-charcoal, lithostratigraphy, pollen, total carbon analyses.	Feurdean *et al.* 2007a
7	Știucii	Transylvanian Basin, northern part 46° 58' 044" N 23° 54' 106" E	Elev. = 239 m a.s.l. Site = 38 ha St = 7.27 m	Lake Mixed origin: salt karst and landslide-dammed	Micro and macro-charcoal, lithostratigraphy, pollen, organic matter content via LOI, magnetic susceptibility, elemental geochemistry; sedimentation rates (SR) using ^{210}Pb, ^{226}Ra, ^{137}Cs, and ^{241}Am.	Hutchinson *et al.* 2015 Feurdean *et al.* 2015
8	Padiș Sondori	Western Carpathians-Apuseni Mts. 46° 35' 44.86" N 22° 44' 00.96" E	Elev. = 1290 m a.s.l. Site = 1 ha St = 0.76 m	Peat bog, infilled sinkhole Located on plateau	Charcoal, lithostratigraphy, pollen.	Feurdean and Willis 2008b Feurdean *et al.* 2009
9	Pietrele Onachii	Western Carpathians-Apuseni Mts. 46° 38' 33" N 22° 50' 43" E	Elev. = 1055 m a.s.l. Site = 3.5 ha St = 1.85 m	Forested peat bog, infilled sinkhole Located on plateau	Charcoal, lithostratigraphy, pollen.	Feurdean and Willis 2008b

10	Molhașul Mare	Western Carpathians-Apuseni Mts. 46° 35' 24" N 22° 45' 51" E	Elev. = 1360 m a.s.l. Site = 1 ha St = 2.24 m	Peat bog, infilled sinkhole Located on plateau	Charcoal, lithostratigraphy, pollen, magnetic susceptibility, organic matter content via LOI.	Feurdean and Willis 2008b
11	Tăul dintre Brazi	Transylvanian Alps-Retezat Mts., northern slope 45° 23' 49.58" N 22° 54' 11.43" E	Elev. = 1730 m a.s.l. Site = 0.11 ha CA = 5.28 ha Water depth = 1.1 m St = 4.9 m Age = 13620 at 5.78 m	Lake Located on the bottom of a glacial valley	Charcoal, lithostratigraphy, elemental geochemistry, organic matter content via LOI, pollen, macrofossils, conifer stomata, diatoms, ostracode, chironomids, ancient DNA.	Magyari *et al.* 2009a, b, 2011, 2013 Finsinger *et al.* 2016
12	Galeș	Transylvanian Alps-Retezat Mts., northern slope 45° 23' 09.69" N 22° 54' 38.51" E	Elev. = 1973 m a.s.l. Site = 3.68 ha CA = 177.5 ha Water depth = 20 m St = 3.28 Age = 13540 at 2.80 m	Lake Located in glacial cirque	Charcoal, pollen, macrofossils, conifer stomata, diatoms, Cladocera, chironomids.	Magyari *et al.* 2009a, b
13	Lia	Transylvanian Alps-Retezat Mts., southern slope 45° 21' 08.73" N 22° 52' 44.24" E	Elev. = 1910 m a.s.l Site = 1.3 ha CA = 431.9 Water depth = 4.3 m St = 7.62 Age = 14200 at 7.62	Lake Located in glacial cirque	Charcoal, diatoms (siliceous algae), pollen, macrofossils, cladoceran, and chironomids.	Buczkó *et al.* 2013 Finsinger *et al.* 2016
14	Bucura	Transylvanian Alps-Retezat Mts., southern slope 45° 21' 38.58" N 22° 52' 34.15" E	Elev. = 2040 m a.s.l. Site = 10 ha CA = 201.4 ha Water depth = 17.5	Lake Located in a complex glacial cirque	Charcoal, pollen, macrofossils, cladocera, chironomids.	Buczkó *et al.* 2013 Magyari *et al.* 2018 Hubay *et al.* 2018
15	Oltina	Floodplain in Danube River, the lower Danube Plain, in southeastern 44° 09′ 16″ N 27° 38′ 13″ E	Elev. = 7 m a.s.l. Site = 33 km^2 Age = 6000 at 9.62	Lake Has a major tributary, Canaraua Fetii, and is connected to two smaller lakes, Ceamurlia and Iortmac	Macro-charcoal, lithostratigraphic, LOI, AMS ^{14}C, ^{210}Pb and ^{137}Cs, pollen, n-alkanes.	Feurdean *et al.* 2021

According to the results of these investigations, the most significant short-term climatic events were recorded in lake and peat sedimentary archives on the Romanian territory within the framework of a regional comparison (Fig. 2).

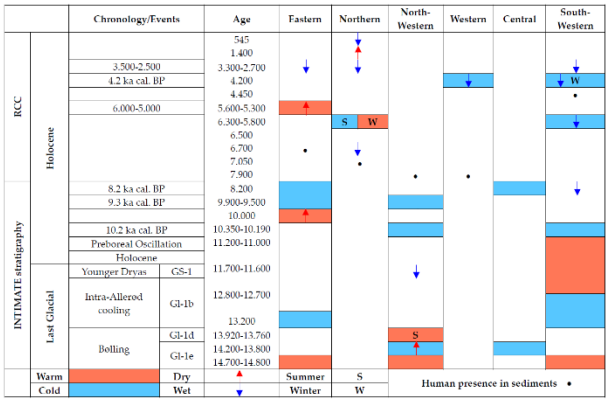

Figure 2. Summary of inferred climatic changes between 14400 and 550 cal. yr BP at reviewed sites from Romania (adapted after Mîndrescu et al. 2017)

These climatic events are further related to the Intimate event stratigraphy (Blockley et al. 2012) from 14400 to 8000 cal. yr BP, whereas the 8000 cal. yr BP to the present period is roughly related to the regional climatic changes documented by Mayewski et al. 2004 and Magny & Haas 2004 cited by Mîndrescu et al. 2013. The characteristics of the climatic stages identified in this area based on the multi-proxy analyses carried out at the sites described in Table 1 and presented in Figure 3 are summarized below according to Blockley et al. 2012 cited by Mîndrescu et al. 2017.

14.4 – 11.7 ka cal. BP. A pollen-based quantitative temperature reconstruction (Feurdean et al., 2008) showed a 2 °C increase in annual temperatures, which reached 4 °C at 14.8 kyr cal. BP. During this period, in the Northern, Eastern, and Southwestern Carpathians, the temperature increase was documented in winter temperatures, whereas summer temperatures remained unchanged. This event is equivalent to the GS-2/GI-1e transition in the Greenland ice core isotope record, which shows an increase in temperature amplitude (Blackley et al., 2012).

11.7 – 8 ka cal. BP. In European regions, climate warming at the Holocene transition resulted in enhanced

vegetation competition and diversity. This major and abrupt climate shift triggered a visible response in vegetation at both lowland and upland sites (Fărcaş et al. 1999, 2006; Björkman et al. 2002; Tanţău et al. 2003, 2006; Feurdean, 2005; Feurdean et al. 2007a, b) which demonstrates that all elevations were comparably vulnerable. Biomass burning reached maximum values due to fire conditions and biomass availability. Charcoal records revealed lower fire activity between 12 and 10.7 kyr cal. BP in the lowland of northern Transylvania due to a shortage in fuel availability against the background of arid and strongly seasonal climatic conditions, i.e., higher summer temperature (4 °C above current mean temperature) and lower precipitation (by 33 %) compared to the present (Feurdean et al., 2013b). Between 9900 and 9500 cal. yr BP, higher lake levels accompanied by decreasing productivity and change in sediment geochemistry, and vegetation (Buczkó et al. 2012, 2013; Magyari et al., 2009b, 2011; Soroczki-Pinter et al., 2015), appear to reflect the shift towards drier conditions from ~ 9200 cal. yr BP.

8.2 - 3 ka cal BP. Between 8000 and 3000 cal. yr BP, in the western sector of the Northern Carpathians, coldest month and annual temperatures were lower compared to current conditions, whereas summer temperatures and precipitation showed increased values, comparable to the present; more stable conditions prevailed compared to the Early Holocene were interrupted by several short-term climate events (Schnitchen et al. 2006; Feurdean et al. 2008). In the SW Carpathians event between 6300 and 5800 cal. yr BP, characterized by summer cooling, a decrease in winter ice-cover season, and an augmenting size of the water body, because of cooler and moister conditions (Buczkó et al., 2013; Magyari et al., 2009a, b). The event is synchronous with a short climatic change recorded in SE Europe and the Northern Mediterranean Region known as 6000-5000 cal. yr BP cold anomaly (Mayewski et al., 2004) characterized by cooler summers and warmer winters (Tanţău et al., 2011a). This anomaly was also identified, albeit with even greater amplitude, in the Eastern Carpathians, at Poiana Știol peatbog (Tanţău and Fărcaş 2004; Tanţău et al., 2011a), in Buzău Subcarpathians (Tanţău et al., 2009) and Southern Transylvania-Făgăraș Depression (Tanţău et al., 2006, 2011b).

3 ka cal. BP to Present. In the Northern Carpathians the last 3000 cal. yr BP was characterized by warm winters (0-1 °C mean temperature of the coldest month) and elevated annual temperatures (7-8 °C), while precipitation decreased by about 100 mm (Mîndrescu et.al., 2017).

Figure 3. Pictures of study sites, upper left corner (Iezerul Sadovei, Molhoșul Mare, Poiana Știol), upper right corner (Tăul dintre Brazi, Lia, Oltina, Galeș), bottom left corner (Bucura, Știucii, Tăul Muced, Tăul Negru)

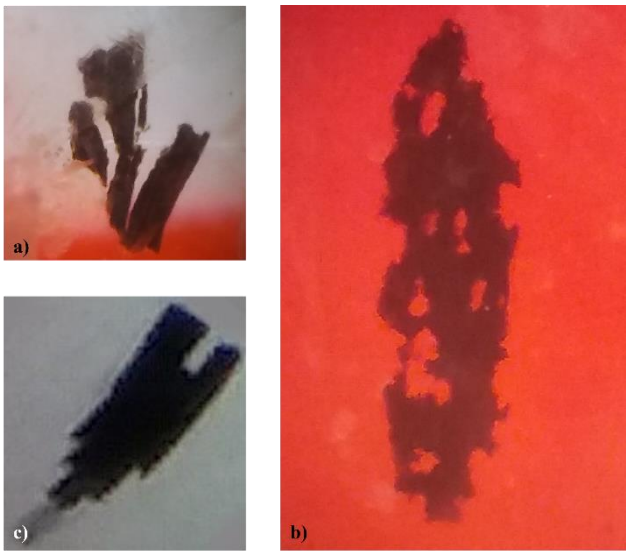

Figure 4. Photographs of representative charcoal morphotypes under a stereomicroscope: a) wood; b) grass (Poaceae) and c) conifer needles

Figure 4 shows the different categories of sedimentary charcoal pieces found in studies. Macroscopic charcoal present in sedimentary records can be classified into these categories. Charcoal morphology can reflect fuel sources with varying degrees of certainty (Scott et al., 2000). As a result, charcoal morphological data can be used to indicate past vegetation assemblages (Mustaphi & Pisaric, 2014) and investigate the different contributions of vegetation types to biomass burning.

Bibliometric analysis on keywords using VOSviewer

The study provides an analysis of recently published literature on paleolimnological studies of wildfires related to ongoing climate change carried out in Romania. The analysis considers papers published from 2004 to 2022 in Web of Science or Scopus (Figure 5).

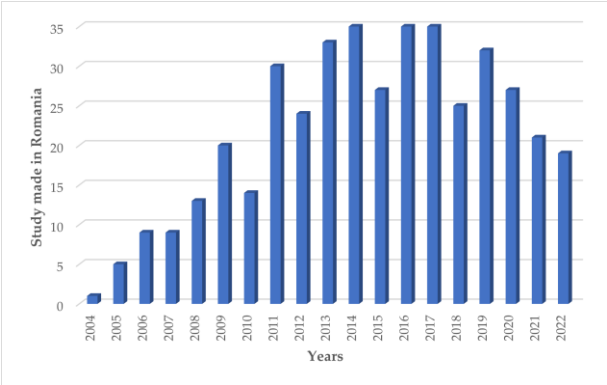

Figure 5. Distribution of review sources from 2004 to 2022 covering studies on paleofires, environmental and climate change carried out in Romania

The study identifies the keywords involved in the selection of the materials, which are necessary for an understanding of the importance of peatbog fire in climate change and how the change of landscape can be influenced by anthropogenic activities. The study also uses bibliographic data and abstracts from Web of Science and Scopus to construct the map based on the data text. The application creates classes of terms, allowing us to preview the selected items, highlighting the links and where they appear in the database.

Climatic and palaeoenvironmental data

The analysis of sediment records from lakes and peatbogs in Romania suggests that the climate during the late Holocene was predominantly affected by natural factors. However, during the late Holocene, it was impacted by a combination of natural and anthropogenic factors. The deforestation of the Romanian Carpathians took place much later than the rest of Europe during the Holocene, resulting in a different pattern of biomass burning in the lowlands compared to the highlands. In Figure 6, the authors who have studied fire regimes in Romania from 2004 to 2022 are highlighted. The figure focuses on identifying climate changes and their impact on the fire regime over time, as well as reconstructing paleofire history. It shows the most relevant contributors in this field, including Feurdean, Tanţău, Fărcaș, Hutchinson, Peters, Magyari, Mîndrescu, Florescu, and Haliuc. The density of the figure is related to the occurrence. The authors' work on climate change and vegetation fires has evolved in terms of research methods over the period in question.

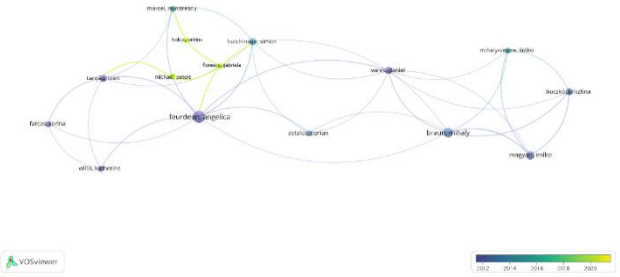

Figure 6. Network visualization map of the main authors who studied wildfires in Romania, showing the evolution from 2004 to 2022

Spatial distribution of wildfires studied in Romania

According to VOSviewer software, the spatial distribution of wildfires studied in Romania is represented by purple dots, which are correlated between articles on the main topic of reconstructing wildfire in the context of climate change using charcoal as the main proxy. Figure 7 illustrates that in 2006, there was a focus on studies related to climate change in Romania, specifically in the Carpathians. The maximum green color in 2014 is followed by a slight decrease in the number of studies, which can be attributed to the studies carried out earlier. Figs. 5 and 7 show that the maximum color, followed by a sharp

decrease in the number of studies, can be observed in the years 2016-2017 and 2019. It seems that the highlighted studies were conducted in Romania, focusing on the Holocene period and forest areas marked with yellow dots. Other relevant topics include climatic change, core and lake sediment analysis, fire activity, macro-charcoal and charcoal particle analysis, land clearance, and studies conducted in the southern Carpathian Mountains, with Lia and Bucura sites, (Finsinger et al. 2018; Pál et al. 2018; Orbán et al. 2018; Buczkó et al. 2013; Magyari et al. 2018; Hubay et al. 2018). In the map with green dots, the smallest items represent the sites in northwest Romania from the Transylvania Basin where studies have been carried out on paleofire regime reconstruction in the Turbuța and Știucii sites (Feurdean et al. 2007, 2015), in Apuseni National Park, studies have been conducted on the following sites: Padiș Sondori (Feurdean et al. 2008, 2009), Pietrele Onachii and Molhașul Mare sites (Feurdean et al. 2004, 2008), Gutâi Mts., with Preluca Țiganului site (Feurdean et al. 2004, 2005a, b, 2007a, b, 2008), Rodna Mts., with Poiana Știol and Tăul Muced sites (Fărcaș et al. 2004; Tanţău et al. 2006; 2011, Feurdean et al. 2015, 2017), and Lăpuș Mountain with Tăul Negru site (Peters et al. 2018). Blue dots indicate reconstruction and environmental change. Human settlements have impacted the landscape and environment in these areas.

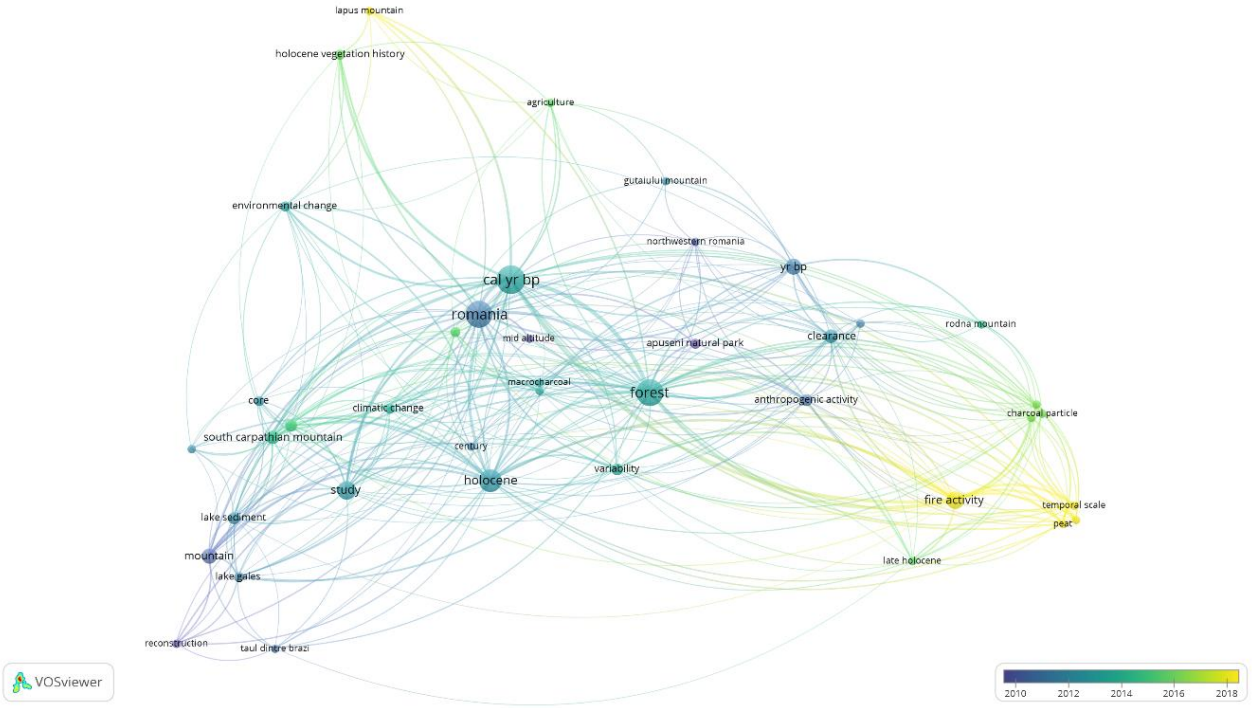

Figure 2. Bibliometric visualization map of studies carried out in Romania from 2004 to 2022

Discussion

In Romania, climate variability has varied by region in the late Holocene. Climate change has led to an increase in extreme weather conditions such as prolonged droughts and wildfires (Beniston et al. 2007, Begović et al. 2020, Vacek et al. 2023). Studies suggest that droughts will become more intense and frequent in central and southern Romania in the foreseeable future. This will affect lakes and peatbogs, which will be more vulnerable to lengthy droughts and frequent wildfires (Vacek et al. 2023). Human activities such as deforestation and mining, as well as landscape changes, will contribute to the occurrence of wildfires. Research conducted over the last two decades should inform the development of sustainable landscape management and environmental protection policies based on scientific evidence.

Studies in low-altitude areas (steppe, forest-steppe)

Feurdean et al. (2021) conducted a study on Lake Oltina, located on the Danube floodplain. The results showed that the lake was formed between 6000 and 2500 cal. yr BP, during a period when there was a vast canopy of xerothermic (*C. orientalis* and *Quercus*) and temperate (*Carpinus betulus, Tilia*) tree taxa. Over time, due to agricultural activities, the tree cover started to decline, while the climate remained humid. At around 2500 cal. yr BP, there was an increase in biomass burning, which suggests that fire was used as a management tool. Over the last millennium, there has been a significant decline in the amount of wooded areas. The landscape openness at Lake Știucii (239 m a.s.l.) during the late Holocene was estimated to be about 20% higher than the actual data.

The open coniferous forest was reduced during the late Holocene, likely indicating a transition. This was due to a higher cover of *Poaceae* and *Picea* and lower values for *Pinus* and *Artemisia*. The Bronze Age was characterized by human activities, including extensive forest clearance after 3700 cal. yr BP, indicating that the Transylvanian Plain was more wooded in the past. However, the forests were never completely closed due to dry growing season conditions, recurrent fires, and anthropogenic impacts that favoured the persistence of grasslands throughout the late Holocene, according to Feurdean et al. 2015. At Turbuța palaeolake in the Transylvanian Basin, the presence of *Pinus* and *Betula* open woodlands with small populations of *Picea*, *Ulmus*, and *Alnus* is indicated before 12000 cal. yr BP. The vegetation dynamics at Turbuța, along with other sites in Romania, suggest a response of the vegetation to regional climatic changes, which indicate that the forests in the lowlands of Turbuța were never closed, as reported by Feurdean et al. 2007b.

Studies in mid-altitude areas (deciduous forest, mixed forest)

At paleolake, Preluca Țiganului (730 m a.s.l.) from Gutâi Mts., the current vegetation types in the area include *Picea* and *Pinus*, and the climate has been relatively stable. Small climate oscillations are recorded at mid-altitude sites because these areas are close to the tree-line ecotone. The development of vegetation shows different responses and amplitudes of response to climatic changes, with local factors determined by the altitude and topography of the study site, as described in Feurdean et al. (2007a). According to Florescu et al. (2017), the data collected from lake Iezerul Sadovei provides the first evidence of environmental changes that have taken place in the mountainous region of Southern Bucovina in the past ~ 950 years. The environmental degradation in this area and its surroundings is primarily caused by human activities such as deforestation. However, it is also influenced by climate-related hydrological conditions such as flooding and the evolution of slope processes. At the Tăul Negru peatbog, there has been a continuous increase in indicators of human activity, such as the presence of *Plantago lanceolata* and *Chenopodiaceae*, and an increase in the abundance of *Poaceae*, *Rumex*, and *Urticaceae* (Peters et al. 2019). The increase in charcoal content is particularly significant in this area, indicating further opening of forests and increasing forest exploitation (charcoal burning) and grazing pressure. The first signs of anthropogenic activity were detected around 6000 cal. yr BP. This pressure was observed in the development of a cultural landscape, which progressed during the Middle Ages and became even more pronounced in modern times. Local disturbances increased during periods of mining activity. It is possible that people used fire to clear forests and open access to mining sites or pastures (Petraș et al. 2021).

Feurdean et al. (2008) conducted a study in the Apuseni National Park, NW Romania, to reconstruct the long-term dynamics of *A. alba*. Three sites – Molhașul Mare, Pietrele Onachii, and Padiș Sondori – were selected for this purpose. The study found that the concentrations of micro-charcoal recorded in Molhașul Mare and Padiș Sondori were highest between 6000 and 4200 cal. yr BP, followed by a decrease and overall low values between 4200 and 500 cal. yr BP. Subsequently, the levels steadily increased again during the last 300-500 years. The study reveals that A. alba has existed in Romania since at least 5700 cal. yr BP. These stands grew in mixed formations until approximately 300 years ago when they were reduced to their present state.

Studies in high altitude areas (coniferous forests, the ecotone at the upper limit of the forest, subalpine and alpine areas)

Gałka et al. (2016) and Diaconu et al. (2017) have reported that Tăul Muced is an ombrotrophic raised bog located in the Eastern Carpathians in Rodna National Park at an altitude of 1.360 m a.s.l. The bog covers an area of approximately 2 hectares, of which about 0.5 hectares has been designated as a scientific reserve under the IUCN category. The bog's surface is mostly covered by spruce trees with small patches of dwarf pine (*Pinus mugo*) scattered around. The dominant species in the moss communities are *Sphagnum russowii* and *S. magellanicum*, along with *Vaccinium microcarpum*, *Carex pauciflora*, *Vaccinium myrtillus*, *Drosera rotundifolia*, *Listera cordata*, and *Polytrichum strictum* (Diaconu et al. 2017; Feurdean et al. 2015). The pollen sequence indicates that *Sphagnum magellanicum* was the most prominent species in the formation of peat for around 8000 years. However, it also reveals ten stages where *Eriophorum vaginatum* had a higher representation at the following times: 8100, 7550, 6850, 6650, 5900, 4650, 3150, 1950, 1450, 750 cal. yr BP. The cyclical analysis of *Sphagnum magellanicum* and *Eriophorum vaginatum* at Tăul Muced suggests that this could be due to regional changes in climatic conditions or the result of autogenic succession (Gałka et al. 2016). Between 4300 and 3300 years ago, there was low fire activity and *Sphagnum macrofossils* were dominant (Gałka et al. 2016). From 2750 to 1300 years ago, the peatland surface conditions were dry, and the air temperature reconstructions suggest relatively warm summers of approximately 14 °C. Charcoal supports the dry conditions with six centennial-scale temperature changes over the last 6550 years. The summers were relatively cold during the periods 6550-5600, 4500-3150, and 1550-600 years ago. However, warm air temperatures were experienced from 5600-4500, 3150-1550, and 100 years ago to the present (Diaconu et al. 2017). Lake Brazi (Tăul dintre Brazi) is situated on the northern slope of the Retezat Mountains at an altitude of 1.740 m a.s.l in the Galeș valley. On the

other hand, Lake Lia is situated at 1.910 m a.s.l on the southern slope. It is noteworthy that the number of fires on the northern slope was relatively lower compared to the southern slope. In the past, the forests on the northern slope around Lake Brazi were mainly dominated by *Picea abies* and they persisted for a long time. During this time, the intervals between fires were comparatively longer, ranging from 1000 to 4000 years. On the other hand, the forests on the southern slope around Lake Lia had a higher abundance of *Pinus mugo* and their fire-return intervals were significantly shorter, ranging from 80 to 1650 years. Forest clearance through burning to increase pasture was moderate compared to the rest of the region. The frequency of fires differed in various areas due to the different microclimates of the northern and southern slopes, and the location of sites above the tree line ecotone. During the last ~ 2000 cal. yr BP, anthropogenic vegetation changes increased, particularly on the southern slope, and were associated with a moderate rise in biomass burning until ~ 1300 cal. yr BP (Finsinger et al., 2016).

It has been suggested by a palaeolimnological investigation that the glacial lakes of the Southern Carpathians – Lia, Bucura, and Galeș – had oligotrophic and oxygenated waters from the late Holocene to the present. This could indicate that forest clearance through burning to reduce pasture was carried out moderately, according to Buczkó et al. 2013. According to Tanţău et al. (2011), the area was covered by dense woodlands containing various tree species such as *Betula*, *Pinus*, *Picea abies*, and *Alnus*. During this period, *Picea abies* was the dominant species. The peat sequence from Poiana Știol provides a detailed account of the forest dynamics and climate history of the Holocene period. The study suggests that human impact on the area became evident approximately 3200 years ago and was mainly due to deforestation and forest grazing (Tanţău et al. 2011).

Conclusions

Paleoenvironmental studies around the world are increasingly focusing on the long-term dynamics of fire, vegetation, and climate. These studies analyze macro-charcoal to better understand the relationship between vegetation fires, anthropogenic impact, and climate changes during the Holocene. The sediment record-based environmental reconstructions highlight the spatial and temporal manifestation of vegetation fires, which is especially relevant given the current global climate change and catastrophic events. Our study is a focused literature review that examines published literature on paleofire reconstruction in lakes and peatbogs in relation to climate variability, both past and present. The impact of global climate change is a significant challenge for Romania. It is important to take timely and appropriate measures to reduce its impact and to adapt ecosystems to the projected changes in environmental conditions. To minimize the ongoing susceptibility of forests, it is necessary to establish and change the species composition of trees in the stand and select suitable tree species that are resistant to adverse abiotic factors such as drought and wildfire. It is crucial to conduct further research to enhance the connection between scientific research and action while developing adaptive responses that are specific to the context of climate change and disturbance regimes. The risk of wildfires is anticipated to increase in the coming years, even in areas that were previously unaffected, like the high and mid-altitude mountain ranges of the Carpathians, leading to expensive economic and environmental consequences.

Code availability

The VOSviewer source code is accessible at https://www.vosviewer.com/.

Access requests can be made by contacting Nees Jan van Eck (http://www.neesjanvaneck.nl/). For this study, we used the model at version 1.6.19.

Author contribution

Conceptualization, A.P., and M.M.; methodology, A.P.; formal analysis, D.I.; investigation, A.F.; writing—original draft preparation, A.P.; writing—review and editing, A.P., D.I., A.F., M.M. All authors have read and agreed to the published version of the manuscript.

Conflicts of interest

The authors declare no conflict of interest.

References

Bal, M.C., Pelachs, A., Perez-Obiol, R., Julia, R., Cunill, R. (2011). Fire history and human activities during the last 3300 cal. yr BP in Spain's Central Pyrenees: the case of the Estany de Burg. *Palaeogeography, Palaeoclimatology, Palaeo-ecology*, 300(1–4), 179–190. https://doi.org/ 10.1016/j.palaeo.2010.12.023.

Barnosky, C. W. (1984). Late Miocene vegetational and climatic variations inferred from a pollen record in northwest Wyoming. *Science*, 223(4631), 49-51, DOI: 10.1126/science.223.4631.49.

Begović, K., Rydval, M., Mikac, S., Čupić, S., Svobodova, K., Mikoláš, M., ... & Svoboda, M. (2020). Climate-growth relationships of Norway Spruce and silver fir in primary forests of the Croatian Dinaric mountains. *Agricultural and Forest Meteorology*, *288*, 108000.

Beniston, M., Stephenson, D. B., Christensen, O. B., Ferro, C. A., Frei, C., Goyette, S., ... & Woth, K. (2007). Future extreme events in European climate: an exploration of regional climate model projections. *Climatic change*, *81*, 71-95, DOI 10.1007/s10584-006-9226-z.

Björkman, L., Feurdean, A., Cinthio, K., Wohlfarth, B., & Possnert, G. (2002). Lateglacial and early Holocene vegetation development in the Gutaiului Mountains, northwestern Romania. *Quaternary Science Reviews*, 21(8-9), 1039-1059, https://doi.org/10.1016/S0277-3791(01)00061-0.

Blarquez, O., Ali, A.A., Girardin, M.P., Grondin, P., Fréchette, B., Bergeron, Y., Hély, C. (2015) Regional paleofire regimes affected by non-uniform climate, vegetation and human drivers. *Scientific Reports*, 5(1), 1–13, https://doi.org/ 10.1038/srep13356.

Blockley, S. P., Lane, C. S., Hardiman, M., Rasmussen, S. O., Seierstad, I. K., Steffensen, J. P., ... & Intimate Members. (2012). Synchronization of palaeoenvironmental records over the last 60,000 years, and an extended INTIMATE event stratigraphy to 48,000 b2k. *Quaternary Science Reviews*, 36, 2-10, https://doi.org/10.1016/j.quascirev.2011.09.017.

Buczkó, K., Magyari, E. K., Braun, M., & Bálint, M. (2013). Diatom-inferred late-glacial and Holocene climatic variability in the South Carpathian Mountains (Romania). *Quaternary International*, 293, 123-135, https://doi.org/10.1016/j.quaint.2012.04.042.

Buczkó, K., Magyari, E., Hübener, T., Braun, M., Bálint, M., Tóth, M., & Lotter, A. F. (2012). Responses of diatoms to the Younger Dryas climatic reversal in a South Carpathian mountain lake (Romania). *Journal of Paleolimnology,* 48, 417-431, DOI 10.1007/s10933-012-9618-1.

Carter, V.A., Moravcová, A., Chiverrell, R.C., Clear, J.L., Finsinger, W., Dreslerová, D., Halsall, K., Kuneš, P. (2018) Holocene-scale fire dynamics of central European temperate spruce-beech forests. *Quaternary Science Reviews*, 191, 15–30, hal-01813530.

Conedera, M., Tinner, W., Neff, C., Meurer, M., Dickens, A.F., Krebs, P. (2009) Reconstructing past fire regimes: Methods, applications, and relevance to fire management and conservation. *Quaternary Science Reviews*, 28(5), 555–576, 10.1016/j.quascirev.2008.11.005.

Diaconu, A. C., Toth, M., Lamentowicz, M., Heiri, O., Kuske, E., Tanţău, I., ... & Feurdean, A. (2017). How warm? How wet? Hydroclimate reconstruction of the past 7500 years in northern Carpathians, Romania. *Palaeogeography, Palaeoclimatology, Palaeoecology*, *482*, 1-12, https://doi.org/10.1016/j.palaeo.2017.05.007.

Enache, M.D., Cumming, B.F. (2006) Tracking recorded fires using charcoal morphology from the sedimentary sequence of Prosser Lake, British Columbia (Canada). *Quaternary Research*, 65(2), 282–292, 10.1016/j.yqres.2005.09.003

Fărcaș, S., & Tanţău, L. (2004). The human presence in pollen diagrams from Romanian Carpathians. *Antaeus (Budapest)*, (27), 227-234.

Fărcaș, S., de Beaulieu, J. L., Reille, M., Coldea, G., Diaconeasa, B., Goeury, C., ... & Jull, T. (1999). First 14C datings of Late Glacial and Holocene pollen sequences from Romanian Carpathes. *Comptes Rendus de l'Académie des Sciences-Series III-Sciences de la Vie*, 322(9), 799-807, https://doi.org/10.1016/S0764-4469(00)80039-6.

Fărcaş, S., Tanţău, I., Mîndrescu, M., & Hurdu, B. (2013). Holocene vegetation history in the Maramureș mountains (Northern Romanian Carpathians). *Quaternary International*, Vol. 293, pp. 92-104, https://doi.org/10.1016/j.quaint.2012.03.057.

Feurdean, A. (2004). Palaeoenvironment in North-Western Romania during the last 15,000 years (Doctoral dissertation, *Institutionen för naturgeografi och kvartärgeologi*).

Feurdean, A. (2005a). Holocene forest dynamics in northwestern Romania. *The Holocene*, 15(3), 435-446.

Feurdean, A., & Astalos, C. (2005b). The impact of human activities in the Gutâiului Mountains, Romania. *Studia UBB Geologia*, 50(1), 63-72.

Feurdean, A., & Willis, K. J. (2008). Long-term variability of Abies alba in NW Romania: implications for its conservation management. *Diversity and Distributions*, Vol. 14, no. 6, pp. 1004-1017, 10.1111/j.1472-4642.2008.00514.x.

Feurdean, A., Florescu, G., Vannière, B., Tanţău, I., O'Hara, R. B., Pfeiffer, M., ... & Hickler, T. (2017). Fire has been an important driver of forest dynamics in the Carpathian Mountains during the Holocene. Forest *Ecology and Management*, Vol. 389, pp. 15-26, 10.1016/j.foreco.2016.11.046.

Feurdean, A., Galka, M., Kuske, E., Tanţău, I., Lamentowicz, M., Florescu, G., ... & Hickler, T. (2015). Last millennium hydro-climate variability in Central-Eastern Europe (northern Carpathians, Romania). *The Holocene*, *25*(7), 1179-1192, https://doi.org/10.1177/0959683615580197.

Feurdean, A., Grindean, R., Florescu, G., Tanţău, I., Niedermeyer, E. M., Diaconu, A. C., ... & Hickler, T. (2021). The transformation of the forest steppe in the lower Danube Plain of southeastern Europe: 6000 years of vegetation and land use dynamics. Biogeosciences, Vol. 18, no. 3, pp. 1081-1103, 10.5194/bg-18-1081-2021.3.

Feurdean, A., Klotz, S., Mosbrugger, V., & Wohlfarth, B. (2008). Pollen-based quantitative reconstructions of Holocene climate variability in NW Romania. Palaeogeography, *Palaeoclimatology, Palaeoecology*, 260(3-4), 494-504, https://doi.org/10.1016/j.palaeo.2007.12.014.

Feurdean, A., Liakka, J., Vannière, B., Marinova, E., Hutchinson, S. M., Mosburgger, V., & Hickler, T. (2013b). 12,000-Years of fire regime drivers in the lowlands of Transylvania (Central-Eastern Europe): a data-model approach. *Quaternary Science Reviews*,

81, 48-61, https://doi.org/10.1016/j.quascirev.2013.09.014.

Feurdean, A., Mosbrugger, V., Onac, B. P., Polyak, V., & Veres, D. (2007a). Younger Dryas to mid-Holocene environmental history of the lowlands of NW Transylvania, Romania. *Quaternary Research*, 68(3), 364-378, DOI: https://doi.org/10.1016/j.yqres.2007.08.003.

Feurdean, A., Tămaş, T., Tanţău, I., & Fărcaş, S. (2012). Elevational variation in regional vegetation responses to late-glacial climate changes in the Carpathians. *Journal of Biogeography*, Vol. 39, no. 2, pp. 258-271, 10.1111/j.1365-2699.2011.02605.x.

Feurdean, A., Vannière, B., Finsinger, W., Warren, D., Connor, S. C., Forrest, M., ... & Hickler, T. (2020). Fire hazard modulation by long-term dynamics in land cover and dominant forest type in eastern and central Europe. *Biogeosciences*, Vol. 17, no. 5, pp. 1213-1230, https://doi.org/10.5194/bg-17-1213-2020.

Feurdean, A., Veski, S., Florescu, G., Vannière, B., Pfeiffer, M., O'Hara, R. B., ... & Hickler, T. (2017). Broadleaf deciduous forest counterbalanced the direct effect of climate on Holocene fire regime in hemiboreal/boreal region (NE Europe). *Quaternary Science Reviews*, Vol. 169, pp. 378-390, 10.1016/j.quascirev.2017.05.024.

Feurdean, A., Wohlfarth, B., Björkman, L., Tantau, I., Bennike, O., Willis, K. J., ... & Robertsson, A. M. (2007b). The influence of refugial population on Lateglacial and early Holocene vegetational changes in Romania. *Review of Palaeobotany and Palynology*, 145(3-4), 305-320, https://doi.org/10.1016/j.revpalbo.2006.12.004.

Finsinger, W., Fevre, J., Orbán, I., Pál, I., Vincze, I., Hubay, K., ... & Magyari, E. K. (2018). Holocene fire-regime changes near the treeline in the Retezat Mts.(Southern Carpathians, Romania). *Quaternary International*, *477*, 94-105, https://doi.org/10.1016/j.quaint.2016.04.029.

Finsinger, W., Kelly, R., Fevre, J., Magyari, E.K. (2014) A guide to screening charcoal peaks in macrocharcoal-area records for fire-episode reconstructions. *The Holocene*, 24(8), 1002–1008, https://doi.org/10.1177/095968361453473.

Florescu, G., Hutchinson, S. M., Kern, Z., Mîndrescu, M., Cristea, I. A., Mihăilă, D., ... & Feurdean, A. (2017). Last 1000 years of environmental history in Southern Bucovina, Romania: A high resolution multi-proxy lacustrine archive. *Palaeogeography, Palaeoclimatology, Palaeoecology*, Vol. 473, pp. 26-40, 10.1016/j.palaeo.2017.01.047.

Florescu, G., Vannière, B., & Feurdean, A. (2018). Exploring the influence of local controls on fire activity using multiple charcoal records from northern Romanian Carpathians. *Quaternary International*, Vol. 488, pp. 41-57, 10.1016/j.quaint.2018.03.042.

Gałka, M., Tanţău, I., Ersek, V., & Feurdean, A. (2016). A 9000 year record of cyclic vegetation changes identified in a montane peatland deposit located in the Eastern Carpathians (Central-Eastern Europe): Autogenic succession or regional climatic influences? *Palaeogeography, Palaeoclimatology, Palaeoecology*, *449*, 52-61, https://doi.org/10.1016/j.palaeo.2016.02.007.

Gasse, F., van Kreveld, S., Holmgren, K., Lee-Thorp, J., Rosqvist, G., & Rack, F. MStaubwasser, R Schneider and E. Steig. (2004). Holocene climate variability, *Quaternary Research*, 62, 243-255, https://doi.org/10.1016/j.yqres.2004.07.001.

Harrison, S.P., Marlon, J.R., and Bartlein, P.J. (2010). Fire in the Earth system, in Changing Climates, Earth Systems and Society. *Springer, Netherland*, 10, 21-48. DOI 10.1007/978-90-481-8716-4_3.

Harrison, S.P., Prentice, I.C., Bloomfield, K.J., Dong, N., Forkel, M., Forrest, M., Ningthoujam, R.K., Pellegrini, A., Shen, Y., Bandena, M., Cardoso, A.W., Huss, J.C., Josh, J., Oliveras, I., Pausas, J., and Simpson, K.J. (2021). Understanding and modelling wildfire regimes: an ecological perspective, Environment *Research Letters*, Vol. 16, no. 12, p. 125008, https://doi.org/10.1088/1748-9326/ac39be.

Harrison, S.P., Villegas-Diaz, R., Cruz-Silva, E., Gallagher, D., Kesner, D., Lincoln, P., Shen, Y., Sweeney, L., Colombaroli, D., Ali, A., Barhoumi, C., Bergeron, Y., Blyakharchuk, T., Bobek, P., Bradshaw, R., Clear, J.L., Czerwinski, S., Daniau, A.-L., Dodson, J., Edwards, K.J., Edwards, M.E., Feurdean, A., Foster, D., Gajewski, K., Gałka, M., Garneau, M., Giesecke, T., Romera, G.G., Girardin, M.P., Hoefer, D., Huang, K., Inoue, J., Jamrichová, E., Jasiunas, N., Jiang, W., Jiménez-Moreno, G., Karpinska-Kołaczek, M., Kołaczek, P., Kuosmanen, N., Lamentowicz, M., Lavoie, M., Li, F., Li, J., Lisitsyna, O., López-Sáez, J.A., Luelmo-Lautenschlaeger, R., Magnan, G., Magyari, E.K., Maksims, A., Marcisz, K., Marinova, E., Marlon, J., Mensing, S., Miroslaw-Grabowska, J., Oswald, W., Pérez-Díaz, S., Pérez-Obiol, R., Piilo, S., Poska, A., Qin, X., Remy, C.C., Richard, P.J.H., Salonen, S., Sasaki, N., Schneider, H., Shotyk, W., Stancikaite, M., Šteinberga, D., Stivrins, N., Takahara, H., Tan, Z., Trasune, L., Umbanhowar, C.E., Väliranta, M., Vassiljev, J., Xiao, X., Xu, Q., Xu, X., Zawisza, E., Zhao, Y., Zhou, Z., and Paillard, J. (2022). The Reading Palaeofire Database: an expanded global resource to document changes in fire regimes from sedimentary charcoal records, *Earth System Science Data*, Vol. 14, no. 3, pp. 1109–1124, https://doi.org/10.5194/essd-14-1109-2022.

Higuera, P. (2009). CharAnalysis 0.9: Diagnostic and analytical tools for sediment-charcoal analysis. User's Guide, *Montana State University*, Bozeman, MT.

Hubay, K., Molnár, M., Orbán, I., Braun, M., Bíró, T., & Magyari, E. (2018). Age–depth relationship and accumulation rates in four sediment sequences from the Retezat Mts, South Carpathians (Romania).

Quaternary International, 477, 7-18, https://doi.org/10.1016/j.quaint.2016.09.019.

Hutchinson, S.M., Akinyemi, F.O., Mîndrescu, M., Begy, R., Feurdean, A. (2016) Recent sediment accumulation rates in contrasting lakes in the Carpathians (Romania): impacts of shifts in socio-economic regime. *Regional Environmental Change*, 16, 501–513, 10.1007/s10113-015-0764-7.

Leys, B., Carcaillet, C. (2016). Subalpine fires: the roles of vegetation, climate and, ultimately, land uses. *Climatic Change*, 135(3–4), 683–697. 10.1007/s10584-016-1594-4.

Leys, B., Carcaillet, C., Dezileau, L., Ali, A.A., Bradshaw, R.H. (2013) A comparison of charcoal measurements for reconstruction of Mediterranean paleo-fire frequency in the mountains of Corsica. *Quaternary Research*, 79(3), 337–349. http://dx.doi.org/10.1016/j.yqres. 2013.01.003.

Magny, M., & Haas, J. N. (2004). A major widespread climatic change around 5300 cal. yr BP at the time of the Alpine Iceman. *Journal of Quaternary Science: Published for the Quaternary Research Association*, 19(5), 423-430, https://doi.org/10.1002/jqs.850.

Magyari, E., Jakab, G., Braun, M., Buczkó, K., & Bálint, M. (2009a, April). High-resolution study of Late Glacial and Early Holocene vegetation and tree line changes in the Southern Carpathian Mountains. In EGU *General Assembly Conference Abstracts* (p. 10549).

Magyari, E., Vincze, I., Orbán, I., Bíró, T., & Pál, I. (2018). Timing of major forest compositional changes and tree expansions in the Retezat Mts during the last 16,000 years. *Quaternary International*, Vol. 477, pp. 40-58, 10.1016/j.quaint.2017.12.054.

Marlon, J. R., Bartlein, P. J., Walsh, M. K., Harrison, S. P., Brown, K. J., Edwards, M. E., ... & Whitlock, C. (2009b). Wildfire responses to abrupt climate change in North America. *Proceedings of the National Academy of Sciences*, Vol. 106, no. 8, pp. 2519-2524, https://doi.org/10.1073/pnas.0808212106.

Marlon, J.R. (2020). What the past can say about the present and future of fire. *Quaternary Research*., vol. 96, pp. 66–87, DOI: https://doi.org/10.1017/qua.2020.48.

Mîndrescu, M., Cristea, A. I., Hutchinson, S. M., Florescu, G., & Feurdean, A. (2013). Interdisciplinary investigations of the first reported laminated lacustrine sediments in Romania. *Quaternary International*, 293, 219-230, https://doi.org/10.1016/j.quaint.2012.08.2105.

Mîndrescu, M., Florescu, G., Grădinaru, I., & Haliuc, A. (2017). Lakes, lacustrine sediments, and palaeoenvironmental reconstructions. Landform Dynamics and Evolution in Romania, *Springer International Publishing*, pp. 699-734, DOI: 10.1007/978-3-319-32589-7_30.

Mîndrescu, M., Petraș, A., Py-Saragaglia, V., Brun, C., Grădinaru, I., Hodor, N., ... & Danu, M. (2023). The complementary use of charcoal number and morphology to reconstruct fire history in a late Holocene peat sequence from NW Romania. *Carpathian Journal of Earth and Environmental Sciences*, *18*(1), 15-25, DOI:10.26471/cjees/2023/018/237.

Mooney, S. D., & Tinner, W. (2011). The analysis of charcoal in peat and organic sediments. *Mires and Peat*, 7(9), 1-18.

Mustaphi, C. J. C., & Pisaric, M. F. (2014). A classification for macroscopic charcoal morphologies found in Holocene lacustrine sediments. *Progress in Physical Geography*, 38(6), 734-754, https://doi.org/10.1177/0309133314548886.

Orbán, I., Birks, H. H., Vincze, I., Finsinger, W., Pál, I., Marinova, E., ... & Magyari, E. K. (2018). Treeline and timberline dynamics on the northern and southern slopes of the Retezat Mountains (Romania) during the late glacial and the Holocene. *Quaternary International*, Vol. 477, pp. 59-78, 10.1016/j.quaint.2017.03.012.

Pál, I., Buczkó, K., Vincze, I., Finsinger, W., Braun, M., Biró, T., & Magyari, E. K. (2018). Terrestrial and aquatic ecosystem responses to early Holocene rapid climate change (RCC) events in the South Carpathian Mountains, Romania. *Quaternary International*, Vol. 477, pp. 79-93, 10.1016/j.quaint.2016.11.015.

Patterson III, W. A., Edwards, K. J., & Maguire, D. J. (1987). Microscopic charcoal as a fossil indicator of fire. *Quaternary Science Reviews*, 6(1), 3-23.

Peters, M., Friedmann, A., Stojakowits, P., & Metzner-Nebelsick, C. (2020). Holocene vegetation history and environmental change in the Lăpuş Mountains, north-west Romania. *Palynology*, *44*(3), 441-452, https://doi.org/10.1080/01916122.2019.1615567.

Petraș, A., Florescu, G., Hutchinson, S. M., & Mîndrescu, M. (2021, April). Fire history and the relationship with late Holocene anthropogenic activity in Tăul Mare peat bog in the Lăpuș Mts (Eastern Carpathians). Romania. *In EGU General Assembly Conference Abstracts*, pp. 15609, 10.5194/egusphere-egu21-15609.

Power, M. J., Marlon, J., Ortiz, N., Bartlein, P. J., Harrison, S. P., Mayle, F. E., ... & Zhang, J. H. (2008). Changes in fire regimes since the Last Glacial Maximum: an assessment based on a global synthesis and analysis of charcoal data. Climate dynamics, 30(7-8), 887-907, DOI 10.1007/s00382-007-0334-x.

Pupysheva, M. A., & Blyakharchuk, T. A. (2023). Fires and their Significance in the Earth's Post-Glacial Period: a Review of Methods, Achievements, Groundwork. *Contemporary Problems of Ecology*, 16(3), 303-315, DOI: 10.1134/S1995425523030095.

Schnitchen, C., Charman, D. J., Magyari, E., Braun, M., Grigorszky, I., Tóthmérész, B., ... & Szántó, Z. (2006). Reconstructing hydrological variability from testate amoebae analysis in Carpathian peatlands. *Journal of*

Paleolimnology, 36, 1-17, DOI: 10.1007/s10933-006-0001-y.

Scott, A. C., Cripps, J. A., Collinson, M. E., & Nichols, G. J. (2000). The taphonomy of charcoal following a recent heathland fire and some implications for the interpretation of fossil charcoal deposits. *Palaeogeography, Palaeoclimatology, Palaeoecology*, 164(1-4), 1-31, https://doi.org/10.1016/S0031-0182(00)00168-1.

Snitker, G. (2020). The charcoal quantification tool (CharTool): A suite of open-source tools for quantifying charcoal fragments and sediment properties in archaeological and paleoecological analysis. *Ethnobiology Letters*, Vol 11, no 1, pp. 103-115, DOI: https://doi.org/10.14237/ebl.11.1.2020.1653.

Soróczki-Pintér, É. (2015). Use of siliceous algae in the environmental reconstruction in the Carpathian Region. (Doctoral dissertation, *Hungarian Natural History Museum*).

Tanţău, I., Feurdean, A., de Beaulieu, J. L., Reille, M., & Fărcaș, S. (2011). Holocene vegetation history in the upper forest belt of the Eastern Romanian Carpathians. *Palaeogeography, Palaeoclimatology, Palaeoecology*, Vol. 309, no. 3-4, pp. 281-290, https://doi.org/10.1016/j.palaeo.2011.06.011.

Tanţău, I., Geantă, A., Feurdean, A., & Tămaș, T. (2014). Pollen analysis from a high altitude site in Rodna Mountains (Romania). *Carpathian Journal of Earth and Environmental Sciences*, Vol. 9, no. 2, pp. 23-30.

Tanţău, I., Reille, M., de Beaulieu, J. L., Fărcaș, S., Goslar, T., & Paterne, M. (2003). Vegetation history in the Eastern Romanian Carpathians: pollen analysis of two sequences from the Mohoş crater. *Vegetation History and Archaeobotany*, *12*, 113-125, DOI: 10.1007/s00334-003-0015-6.

Vacek, Z., Vacek, S., & Cukor, J. (2023). European forests under global climate change: Review of tree growth processes, crises and management strategies. *Journal of Environmental Management*, *332*, https://doi.org/10.1016/j.jenvman.2023.117353.

Van Eck, N. J., & Waltman, L. (2018). Manual for VOSviewer version 1.6. 8. CWTS Meaningful Metrics. *Universiteit Leiden*, pp. 1–51, https://www.vosviewer.com.

Vannière, B., Blarquez, O., Rius, D., Doyen, E., Brücher, T., Colombaroli, D., Connor, A., Feurdean, A., Hickler, T., Kaltenrieder, P., Lemmen, C., Leys, B., Massa, C., Olofsson, J. (2016) 7000-year human legacy of elevation-dependent European fire regimes. *Quaternary Science Reviews*, 132, 206–212. https://doi.org/ 10.1016/j.quascirev.2015.11.012.

Whitlock, C., & Larsen, C. (2002). Charcoal as a fire proxy. *Tracking environmental change using lake sediments: terrestrial, algal, and siliceous indicators*, pp. 75-97, DOI: 10.1007/0-306-47668-1_5.

Whitlock, C., Colombaroli, D., Conedera, M., Tinner, W. (2018) Land-use history as a guide for forest conservation and management. *Conservation Biology*, 32(1), 84–97, https://doi.org/10.1111/cobi.12960.

Whitlock, C., Higuera, P. E., McWethy, D. B., & Briles, C. E. (2010). Paleoecological perspectives on fire ecology: revisiting the fire-regime concept. *The Open Ecology Journal*, Vol. 3, no. 2, pp. 6-23, 10.2174/1874213001003020006.

Forum geografic. Studii și cercetări de geografie și protecția mediului
Volume **XXII**, Issue **1** (**June 2023**), pp. **92-108;** DOI: **10.5775/fg.2023.070.i**

Geographical analysis of multidimensional poverty in India from 2005-2006 to 2021: An emerging scenario

Soumyabrata MONDAL[1,*], Saheli KUMAR[1], Anand Prasad MISHRA[1]

[1] Institute of Science, Department of Geography, Banaras Hindu University, Varanasi, India
* *Corresponding author*: soumyamondal1992@gmail.com

Received on 12-01-2023, reviewed on 17-06-2023, accepted on 30-06-2023

Abstract

The present study has made a thorough investigation into the spatial clustering, trend, and intensity of multidimensional poverty in India between 2005–2006 and 2021. Data has been obtained from the global multidimensional poverty report [developed by the Oxford Poverty and Human Development Initiative (OPHI) and UNDP] and the national report of the Multidimensional Poverty Index (MPI) for 2021 [prepared by NITI Aayog] for India based on the NFHS-3 and NFHS-4 datasets. The study shows that, despite significant interstate disparities, multidimensional poverty in India has decreased from 0.279 in 2005–2006 to 0.118 in 2021. States like Bihar, Jharkhand continue to experience extreme multidimensional poverty. The study demonstrates that even though the intensity of poverty has remained relatively constant, the poorer states are significantly more advanced in reducing poverty than the nation's wealthier states. This suggests a pattern of pro-poor poverty reduction. Besides the study explores indicator-wise deprivation of MPI among the states and it is witnessed that Chhattisgarh, Jharkhand, Tripura, and Bihar have made splendid progress in reducing deprivation in different indicators (antenatal care, electricity, drinking water, assets) of multidimensional poverty, while the magnitude of deprivation is acute in several indicators like nutrition, cooking fuel, sanitation, and housing in these states. Based on the analysis, the present study suggests that India should undertake target-based interventions in poverty-prone regions to reduce poverty.
Keywords: *poverty in India, multidimensional poverty, Multidimensional Poverty Index (MPI), spatial pattern of poverty, decomposition, deprivation*

Introduction

During the previous two decades, India has attained remarkable progress in its growth trajectory (World Bank 2018). However, the growth performance of the Indian subcontinent has been exclusive and inconsistent. As a result, regional disparities, the rural-urban divide, and socio-economic and gender inequities have all worsened (Dev, 2010). Various studies (Das & Barua, 1996; Ohlan, 2013) have discussed that over the years, regional disparities in India have been increasing at an alarming rate. Even after seven decades of independence, a large section of Indian society does not have access to essential services including health, education, housing, and safe drinking water. The government of India faces challenges to overcome the problem of inter-regional poverty and income disparity that are not explicit at aggregative levels.

During the first four decades of development studies (1950–90), poverty was mainly measured in money-metric terms, either from household income or consumption expenditure. The World Bank sets poverty line at $2.15 a day in 2017 PPP (Purchasing Power Parity). Although the monetary-based poverty estimates have provided valuable insights into poverty, they have some flaws. The major limitation of money-metric poverty is its inability to express the multiple deprivations of human life. Sen (1980, p-198) stated that "income may not be translated into basic needs. As a result, deprivations in education, health, social, and political dimensions are critical in determining poverty because they are difficult to define through price". Moreover, there is ample possibility of inaccurate measurement of a household's income and expenditure (Deaton, 1997). Apart from income, poverty measure fails to consider the spatiality of living costs, which are considerably higher in urban areas than in rural areas (Wratten, 1995). These limitations of money-metric poverty put emphasis on developing the multidimensional approach to poverty measurement, which considers poverty as i) capability deprivation (Sen, 1993) and ii) a counting measure of deprivation (Atkinson, 2003). The emergence of the human development paradigm during 1990 provided a solid theoretical framework for measuring multidimensional poverty. The United Nations Development Programme (UNDP) developed a set of composite indices such as the Capability Poverty Measure (CPM), Human Poverty Index 1 (HPI-1), and Human Poverty Index 2 (HPI-2) to compute multidimensional poverty (UNDP, 1996). The Multidimensional Poverty Index (MPI) differs from the HPI in that it identifies people at the micro level who are disadvantaged in a variety of overlapping ways and captures both the amount and intensity of poverty in a more appropriate way (Alkire & Santos, 2010). The Oxford Poverty and Human Development Initiative (OPHI), jointly with UNDP,

developed the Multidimensional Poverty Index (MPI) in 2010. The major goal of MPI was to identify those who were unable to meet a certain level of resources, requirements, or functioning in order to maintain a minimum standard of living (Alkire & Santos, 2014; Walker, 2015). MPI has grown into a formidable instrument that is now used by over 18 nations to track poverty alleviation (UNDP, 2019). The index's strength comes from its capacity to disaggregate the MPI into numerous categories, ensuring that no region is left behind. It also serves as a powerful tool for assessing a country's progress toward reaching the Sustainable Development Goals (UNDP, 2019).

The study of multidimensional poverty and deprivation on a regional scale is critical in such a large country as India. The extant seam of literature on multidimensional poverty has significantly expanded in recent years following the ground breaking contributions of Atkinson and Bourguignon (1982), Bourguignon and Chakravarty (2003), and later the significant theoretical as well as empirical contributions of Alkire and Foster (2011), Alkire and Seth (2015), Das et al. (2021), and Alkire et al. (2021). In order to measure and estimate multidimensional poverty, a number of researchers (Chakravarty & D'Ambrosio, 2006; Alkire & Foster, 2008, 2011; Calvo, 2008; Wagle, 2008; Alkire & Santos, 2010; Mohanty, 2011; Mishra & Ray, 2013; Alkire & Seth, 2015) around the world have made significant contributions. Most of these studies used education, health, and standard of living as criteria for defining multidimensional poverty, while a few studies also took into account subjective well-being factors like fear of hardship (Calvo, 2008). Regarding measurement of multidimensional poverty, some researchers have considered the "union" (poor in any dimension) approach (Bourguignon & Chakravarty, 2003); while others have applied the "intersection" (poor in two or more dimensions) or "relative" approach (Wagle, 2008).

Though a large number of studies have delved into the dynamics of multidimensional poverty at the global level, studies on multidimensional poverty at a regional level for developing nations in general and India, in particular, are few and far between. Following the methodology of Alkire and Foster (2011), Alkire et al. (2015), Das et al. (2021), and Alkire et al. (2021), this paper revisits the measurement of multidimensional poverty in the Indian context during two different periods of time: 2005–2006 and 2021.

The contribution of the paper is threefold. The primary objective of this study is to investigate the spatial disparities in the concentration of multidimensional poverty among the different states of India during two distinct periods, i.e., 2005–06 and 2021. In addition, the study has attempted to investigate the trends of changes in the MPI's absolute and relative dimensions, headcount ratio (H), and poverty intensity (A), over these periods, across the states of India. The paper's final section further explores the disparities in MPI indicators across the states. The study will make a novel contribution to understanding the recent scenario of multidimensional poverty, intensity, and deprivation across the states of India, which may be helpful for the easy formulation of state-level policies.

Literature review

The existing literature on development economics suggests that assessing poverty across several dimensions of deprivation provides a more comprehensive picture of poverty. In India a plethora of studies have addressed the relevance of multidimensional poverty measurement using variety of indicators.

Alkire and Seth (2008) calculated the MPI in the context of India using the Below Poverty Line (BPL), 2002 methodology, with the help of NFHS (National Family Health Survey) dataset. Mohanty (2011) tried to assess multidimensional poverty using NFHS-3 unit-level data and discovered that infant mortality and under-five mortality rates are particularly high among people living in abject multidimensional poverty. Sarkar (2012) calculated multidimensional poverty using data from the National Sample Survey Organization (NSSO) and concluded that while rural poverty has declined over time in India, it is still very acute among socially vulnerable groups. Using NFHS data, Alkire and Seth (2013) looked at how multi-dimensional poverty changed in India between 1999 and 2006 and found that some indicators of the standard of living—like access to electricity, decent housing, safe drinking water, and improved sanitation—were comparatively more significant than other social indicators in promoting national poverty reduction. However, the reduction was not consistent across different population subgroups, and the pattern of reduction among states was less pro-poor than the pattern of income poverty. Mishra and Ray (2013) performed a wide-ranging analysis of the Indian population's living standards using NFHS and NSSO data between 1992 and 2005 and concluded that the decomposable dimensions of poverty deprivation explained vulnerability across socio-economic groups better than total deprivation levels. Using NFHS data, Alkire and Seth (2015) observed that although poverty level in India has decreased during 1999 to 2006, the reduction in poverty among the lower sub-groups has been modest, resulting in a widening of the income gap throughout the population. Gathering data from several issues of periodic reports produced by OPHI as well as various other research reports, Kumar et al. (2015) have calculated the MPI for India based on health and household status and contend that Kerala is the most secure in multidimensional poverty, while Goa, Punjab, Himachal Pradesh, and Tamil Nadu are the most susceptible. While the rest of the states are in a miserable state of affairs. Dehury and Mohanty (2015) estimated and decomposed multidimensional poverty in 82 natural regions of India using unit data from the Indian Human Development Survey (IHDS), 2011–2012. According to the findings, around 43 per cent of India's population is

multidimensionally poor, with considerable regional differences. Based on data from three NFHS rounds: 1992–1993, 1998–1998, and 2005–2006, Chaudhuri et al. (2017) determined the state-level MPI in India and revealed that the country's progress has been unbalanced, with poorer states (like Bihar) continuing to stay impoverished and there is a prevalence of intra-urban inequities and female multi-dimensional destitution. Using the NFHS-3 and NFHS-4 datasets, Alkire et al. (2018) attempted to analyze the changes in the MPI from 2005–2006 to 2015–2016 and found that multidimensional poverty in India decreased from 54.7 percent in 2005–2006 to 27.5 percent in 2015–2016. As per their observation, the reductions in MPI are rarely connected with GDP growth at the state level. Using NSSO data on consumer expenditure Tripathi and Yenneti (2020) tried to estimate multidimensional poverty across Indian states and disclosed that household members' lack of education, followed by their income, was the biggest factor contributing to their poverty. Between 2005–2006 and 2015–2016, Alkire, et al. (2021) looked at how poverty levels changed across socioeconomic groups and among the poorest of the poor in India. Using NFHS-4 datasets, Vasishtha and Mohanty (2021) investigated the spatial clustering and association of multidimensional and consumption poverty in Indian districts and unveiled that in comparison to consumption poverty, multidimensional poverty is spatially more concentrated. Based on the results, they suggested multidimensional poverty measures should be integrated with consumption poverty measures and those districts with high levels of multidimensional and consumption poverty should be prioritized for evidence-based planning. Das et al. (2021) used NSSO data to examine how consumption and multidimensional poverty changed in India between 2004–2005 and 2011–2012 as a result of changes in population subgroups and household characteristics. According to their observations, multidimensional poverty has dropped for both consumption-poor and non-poor people, but the decline is more rapid among the poorest segments, which is encouraging. Additionally, they concluded that a sizable portion of Indians is multidimensionally poor but not consumption poor, making it ineffective to combat poverty using conventional methods due to exclusionary bias. Mohanty and Vasishtha (2021) estimated and decomposed multidimensional poverty in urban India using the urban sample from the NFHS-4. According to the findings, approximately one-third of the urban Indian population is multidimensionally poor, one-sixth is vulnerable to multidimensional poverty, and poverty is more prevalent among large households, female-headed households, widowed individuals, and scheduled tribes. Based on NFHS-4 dataset Mondal et al. (2023) tried to estimate the spatial pattern of multidimensional poverty in both rural and urban context across the states of India and confirms that the magnitude of poverty and deprivation is acute in most of the poverty indicators in the poorer states of India like Bihar, Jharkhand, Uttar Pradesh, Madhya Pradesh etc. The study further revealed that in both rural and urban space among the dimension health and among the indicators nutrition have made most significant contribution in overall score of multidimensional poverty in India. Not only at national level but also at micro level several studies have been performed in India to investigate the pattern and intensity of multidimensional poverty. Like Mondal and Mishra (2021) in their study have tried to explore and analyze spatial interlinkages of poverty in Hooghly district of West Bengal with the help of twelve indicators and unveiled that geographical dimension of poverty has many linkages with the socio economic and cultural aspects of society.

Even though numerous studies have been carried out at the national level, no comparisons between the states using the MPI for the years 2005–2006 and 2021 have been made so far in India. The current study aims to fill this significant gap in the body of existing literature. This type of research will shed light on the spatial and temporal dimensions of multidimensional poverty in the context of a vastly dispersed country like India.

Data and methods

The present study is based on secondary sources of data. The data relating to the MPI of India for the year 2005–2006 has been obtained from the Global Multidimensional Poverty Index prepared by UNDP and OPHI using the Alkire–Foster (A–F) Method. The data on multidimensional poverty in India for 2021 is gathered from the report prepared by the National Institution for Transforming India (NITI) Aayog using the same methodology as UNDP and OPHI. The widely used Foster-Greer-Thorbecke (FGT) class of poverty measures is extended by the A-F methodology, which has several technical and practical benefits that make it suitable for use in non-monetary poverty estimation. While the MPI of 2021 has used the NFHS-4 dataset collected during 2015–16, the MPI of 2005–06 is based on NFHS-3 datasets. The NFHS is conducted by the International Institute of Population Sciences (IIPS), Mumbai and is the major source for demographic and health indicators in India with support from the ICF International, the National AIDS Research Institute (NARI) and Demographic Health Surveys (DHS). It should be noted that it will be NFHS 4 which is representative at both the state and district levels, as opposed to NFHS 3, which is only representative at the state level. The sample size thus increased almost six-fold between NFHS-3 and NFHS-4. Both surveys use a two-stage stratified sampling design. The two datasets are thus comparable at the state level, though not at the district level. Therefore, we have used these two data sets for inter-spatial and temporal comparisons.

According to the UNDP's Human Development Reports (2015 and 2019), the MPI of 2005–2006 and 2021 both have considered three dimensions, namely health, education, and standard of living. The global MPI used 10

indicators (two from health, two from education and six from standard of living) for the construction of MPI for India in 2005-06 while NITI Aayog has used twelve indicators with the inclusion of two new indicators (Child and adolescent mortality from health and bank account from standard of living) for 2021 (Fig. 1).

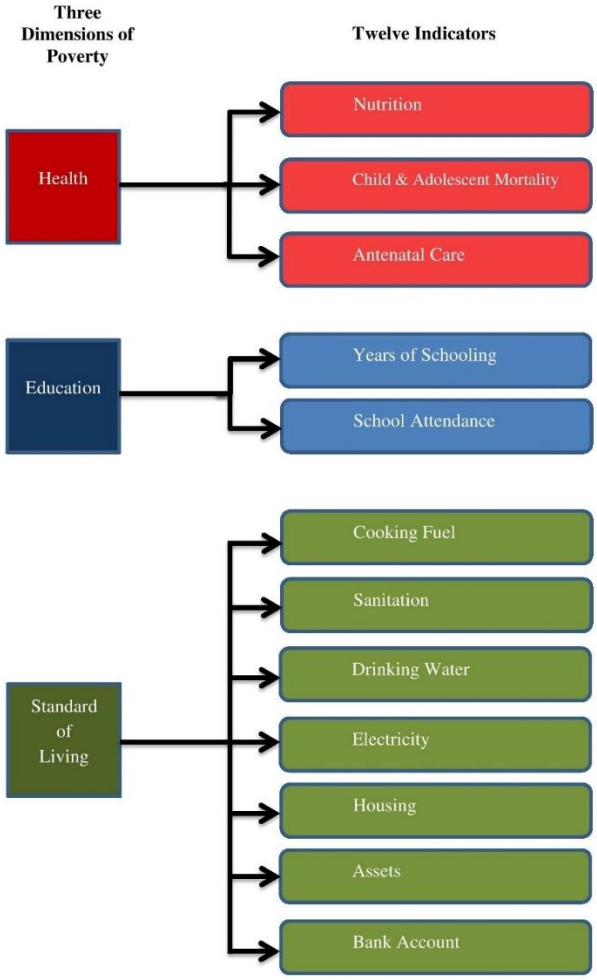

Figure 1. Dimensions and indicators of MPI for India 2021 *Source:* Prepared by the authors based on NITI Aayog Report of MPI, 2021

These indicators reflect different Sustainable Development Goals (SDGs). The descriptions of the dimensions, the indicators, and the cut-off point that have been considered by NITI Aayog have been enlisted in Table 1. Equal weights were assigned to each dimension, and within each dimension, equal weights were given to each indicator (Alkire & Santos, 2010; Alkire & Seth, 2015; UNDP, 2015, 2019). The percentage of weighted deprivations that the state's population experiences is shown in the deprivation score, which adds up the weights on each indicator of deprivation and summarizes the state's deprivation profile. After Sen (1976), the next step is to determine who is poor using the poverty cut-off. If they experience one-third of the weighted deprivations or more, they are identified as MPI poor.

Thereafter, the proportion of multidimensionally poor individuals in the total population has been determined which is known as the Headcount Ratio (H) of multidimensional poverty and is the first of two partial indices used to determine the MPI.

Percentage of multidimensionally poor is denoted by H and defined as

$$H = \frac{q}{n} * 100$$

Where, q is the number of multidimensional poor households and n is the total population.

Thereafter intensity of poverty (A) which is the second partial index to formulate MPI has been calculated. The intensity of poverty (denoted by A) is the average proportion of deprivations which is experienced by multidimensionally poor individuals.

In percentage form, it is expressed as

$$A = \frac{1}{q}\sum_{i=1}^{q} Ci(k)$$

Where, Ci(k) is the deprivation score of multidimensionally poor individuals up to the ith individual and q is the number of multidimensionally poor individuals.

The Multidimensional Poverty Index (MPI) is the product of the two partial indices, the (H) and (A). Hence, the index reflects both the incidence and the intensity of poverty.

Thus MPI is calculated as

$$MPI = H * A$$

Further we have decomposed the MPI by dimensions and indicators to assess the contribution of the various dimension/indicators to overall poverty. The contribution of a particular indicator to overall multidimensional poverty is computed as

$$Contribution\ of\ indicator\ i\ to\ MPI = \frac{wiCHi}{MPIc} \times 100$$

Where wi is the weight of the ith indicator (Table 1) CHi is the censored headcount ratio of the ith indicator and MPIc denotes the India's national MPI.

The study has made use of a variety of analytical tools, including tabular analysis, absolute and relative change detection, scatter plots, bubble charts, etc. With the aid of ArcGIS 10.5, SPSS 22, and MS-Excel 2010 software, a number of maps, charts, and diagrams have been prepared for better visual representation.

Table 1. Dimensions, indicators, deprivation cut-offs and weights of the multidimensional poverty

Dimension	Indicator (Weight)	Deprivation cut-off
Health (1/3)	Nutrition (1/6)	A household is considered deprived if any child between the ages of 0 to 59 months, or woman between the ages of 15 to 49 years, or man between the ages of 15 to 54 years -for whom nutritional information is available - is found to be undernourished.
	Child and Adolescent Mortality (1/12)	A child/adolescent under 18 years of age has died in the family in the five-year period preceding the survey.
	Antenatal Care(1/12)	A household is deprived if any woman in the household who has given birth in the 5 years preceding the survey, has not received at least 4 antenatal care visits for the most recent birth, or has not received assistance from trained skilled medical personnel during the most recent childbirth.
Education (1/3)	Years of Schooling (1/6)	Not even one member of the household aged 10 years or older has completed six years of schooling.
	School Attendance (1/6)	Any school-aged child is not attending school up to the age at which he/she would complete class 8.
Standard of Living (1/3)	Cooking Fuel (1/21)	A household cooks with dung, agricultural crops, shrubs, wood, charcoal or coal.
	Sanitation (1/21)	The household has unimproved or no sanitation facility or it is improved but shared with other households.
	Drinking Water (1/21)	The household does not have access to improved drinking water or safe drinking water is at least a 30-minute walk from home (as a round trip).
	Electricity (1/21)	The household has no electricity.
	Housing (1/21)	The household has inadequate housing: the floor is made of natural materials, or the roof or walls are made of rudimentary materials.
	Assets (1/21)	The household does not own more than one of these assets: radio, TV, telephone, computer, animal cart, bicycle, motorbike, or refrigerator; and does not own a car or truck.
	Bank Account (1/21)	No household member has a bank account or a post office account.

Source: National Multidimensional Poverty Index, 2021 Based on NFHS-4 (2015-16), NITI Aayog

Results and discussions

Spatial pattern of MPI, H and A of poverty in 2005-2006 and 2021

India has achieved a momentous progress in reducing multidimensional poverty and headcount ratio in between 2005-06 and 2021. The headcount ratio has dropped down from 54.7 percent in 2005-2006 to 25.0 percent in 2021. The MPI score has more than halved during this period from 0.279 to 0.118. Though intensity of poverty has remained more or less the same during 2005-2006 (51.1 percent) and 2021 (47.1 percent) which is a serious concern among the policy makers and social scientists in respect to poverty in India. Though poverty has been reduced at the national level, large interregional disparities in the pattern of multidimensional poverty persist in our country. The section that follows provides an example of a comparative analysis of the regional variation in multidimensional poverty, headcount Ratio, and poverty intensity over two distinct time periods, namely 2005–2006 and 2021.

State wise pattern of poverty in 2005-2006

Table 2 and Figure 2 reveal that during 2005-2006 very high multidimensional poverty (MPI>0.198) persisted in 16 out of 28 states in India. Among the states Bihar was the poorest in multidimensional poverty followed by Jharkhand and Uttar Pradesh. Lack of education, a high rate of illiteracy, a lack of infrastructure and industries, unequal land distribution, caste-based politics, a heavy population burden on natural resources, a problem with youth unemployment, and a lack of urbanization are the main causes of the high incidence of poverty in these states (Mondal et al., 2023).

Table 2. State wise MPI, Headcount Ratio (H) and Intensity (A) in 2005-2006 and 2021

State	2005/06*			2021**		
	MPI	H Incidence	A Intensity	MPI	H Incidence	A Intensity
INDIA	0.279	54.7	51.1	0.118	25.0	47.1
Andhra Pradesh	0.234	49.9	47.0	0.053	12.3	43.2
Arunachal Pradesh	0.309	59.7	51.8	0.115	24.3	47.3
Assam	0.312	60.7	51.4	0.156	32.7	47.9
Bihar	0.446	77.1	57.8	0.265	51.9	51.0
Chhattisgarh	0.353	70.0	50.5	0.134	29.9	44.6
Goa	0.087	20.4	42.5	0.015	3.8	40.2
Gujarat	0.185	38.5	48.0	0.084	18.6	45.0
Haryana	0.182	38.5	47.2	0.055	12.3	44.4
Himachal Pradesh	0.129	31.1	41.5	0.03	7.6	39.4
Jammu & Kashmir* **	0.189	40.8	46.4	0.055	12.6	44.1
Jharkhand	0.425	74.7	57.0	0.202	42.2	47.9
Karnataka	0.224	48.1	46.5	0.056	13.2	42.7
Kerala	0.052	13.2	39.6	0.003	0.7	39.0
Madhya Pradesh	0.358	67.7	52.8	0.173	36.7	47.3
Maharashtra	0.182	39.4	46.2	0.065	14.9	43.8
Manipur	0.207	45.1	45.8	0.08	17.9	44.4
Meghalaya	0.334	60.5	55.2	0.157	32.7	48.1
Mizoram	0.139	30.8	45.0	0.046	9.8	47.4
Nagaland	0.294	56.9	51.6	0.117	25.2	46.3
Odisha	0.330	63.5	52.0	0.136	29.4	46.4
Punjab	0.108	24.0	45.0	0.024	5.6	43.8
Rajasthan	0.327	61.7	52.9	0.140	29.5	47.4
Sikkim	0.176	37.6	46.7	0.016	3.8	41.2
Tamil Nadu	0.155	37.0	41.8	0.02	4.9	40.0
Telangana	-	-	-	0.059	13.7	43.2
Tripura	0.265	54.4	48.6	0.075	16.7	45.0
Uttar Pradesh	0.360	68.9	52.2	0.180	37.8	47.6
Uttarakhand	0.179	38.7	46.1	0.079	17.7	44.4
West Bengal	0.298	57.3	52.0	0.097	21.4	45.5

*Source: * Global Multidimensional Poverty Index 2018, Oxford Poverty and Human Development Initiative (OPHI), University of Oxford, P. 31 ** National Multidimensional Poverty Index, 2021 Based on NFHS-4 (2015-16), NITI Aayog *** Value of Jammu & Kashmir includes J & K and Ladakh UT*

Table 2 also shows that during the years 2005–2006, 11 of the 16 states with the highest rates of poverty exceeded the national MPI value of 0.279. As shown in Fig. 2, these states are primarily located in India's central and eastern regions. Table 2 further reveals that high MPI (considering cut off 0.133) is observed in eight states in the country during 2005-06 with highest MPI 0.189 for Jammu and Kashmir to 0.139 MPI of Mizoram falling in this category. These states do not follow any spatial clustering, rather they are scattered. Only three states, Goa, Punjab, and Himachal Pradesh, fall within the MPI's moderate category (considering cut off 0.068). While only the state Kerala having the lowest MPI value of 0.052 falls under the low poverty category (Fig. 2 and Table 2).

Table 2 also portrays the spatial pattern of the headcount ratio of multidimensional poverty in India during 2005-2006. As shown in Table 2, 12 states have surpassed the country's headcount ratio of 54.7 percent. Similar to MPI, Bihar (77.1%) had the highest headcount ratio, followed by Jharkhand, Chhattisgarh, and Uttar Pradesh. In contrary, Kerala (13.2%) had the lowest multidimensional poverty headcount ratio in 2005–2006 (Table 2). Figure 3 exhibits that, of the 28 states in our nation, 18 had very high multidimensional headcount ratios (using a cut-off of 39.10 percent) at that time. While, seven states continued to have high multidimensional poverty headcount ratios (using 26.31 percent as the cut-off). As witnessed in Figure 3, these states are primarily located in the country's central, eastern, and north-eastern regions, with a few small pockets in the western and northern regions. The remaining three states had a moderate or low multidimensional headcount ratio in 2005-06.

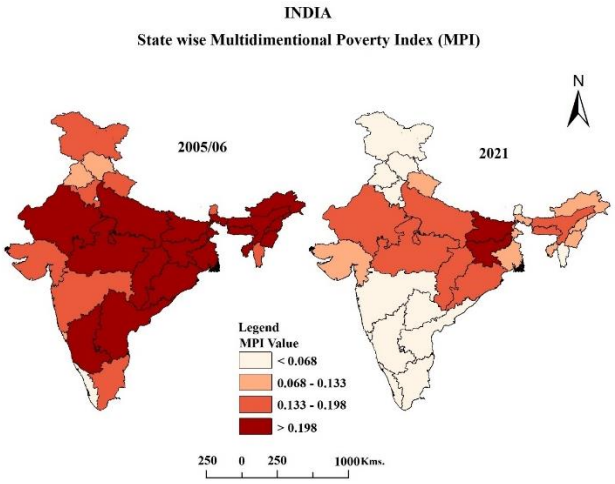

Figure 2. Spatial pattern of MPI in 2005-2006 and 2021 ***Source: Prepared by authors***

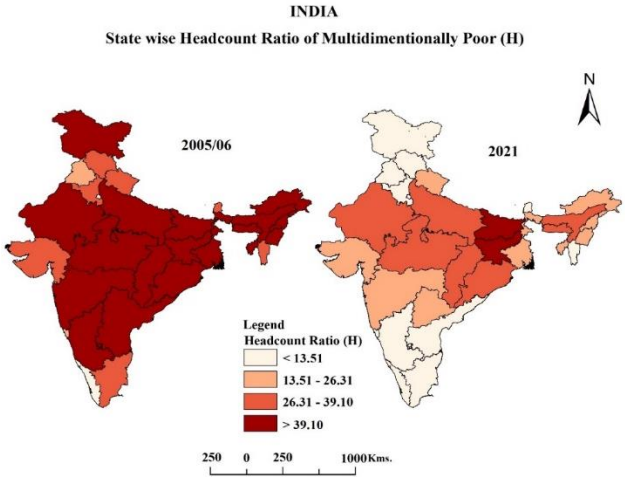

Figure 3. Spatial pattern of Headcount Ratio of Multidimensionally Poor in 2005-2006 and 2021 ***Source: Prepared by authors***

Table 2 further reveals that Bihar had the highest intensity of poverty, at 57.8 percent in 2005–06, followed by Jharkhand and Meghalaya. While, Kerala had the lowest intensity, followed by Himachal Pradesh and Tamil Nadu. The spatial pattern of poverty intensity shows that intensity is not always associated with the MPI and headcount ratio. Even though Chhattisgarh has an MPI score of 0.353 and a headcount ratio of 70.0 percent, its poverty intensity is lower (50.5 percent) than the national average. It may be due to the result of focusing on the poorest of the poor (OPHI, 2018). Likewise in Tripura, the headcount ratio is 54.4 percent and the poverty intensity is 48.6 percent. Figure 4 portrays state-wise intensity of poverty in India during 2005-2006, and it is observed that a very high intensity of poverty (considering the cut-off point of 48.02 percent) is concentrated among the states located in the central and eastern parts of our country, while the low intensity of poverty is found in the southern portion (Kerala and Tamil Nadu) of the country with an isolated patch in the northern part (Himachal Pradesh). During 2005-2006, out of 28 states, 11 states exceeded the national intensity of poverty, which was 51.1 percent.

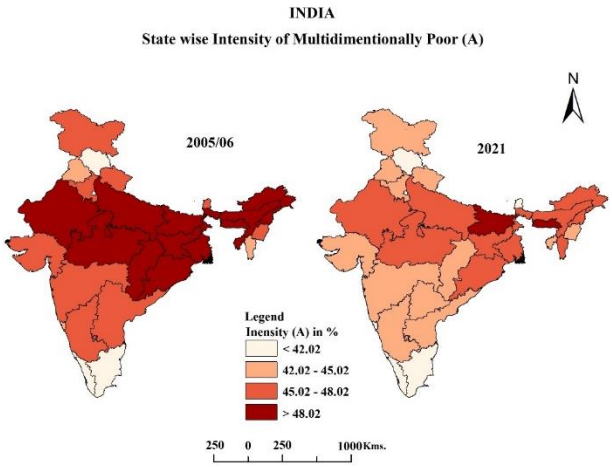

Figure 4. Spatial pattern of Intensity (A) of Poverty in 2005-2006 and 2021 ***Source: Prepared by authors***

State wise pattern of poverty in 2021

This section of our study focuses on exposing regional disparities in the pattern of multidimensional poverty, headcount ratio, and intensity of poverty in India according to the most recent report from NITI Aayog, 2021. According to Table 2, Bihar has achieved the highest MPI score in 2021 (0.265), while Kerala has the lowest (0.003). Among the states except for Bihar, a very high level of multidimensional poverty (>0.198) also persists in Jharkhand (Table 2). Consequently, only two Indian states have experienced extremely high levels of multidimensional poverty in 2021, as opposed to sixteen states in 2005–2006. In addition, high poverty (0.133-0.198) persists in seven states, ranging from Chhattisgarh (0.134) to Uttar Pradesh (0.180) in terms of MPI scores. Figure 2 shows that, even in 2021, the central and eastern parts of India have remained significantly poorer than the rest of the country. As shown in Table 2, eight states—out of the total 29 states, including Jammu and Kashmir—have crossed the national MPI threshold of 0.118 in 2021, necessitating special attention. The spatial pattern of MPI reveals that severe conditions of poverty are still being persisted in 28 percent of areas of India. Six states—Nagaland, Arunachal Pradesh, West Bengal, Gujarat, Uttarakhand, and Tripura—fall into the moderate MPI (0.068–0.133) score category in 2021 (Fig. 2). The remaining 14 states are under the low MPI score category, with a score of less than 0.068. According to Figure 2, most of the states located in the southern and northern parts of India have a low concentration of multidimensional poverty. It should be noted that only the state of Kerala fell into the low MPI category in 2005–06; whereas during

2021, nearly half of the states in India fall into this category.

In terms of headcount ratio, Bihar has the highest percentage (51.9 percent) in 2021, followed by Jharkhand. In India, the patterns of MPI and headcount ratio are more or less similar in 2021. According to the NITI Aayog report, 25.0 percent of Indians are now multidimensionally poor. A state-by-state analysis shows that 10 out of the 29 Indian states have surpassed this threshold. Kerala, on the other hand, with a poverty rate of just 0.7 percent, has the lowest headcount ratio of multidimensional poverty. It is encouraging from the standpoint of India's poverty that during 2021 few states like Goa, Sikkim, and Tamil Nadu have multidimensional poverty headcount ratios of less than 5 percent. Figure 3 also shows that in 2021, the central, eastern, and north-eastern parts of India have a moderate to high poverty headcount ratio, while the southern and northern parts have a low multidimensional headcount ratio.

To comprehend the ground reality of poverty disparities, it is necessary to discuss the spatial pattern of poverty intensity among India's states. As per the latest estimate, the highest intensity of poverty is observed in Bihar, followed by Meghalaya (Table 2). Besides these two states, a high intensity of poverty is noticed (Fig. 4) in eleven states ranging from Jharkhand (47.9 percent) to Tripura (45.0 percent). According to NITI Aayog estimates for 2021, nine Indian states have exceeded the national intensity of poverty, i.e., 47.1 percent, while the remaining 19 states are below the national average. Table 2 shows that even in states with low multidimensional poverty rates (less than 15 percent), such as Mizoram, Punjab, Haryana, Jammu and Kashmir, and Karnataka, the intensity of poverty is higher than average (more than 42 percent). The spatial analysis of poverty explains that poverty intensity often deviates from the pattern of the MPI and headcount ratio and is associated with other socioeconomic and cultural dynamics.

Changes in Multidimensional Poverty Index, Headcount Ratio and Intensity of Poverty between 2005-2006 and 2021

The spatial pattern of absolute and relative changes in multidimensional poverty, headcount ratio, and intensity of poverty from 2005-06 to 2021 is more relevant to understanding the poverty scenario in India in greater detail. According to Table 3, between 2005–2006 and 2021, India has succeeded to reduce MPI by more than half (from 0.118 to 0.279), which represents a significant accomplishment. Similar to MPI, the multidimensional poverty headcount ratio has significantly decreased over the same period, falling from 54.7 to 25.0 percent, or 29.7 percent. In addition, Table 3 further shows that during this time, the intensity of poverty has also lessened from 51.1 percent to 47.1 percent, or 4 percent, which is not particularly impressive. To further explain the interstate disparities in the reduction of poverty in India from 2005–2006 to 2021, the study also makes an effort to assess the state-by-state pattern of changes in absolute and relative terms.

It is noteworthy that all Indian states have been successful in lowering MPI, H, and A. However, large interstate disparities persist in poverty reduction. Fig. 5 plots the absolute change in MPI on the vertical axis and the initial 2005–06 levels of MPI at the state level horizontally. It demonstrates that between 2005–2006 and 2021, 14 of 28 states were successful in reducing MPI at an apprehending rate (>0.165). During this period, it is clear that the poorer states of India are far ahead of the better-off states in terms of poverty reduction. The state's highest absolute change in MPI is observed in Jharkhand (-0.223), followed by Chhattisgarh and West Bengal (Table 3). Alkire and Seth (2015) in their study revealed that from 1998–99 to 2005–06, the reduction of monetary poverty had been faster among the slowest states, and progress in terms of the MPI headcount ratio, as well as the MPI value, had been slower for the poorer states.

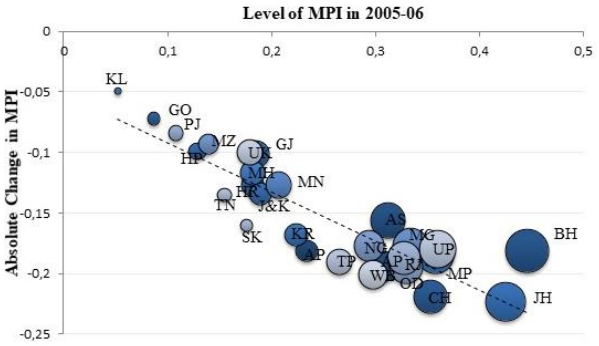

Figure 5. Absolute changes in MPI across Indian states between 2005-06 and 2021, *Source: Prepared by authors*

Several states like Arunachal Pradesh, Odisha, Tripura, Rajasthan, Madhya Pradesh, Andhra Pradesh, Uttar Pradesh, Meghalaya, Nagaland, and Karnataka have also made significant advancements in the absolute change of MPI (Fig. 5). On the other hand, Kerala (-0.049) has the lowest MPI reduction in absolute terms, followed by Goa and Punjab (Table 3). As a result, we can conclude that the rate of poverty reduction is much faster in poverty striken states compared to the less poorer states of India. It is mainly because the rate of absolute change is capped in less poor areas. Most Indian states attempt to explain this emerging dynamics of poverty through their spatial patterns.

Table 3. State wise Absolute and Relative Change in MPI, H and A

State	Absolute Change			Relative Change		
	MPI	H	A	MPI	H	A
INDIA	-0.161	-29.7	-4.0	-57.7	-54.3	-7.8
Andhra Pradesh	-0.181	-37.6	-3.8	-77.4	-75.3	-8.0
Arunachal Pradesh	-0.194	-35.4	-4.5	-62.8	-59.4	-8.7
Assam	-0.156	-28.0	-3.5	-50.0	-46.2	-6.8
Bihar	-0.181	-25.2	-6.8	-40.6	-32.7	-11.7
Chhattisgarh	-0.219	-41.0	-5.9	-62.0	-57.3	-11.6
Goa	-0.072	-16.6	-2.3	-82.8	-81.6	-5.5
Gujarat	-0.101	-19.9	-3.0	-54.6	-51.7	-6.3
Haryana	-0.127	-26.2	-2.8	-69.8	-68.1	-5.9
Himachal Pradesh	-0.099	-23.5	-2.8	-76.7	-75.5	-5.0
Jammu & Kashmir*	-0.134	-28.2	-2.3	-70.9	-69.2	-4.9
Jharkhand	-0.223	-32.5	-9.1	-52.5	-43.6	-16.0
Karnataka	-0.168	-34.9	-3.8	-75.0	-72.6	-8.2
Kerala	-0.049	-12.5	-0.6	-94.2	-94.6	-1.5
Madhya Pradesh	-0.185	-31.1	-5.6	-51.7	-45.9	-10.5
Maharashtra	-0.117	-24.6	-2.4	-64.3	-62.3	-5.2
Manipur	-0.127	-27.2	-1.4	-61.4	-60.3	-3.0
Meghalaya	-0.177	-27.8	-7.1	-53.0	-46.0	-12.9
Mizoram	-0.093	-21.0	2.4	-66.9	-68.2	5.3
Nagaland	-0.177	-31.7	-5.3	-60.2	-55.7	-10.2
Odisha	-0.194	-34.2	-5.6	-58.8	-53.8	-10.7
Punjab	-0.084	-18.4	-1.3	-77.8	-76.7	-2.8
Rajasthan	-0.187	-32.2	-5.5	-57.2	-52.3	-10.3
Sikkim	-0.160	-33.8	-5.5	-90.9	-89.8	-11.8
Tamil Nadu	-0.135	-32.1	-1.8	-87.1	-86.8	-4.4
Tripura	-0.190	-37.8	-3.6	-71.7	-69.4	-7.4
Uttar Pradesh	-0.180	-31.1	-4.6	-50.0	-45.2	-8.8
Uttarakhand	-0.100	-21.0	-1.7	-55.9	-54.2	-3.8
West Bengal	-0.201	-35.9	-6.5	-67.5	-62.6	-12.5

** Value of Jammu & Kashmir includes J & K and Ladakh UT*
Source: Authors' own calculation

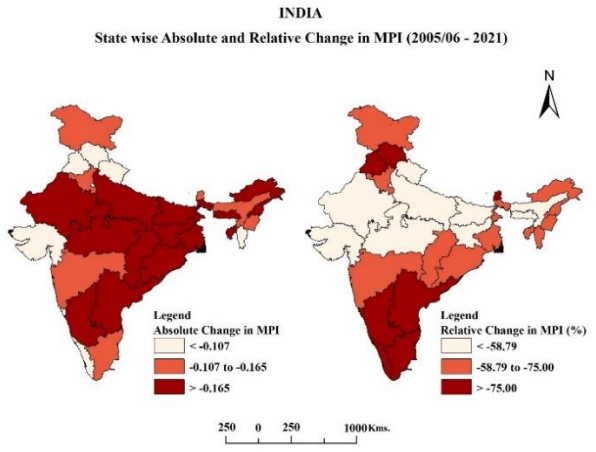

Figure 6. Absolute and relative changes in MPI across Indian states from 2005-2006 to 2021 Source: Prepared by authors

However, the scenario is completely different if we consider the relative change in poverty reduction. A relative measure shows what percentage of change occurred in the present year compared to the previous year. Table 3 shows that from 2005–06 to 2021; Kerala was able to reduce its MPI by approximately 94.23 percent. In a similar vein, Sikkim has dramatically decreased its MPI during that time by 90.91 percent. Figure 6 shows that eight states have been able to reduce poverty by more than seventy-five percent. It should be noted that eight of the nine states with the lowest levels of per capita income in 2021, including Chhattisgarh, Odisha, Rajasthan, Meghalaya, Jharkhand, Madhya Pradesh, Assam, and Uttar Pradesh, have been able to reduce their starting MPI levels by more than 50 percent (Table 3). In terms of the relative change in multidimensional poverty, the majority of the southern states and some of the northern states in India are significantly ahead than the rest of the states of India. On the other hand, from 2005–2006 to 2021, the central and some eastern states of the nation lag behind in terms of relative poverty reduction.

Is this same result noticeable if we consider Headcount Ratio (H), instead of the MPI? To solve this dilemma here we have plotted state-level absolute changes of H in Y-axis and level of H in 2005-06 on X-axis (Fig. 7).

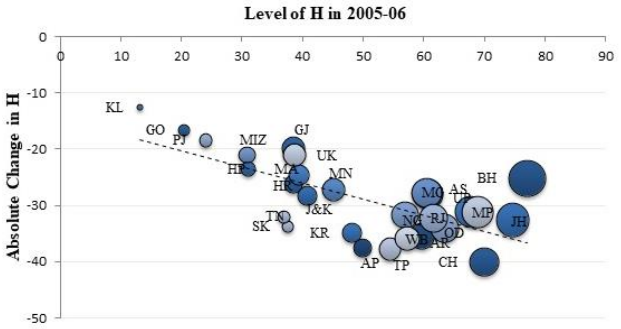

Figure 7. Changes in Headcount ratio (H) across Indian states between 2005-2006 and 2021, *Source: Prepared by authors*

After plotting, the true picture of poverty becomes more visible. Table 3 displays the type and pattern of India's absolute change in the number of people living in poverty, which decreased from 54.07 in 2005–2006 to 25.01 in 2021. Chhattisgarh (-40.09 percent), followed by Tripura and Andhra Pradesh, has experienced the highest absolute headcount ratio reduction (Table 3). In addition, states like West Bengal, Arunachal Pradesh, Karnataka, and Odisha have fair headcount reductions. In contrast, Kerala (-12.49 percent) has the lowest reduction in absolute headcount, followed by Goa and Punjab. Additionally, the rate of reduction is modest in states like Gujarat, Uttarakhand, Mizoram, Himachal Pradesh, Maharashtra, and Bihar (Fig. 7). While the highest relative change of H is found in Kerala (94.62 percent), then Sikkim, Tamil Nadu, and Goa (Table 3). Contrarily, Bihar (32.67 percent) has the lowest relative change in H reduction, followed by Jharkhand, Uttar Pradesh, and Madhya Pradesh (Table 3). Thus, the study shows that between 2005–2006 and 2021, the states with the highest levels of poverty performed worse in terms of the relative change of H reduction among the states of India.

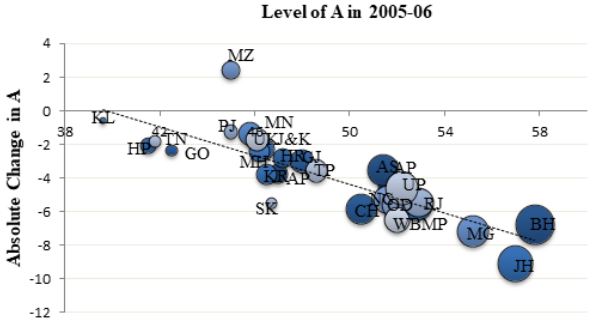

Figure 8. Changes in intensity of poverty (A) across Indian states between 2005-2006 and 2021 *Source: Prepared by authors*

Why are these two depictions of MPI and H changes so dissimilar? Which is the correct one? To answer this conundrum, we look at trends in poverty intensity (A), the overlapping deprivations among the poor, which is the second component of the MPI after H. Figure 8 displays the absolute change in poverty intensity (A), which has been plotted on the Y-axis against the baseline level of poverty intensity in 2005/06 on the X-axis.

According to Figure 8, the poorest states are experiencing a markedly faster decline in poverty intensity. Jharkhand, for example, leads all other Indian states in terms of reducing the intensity of poverty (A), followed by Meghalaya, Bihar, and then West Bengal in both absolute and relative terms (Table 3). On the other hand, Kerala has experienced the smallest reduction in the severity of poverty (Table 3), followed by Punjab, Manipur, and Uttarakhand (Fig. 8). It should be noted that the intensity of poverty in Mizoram has increased from 45 to 47 percent (Table 3), despite decreases in MPI and H from 2005-06 to 2021.

Indicator wise Deprivation of Multidimensional Poverty

Even though we looked at how multidimensional poverty changed in terms of its distribution across the states of India from 2005–2006 to 2021, we still need to understand how deprivations varied by indicator over these years to fully grasp the situation. As opposed to the headcount ratio, the MPI can be broken down into its component indicators, and hence there is a direct relationship between each indicator and the MPI. So how did the indicators of deprivation change among the poor in India? To answer this question, a comparison of each indicator's censored headcount ratio between 2005–2006 and 2021 was performed because the censored headcount ratio indicates the proportion of the population that is MPI poor and deprived for each indicator.

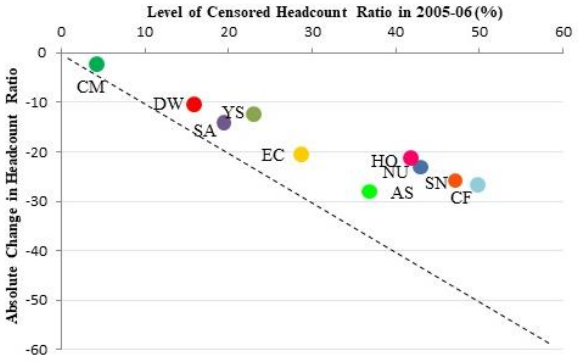

Figure 9. Change in censored headcount (CH) ratios of 10 indicators, *Source: Prepared by authors*

Figure 9 shows how each of the ten indicators has contributed to India's progress in reducing multidimensional poverty. Malnutrition is one of the indicators that are typically high in India, despite having

decreased by half between 2005–2006 and 2021. With at least one malnourished child or adult in the household in 2005–2006, 43 percent of India's population was multidimensionally poor (Table 4); however, by 2021, this proportion has dropped to 19.9 percent (Table 5).

Table 4. Censored Headcount Ratio by Indicator (in Percentage Points) in 2005-2006

Censored Headcount Ratio	Education		Standard of Living							
	Nutrition	Child & Adolescent Mortality	Years of Schooling	School Attendance	Cooking Fuel	Sanitation	Drinking Water	Electricity	Housing	Assets
INDIA	43.0	4.2	23.0	19.4	49.8	47.1	15.9	28.7	41.9	36.9
Andhra Pradesh	36.7	2.2	24.3	12.7	43.2	42.1	11.9	8.7	29.4	34.8
Arunachal Pradesh	39.0	6.1	31.1	31.0	54.0	44.6	16.0	20.9	55.9	47.1
Assam	45.9	4.6	24.8	15.4	55.8	47.2	22.1	51.0	55.6	43.4
Bihar	63.9	7.5	39.8	42.7	74.9	70.4	6.6	63.7	67.3	55.8
Chhattisgarh	51.9	5.5	29.5	19.8	62.1	60.9	29.1	23.8	58.0	41.5
Goa	14.9	0.4	5.8	5.9	15.6	14.5	9.7	2.3	12.6	11.9
Gujarat	30.0	2.8	15.0	11.0	32.7	32.1	11.7	8.8	23.7	27.0
Haryana	33.4	2.9	13.6	15.6	38.6	33.7	12.6	7.5	27.6	23.6
Himachal Pradesh	26.8	1.2	6.4	4.7	29.3	26.9	9.2	1.5	23.5	19.0
Jammu & Kashmir*	29.4	2.8	10.5	17.1	35.7	37.5	17.7	4.8	30.7	25.4
Jharkhand	57.3	7.0	32.9	33.9	70.0	67.6	46.5	55.0	59.8	50.9
Karnataka	38.6	2.2	14.6	15.3	42.1	41.3	17.5	8.4	32.0	32.1
Kerala	10.7	0.5	2.3	2.4	12.7	4.0	8.1	4.4	6.1	10.3
Madhya Pradesh	52.6	5.6	29.4	24.1	62.2	60.8	40.0	25.3	57.8	47.6
Maharashtra	33.1	1.9	10.6	10.9	34.0	35.2	10.1	13.7	29.6	26.8
Manipur	29.3	2.3	9.0	18.4	37.4	33.2	26.9	9.5	40.0	23.2
Meghalaya	41.8	3.8	31.8	38.0	58.9	44.3	32.4	27.3	46.2	51.6
Mizoram	23.5	2.4	8.7	11.1	24.1	13.0	8.7	6.1	29.2	27.9
Nagaland	39.7	4.8	23.1	31.4	54.6	36.8	28.6	17.5	54.3	46.8
Odisha	45.6	4.0	29.6	15.8	57.1	56.0	26.4	43.9	48.2	47.0
Punjab	16.5	1.4	11.9	10.2	20.2	19.5	1.1	2.5	16.1	10.9
Rajasthan	46.9	5.6	28.7	25.3	57.9	56.6	29.5	30.4	40.9	44.3
Sikkim	17.9	1.3	21.8	17.4	31.8	21.3	15.5	7.5	29.0	32.0
Tamil Nadu	26.6	0.8	13.8	3.9	32.7	33.7	11.1	8.2	18.8	26.6
Tripura	41.0	3.0	22.4	11.2	49.8	27.4	27.3	26.6	50.6	39.4
Uttar Pradesh	56.5	7.2	26.2	27.9	62.8	58.9	9.2	48.2	56.0	40.0
Uttarakhand	32.9	2.5	12.5	9.1	37.8	32.4	12.2	14.6	32.8	26.0
West Bengal	42.8	3.1	30.3	16.7	52.3	42.4	11.6	41.4	44.6	41.3

Source: Author's calculation based on Alkire et al. (2021)

In terms of health, the censored headcount ratio of child mortality has decreased from 4.18 percent to 1.88 percent in only 15 years during the same period. A notable improvement in education is also readily apparent: between 2005–2006 and 2021, the censored headcount ratios for years of schooling and school attendance have more than halved. Similarly, the censored headcount ratio of each indicator of standard of living has improved during this period. The proportion of people who are deprived of housing has decreased from 41.9 percent to 20.6 percent. While deprivation in drinking water has reduced from 15.9 percent to 5.5 percent, the percentage of people using solid cooking fuel has lessened from 49.8 percent to 23.1 percent (Tables 4 and 5). Similarly, the sanitation sector's censored headcount ratio has dropped from 47.1 to 21.3 percent. The lack of access to electricity and asset ownership also more than halved between 2005–2006 and 2021.

Table 5. State wise Censored Headcount Ratio of MPI Indicators in 2021

Censored Headcount Ratio	Health			Education		Standard of Living						
	Nutrition	Child & Adolescent Mortality	Maternal Health	Years of Schooling	School Attendance	Cooking Fuel	Sanitation	Drinking Water	Electricity	Housing	Assets	Bank Account
INDIA	19.9	1.9	14.7	10.7	5.2	23.1	21.3	5.5	8.3	20.6	8.9	5.4
Andhra Pradesh	9.2	0.9	4.8	7.7	1.5	9.7	10.5	4.4	0.6	5.7	4.8	1.7
Arunachal Pradesh	13.8	1.2	14.9	13.5	5.9	21.3	16.7	6.2	7.2	23.3	12.9	9.2
Assam	25.5	2.2	17.8	14.3	5.6	31.6	24.4	8.3	14.7	31.4	13.9	10.5
Bihar	41.6	3.9	36.5	24.7	11.6	50.2	46.6	1.6	28.8	47.1	18.7	19.6
Chhattisgarh	24.0	2.3	17.0	10.9	4.3	29.1	26.6	10.2	2.8	26.8	10.4	3.4
Goa	3.0	0.2	1.4	2.2	0.6	2.1	2.8	0.3	0.0	1.8	0.9	0.8
Gujarat	15.4	1.1	8.7	6.7	4.8	17.3	15.5	4.7	2.9	11.4	8.2	4.4
Haryana	10.4	1.2	9.4	4.6	2.8	10.2	6.2	3.4	0.8	7.4	2.6	2.9
Himachal Pradesh	6.8	0.6	5.7	1.5	0.4	7.1	4.8	1.4	0.2	5.2	2.2	0.7
Jammu & Kashmir*	9.7	0.9	6.1	4.5	2.5	11.3	10.6	5.0	1.7	9.4	6.7	1.4
Jharkhand	34.4	2.7	26.5	16.5	7.2	41.3	39.4	17.5	13.6	35.9	15.5	6.6
Karnataka	10.1	0.7	5.4	5.5	2.4	11.6	11.0	3.5	1.0	9.4	5.0	3.4
Kerala	0.6	0.0	0.2	0.2	0.2	0.6	0.3	0.1	0.2	0.4	0.3	0.2
Madhya Pradesh	29.1	2.7	20.9	14.0	7.3	34.9	33.2	17.6	6.5	32.7	13.7	7.4
Maharashtra	12.4	0.8	7.1	4.3	3.0	12.5	12.5	5.3	3.1	10.1	6.7	3.8
Manipur	13.4	1.0	10.1	4.7	1.8	16.3	11.7	13.6	3.5	17.3	6.9	8.9
Meghalaya	23.8	2.1	22.5	16.7	5.3	31.8	18.6	13.7	6.4	23.3	19.4	12.9
Mizoram	6.2	0.6	6.0	5.5	2.3	8.7	5.7	2.8	3.0	7.6	6.7	2.7
Nagaland	17.2	1.4	18.3	11.3	3.7	24.0	8.7	6.9	2.5	24.0	16.7	15.8
Odisha	22.4	1.5	12.8	13.8	4.3	28.8	27.1	9.9	8.9	24.9	13.3	6.5
Punjab	4.4	0.5	3.1	3.4	1.4	4.2	3.0	0.3	0.2	3.3	0.6	1.0
Rajasthan	23.3	2.1	17.1	13.4	7.2	27.7	24.8	13.1	6.6	18.7	13.3	2.2
Sikkim	2.9	0.3	1.8	2.5	0.4	2.9	1.1	0.2	0.1	2.3	1.8	1.1
Tamil Nadu	3.6	0.3	1.7	2.3	0.5	3.6	4.5	1.2	0.4	2.6	1.4	1.5
Telangana	10.2	0.8	0.1	8.5	1.1	10.5	12.2	4.5	0.9	8.3	6.0	2.7
Tripura	12.0	0.9	7.8	8.1	1.7	15.5	11.1	7.3	4.3	16.2	9.4	2.2
Uttar Pradesh	30.5	3.8	25.3	15.1	10.0	34.3	31.8	2.4	18.4	33.4	8.9	3.3
Uttarakhand	14.7	1.6	13.1	6.7	3.2	15.8	11.2	3.2	1.4	12.4	6.2	3.2
West Bengal	16.2	1.0	9.4	11.3	2.8	20.8	16.9	4.4	3.7	18.8	8.7	7.1

*Source: National Multidimensional Poverty Index, 2021 Based on NFHS-4 (2015-16), NITI Aayog * Value of Jammu & Kashmir includes J & K and Ladakh UT*

In Figure 9, the Y-axis represents the change in the censored headcount ratio in absolute terms, and the 45-degree line represents the change necessary to achieve a 100 percent decrease in each indicator. Therefore, the distance between each indicator bubble and the 45-degree line represents the amount required to completely remove the deprivation. Additionally, it offers details on the relative decline of each indicator. The larger the relative reduction, the closer the bubble is to the line. For example, despite the small absolute change in child mortality, the relative rate of reduction has been enormous. Large deprivation is still present across several indicators, including housing, sanitation, cooking fuel, and nutrition, which call for special attention if India wants to end multidimensional poverty in near future.

Though India has made sensational improvements in reducing deprivation in each indicator of MPI, the question still arises: have all the states been equally successful in reducing multidimensional deprivation? A comparison of the state-by-state censored headcount ratios for each MPI indicator between 2005–2006 and 2021 is necessary to provide the answer (Fig. 10 and 11).

Among the states, Tripura, Karnataka, Chhattisgarh, and Andhra Pradesh have made outstanding strides in terms of the magnitude of the reduction in nutritional deprivation (Table 6). Arunachal Pradesh and Jharkhand have made significant progress in lowering child and adolescent mortality. In a similar vein, Table 6 shows that Sikkim, West Bengal, and Chhattisgarh have greater reductions in the deprivation of school years. In school attendance criteria, states like Meghalaya, Nagaland, and

Jharkhand have made notable progress. When it comes to cooking fuel, Tripura, Andhra Pradesh, and Chhattisgarh have been able to significantly reduce deprivation (Table 6). Similar improvements in sanitation have been countersigned by Chhattisgarh, Rajasthan, and Andhra Pradesh. Among the states, Jharkhand, Madhya Pradesh, and Nagaland have made a notable advancement in the degree of reduction in the lack of access to clean drinking water (Table 6). Deprivation from electricity has been reduced mostly in states like Jharkhand, West Bengal, Assam and Odisha. Table 6 also depicts that Tripura, Arunachal Pradesh and Chhattisgarh had larger reductions in housing. While magnitude of asset deprivation has reduced sharply in states like Bihar, Jharkhand and Arunachal Pradesh (Table 6). Overall we can state that in between 2005-06 to 2021 among the states of India 5 states, namely Chhattisgarh, Jharkhand, Tripura, Bihar and Andhra Pradesh have made splendid progress in reducing deprivation in different indicators of multidimensional poverty.

Even though the indicator-wise reduction rate of the censored headcount ratio is discernible among the poorer states, the situation of extreme deprivation still exists in these states that require serious attention. Figure 10 and Figure 11 illustrate the scenario of state-by-state censored headcount ratios in various MPI indicators between 2005–2006 and 2021.

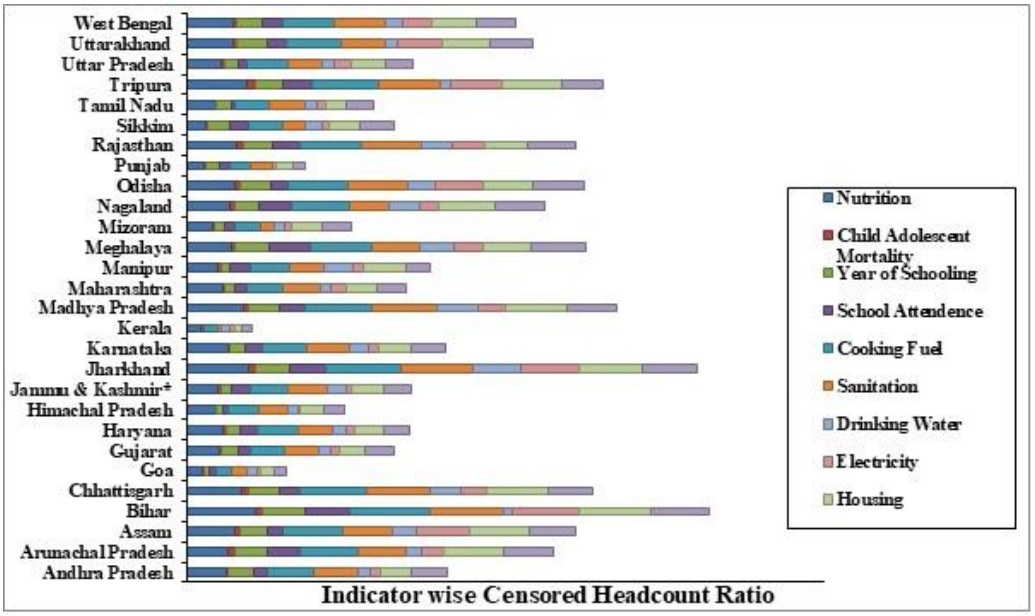

Figure 10. Indicator wise censored headcount ratio in states of India, 2005-2006, *Source: Prepared by authors*

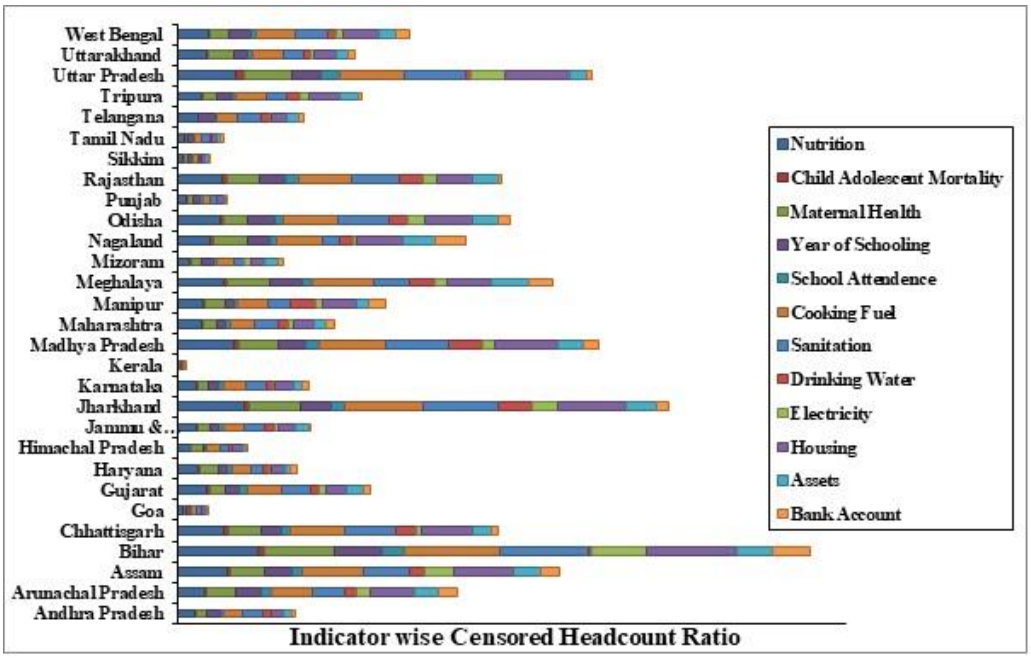

Figure 11. Indicator wise censored headcount ratio in states of India, 2021, *Source: Prepared by authors*

Table 6. Indicator Wise Reduction in Censored Headcount Ratio across the States of India from 2005-2006 to 2021

States	Nutrition	Child & Adolescent Mortality	Years of Schooling	School Attendance	Cooking Fuel	Sanitation	Drinking Water	Electricity	Housing	Assets
India	23.1	2.3	12.3	14.2	26.7	25.8	10.4	20.4	21.3	28.0
Andhra Pradesh	27.5	1.3	16.6	11.2	33.5	31.6	7.5	8.1	23.7	30.0
Arunachal Pradesh	25.2	4.9	17.6	25.1	32.7	27.9	9.8	13.7	32.6	34.2
Assam	20.4	2.4	10.5	9.8	24.2	22.8	13.8	36.3	24.2	29.5
Bihar	22.3	3.6	15.1	31.1	24.7	23.8	5	34.9	20.2	37.1
Chhattisgarh	27.9	3.2	18.6	15.5	33.0	34.3	18.9	21.0	31.2	31.1
Goa	11.9	0.2	3.6	5.3	13.5	11.7	9.4	2.3	10.8	11.0
Gujarat	14.6	1.7	8.3	6.2	15.4	16.6	7.0	5.9	12.3	18.8
Haryana	23.0	1.7	9.0	12.8	28.4	27.5	9.2	6.7	20.2	21.0
Himachal Pradesh	20.0	0.6	4.9	4.3	22.2	22.1	7.8	1.3	18.3	16.8
Jammu & Kashmir*	19.7	1.9	6.0	14.6	24.4	26.9	12.7	3.1	21.3	18.7
Jharkhand	22.9	4.3	16.4	26.7	28.7	28.2	29.0	41.4	23.9	35.4
Karnataka	28.5	1.5	9.1	12.9	30.5	30.3	14.0	7.4	22.6	27.1
Kerala	10.1	0.5	2.1	2.2	12.1	3.7	8.0	4.2	5.7	10.0
Madhya Pradesh	23.5	2.9	15.4	16.8	27.3	27.6	22.4	18.8	25.1	33.9
Maharashtra	20.7	1.1	6.3	7.9	21.5	22.7	4.8	10.6	19.5	20.1
Manipur	15.9	1.3	4.3	16.6	21.1	21.5	13.3	6.0	22.7	16.3
Meghalaya	18.0	1.7	15.1	32.7	27.1	25.7	18.7	20.9	22.9	32.2
Mizoram	17.3	1.8	3.2	8.8	15.4	7.3	5.93	3.1	21.6	21.2
Nagaland	22.5	3.4	11.8	27.7	30.6	28.1	21.7	15.0	30.3	30.1
Odisha	23.2	2.5	15.8	11.5	28.3	28.9	16.5	35.0	23.3	33.7
Punjab	12.1	0.9	8.5	8.8	16.0	16.5	0.8	2.3	12.8	10.3
Rajasthan	23.6	3.5	15.3	18.1	30.2	31.8	16.4	23.8	22.2	31.0
Sikkim	15.0	1.0	19.3	17.0	28.9	20.2	15.3	7.4	26.7	30.2
Tamil Nadu	23.0	0.5	11.5	3.4	29.1	29.2	9.9	7.8	16.2	25.2
Tripura	29.0	2.1	14.3	9.5	34.3	16.3	20.0	22.3	34.4	30.0
Uttar Pradesh	26.0	3.4	11.1	17.9	28.5	27.1	6.8	29.8	22.6	31.1
Uttarakhand	18.2	0.9	5.8	5.9	22.0	21.2	9.0	13.2	20.4	19.8
West Bengal	26.6	2.1	19.0	13.9	31.5	25.5	7.2	37.7	25.8	32.6

Source: Author's own calculation

Tables 4 and 5 portray that between 2005–2006 and 2021, the poorer states in India display acute deprivation in the majority of the indicators. Bihar has the worst situation of the states, with the highest deprivation in ten out of twelve indicators, including nutrition, child and adolescent mortality, maternal health, years of schooling, school attendance, cooking fuel, sanitation, electricity, housing, and bank account in 2021. Except for electricity, assets, and bank accounts, Jharkhand's level of deprivation is similarly severe to Bihar's in most MPI indicators (Table 5). Uttar Pradesh, the most populous state of India is also facing the problem of intense deprivation in most of the indicators except drinking water, assets and bank account. According to Table 5, Madhya Pradesh has the highest level of drinking water deprivation in 2021. In Madhya Pradesh, the magnitude of deprivation is also severe in indicators like child mortality, cooking fuel, and sanitation. Meghalaya and Assam are the two northeastern states where the situation is the worst (Fig. 11). Table 5 portrays that in 2021, among the states of northeast India, the highest deprivation in assets is observed in Meghalaya. The opposite scenario is observed in all the southern states like - Kerala, Karnataka, Andhra Pradesh, Tamil Nadu and Telangana (Fig. 11). The magnitude of deprivation in all the indicators in these states is far below the national average. Except for Rajasthan, none of the western states' censored headcount ratios are particularly extreme (Table 5).

Therefore, it can be said that the poorer states of India (Bihar, Jharkhand, Uttar Pradesh, Madhya Pradesh, and Chhattisgarh) require special attention in order to overcome multidimensional poverty, despite the significant decrease in the censored headcount ratio even after seven decades of independence. In addition, indicator-based special assistance programs must be developed in the country's poorest states.

Decomposition of Multidimensional Poverty

All of the indicators are crucial to the final MPI value. However, it may be a significant task for researchers to determine which indicators are more important to the final MPI score during these two distinct time periods (2005–06 and 2021). The contribution of an indicator offers insight into the relative deprivation of a particular indicator based on the weight assigned to that indicator, which is crucial to understanding where interventions would lead to a decrease in the overall MPI. The contribution of a particular indicator to overall multidimensional poverty can be estimated with the help of decomposition analysis.

Table 7. Indicator wise contribution to MPI for 2005-2006 and 2021

Indicators	Contribution in % (2005-2006)	Contribution in % (2021)
Nutrition	25.89	28.14
Child-Adolescent Mortality	2.75	1.33
Maternal Health	-	10.40
Years of Schooling	14.22	15.14
School Attendance	12.04	7.39
Cooking Fuel	10.13	9.34
Sanitation	9.59	8.61
Drinking Water	3.38	2.23
Electricity	5.92	3.35
Housing	8.54	8.31
Assets	7.55	3.58
Bank Account	-	2.17

Source: Compiled by authors based on NITI Aayog Report on MPI, 2021

Table 7 shows that, between 2005 and 2006, undernutrition contributed the most (about 26 percent) to multidimensional poverty, followed by years of schooling (14.22 percent) and school attendance (12.04 percent). The least significant factors in multidimensional poverty were found to be unimproved access to water and electricity, at 3.38 percent and 5.92 percent, respectively. Similarly, in 2021, undernutrition (28.14 percent) has become the MPI indicator with the highest influence, followed by years of education (15.14 percent) and maternal health (10.40 percent). Child and adolescent mortality (1.33%) and bank account (2.17%), on the other hand, are the least important contributors to MPI in 2021. If we look at contribution in terms of dimensions, the highest contribution among the three domains in 2005 belonged to standard of living, while the highest contribution to MPI in 2021 came from the health dimension. This change may be the result of the addition of two new indicators, such as maternal health in the "health" dimension and banking access in the "standard of living" dimension. This type of addition leads to a change in the weights assigned to the indicators, as the overall weight of MPI is now distributed among twelve indicators. This lessens the significance of each of the seven indicators in terms of both the health and standard of living dimensions (Maiti & Mehrotra, 2022).

Conclusions

The present study has made a thorough comparative assessment of the pattern of multidimensional poverty across the states of India between two different periods, namely 2005–2006 and 2021. The major findings of our study are as follows:

Firstly, the study looked at the spatial distribution of multidimensional poverty in India throughout the aforementioned two time periods. It is found that, while India has made significant progress in lowering its MPI score from 0.279 in 2005–2006 to 0.118 in 2021, there are still significant interstate disparities in the country. The spatial pattern indicates that, despite nearly seven decades of independence, extreme multidimensional poverty persists in several Indian states, including Bihar, Jharkhand, and others. Geographically, India's central and eastern regions continue to be the poorest.

Secondly, the paper also focuses on the state-level absolute and relative changes in the multidimensional poverty, headcount ratio, and intensity of poverty over the period of 2005–2006 to 2021. The study unveils that the poorer states are much ahead in reducing poverty than the better-off states of India which implied a pattern of pro-poor poverty reduction. According to the study, while most states were able to reduce MPI and headcount ratios during this period, the intensity of poverty remained relatively constant, requiring special attention from policymakers and practitioners.

Thirdly, the study investigates indicator-wise deprivation in 2005–06 and 2021, not only at the national level but also among the states. The analysis claims that during this period, most of India's states have succeeded in reducing the severity of deprivation in several indicators like nutritional security, educational opportunities, access to electricity, and housing facilities. The Indian government has implemented a number of development initiatives, including the Integrated Child Development Service, Rashtriya Swasthya Bima Yojana, Mission Indradhanush, Pradhan Mantri Swasthya Suraksha Yojana, Mid Day Meal Programme, Universalizing Education and Enacting the Right to Education for All (2009), Beti Bachao Beti Padhao, Swachh Bharat Mission, National Rural Drinking Water Program, etc., which have played a crucial role in reducing deprivation in MPI (Das et al. 2021). Although India has made outstanding progress in reducing deprivation in the censored headcount ratio for the majority of the indicators, the study discloses that significant deprivation is still present in indicators like nutrition, cooking fuel, sanitation, and housing, which calls for further research.

Fourthly, the current study investigates whether or not all the states have equally succeeded in lowering the deprivation of the multidimensionally poor. And it has been revealed that, compared to the other states, Chhattisgarh, Jharkhand, Tripura, Bihar, and Andhra Pradesh have made excellent progress in reducing deprivation in various indicators of multidimensional poverty between 2005–2006 and 2021. Nevertheless, the severity of poverty is particularly acute in India's poorer states (Bihar, Jharkhand, Uttar Pradesh, Madhya Pradesh, and Chhattisgarh).

Finally, the decomposition analysis of each MPI indicator sheds additional light on the study and demonstrates that undernutrition played a major role in multidimensional poverty in both 2005–06 and 2021. While, dimension-wise, the highest contribution among the three domains during 2005–06 belonged to standard of living, for 2021 the highest contribution is made by the health dimension to MPI.

Based on the above mentioned findings targeted interventions at the grassroots level in the deprived regions of our country should be introduced with special emphasis on several dimensions like health, education and standard of living to reduce poverty and inequality. This study, apart from contributing to the growing literature on poverty studies in the context of India, has identified the geographic dimension of multi-dimensional poverty over space and time. The study ensures that in addition to social and economic dimensions, policymakers should additionally incorporate spatial dimensions and spatial interventions into poverty eradication programs during plan formulation.

Funding

This research received no external funding.

Author contribution

Conceptualization, methodology, writing – original draft – S.M.; Reviewing and Preparing Maps – S.K.; Reviewing and Editing – A.P.M. All authors have read and agreed to the published version of the manuscript.

Conflicts of interest

The authors declare no conflict of interest.

References

Alkire, S. & Foster, J. (2011). Counting and multidimensional poverty measurement. *Journal of Public Economics*, 95(7–8), 476–487. https://doi.org/10.1016/j.jpubeco.2010.11.006

Alkire, S. & Santos, M. E. (2010). Acute Multidimensional Poverty: A New Index for Developing Countries. *OPHI Working Paper* No. 38, University of Oxford

Alkire, S. & Santos, M. E. (2014). Measuring acute poverty in the developing World: robustness and scope of the multidimensional poverty index. *World Development*, 59, 251–274. https://doi.org/10.1016/j.worlddev.2014.01.026

Alkire, S. & Seth, S. (2015). Multidimensional poverty reduction in India between 1999 and 2006: Where and how? *World Development*, 72(C), 93–108, https://doi.org/10.1016/j.worlddev.2015.02.009

Alkire, S. & Foster, J. (2008). Counting and multidimensional poverty measures, *Oxford Poverty and Human Development Initiative (OPHI)* Working Paper 7, Oxford Department of International Development, University of Oxford. http://www.ophi.org.uk/wp-content/uploads/ophi-wp7.pdf

Alkire, S. & Seth, S. (2013). Selecting a targeting method to identify BPL households in India. *Social Indicators Research*, 112 (2), 417–446, https://doi.org/10.1007/s11205-013-0254-6

Alkire, S., Oldiges, C. & Kanagaratnam, U. (2018). Multidimensional Poverty Reduction in India 2005 /6 – 2015 /16: Still a Long Way to Go but the Poorest Are Catching Up. *Research in Progress Series* 54A, Oxford Poverty and Human Development Initiative, University of Oxford

Alkire, S., Oldiges, C. & Kanagaratnam, U. (2021). Examining multidimensional poverty reduction in India 2005/6–2015/16: Insights and oversights of the headcount ratio. *World Development*, https://doi.org/10.1016/j.worlddev.2021.105454

Alkire, S. & Seth, S. (2008). Measuring Multi-dimensional Poverty in India: A New Proposal, *OPHI Working Paper* No. 15, Available at http://ssrn.com/abstract=1815355orhttp://dx.doi.org/10.2139/ssrn.1815355

Atkinson, A. B. (2003). Multidimensional Deprivation: Contrasting Social Welfare and Counting Approaches. *Journal of Economic Inequality*, 1, 51–65. https://doi.org/10.1023/A:1023903525276

Atkinson, A. B. & Bourguignon, F. (1982). The comparison of multi-dimensioned distributions of economic status. *The Review of Economic Studies*, 49(2), 183–201, https://doi.org/10.2307/2297269

Bourguignon, F. & Chakravarty, S. R. (2003). The measurement of multidimensional poverty. The *Journal of Economic Inequality*, 1(1), 25–49, https://doi.org/10.1023/A:1023913831342

Calvo, C. (2008). Vulnerability to Multidimensional Poverty: Peru, 1998–2002. *World Development*, 36(6), 1011–1020. https://doi.org/10.1016/j.worlddev.2007.10.001

Chakravarty, S.R. & D'Ambrosio, C. (2006). The measurement of social exclusion. *Review of Income and Wealth*, 52(3), 377–398. https://doi.org/10.1111/j.1475-4991.2006.00195.x

Chaudhuri, B., Gulati, N., Banerjee, A., Roy, A., Halder, I., Karim, S. & Vertier, P. (2017). Multi-dimensional poverty index-a state level analysis of India. *Working Paper Brussels: European Commission*

Das, P., Paria, B. & Firdaush, S. (2021). Juxtaposing consumption poverty and multidimensional poverty: A study in Indian context. *Social Indicators Research*, 153(2), 469–501. https://link.springer.com/article/10.1007/s11205-020-02519-0

Das, S. K. & Barua, A. (1996). Regional inequalities, economic growth and liberalisation: A study of the Indian economy. *The Journal of Development Studies*, 32(3), 364–390. https://doi.org/10.1080/00220389608422420

Deaton, A. (1997). The analysis of household surveys: A micro econometric approach to development policy. *United States: John Hopkins University Press*

Dehury, B. & Mohanty, S. (2015). Regional Estimates of Multidimensional Poverty in India. *Economics*, 9(1), 1-

35. http://dx.doi.org/10.5018/economics-ejournal.ja.2015-36

Dev, M. S. (2010). Inclusive growth in India: Agriculture poverty and human development. *Oxford India Paperback*

Kumar, V., Kumar, S. & Sonu. (2015). Multi-dimensional poverty index (MPI): A state wise study of India in SAARC countries, *International Journal of Enhanced Research in Educational Development*. 3 (1), 14-21

Maiti, K. D. & Mehrotra, S. (2022). A Curious Case of the Millions of "Disappeared" Poor in India. Retrieved February 4, 2022, from https://www.impriindia.com/insights/poor-disappeared-millions/

Mishra, A. & Ray, R. (2013). Multi-dimensional deprivation in India during and after the reforms: Do the household expenditure and the family health surveys present consistent evidence? *Social Indicators Research*, 110(2), 791–818, https://doi.org/10.1007/s11205-011-9959-6

Mohanty, S. K. (2011). Multidimensional poverty and child survival in India. *PLOS One*, 6(10), https://doi.org/10.1371/journal.pone.0026857

Mohanty, S. K. & Vasishtha, G. (2021). Contextualizing multidimensional poverty in urban India. *Poverty & Public Policy*, 13(3), https://doi.org/10.1002/pop4.314

Mondal, S. & Mishra, A. P. (2021). Spatial interlinkages of poverty determinants and social space of poverty in Hooghly District of West Bengal: A geographical perspective. *Forum Geografic*, XX(2), 212-223. http://dx.doi.org/10.5775/fg.2021.063.d

Mondal, S., Kumar, S. & Mishra, A. P. (2023). Contextualizing spatiality of multidimensional poverty in rural and urban India: A geographical perspective. *Belgeo*, 1, https://doi.org/10.4000/belgeo.59421

Ohlan, R. (2013). Pattern of regional disparities in socio-economic development in India: District level analysis. *Social Indicators Research*, 114(3), 841–873, http://dx.doi.org/10.1007/s11205-012-0176-8

OPHI (2018). Multidimensional Poverty in Chhattisgarh: A Measure for Action. Retrieved from https://ophi.org.uk/wp-content/uploads/Chhattisgarh_2020_online_4vs.pdf

Sarkar, S. (2012). Multi-dimensional Poverty in India: Insights from NSSO data. *OPHI Working Paper*. Retrieved on 6th May, 2021 from http://www.ophi.org.uk/wp-content/uploads/Sandip-Sarkar-Multi dimensional-Poverty-in-India.pdf.

Sen, A. (1976). Poverty: An ordinal approach to measurement. *Econometrica: Journal of the Econometric Society*, 44(2), 219–231, https://doi.org/1912718

Sen, A. K. (1980). Equality of What? In McMurrin, S (Ed.) The Tanner Lectures on Human Values, *University of Utah Press*, Salt Lake City, 197-220

Sen, A. (1993). Capability and Well-Being. In Nussbaum, M. and Sen, A. (Ed.) The Quality of Life. *Oxford: Clarendon Press*, 30-53

Tripathi, S. & Yenneti, K. (2020). Measurement of multidimensional poverty in India: A State-level analysis. *Indian Journal of Human Development*, 14(2), 257–274, https://doi.org/10.1177%2F0973703020944763

UNDP (2015). Human development report 2015: Work for human development. *United Nations Development Programme*. Retrieved February 3, 2021, from http://hdr.undp.org/sites/default/files/2015_human_development_report.pdf

UNDP (2019). The 2019 Global Multidimensional Poverty Index (MPI). Retrieved February 6, 2021, from http://hdr.undp.org/en/2019-MPI

Vasishtha, G. & Mohanty, S.K. (2021). Spatial Pattern of Multidimensional and Consumption Poverty in Districts of India. *Spatial Demography*, 9, 213-240, https://doi.org/10.1007/s40980-021-00089-4

Wagle, U.R. (2008). Multidimensional poverty: An alternative measurement approach for the United States? *Social Science Research*, 37(2), 559–580, https://doi.org/10.1016/j.ssresearch.2007.06.013

Walker, R. (2015). Multidimensional poverty. *GSDRC professional development* reading pack no. 22, Birmingham: University of Birmingham.

World Bank (2018). India development update India's growth story (English). *Washington, D.C. World Bank Group*. Retrieved, 17, May 2021 from http://documents.worldbank.org/curated/en/814101517840592525/Indiadevelopment-update-Indias-growth-story

Wratten, E. (1995). Conceptualizing urban poverty. *Environment and Urbanization*, 7(1), 11-38, https://doi.org/10.1177%2F095624789500700118